INTRODUCTION

Everyone could observe as a little child meets with a playground swing for first time. It seems that the swing is very easily, without any busy, since, and it is almost obvious that this game is naturally given to children, maybe, from the birth. At the same time, the child, being loaded into the swing, would get a first small amazement – all is ready to enjoy, but this swing does not want to sway for some reason. Initially, someone may help him by swaying. Then, maybe not immediately, but still soon enough, the understanding, how to get rid of helper and any troublesome custody assistants, will come: it is necessary to be simply adjusted to the rhythm and small, almost imperceptible, pushes are need to master the game completely. Maybe, one can remember a school basketball court: it is so easy to navigate through it, just holding the ball in any position by some "van der Waals" forces at the fingertips, and playing, thus, a split second to take the next tricky maneuver. Thus, the concept of resonance is very affordable intuitively almost for everybody.

When the time will come not to play, but for a working activity, for example, as a mechanical engineer, then this is the time finally to answer on the essential question: what is the resonance? One can read in "Encyclopedia Britannica" the following lines: "*resonance, in physics, relatively large selective response of an object or a system that vibrates in step or phase, with an externally applied oscillatory force. Resonance was first investigated in acoustical systems such as musical instruments and the human voice. An example of acoustical resonance is the vibration induced in a violin or piano string of a given pitch when a musical note of the same pitch is sung or played nearby...*"

The above text has an undoubted value: now it is obvious that in the case of the experience in life with a swing, the so-called parametric resonance is emerged, and the controlled pushes in a basketball court can be attributed to the ordinary resonance. But the mentioned above definition leaves some dissatisfaction: it seems that once again we have got only small and insignificant details, while the nature of this phenomenon has already known before the reading *a priori*. Also, somewhat is alarming in the frequently cited phrase characterizing the resonance which is "accompanied with a sharp increase in the amplitude". This passage associated with something uncontrolled. Though, almost any child had a chance to make sure: it is very easily to handle and gently drive by the resonance. The question is never disclosed to the end: it is not clear how to recognize the resonant phenomena in practice, how this may be formalized mathematically, whether the resonance has place or not in any specific case? Also, there are many adjectives to

the word “resonance” in the literature, for example: external and internal resonance, the absolute and stochastic resonance, linear and nonlinear one, etc. And how can one do recognize the essence of this physical phenomenon for such an abundance of terms? It turns out that the mathematical formalization of the resonant phenomenon is difficult enough. Let us refer back to one more appropriate definition: “*Let* $\gamma(\zeta)$ *is the Hamiltonian, then zero* $\zeta = \mathbf{0}$ *is a fixed point of the set* (1.1) *and* $\boldsymbol{\lambda} = (\lambda_1,..,\lambda_n)$ *is the vector of eigenvalues* $\boldsymbol{\lambda}$ *of the linear part of the system, so that* $\boldsymbol{\lambda}$ *exhausts all its eigenvalues. The Hamiltonian* $\gamma(\zeta)$ (*and the system* (1.1)) *is in resonance, if the equation*

$$\langle \mathbf{p}, \boldsymbol{\lambda} \rangle = 0 \tag{3.1}$$

has a nonzero integer solution $\mathbf{p} \in \mathbf{Z}^n$, $\mathbf{p} \neq \mathbf{0}$ (*$\mathbf{Z}^n$ is a group of all n-dimensional integer vectors) ... In general, if at least one* $\lambda_j = 0$, *there is a resonance and its order is equal to unity, since the equation (3.1) has a solution* $\mathbf{p} = \mathbf{e}_j$ “. The set of equations (1.1) is the following: $\dot{\zeta}_j = \partial\gamma / \partial\eta_j$; $\dot{\eta}_j = -\partial\gamma / \partial\zeta_j$ $\left(j = \overline{1,n}\right)$, where ζ_j and η_j are canonically conjugate coordinates[1].

From this definition it follows that the resonance may present in Hamiltonian systems[2], which must possess, at least, the first integral. In addition, the phenomenon of resonance can be observed not only in non-autonomous systems, but also in the autonomous Hamiltonian systems, where no external forces act. Moreover, it is not required a proximity or coincidence between the resonant frequencies or eigenvalues. One would ask what can be found of interest in Hamiltonian systems which are almost absent in engineering practice? But, the Hamiltonian systems are general in the nature. For example, one can refer to the stability of the solar system that conserves quasi-periodic motions during milliards years. On the contrary, the instability of the Pluto's orbit due to the resonance caused the recent exception of this celestial body from the family of planets of our solar system. Most phenomena in the microcosm are also described by the Hamiltonian mechanics.

Let us pay attention to another pragmatic definition of the resonance adapted for oscillating systems: “*First of all it is necessary to define the resonance and indicate on what grounds can es-*

---

[1] Bruno, A.D.: *Bounded Three-Body Problem.* Nauka: Moscow (1990) [in Russian]

[2] A similar approach can be found in Arnold, V.I. et al in *Mathematical aspects of classical and celestial mechanics.* VINITI: Moscow (1985) [in Russian]

tablish its presence in the system (22.2) *before solving the problem. We give a definition for this purpose through the time-average of functions* $\mathbf{\Phi}(\varphi, \mathbf{x}, \varepsilon)$ *and* $\mathbf{X}(\varphi, \mathbf{x}, \varepsilon)$:

$$\begin{aligned} \mathbf{\Phi}_0^*(\varphi, \mathbf{x}, \varepsilon) &= \lim_{T\to\infty} \frac{1}{T} \int_0^T \mathbf{\Phi}(\omega_1 t + \theta_1, ..., \omega_m t + \theta_m, \mathbf{x}, \varepsilon) dt, \\ \mathbf{X}_0^*(\varphi, \mathbf{x}, \varepsilon) &= \lim_{T\to\infty} \frac{1}{T} \int_0^T \mathbf{X}(\omega_1 t + \theta_1, ..., \omega_m t + \theta_m, \mathbf{x}, \varepsilon) dt. \end{aligned} \tag{22.9}$$

These expressions represent the average values of the right-hand terms of the system (22.2) *with respect to the time, calculated along the trajectory of the degenerated system* $(\varepsilon = 0)$:

$$\mathbf{x} = \text{const}, \quad \varphi = \boldsymbol{\omega} t + \boldsymbol{\theta}.$$

The function (22.9)*, considered as functions of* $\boldsymbol{\omega} = (\omega_1, ..., \omega_m)$*, can have a point of discontinuity. That is the frequencies at which the functions* (22.9) *are discontinuous, and thus is called as resonant*[3]*"*. Here, the equations (22.2) are the following: $\dot{\varphi} = \boldsymbol{\omega}(x) + \varepsilon \mathbf{\Phi}(\varphi, \mathbf{x}, \varepsilon)$; $\dot{\mathbf{x}} = \varepsilon \mathbf{X}(\varphi, \mathbf{x}, \varepsilon)$, where $\mathbf{\Phi}$ and $\mathbf{X}$ are 2π -periodic functions for all phases.

From the above quotations, we can conclude that it is very difficult, and perhaps impossible to create a context-free (i.e., devoid of any reference to additional information) definition of the resonance phenomenon. It is too capacious concept, maybe the same as a concept of information or a concept of algorithm. It is possible to give a set of various definitions, and all will be OK in their own aspect, but almost all would be incomplete. Therefore, there is no place to fundamental, theoretical and mathematical foundations describing the resonant phenomena in this booklet. This deals with some specific applied problems of engineering only, where the resonant phenomenon plays a key role.

This monograph consists of seven chapters. In the first one, on the basis of specific examples, some general information is referred to mathematical methods from the theory of nonlinear oscillations. The reader, having enough skill over this subject, may pass immediately to the second part, which discusses some new aspects related to the Sommerfeld effect, well-known in mechanics. The third chapter describes the synchronization phenomenon of a pair of asynchronous rotors mounted on an elastic foundation. The question how to control the synchronous motion by

---

[3] Zhuravlev, V.F. and Klimov, D.M.: *Applied Methods in Theory of Oscillations.* Nauka: Moscow (1988) [in Russian]

dampers is posed, as well. The fourth chapter examines the effect of thermo-mechanical instability in dampers, which can lead to undesirable dynamical regimes in the system. The fifth chapter examines dynamical effects of the geometric nonlinearity of the ring resonator of a solid state gyro, which represents an angle sensor for aims of inertial navigation. The sixth part is devoted to the theory of the resonant bolometer. This is a high precision instrument for measuring under cryogenic temperatures. The seventh chapter studies nonlinear resonant interactions between quasi-harmonic waves in a one-dimensional anharmonic chain, based on a simple mathematical model originated from the geometry of central and noncentral interactions between particles, within the so-called harmonic approximation. It is shown that an ideal crystal structure allows for stationary coherent wave ensembles which can significantly influence upon the heat properties of the system, especially at low temperatures. The main idea is to find the most optimal version of the absorber of the resonant bolometer. All these questions, discussed throughout the text, are almost independent problems from the viewpoint of engineering, though being united by a common analytic approach based on asymptotic methods from the nonlinear theory of oscillations.

The main purpose of the first four chapters is to master the mathematical apparatus of asymptotic methods to study specific dynamic properties of mechanical systems in the presence of the Sommerfeld effect, the synchronization phenomenon and the thermo-mechanical instability, as well. This should help to understand how to manifest these physical effects in practice, when one operates with complex technical system, for example, such as railway equipment, where, as a rule, there is a variety of electro-mechanical and thermal phenomena.

In the fifth chapter, we propose a new type of the wave excitation of a ring resonator gyro, associated with navigation systems for long-term space missions up to fifteen years. The main idea is to use the instable properties of the axisymmetric oscillatory mode in the axisymmetric thin-walled ring resonator. The break-up instability of the high-frequency axisymmetric mode is accompanied by the resonant excitation of a pair of precessing bending waves due to the so-called triple-wave resonant interactions between oscillatory modes entering this resonant ensemble. The triple-wave resonance combines advantageously both the parametric and the position types of wave excitation in the presence of energy dissipation.

The sixth chapter examines a model of the resonant bolometer, the operation of which is based on the conversion of the electromagnetic radiation into the heat energy by a heat sensor integrated into a high-Q resonant circuit. Oscillations in the resonant circuit are supported by the low noise self-excited generator of periodic oscillations at given amplitude and frequency, which op-

erates based on the physical properties of the Josephson junction. The heat-sensitive receiving element, implemented into the resonant circuit, experiences a transition from the superconducting phase to the normal resistive state. The measurement procedure is to register a change in the amplitude and phase envelopes under the incoming electromagnetic radiation flux. The resonant bolometer relates to measuring equipment and can be used in devices detecting electromagnetic radiation, especially to determine the weak signals in submillimeter-wave spectral range.

The seventh chapter reveals the multi-wave resonant ensembles in a one-dimensional anharmonic chain of particles with allowances for the central and noncentral internal forces. These ensembles are formed both due to the quadratic nonlinearity of the system, and due to satisfying the phase-matching conditions. The resonant triads entering the multi-wave ensemble can be of three different types only, though each resonant triad consists necessarily of one longitudinal and two transversal wave modes. These resonant triads are nonlinearly coupled. In general case, this leads to a creation of the resonant lattices formed from resonant triads of three different types and the spectral scales. Cascade processes of energy exchange between the oscillatory modes are characterized not only by complex chaotic dynamics, inherent in nonintegrable Hamiltonian dynamical systems, but also by the presence of multi-mode stationary motions, which are stable by the Lyapunov criterion. In the ideal crystals such stationary coherent wave ensembles can significantly influence on the energy partition between waves, especially at low temperatures. This is a relevance of their theoretical and experimental study in micromechanics.

The monograph is written based on the resent papers [1-5]. This one is recommended to undergraduate and graduate students of technical specialties, and may also be useful to my dear colleagues, researchers, with my wishing them many successes.

SIMPLE PROBLEMS OF THE APPLIED THEORY OF OSCILLATIONS

This chapter provides typical examples to the basic problems from the theory of nonlinear vibrations. We consider a pendulum described by the Mathieu equation, Düffing oscillators possessing different nonlinear elastic characteristics, and the van der Pol generator. At the end of some subsections, some questions may be proposed for self-reflection, since the state of the art in science and technology requires from any specialist not only good skill, knowledge in the problem formulation, creating mathematical models and solving basic differential equations, but also the ability to obtain applied results.

Asymptotic methods

These state the basis of the mathematical analysis in a certain sense. The concept of infinitesimals and infinite values are general. The traditional questions, including, in particular, the series convergence, represent key theoretical problem for asymptotic analysis. Unfortunately, absolutely convergent series are almost absent in the theory of dynamical system. Let us recall standard expansions of the sine-function and the logarithm in the neighborhood of a point. In the case of the sine, it is sufficiently to use about three first terms from the Taylor series to access adequate calculations up to the sixth decimal sign. In the case of the logarithm, one needs about five hundred terms in order to ensure the same accuracy of calculations. Obviously, any calculator can cope with much more accurate calculations of the logarithm. Though, it is natural to assume that the algorithm for calculating the logarithm cannot follow directly to the formal Taylor expansions. Otherwise, one could unnecessarily spend all PC resources to calculate a logarithm value. Nonetheless, the accuracy, up to the sixteenth decimal sign, is not a problem for any cheap calculator, using somewhat different algorithm. Similar situations are quite frequent in the dynamics of systems, since the divergent series in the asymptotic methods are often caused by the *phenomenon of resonance*.

The concept of resonance is not a primary category. This requires, at least, good-quality knowledge in the mathematical analysis and the theory of ordinary differential equations. It should be noted, that the understanding cannot be reduced to a formal definition given, for instance, in

"Encyclopedia Britannica". Nonetheless, one can find rigorous mathematical definitions of the resonance in literature. These definitions serve as pragmatic tools in practice[4].

The question of divergent or conditionally convergent series, representing asymptotic solutions to the problems of nonlinear dynamics, is usually solved by separating the motion on the so-called "slow" and "fast" patterns. The "slow" motion is often caused by the resonant phenomena. Most effective tools for studying this remarkable phenomenon are the joint methods of the algebra and mathematical analysis, united in the theory of groups that is used almost everywhere in the modern physics today[5]. The next section provides some information related to the resonant phenomenon along basic examples in mechanical engineering.

Resonance in simplest systems

When studying the resonant phenomena in dynamical systems by asymptotic methods, first of all, one should define a form of the generating solution. First, the original set of equations governing the motion should be transformed to standard equations resolved for the first derivatives, and then, one can solve the problem using, for example, a technique of variation of arbitrary integration constants. The meaning of these preliminary steps is the following. In the generating solution, the integration constants are invariants of motion[6]. In the same generating solution, the perturbed invariants play the role of independent variables, slowly evolving in the time. Thus, we should trace the rate of "destruction" of these invariants by the method of variation of arbitrary constants. Usually, there are no problems to solve the resulting differential equations describing the evolution of these invariants. The experience shows that final differential equations usually get a very simple mathematical structure, so that one can often obtain their analytical solution[7]. Before the solving, the right-hand terms of the obtained equations are subject to a qualitative

---

[4] Zhuravlev, V.F. and Klimov, D.M.: *Applied Methods in Theory of Oscillations.* Nauka: Moscow (1988) [in Russian]

[5] Zhuravlev, V.F.: *Fundamentals of Theoretical Mechanics.* Nauka: Moscow (1997) [in Russian]

[6] The invariants (from Lat. invarians, gen.: invariantis) are physical values, algebraic expressions, etc., associated with any mathematical object and remain unchanged under certain transformations of the object with respect to a group of frames of references, relatively which the object is described.

[7] In this case, the original problem should not be integrable by simple methods, or even, be such in principle.

analysis. Let us suppose that the averaging is performed over the right-hand terms with respect to time, and then the problem would reveal the "fast" variables, e.g., the fast rotating phases, and the "slow" motions, e.g., the slowly varying amplitudes. The average of any function $f(\alpha,\phi,\rho,\omega)$ is calculated as

$$F(\rho,\omega)=\langle f(\alpha,\phi,\rho,\omega)\rangle=\frac{1}{(2\pi)^2}\int_0^{2\pi}d\alpha\int_0^{2\pi}f(\alpha,\phi,\rho,\omega)d\varphi,$$

where some function, for example ρ, is referred to the "slow" motion. Now, the average $F(\rho,\omega)$ is examined for the presence of jumps of this function, when smoothly scanning the parameters, which are some suitable parameters of the problem. For example, in the problem of oscillations of a simple pendulum, this parameter is single: this is the frequency of linear oscillations ω. The jump, or nonzero, in averages indicate the presence of *resonance* in the system. This means that the perturbed solution would be qualitatively different from the generating solution. Otherwise, the motion obtains just small corrections, which may be neglected in many practical cases.

Mathematical pendulum

This is an abstract object in physics, undeniable convenient in modeling many natural phenomena. A mathematical pendulum is isomorphic to the so-called physical oscillator. For example, this is a weight suspended from a pivot in mechanics. This weight can swing freely about the pivot under the gravity.

Harmonic oscillators, occurring in a number of areas of electrodynamics, physical chemistry, engineering and other natural sciences, are equivalent in the sense that their mathematical models are represented by the following ordinary differential equation

$$\ddot{x}+\omega^2\sin x=0,$$

where ω is a positive constant related to the natural frequency; the unknown function $x(t)$ depends upon the time t. For example, in the mechanics, the oscillation frequency is given by $\omega=\sqrt{g/l}$, where l is the length of the suspension; g is the acceleration of gravity, $x(t)$ denotes the angle of deflection of the pendulum from the lower equilibrium position. The equation of small oscillations of the pendulum near the equilibrium is given by

$$\ddot{x}+\omega^2 x=0.$$

This is the equation of motion of the second order, therefore, the law of motion is called harmonic oscillations of the pendulum:

$$x(t) = A\sin(\omega t + \varphi),$$

and determined by two independent constants, i.e., by the initial amplitude A and the initial phase φ.

Mathieu equation

This is an ordinary nonautonomous linear differential equation of the following form [6]

$$\frac{d^2y}{dx^2} + [a - 2q\cos(2x)]y = 0, \qquad (1.1)$$

where a and q are parameters defining the stability properties of solutions[8]. In particular, this equation is used to study the *parametric resonance* phenomenon, and quasi-linear patterns in various applications of theoretical and experimental physics, as well. The well-known example, manifesting the parametric resonance, is a playground swing. The height of the center of mass is varied periodically; therefore, the moment of inertia also follows these changes. This can lead to increase in the amplitude of oscillations. Another example represents a mechanical oscillator the pivot of which performs a periodic motion in the direction perpendicular to oscillations.

The equation (1.1) possesses well-known analytical solutions, though this importance is not so valuable. In the case of quasi-periodic coefficients or a quasilinear system, some modifications to this equation ensure the effectiveness of asymptotic methods, and unnecessary in the absolutely accurate solution.

The equation (1.1) is transformed to the following standard set

$$\dot{x} = y; \quad \dot{y} + \omega^2 x = \mu x\cos\Omega t, \qquad (1.2)$$

[8] The equation, being a special case of Hill's equations, was introduced by E. Mathieu in a context of vibrations of the elliptic membrane [6]. The stability properties are illustrated by the so-called *Ince-Strutt diagram* [7]. The fundamental solutions to Eq. (1) are expressed in the Mathieu functions, i.e., special functions which represent periodic solutions to the Mathieu equation [8, 9].

where ω is the frequency of the pendulum in the absence of the parametric excitation at the frequency Ω. The small parameter of the problem is small: $\mu << 1$.

Let us suppose $\mu = 0$, then the *generating* solution to the set (1.2) is exactly the same as for the harmonic oscillator:

$$x(t) = A\sin(\omega t + \varphi_1); \quad y(t) = \omega A\cos(\omega t + \varphi_1), \tag{1.3}$$

where A and φ_1 are the amplitude and phase, respectively. These are the integration constants determined from the standard initial conditions, defining the state of the system at the initial time, i.e., $x(0)$ and $y(0)$.

Let the parameter μ is small, but finite, then Eq. (1.2) can be solved using the method of variations of arbitrary integration constants. The transform from the old variables of the problem, $x(t)$ and $y(t)$, to the new coordinates, $A(t)$ and $\varphi_1(t)$, using the same representation (1.3), where the constants of integration are formally replaced by functions $A(t)$ and $\varphi_1(t)$, i.e., $x(t) = A(t)\sin(\omega t + \varphi_1(t))$ and $y(t) = \omega A(t)\cos(\omega t + \varphi_1(t))$, is resulted, after the substitution into the set (1.2), in the following differential equations

$$\begin{aligned} \dot{A} &= \mu\omega A\cos(\omega t + \varphi_1)\sin(\omega t + \varphi_1)\cos\Omega t; \\ \dot{\varphi}_1 &= -\mu\omega^2\left(1 - \cos^2(\omega t + \varphi_1)\right)\cos\Omega t. \end{aligned} \tag{1.4}$$

Within the first-order approximation, it is natural to interpret the values A and φ_1 as invariants or ordinary solutions to the generating equations at $\mu = 0$. The right-hand terms of this set (1.4) are of the first power in μ, after the applying the asymptotic procedure. The evidence of the resonance is reduced to finding the jumps in the time-averaged right-hand terms of Eq. (1.4), by scanning the frequencies ω and Ω. Formally, the averaging procedure is performed:

$$\begin{aligned} R_A &= \lim_{T\to\infty}\frac{1}{T}\int_0^T \mu\omega A\cos(\omega\tau + \varphi_1)\sin(\omega\tau + \varphi_1)\cos\Omega\tau d\tau; \\ R_{\varphi_1} &= -\lim_{T\to\infty}\frac{1}{T}\int_0^T \mu\omega^2\left(1 - \cos^2(\omega\tau + \varphi_1)\right)\cos\Omega\tau d\tau. \end{aligned} \tag{1.5}$$

The calculated values of these integrals, provided that the parameters ω and Ω satisfy the following matching condition $\Omega = 2\omega$, are such: $R_A = \frac{\mu\omega A}{2}\cos\varphi_1\sin\varphi_1$ and

$R_{\varphi_1} = -\frac{\mu}{4}\left(2\cos^2\varphi_1 - \omega\right)$. For all other relations between ω and Ω, the average values, R_A and R_{φ_1}, are zeroes. Consequently, the jump in the averages is observed when the following *phase matching condition* is satisfied:

$$\Omega = 2\omega + \mu\Delta, \tag{1.6}$$

where Δ is a small frequency *detuning*, introduced to study the behavior of the system in the vicinity of resonance. Consequently, the first-order approximation procedure, applied to the set (1.2), reveals the single resonance. To construct the higher-order approximations, the anzats (1.3) is modified by introducing the so-called nonresonant corrections $X(t)$ and $Y(t)$:

$$x(t) = A(t)\sin\left(\omega t + \varphi_1(t)\right) + \mu X(t); \quad y(t) = \omega A(t)\cos\left(\omega t + \varphi_1(t)\right) + \mu Y(t), \tag{1.7}$$

Now, the motions are separated into the "fast" and "slow" ones, when replacing the constant of integration by the new unknown functions, $A(t)$ and $\varphi_1(t)$, slowly varying in the time. The role of the nonresonant corrections, $X(t)$ and $Y(t)$, is to compensate the difference between the exact and averaged solutions, since $A(t) = \langle A(t)\rangle + O(\mu\Delta t)$ and $\varphi_1(t) = \langle\varphi_1(t)\rangle + O(\mu\Delta t)$, where the brackets denote the time averages. Let us introduce the following notations: $\langle A(t)\rangle = B(t)$ and $\langle\varphi_1(t)\rangle = \alpha_1(t)$

To bring the system to the autonomous form, we introduce the new additional coordinate $\varphi_2(t) = 2\omega t$, and the related equation $\dot{\varphi}_2 = 2\omega$. The substitution from (1.7) into (1.2), with the allowances for the phase matching condition (1.6), leads to the so-called truncated or evolution differential equations governing the "slow" motions:

$$\dot{B} = \frac{\mu\omega B}{4}\sin 2\alpha_1; \quad \dot{\alpha}_1 = \frac{\mu\omega^2}{4}\cos 2\alpha_1 - \mu\Delta. \tag{1.8}$$

This system is characterized by that its right-hand terms are of the order of μ. Evidently, the variables of the problem, B and α_1, should change slowly. Furthermore, the system (1.8) has the following formal analytical solution

$$\begin{aligned} B(t) &= c_1 \exp\left(\mu\omega\int \sin\left(2\alpha_1(t)\right)dt/4\right); \\ \alpha_1(t) &= -\arctan\left(\frac{1}{\omega + 4\Delta}\left[\tan\left(\frac{\mu t}{4}\sqrt{\Theta} + \frac{1}{4}c_2\sqrt{\Theta}\right)\sqrt{\Theta}\right]\right), \end{aligned} \tag{1.9}$$

where $\Theta = 16\Delta^2 - \omega^2$; c_1 and c_2 are arbitrary constants of integration determined by the initial conditions to the original problem, according to the formulae

$$B(0) = \frac{\sqrt{\omega^2 x^2(0) + y^2(0)}}{\omega}; \quad \alpha_1(0) = \arctan\left(\frac{\omega x(0)}{y(0)}\right). \tag{1.10}$$

The solution (1.9) is easily obtained by eliminating the time parameter, and then, by simply dividing one equation of the system (1.8) on the other, to apply the methods of integrating the first-order differential equations.

The "fast" motions of the problem are naturally represented by the functions $\sin\omega t$ and $\cos\omega t$, and the third harmonics, as well. The equations for the rapidly changing nonresonant corrections would be written as it follows:

$$\begin{aligned} \dot{X} &= \omega^2 B\sin(3\omega t + \alpha_1)/2 - \omega^2 A\sin(\omega t - \alpha_1)/2 - \omega^2 Y; \\ \dot{Y} &= \omega B\cos(\omega t - \alpha_1)/4 + X, \end{aligned} \tag{1.11}$$

The exact solution to this system is irrelevant, because it would have unnecessarily inflated degree of accuracy within the first-order approximation analysis. It is sufficiently to express one variable, does not matter $X(t)$ or $Y(t)$, through the other variable. It is obvious that such a procedure, after dropping the terms of order μ, would be resulted in the following oscillatory equation

$$\ddot{X} + \omega^2 X = \frac{3}{2}\omega^2 B\cos(3\omega t + \alpha_1). \tag{1.12}$$

The trivial initial conditions are natural for this equation. Now, it is useful to summarize some results of the present study:

- The original problem is related to the nonautonomous second-order differential equation (1.2). In the first-order approximation, the asymptotic procedure reduces the problem to the autonomous set (1.8).
- The averages of the right-hand terms of the original set, which are obtained by substituting from (1.3) into (1.2), is clearly dependent upon the nonresonant corrections $X(t)$ and $Y(t)$: $T_A = \mu\left(-\dot{X}\cos\Xi - \omega\dot{Y}\sin\Xi + \omega X\sin\Xi - \omega^2 Y\cos\Xi\right)/\omega$,
  $T_{\varphi_1} = -\mu\left(-\dot{X}\sin\Xi + \omega\dot{Y}\cos\Xi - \omega X\cos\Xi - \omega^2 Y\sin\Xi\right)/B$, where $\Xi = \omega t + \varphi_1$. Though, these average values must be zero.

- The set (1.8) describes the "slow" motions, due to the presence of the resonance in the system (1.2). The resonance is specified by the given structure of the governing equations (1.2). Therefore, the phase matching condition (1.6) is the necessary condition of resonance.
- The equation (1.11) describes the small nonresonant corrections to the basic solution (1.3) within the first-order approximation analysis. These corrections are not relevant to the first-order approximation, however, these are necessary to refine the higher-order approximations, following the asymptotic procedure.

For example, let us select the following specific parameters of the problem: $\mu = 0.1$, $\omega = 1$, $\Omega = 2$, $x(0) = 0.01$, $y(0) = 0.01$, $\Delta = 0.01$. The time history of the system (1.8) is represented in Fig. 1.1.

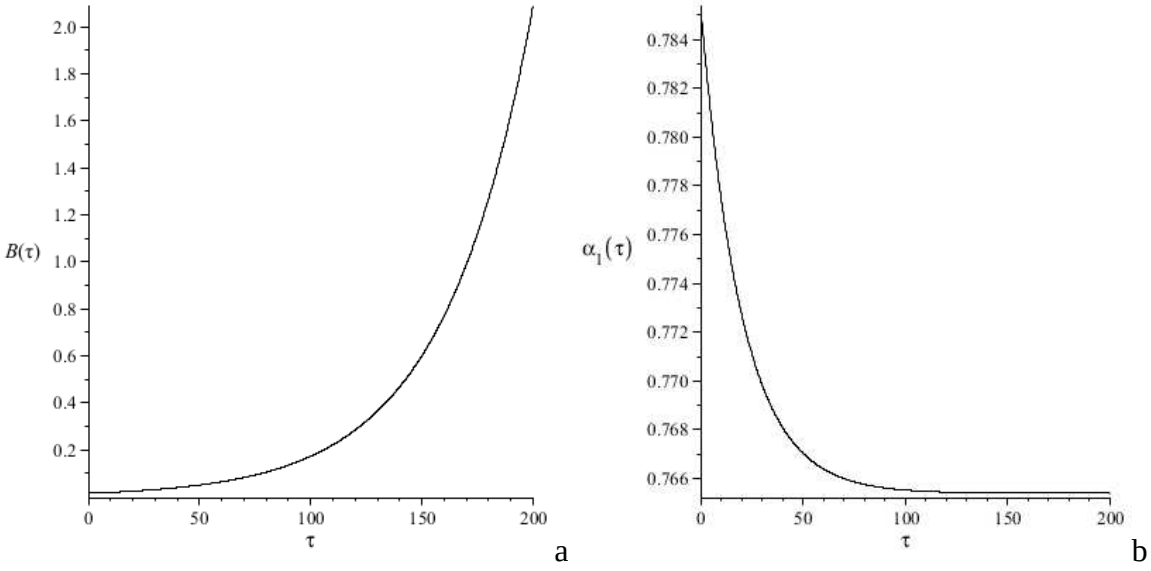

Fig. 1.1 Amplitude envelope and phase: a – $B(t)$; b – $\alpha_1(t)$

Obviously, a comparison between the analytical and numerical results displays that these are indistinguishable (Fig. 1.2). However, the analytical solution is much more informative in terms of parametric analysis, while the numerical solution gives just one more simulation of the process. On this stage of the study we can formulate following problems:

- *How does the phase matching condition* (1.6) *influence upon the dynamics of the system?*
- *Let the phase matching condition has the following form* $\Omega \approx \omega$. *How do the evolution equations for the "slow" motions change?*

- *Let the phase matching condition is the following* $n\Omega \approx m\omega$, *where* n *and* m *are non-zero integers. What form of evolution equations for the variables* $B(t)$ *and* $\alpha_1(t)$ *would be resulted?*

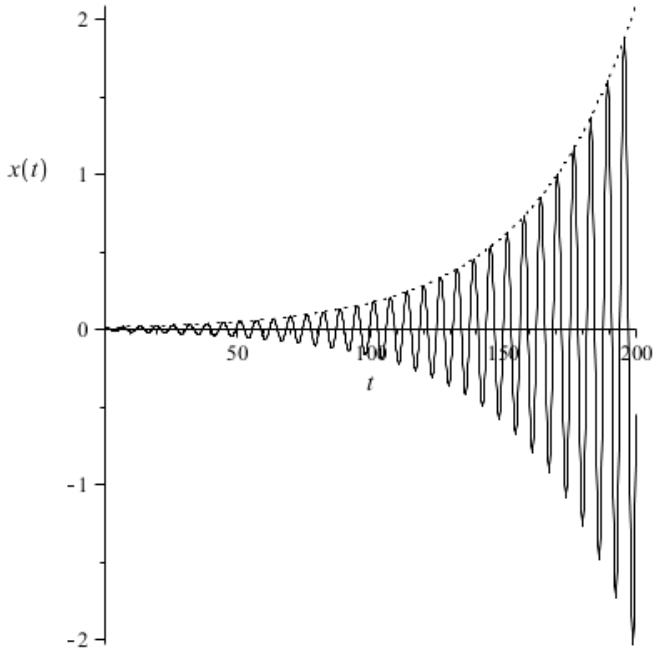

Fig. 1.2 Asymptotic solution vs. numerical integration: dotted line traces the amplitude envelope $B(t)$; solid line corresponds to exact solutions

Düffing Oscillator

The equation governing the motion of the Düffing oscillator has the following form[9]

$$\begin{aligned} &\dot{x} = y; \\ &\dot{y} + \omega^2 x + 2\mu\delta y = \mu\left(f\cos\Omega t - \eta x^3\right), \end{aligned} \tag{1.13}$$

where $x = x(t)$ is the sought variable; ω denotes the natural frequency of the oscillator when the small parameter of the problem μ is zero; δ stands for the coefficient of energy dissipation; η is the nonlinearity coefficient; f is the magnitude of the external periodic force oscillating at the frequency Ω; t is the time. Let $\mu = 0$, then the set (1.13) describes linear harmonic oscillations. In the absence of dissipation of energy $\delta = 0$, and at infinitely small oscillations, one can neglect the nonlinearity, $\eta = 0$. As a result, one can conclude that the linear harmonic oscillator, under the periodic force $F = f\cos\Omega t$, performs finite forced oscillations at the same frequency that

[9] The simplest nonlinear system, first studied by the German engineer *Georg Düffing* in 1918.

the external force[10]. Though, when the natural frequency coincides with the of the external force, $\omega = \Omega$, the system experiences the resonance, expressed in the unlimited growth in the amplitude. It is well known that the solution would be always limited in the damped forced case, at $\delta \neq 0$. After performing the change of variables

$$x(t) = \rho(t)\sin(\omega t + \varphi_1(t)); \quad y(t) = \omega\rho(t)\cos(\omega t + \varphi_1(t)), \tag{1.14}$$

Eq. (1.13) turns into the so-called *standard form* of differential equations, resolved relatively to the first derivatives. The dynamical patterns of the system are studied in the vicinity of the resonance $\omega \approx \Omega$. It is reasonable to introduce the new coordinates, $\varphi_1(t) = \omega t + \alpha_1$ and $\varphi_2(t) = \Omega t + \alpha_2$. On the one hand, this allows to obtain the autonomous standard form, while on the other hand, to separate the motions into "fast" and "slow" ones.

The standard form reads

$$\dot{\rho} = -\frac{\mu}{8\omega}\begin{bmatrix} 8\delta\omega\rho\cos(2\omega t + 2\alpha_1) + 8\delta\omega\rho \\ +\eta\rho^3\sin(4\omega t + 4\alpha_1) - 2\eta\rho^3\sin(2\omega t + 2\alpha_1) \\ +4f\sin(2\omega t + \mu\Delta t + \alpha_1 + \alpha_2 + \Phi) + 4f\sin(\mu\Delta t - \alpha_1 + \alpha_2 + \Phi) \end{bmatrix};$$

$$\dot{\alpha}_1 = \frac{\mu}{8\omega\rho}\begin{bmatrix} 8\delta\omega\rho\sin(2\omega t + 2\alpha_1) \\ +3\eta\rho^3 + \eta\rho^3\cos(4\omega t + 4\alpha_1) - 4\eta\rho^3\cos(2\omega t + 2\alpha_1) \\ -4f\cos(2\omega t + \mu\Delta t + \alpha_1 + \alpha_2 + \Phi) + 4f\cos(\mu\Delta t - \alpha_1 + \alpha_2 + \Phi) \end{bmatrix}. \tag{1.15}$$

Here, the detuning Δ is associated with the phase matching of the system: $\Omega = \omega + \mu\Delta$. This relationship must be necessarily satisfied in the presence of resonance.

To obtain an analytical solution, the standard form (1.15), being completely equivalent to the original equations, is truncated to the evolution equations by calculating the averages of the right-hand terms entering there:

[10] When studying the forced oscillations, one usually neglects the solution to the corresponding homogeneous subsystems, evolving accordingly to the harmonic or exponential law.

$$\dot{\rho} = -\frac{\mu}{2\omega^2}\left[2\delta\omega\rho + f\sin\left(\mu\Delta t - \alpha_1 + \alpha_2 + \Phi\right)\right];$$
$$\dot{\alpha}_1 = \frac{\mu}{8\omega^2\rho}\left[-3\eta\rho^3 + 4f\cos\left(\mu\Delta t - \alpha_1 + \alpha_2 + \Phi\right)\right], \tag{1.16}$$

After the introducing the new angular variable $\psi(t) = \mu\Delta t - \alpha_1 + \alpha_2 + \Phi$, and the "slow" time scale $\tau = \mu t$, this system becomes suitable for analytical study:

$$\frac{d\rho}{d\tau} = -\frac{\delta}{\omega}\rho - \frac{f}{2\omega^2}\sin\psi; \quad \frac{d\psi}{d\tau} = \Delta - \frac{4f\cos\psi - 3\eta\rho^3}{8\omega^2\rho}. \tag{1.17}$$

The solution to this set describes the evolution of the amplitude ρ and phase ψ of the Düffing oscillator within the first-order perturbation analysis. In the absence of the external force and the energy dissipation, the set (1.17) is essentially simplified:

$$\frac{d\rho}{d\tau} = 0; \quad \frac{d\psi}{d\tau} = \Delta - \frac{3\eta\rho^2}{8\omega^2}, \tag{1.18}$$

and can be easily integrated:

$$\rho = \rho_0; \quad \psi = \psi_0 + \left(\Delta - \frac{3\eta\rho_0^2}{8\omega^2}\right)\tau,$$

where ρ_0 and ψ_0 are the integration constants determined from the initial conditions.

Let us analyze this solution, together with the phase-matching condition $\Omega = \omega + \mu\Delta$, and the form of the substitution (1.14). We can find the deviation of the oscillatory frequency, caused by the nonlinearity: $\nu = -3\mu\eta\rho_0^2/8\omega^2$. It is obvious that if the nonlinearity coefficient is positive, i.e., $\eta > 0$, then the effective frequency of the Düffing oscillator, $\omega_{eff} = \omega + \nu$, would decrease. Otherwise, the effective frequency increases, if the nonlinearity coefficient is negative.

Among all the solutions to the set (1.17), the stationary oscillatory modes and their stability properties are of interest. The stationary states can be obtained from the algebraic system of equations, which is resulted by equating to zeroes the derivatives in the differential equations (1.17). This set of algebraic equations is associated with the frequency response of the Düffing oscillator:

$$\left(64\omega^4\Delta^2 + 48\omega^2\Delta\eta\rho_0^2 + 9\eta^2\rho_0^4 + 64\delta^2\omega^4\right)\rho_0^2 = 16f^2, \tag{1.19}$$

depicted in Fig. 1.3. Each point on this curve corresponds to the stationary solutions, which can be stable or not. To investigate the stability, one can use a variety of well-known criteria[11]. We would consider an application of the Hurwitz criterion below.

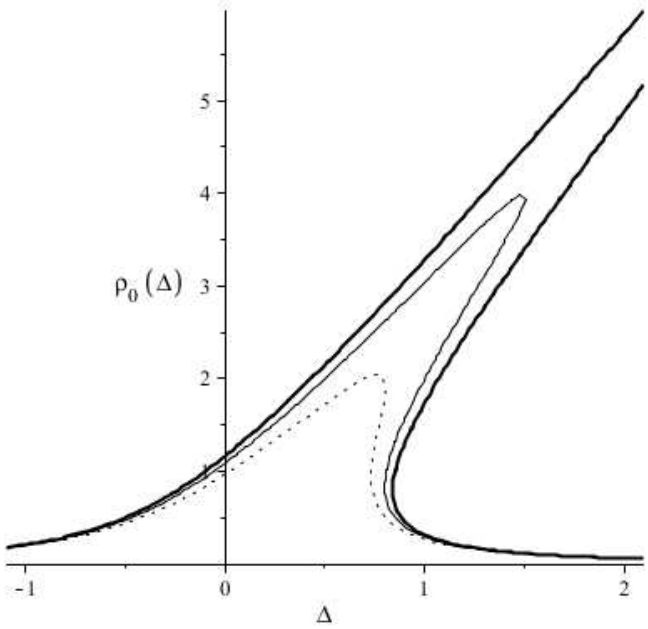

Fig. 1.3 Amplitude-frequency relation to the Düffing equation at $f=1;\ \omega=1;\ \eta=1$. Higher the amplitude, lower the damping ($\delta = 0.15, 0.25, 0.35$)

First, the so-called set of equations describing small perturbations is prepared. After using the following transform to the set (1.17):

$$\psi(\tau)\to\psi_0+\varepsilon\psi(\tau);\quad \rho(\tau)\to\rho_0+\varepsilon\rho(\tau),$$

where ε is an infinitesimal, these equations obtain the form

$$\begin{aligned}\frac{d\rho}{d\tau}&=-\frac{2\delta\rho\omega\rho_0+f\cos\psi_0\psi}{\omega^2};\\ \frac{d\psi}{d\tau}&=\frac{4\rho_0 f\sin\psi_0\psi-3\eta\rho_0^3\rho+2\rho f\cos\psi_0}{4\omega^2\rho_0^2}.\end{aligned}\qquad(1.20)$$

[11] Goryachenko, V.D., Prigorovsky, A.L. and Sandalov, V.M. *Problems in the theory of oscillations, stability of motion and the qualitative theory of differential equations*. Textbook. 2nd ed., Nizhny Novgorod: Publishing House of the Nizhny Novgorod State University (2007) [in Russian]

The linear differential equations (1.20) describe the dynamics of the system (1.17) in a small neighborhood of stationary regimes. If these solutions will increase without limit, the steady state motion will be unstable. To solve the problem of stability, it is sufficient to use solutions to the eigenvalue problem. If the real parts of the eigenvalues will be negative, then we can talk about the stabile motion, otherwise, the stationary regimes would be unstable. One of the universal tools to solve the problem of stability is the Hurwitz criterion, well-known from the course of algebra and geometry. There are some concrete steps for calculating the criterion Hurwitz. First, the characteristic polynomial of the system (1.20) is prepared as it follows:

$$P(\lambda)=\lambda^2-\frac{f\sin\psi_0-2\delta\omega\rho_0}{2\omega^2\rho_0}\lambda+\frac{2f\cos^2\psi_0+3\eta\rho_0^3\cos\psi_0-4\rho_0\omega\sin\psi_0}{8\omega^4\rho_0^2}.$$

Then, accordingly to a paradigm of practical applications of the Hurwitz criterion, we introduce the following notation for the coefficients of the polynomial:

$$g_0=1;\ g_1=\frac{2\delta\omega\rho_0-f\sin\psi_0}{2\omega^2\rho_0};\ g_2=\frac{2f\cos^2\psi_0+3\eta\rho_0^3\cos\psi_0-4\rho_0\omega\sin\psi_0}{8\omega^4\rho_0^2};\ g_3=g_4=g_5=0,$$

and write out the following determinants:

$$T_2=\begin{bmatrix}g_1 & g_0\\ g_3 & g_2\end{bmatrix};\ T_3=\begin{bmatrix}g_1 & g_0 & 0\\ g_3 & g_2 & g_1\\ g_5 & g_4 & g_3\end{bmatrix},$$

For consistency, we introduce the final determinants: $T_0=g_0$, $T_1=g_1$. If all four values of T_0, T_1, T_2 and T_3 would be positive, then the stationary regime is reported as stable. Although, if, at least, one of these numbers will be negative or approaches zero, then the motion is considered to be unstable.

Now, the information received is sufficient to formulate the following questions:

- *Assume that in the Düffing equation is subject to the following transform of variables,* $x(t)=\rho(t)\sin(\omega t+\varphi_1(t))+\mu X(t);\quad y(t)=\omega\rho(t)\cos(\omega t+\varphi_1(t))+\mu Y(t)$. *What form of equations for the "nonresonant" corrections,* $X(t)$ *and* $Y(t)$*, will be?*
- *Would the stationary oscillations be stable for the Düffing oscillator, using the Hurwitz criterion?*

Oscillator with quadratic nonlinearity

The equations of motion of this oscillator are the following

$$\begin{aligned} &\dot{x} = y; \\ &\dot{y} + \omega^2 x + 2\mu\delta y = \mu\left(f\cos\Omega t - \eta x^2\right), \end{aligned} \tag{1.21}$$

wherein all the symbols are exactly the same as in the case of the classical Düffing oscillator.

Let $\mu = 0$, then the system (1.21), as before, describes the motion of a linear harmonic oscillator. If $\mu \neq 0$, and the energy dissipation presents, $\delta \neq 0$, but there is no external periodic force, $f = 0$, then one obtains a nonlinear oscillator with the asymmetric restoring force. Solution to this system is sought in the form

$$\begin{aligned} &x(t) = A(t)\sin(\omega t) + B(t)\cos(\omega t) + \mu x_1(t); \\ &y(t) = \omega A(t)\cos(\omega t) - \omega B(t)\sin(\omega t) + \mu y_1(t), \end{aligned} \tag{1.22}$$

where $y_1(t) = \dot{x}_1(t)$. After the substitution from (1.22) into the set (1.21), we determine the evolution equations in terms of new unknown functions $A(t)$, $B(t)$ and $x_1(t)$, $y_1(t)$. It is obvious that since the order of the original system is two, then the variable $x_1(t)$, which represents a small nonresonant additive correction should be linked to the two remaining unknowns $A(t)$ and $B(t)$, representing the slowly varying amplitudes.

It is remarkable, although the system (1.21) experiences the resonance, nonetheless, this one cannot be detected within the first-order approximation analysis as it has be done in the previous examples. After the reduction of the original set to the standard form and the averaging procedure, one can obtain the following very simple equations:

$$\dot{A} = -\mu\delta A; \quad \dot{B} = -\mu\delta B. \tag{1.23}$$

The equation for the nonresonant correction reads

$$\ddot{x}_1 + \omega^2 x_1 = \eta\frac{\eta\left(B^2 + A^2\right)}{2} + \frac{\eta\left(B^2 - A^2\right)}{2}\cos 2\omega t + \eta AB\sin 2\omega t\,. \tag{1.24}$$

When solving the last equation (1.24), we should remember that the accuracy of the asymptotic procedure is of order μ, accordingly to the expression (1.22). Therefore, it becomes evident that within the first-order nonlinear approximation, the correction $x_1(t)$ can not depend explicitly upon the small parameter μ. Thus, the solution to Eq. (1.24) is also very simple:

$$x_1 = \frac{\eta}{6\omega^2}\left[3\left(B^2 + A^2\right) + \left(A^2 - B^2\right)\cos(2\omega t) - 2AB\sin(2\omega t)\right],$$

where the amplitudes $A(t)$ and $B(t)$ are considered as constants, accordingly to the solution to Eq. (1.23), when $\mu = 0$. Consequently, in the first-order nonlinear approximation, the solution to the set (1.21) is almost indistinguishable from the linear solution, as $\mu = 0$. This case requires applying the tools of the second-order nonlinear approximation analysis, to have some nontrivial result. Now the solution of the system is modified with the allowances for the above information:

$$\begin{aligned} x(t) &= A\sin\omega t + B(t)\cos\omega t + \\ &+ \mu\frac{\eta}{6\omega^2}\left[3\left(B^2 + A^2\right) + \left(A^2 - B^2\right)\cos 2\omega t - 2AB\sin 2\omega t\right] + \mu^2 x_2(t); \\ y(t) &= \omega A\cos\omega t - \omega B\sin\omega t + \\ &+ \mu\frac{\eta}{3\omega}\left[-\left(A^2 - B^2\right)\sin 2\omega t - 2AB\cos 2\omega t\right] + \mu^2 y_2(t), \end{aligned} \tag{1.25}$$

where $y_2(t) = \dot{x}_2(t)$. After substituting the expression (1.25) into the set (1.21) once again, one can obtain the evolution equations for the new unknown functions $A(t)$, $B(t)$ and $x_2(t)$. Obviously, the variable, responsible for the second-order nonresonant additive correction $x_2(t)$, should also be linked with the slowly varying amplitudes $A(t)$ and $B(t)$.

In the second-order nonlinear approximation, the resonance in the system (1.21) is already present. The nontrivial evolution equations are the following

$$\begin{aligned} \dot{A} &= -\mu\delta A + \frac{5}{12\omega^3}\mu^2 B\left(A^2 + B^2\right); \\ \dot{B} &= -\mu\delta B - \frac{5}{12\omega^3}\mu^2 A\left(A^2 + B^2\right). \end{aligned} \tag{1.26}$$

These equations, in the absence of the energy dissipation, $\delta = 0$, can be easily resolved:

$$A(t) = A(0)\sin\left[\frac{5\mu^2}{12\omega^3}\left(A^2(0) + B^2(0)\right)t\right]; \quad B(t) = B(0)\cos\left[\frac{5\mu^2}{12\omega^3}\left(A^2(0) + B^2(0)\right)t\right],$$

where $A(0)$ and $B(0)$ are the initial values of amplitudes. Obviously, that *in vacuo*, $\delta = 0$, the corresponding solution would be very primitive. And now, an answer on the question how does the quadratic nonlinearity effect on the dynamics of the nonlinear oscillator is ready. This type of nonlinearity, as in the case of the classic Düffing oscillator, causes the frequency deviation of

order μ^2, within the second-order approximation procedure. This effect is very weak, but has a significant impact on the evolution of dynamic systems.

Van der Pol generator

Van der Pol generator is an important special case of the Liénard equation [10], describing the motion of simplest nonlinear oscillatory systems[12]. In particular, the following second-order ordinary nonlinear differential equation is a mathematical model of self-excited electric oscillations:

$$\dot{x} = y; \quad \dot{y} + \omega^2 x = \mu\left(x^2 - \delta\right)y, \tag{1.27}$$

where $x = x(t)$ is the dependent variable; ω is the natural frequency of the oscillator when the small parameter of the problem μ is zero; δ is non-negative rate of energy dissipation; t denotes the time. Let $\mu = 0$, then the set (1.27) describes the oscillations of a simple harmonic oscillator, therefore, its solution for small μ, can be found in the form:

$$x(t) = A(\tau)\sin(\omega t + \varphi(\tau)) + \mu X(t); \; y(t) = \omega A(\tau)\cos(\omega t + \varphi(\tau)) + \mu \dot{X}(t), \tag{1.28}$$

where $X(t)$ is a small nonresonant correction. The substitution from (1.28) into Eq. (1.27) leads to the following evolution equations describing the "slow" motion:

$$\frac{dA(\tau)}{d\tau} = -\frac{1}{8}A(\tau)\left[A^2(\tau) - 4\delta\right]; \quad \frac{d\varphi(\tau)}{d\tau} = 0, \tag{1.29}$$

where the differentiation is carried out with respect to the "slow" time $\tau = \mu t$. This set of equations (1.29) has an analytic solution:

---

[12] Balthasar van der Pol (1889 – 1959) was a Dutch physicist. and mathematician. He was born in Utrecht. He graduated from the University of Utrecht (1916), then studied with John Ambrose Fleming and Sir J.J. Thomson, the Cavendish Lab at Cambridge University (1916 – 1919). In 1922 – 1949 he headed the research in electrical laboratory in Eindhoven. Basic mathematical works relate to the theory of oscillations. In 1920, the famous equation, describing the oscillations in vacuum-tube oscillator, was born. The method of slowly varying coefficients to solve this equation had been also suggested, which gave start in the development of the modern theory of nonlinear oscillations.

$$A(\tau)=2\frac{\sqrt{\delta\left(1-\dfrac{\left(x_0+\omega^2y_0^2-4\delta\omega^2\right)\exp(-\delta\tau)}{x_0+\omega^2y_0^2}\right)}}{1-\dfrac{\left(x_0+\omega^2y_0^2-4\delta\omega^2\right)\exp(-\delta\tau)}{x_0+\omega^2y_0^2}};\quad \varphi(\tau)=\arctan\left(\frac{\omega x_0}{y_0}\right). \tag{1.30}$$

The integration constants are determined from the initial conditions of the original problem, accordingly to the following formulae:

$$A(0)=\frac{\sqrt{\omega^2x_0^2+y_0^2}}{\omega};\quad \varphi(0)=\arctan\left(\frac{\omega x_0}{y_0}\right),$$

where $y_0=y(0)$ and $x_0=x(0)$. The equation for the nonresonant corrections $X(t)$ is the following

$$\ddot{X}+\omega^2X=\frac{\omega A\left(-4\delta+A^2-4\omega\delta A+8\left(\delta-A^2\right)\cos^2(\omega t+\varphi)+8A^2\cos^4(\omega t+\varphi)\right)}{8\cos(\omega t+\varphi)}.$$

Let our attention be drawn to the fact that the last equation evolves in the physical time scale t, but not in the "slow" time τ. Assuming that the times t and τ are independent, it is a fairly simple to obtain analytical expression for the solution to this equation:

$$X(t)=-\frac{A}{2(\cos2\varphi+1)}\left[\begin{array}{l}\dfrac{(\cos2\varphi+1)\left(\delta-\dfrac{A^2}{4}\right)\ln(\cos(2\omega t+2\varphi)+1)}{2}\cos(\omega t+\varphi)+\\ \dfrac{A^2\cos(2\omega t+2\varphi)\cos(\omega t+\varphi)(\cos2\varphi+1)}{8}-\\ \left(\dfrac{\cos2\varphi+1}{2}\right)\left(\delta-\dfrac{A^2}{4}\right)\ln(\cos2\varphi+1)-\dfrac{A^2\cos^2 2\varphi}{8}-\\ \dfrac{A^2}{4}\cos(\omega t+\varphi)\left[\begin{array}{l}(\cos2\varphi\sin2\varphi\sin\varphi+1/2)\cos2\varphi\\ -\delta\sin2\varphi\cos\varphi\sin\varphi\end{array}\right]+\\ \left(\delta+\dfrac{A^2\cos2\varphi}{4}\right)\sin(\omega t+\varphi)\sin2\varphi\cos^2 2\varphi.\end{array}\right].$$

Obviously, the values A and φ, describing the "slow" motions, are the functions of the "slow" time τ. They vary accordingly to the expressions (1.30), governed by the equations of motion (1.29). For a visualization, the following specific parameters of the problem are selected: $\mu=0.1$, $\omega=1$, $\delta=1$, $x_0=0.1$, $y_0=0.01$. The time history of the solution $x(t)=A(t)\sin(\omega t+\varphi(t))+\mu X(t)$ is shown in Fig. 1.4. Here the time evolution of the amplitude

$A(t)$ and phase $\varphi(t)$ is described by the expressions (1.30) and the formula for the small additive term $X(t)$. Figure 1.4 shows the numerical solution to the original problem (1.27) with the same data, as in the case of the asymptotic solution. Apparently, these plots almost coincide. This indicates a good quality of the asymptotic approximation.

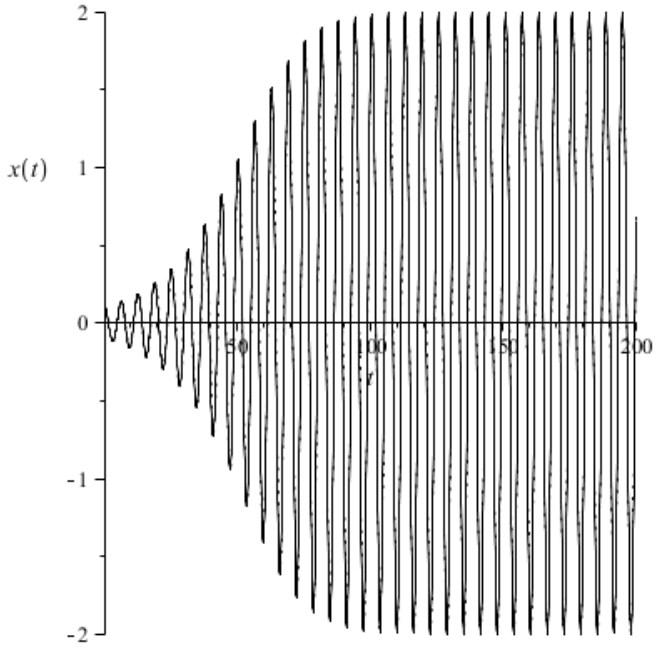

Fig. 1.4 Time history (dotted line – analytical solution of the first-order approximation; solid line – direct numerical integration)

Nonlinear waves in a thin infinitely long bar

We concern with the essentials of nonlinear wave properties in typical mechanical systems such as an infinite straight bar and a circular ring. It is found that the triple-wave resonance can be experienced in systems with continuous and discrete spectra. The circular ring is studied in detail in the context of the solid state wave gyro in the fifth chapter. Much more complicated cascade wave processes and the stability properties of coupled modes with respect to small perturbations are discussed in the seventh chapter.

We consider mechanical vibrations of a thin bar performing plane oscillations along the longitudinal and transverse directions. The elongation of a segment in the bar, Λ, and the curvature of the median line, K, in the vicinity of the point x at the time t can be expressed as it follows: $\Lambda = \sqrt{(1+U_X)^2 + W_X^2} - 1$ and $\mathrm{K} = \left(\arctan\left(W_X/(1+U_X)\right)\right)_X$, where $U = U(X,T)$ and $W = W(X,T)$ are the longitudinal and transverse displacements, respectively. Then the Lagrangian density of the system in the harmonic approximation takes the form

$$L = \frac{\rho A}{2}\left(U_T^2 + W_T^2\right) - \frac{EA}{2}\Lambda^2 - \frac{EJ}{2}\mathrm{K}^2,$$

where ρ is the mass density; A denotes the cross section area; E is the Young modulus; J stands for moment of inertia of the cross section. In a dimensionless notation, this Lagrange density function reads

$$l = \left(u_t^2 + w_t^2 - \varepsilon^2 - \alpha^2\kappa^2\right)/2. \tag{1.31}$$

The related algebra is not cumbersome, though is omitted. It can be found in lengthy original reports. We just emphasize here on the mechanical consequences of the analysis. The relevant dimensionless equations are the following [11]:

$$u_{tt} - u_{xx} = \mu\left(w_x^2\right)_x/2; \quad w_{tt} + \alpha^2 w_{xxxx} = \mu\left(u_x w_x\right)_x \tag{1.32}$$

where α is the dimensionless radius of inertia of the bar; μ is a small parameter arising from asymptotic considerations. Equations (1.32) are established under the working hypotheses of Bernoulli and Euler. Only second-order couplings between the longitudinal mode u and the bending mode w are kept. The linear analysis of Eq. (1.32) yields straightforwardly the dispersion relation for the longitudinal waves propagating without dispersion:

$$\omega_l = \pm k\,, \tag{1.33}$$

and that for the highly dispersive bending waves:

$$\omega_b = \pm\alpha k^2, \tag{1.34}$$

where ω and k denote the natural frequencies and wave numbers, respectively.

The spectra are sketched in Fig. 1.5. Now, we consider the possible coupling between three waves selected at working points in this figure in a typical parallelogram form such that we satisfy the so-called three-wave phase matching conditions

$$\omega_3 = \omega_1 + \omega_2 + \Delta\omega; \quad k_3 = k_1 + k_2 + \Delta k. \tag{1.35}$$

That is, we consider the energy exchange between a large-amplitude high-frequency longitudinal wave coupled to two low-frequency bending wave perturbations propagating in opposite directions. These three waves create a resonant triad. The nonlinear resonant coupling between these

modes is now examined on the basis of the average Lagrangian in the first-order approximation analysis in μ. Coupled solutions are sought in the form

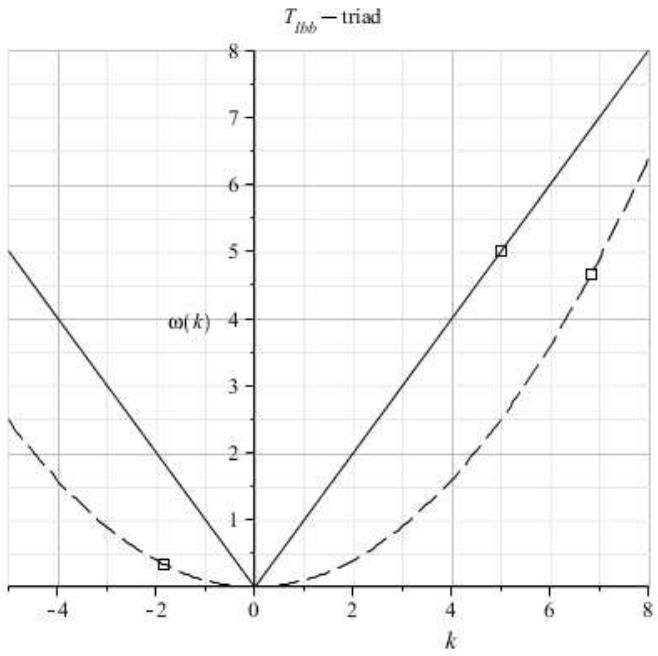

Fig. 1.5 Triple-wave phase matching between high-frequency longitudinal and a pair of low-frequency bending waves in a bar. The bending dispersion branch is traced by the dashed line, while the boxes correspond to the waves of the triad

$$u(x,t) = A_3(\chi,\tau)\exp i\phi_3 + c.c.;$$
$$w(x,t) = A_1(\chi,\tau)\exp i\phi_1 + A_2(\chi,\tau)\exp i\phi_2 + c.c.; \qquad (1.36)$$

where $\chi = \mu x$, $\tau = \mu t$ ($\mu << 1$); A_n are the slowly varying complex amplitudes; $\phi_n = \omega_n t - k_n x$ are the phases. Each couple (ω_n, k_n) satisfies to the correspondingly numbered dispersion relation, and altogether the phase matching conditions (1.35). The symbol *c.c.* denotes the complex conjugate.

On substituting from the anzats (1.36) into the Lagrangian (1.31), and averaging the result over both the space and the time scales, we obtain a set of three coupled hyperbolic-type partial differential equations for the complex amplitudes:

$$\frac{\partial A_n}{\partial \tau} + v_n \frac{\partial A_n}{\partial \chi} = \frac{\beta}{\omega_n}\frac{\partial U}{\partial \overline{A}_n}. \qquad (1.37)$$

Here, $v_n = d\Omega_n(k)/dk\big|_{k=k_n}$ are the group velocities of these three modes; $\beta = -\alpha k_1 k_1 k_1/2$ is the nonlinearity coefficient, while $U = A_1 A_2 \overline{A}_3 \exp i(\Delta\omega t - \Delta k x) + \overline{A}_1 \overline{A}_2 A_3 \exp i(-\Delta\omega t + \Delta k x)$ is the average potential. The Cauchy problem associated with Eq. (1.37) requires the initial conditions:

$A_n(\chi,0)=a_n(\chi)\ \ \left(n=\overline{1,3}\right)$. Let us denote the energy and the energy flux, associated with each linear mode, as it follows:

$$E_n=\omega_n^2\left|A_n\right|^2;\quad S_n=v_nE_n. \tag{1.38}$$

We can establish several consequences of Eq. (1.37) and (1.38) such as the equation

$$\frac{\partial}{\partial\tau}\left(E_1+E_2+E_3\right)+\frac{\partial}{\partial\chi}\left(S_1+S_2+S_3\right)=0. \tag{1.39}$$

It is clear that the following conservation also hold true:

$$\begin{aligned}&\frac{\partial}{\partial\tau}\left(\frac{E_1}{\omega_1}-\frac{E_2}{\omega_2}\right)+\frac{\partial}{\partial\chi}\left(\frac{S_1}{\omega_1}-\frac{S_2}{\omega_2}\right)=0;\\&\frac{\partial}{\partial\tau}\left(\frac{E_1}{\omega_1}+\frac{E_3}{\omega_3}\right)+\frac{\partial}{\partial\chi}\left(\frac{S_1}{\omega_1}+\frac{S_3}{\omega_3}\right)=0.\end{aligned} \tag{1.40}$$

In the case of spatially uniform processes, direct consequences of these divergent laws are the well-known Manley-Rowe relations (first integrals of Eq. (1.39) and (1.40) characterizing the energy partition between modes):

$$\frac{E_1}{\omega_1}-\frac{E_2}{\omega_2}=\text{constant};\quad \frac{E_1}{\omega_1}+\frac{E_3}{\omega_3}=\text{constant}. \tag{1.41}$$

The total mechanical energy is conserved: $E=E_1+E_2+E_3=\text{constant}$, while the evolution equations (1.37) are reduced to the following ones

$$\dot{A}_n=\frac{\beta}{\omega_n}\frac{\partial U}{\partial A_n^*}, \tag{1.42}$$

These are identical to the Euler equations of motion for a rigid body about a fixed point (for real-valued variables [12]). At the degree of approximation (cf. (1.36)), in the present approach, we have the following easily established results concerning the stability of modes:

- Longitudinal waves are unstable with respect to small low-frequency perturbations (so-called break-up instability).
- Bending waves are stable, at least, within the present first-order nonlinear approximation, with respect to small high-frequency perturbations.
- The loss of stability against the high-frequency wave can lead to a dynamic stress growth caused by the resonant excitation of two low-frequency waves.

As a consequence, one may pay special attention to the initial stress level, for example, one may envisage a restriction on it so as to stay in the elastic regime. Finally, one may inquire about the temporal evolution of the considered triad. This requires exploiting a technique such as the inverse scattering method in the general case [13], or to find out much simpler analytical expressions, in terms of Jacobi elliptic functions.

Exploring the Lie series

We consider the problem of two coupled oscillators. The expressions for the kinetic and potential energy are follows

$$\mathrm{K} = \frac{1}{2} m_1 \dot{x}_1^2 + \frac{1}{2} m_2 \dot{x}_2^2; \quad \Pi = \frac{c_1 x_1^2}{2} + \frac{c_2 \left(x_2 - x_1\right)^2}{2} + \frac{c_3 x_3^2}{2}.$$

Using the Euler-Lagrange method, with the help Lagrangian $L = \mathrm{K} - \Pi$, we can obtain the equations of motion, and then derive the characteristic equation for the eigenvalues and eigenvectors of the problem. This equation, represented in an implicit form

$$\lambda^4 m_1 m_2 + \left(\left(m_1 + m_2\right)c_2 + c_1 m_2 + c_3 m_1\right)\lambda^2 + \left(c_1 + c_3\right)c_2 + c_1 c_3 = 0, \tag{1.43}$$

is biquadratic, and therefore, it is easy to solve this analytically. Let us suppose that the parametric dependence $\lambda(m_1)$ is of interest. How do the eigenvalues of the problem change with the variation of the mass, number one? For equation (1.43) this problem is easily solved: one needs to define explicitly the expression for λ. For example, one of the four roots to the equation (1.31) at the given parameters: $m_2 = 1$; $c_i = 1$ $\left(i = \overline{1,3}\right)$, can be expressed as $\lambda = \sqrt{m_1\left(1 + m_1 - \sqrt{1 - m_1 + m_1^2}\right)} / m_1$.

Let us suppose that the equation (1.31) is transcendental, and then the analytic solution to the problem would not so obvious. Here we trace a technique building a solution in the form of the so-called formal series Lie, regardless of the form of the implicit function. This one still should be enough differentiable.

Equation (1.31) can be rewritten in the form $D(\lambda, m_1) \equiv 0$. The parameterization relates to the variables $\lambda = \lambda(\mu)$ and $m_1 = m_1(\mu)$, using the argument μ. Now one can write the Hamiltonian equations

$$m_{1\mu} = -\frac{D_\mu(\lambda, m_1)}{\lambda_\mu}; \quad \lambda_\mu = \frac{D_\mu(\lambda, m_1)}{m_{1\mu}}, \tag{1.44}$$

where the subscript denotes differentiation with respect to the parameter μ. If the original data of the problem are known, for example: $m_j = 1 \quad \left(j = \overline{1,2}\right)$, $c_i = 1 \quad \left(i = \overline{1,3}\right)$, then the Eq. (1.44) can put the Cauchy problem with the initial conditions. Let these conditions would be:

$$\lambda(0) = 1; \quad m_1(0) = 1. \tag{1.45}$$

In other words, we study the evolution of one of roots to the original equation depending on the parameter μ. The Cauchy problem (1.44), (1.45) can be easily solved numerically.

If the parameter μ varies in a small neighborhood of zero only, then it is easy to get a formal analytical solution in the form of the Lie series. For this purpose, by virtue of Eq. (1.44), it is compiled a pair of functions

$$\zeta(\lambda, m_1) \equiv m_{1\mu}; \quad \eta(\lambda, m_1) \equiv \lambda_\mu. \tag{1.46}$$

A parameterization over the variable μ in the expressions (1.46) is insignificant, since the set (1.32) is autonomous. Now the following differential operator is defined

$$\mathbf{G} \equiv \zeta(\lambda, m_1)\frac{\partial}{\partial \lambda} + \eta(\lambda, m_1)\frac{\partial}{\partial m_1}, \tag{1.47}$$

which is called the generator of the group.

Formal Lie series for an arbitrary function of two variables is constructed using the following rule:

$$F\left(\lambda^*, m_1^*\right) = F(\lambda, m_1) + \mu \mathbf{G} F(\lambda, m_1) + \frac{\mu^2}{2!}\mathbf{G}^2 F(\lambda, m_1) + \ldots, \tag{1.48}$$

where $F(\lambda, m_1)$ is the value of the function when its arguments are determined by the initial conditions (1.45), for example: $\lambda(0) = 1;\ m_1(0) = 1$. Here $F\left(\lambda^*, m_1^*\right)$ is the value of the same function at the explicit dependence upon the small parameter μ. In the particular case $F(\lambda, m_1) = \lambda$, we obtain a formal series, describing small variations of the eigenvalue upon the variable μ. Similarly, a particular relationship $F(\lambda, m_1) = m_1$ describes the mass as a function of μ. With regard to the problem of the Lie series describing the variation of mass, one can obtain:

$$m_1^* = 1 - \mu + 2\mu^2 - 6\mu^3 + 26\mu^4 - \frac{698}{5}\mu^5 + \ldots \tag{1.49}$$

The result for the eigenvalue is obtained in a similar manner:

$$\lambda^* = 1 + 4\mu - 6\mu^2 + 28\mu^3 - 151\mu^4 + \frac{4332}{5}\mu^5 + \ldots \qquad (1.50)$$

Obviously, the specific cases of the Lie series (1.49) and (1.50) are sign-alternating conditionally convergent, or even divergent, series. However, they give a good approximation for small values of the parameter of group μ (Fig. 1.6).

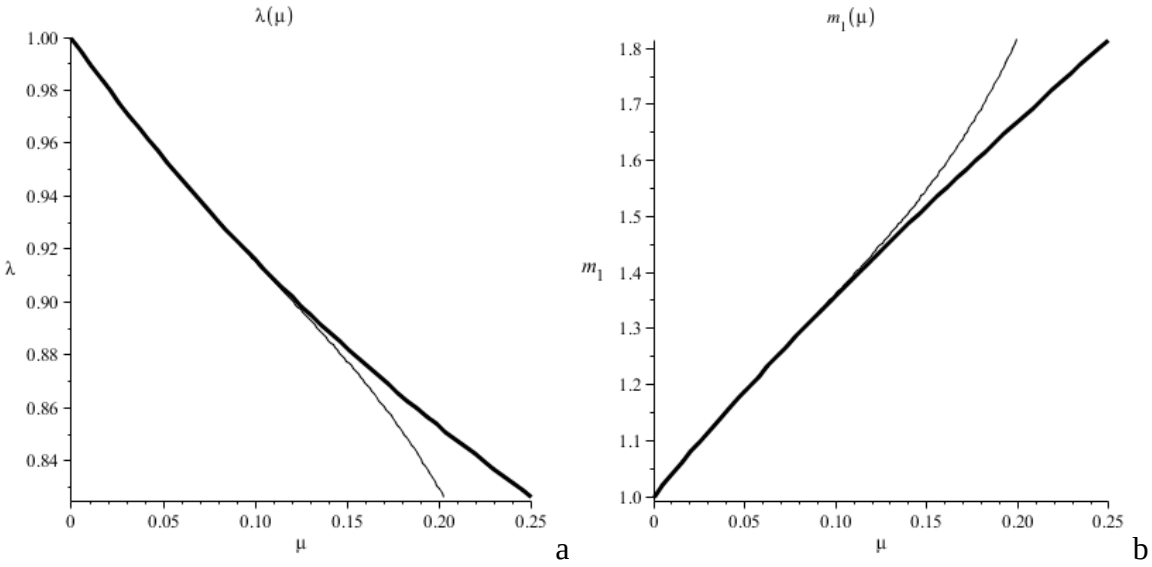

Fig. 1.6 Approximation by the Lie series: a – eigenvalue; b – mass. Thin lines show the Lie partial sums. Thick lines correspond to exact analytical solution

SOMMERFELD EFFECT

We analyze a classical problem of oscillations arising in an elastic base caused by rotor vibrations of an asynchronous driver near the critical angular velocity. The nonlinear coupling between oscillations of the elastic base and rotor takes place naturally due to unbalanced masses. This provides typical frequency–amplitude patterns, even let the elastic properties of the base be linear one. As the measure of energy dissipation increases, the effect of bifurcated oscillations can disappear. The latter circumstance indicates the efficiency of using vibration absorbers to stabilize the dynamics of the electromechanical system. The fourth chapter of this monograph presents results of theoretical studies inspired by the problem of reducing the noise and vibrations by using hydraulic absorbers as dampers to dissipate the energy of oscillations in railway electric equipments. The results of experimental trials over this problem and some theoretical calculations, discussed in the text, are demonstrated the ability to customize the damping properties of hydraulic absorbers to save an electric power and to protect the equipment itself due to utilizing the synchronous modes of rotation of the rotors.

The phenomenon of bifurcated oscillations of an elastic base, while scanning the angular velocity of an asynchronous driver, is referred to the well-known Sommerfeld effect [14–19]. Nowadays, this plays the role of one of classical representative examples of unstable oscillations in electromechanical systems, even being the subject of student laboratory work in many mechanical faculties. This effect is manifested in the fact that the descending branch of resonant curve cannot be experienced in practice. A physical interpretation is quite simple. A driver of limited power cannot maintain given amplitude of stationary vibrations of the elastic base. Detailed measurements can reveal that the oscillation frequency of the base is always somewhat higher than that predicted by the linear theory. This implies a very reasonable physical argument. With an increase in base vibrations, for example, the geometric nonlinearity of the elastic base should brightly manifest itself, so that this assuredly may lead to the so-called phenomenon of “pulling”, or even, chaotic oscillations [20–22]. However, a more detailed mathematical study can demonstrate that the dynamic phenomena associated with the Sommerfeld effect are of more subtle nature. If one interprets this effect as a typical case of resonance in nonlinear systems [23–25], then one should come to a very transparent conclusion. The appearance of the amplitude-versus-frequency response characteristic naturally encountered in nonlinear systems, say, when regarding the Düffing-type equations, does not necessarily have place due to the geometric nonlinearity of the elastic base. This dependence appears as a result of nonlinear resonant coupling between oscillations of the elastic base and rotor vibrations, even when the elastic properties are abso-

lutely linear. The latter circumstance attracts a practical interest in such a remarkable phenomenon, as the effect of Sommerfeld, which is focused in the present study. Namely, some recent numerical simulations [26] lead to idea of efficiency of utilizing vibration absorbers to stabilize the motion of electromechanical systems. The first section of the present study drafts a simple analytical approach to the same problem.

Equations of motion

The equations governing a rotor rolling on an elastic base read [15–18]

$$\begin{aligned} &m\ddot{\eta} + p\eta + 2q\dot{\eta} - m_1 r_1\left(\ddot{\varphi}_1 \sin\varphi_1 + \dot{\varphi}_1^2 \cos\varphi_1\right) = 0; \\ &J_1\ddot{\varphi}_1 + H_1(\varphi_1, \dot{\varphi}_1) - L_1(\varphi_1, \dot{\varphi}_1) - m_1 r_1 \ddot{\eta}\sin\varphi_1 = 0, \end{aligned} \tag{2.1}$$

where m is the mass of a base with one degree of freedom, characterized by the linear displacement η; p is the elasticity coefficient of the base; q is the damping coefficient; m_1 stands for the mass of an eccentric; r_1 denotes the radius of inertia of this eccentric; J_1 is the moment of inertia of the rotor in the absence of imbalance; $H_1(\varphi_1, \dot{\varphi}_1)$ is the driving moment; $L_1(\varphi_1, \dot{\varphi}_1)$ describes the torque resistance of the rotor. The single device (unbalanced rotor) set on the platform, while the rotation axis is perpendicular to the direction of oscillation η. The angle of rotation φ_1 of the rotor is measured counter-clockwise. Assume that the moment characteristics and the driver drag torque are modeled by the simple functions: $H_1 = M_1 - k_1\dot{\varphi}_1$ and $L_1 = k_{10}\dot{\varphi}_1$, where M_1 is the starting point, k_1 is the coefficient characterizing the angular velocity of the rotor, i.e., M_1 / k_1; k_{10} is the resistance coefficient. Then the equations of motion are rewritten as

$$\begin{aligned} &m\ddot{\eta} + p\eta + 2q\dot{\eta} - m_1 r_1\left(\ddot{\varphi}_1 \sin\varphi_1 + \dot{\varphi}_1^2 \cos\varphi_1\right) = 0; \\ &J_1\ddot{\varphi} + \left(k_{10} + k_1\right)\dot{\varphi}_1 - M_1 - m_1 r_1 \ddot{\eta}\sin\varphi_1 = 0. \end{aligned} \tag{2.2}$$

After introducing the dimensionless variables, the basic equations hold true:

$$\begin{aligned} &\ddot{x} + x + 2\mu d\dot{x} - \mu\left(\ddot{\varphi}_1 \sin\varphi_1 + \dot{\varphi}_1^2 \cos\varphi_1\right) = 0; \\ &\ddot{\varphi} + a_1\dot{\varphi} - b_1 - \mu c_1 \ddot{x}\sin\varphi_1 = 0, \end{aligned} \tag{2.3}$$

where $\mu = m_1 / m << 1$ is the small parameter; $a_1 = \left(k_{10} + k_1\right) / J_1\omega_0$, $b_1 = M_1 / J_1\omega_0^2$, $c_1 = m_1 r_1 / J_1$. Here, $\omega_0 = \sqrt{p / m}$ stands for the oscillation frequency of the base; x is the new dimensionless linear coordinate measured in fractions of the radius of inertia of the eccentric; $d = r_1\omega_0 q / m_1$ is the dimensionless coefficient of energy dissipation; $\tau = \omega_0 t$ is the new dimensionless time.

The set (2.3) is now normalized at the linear part approaching a standard form. First, the equations can be written as a system of four first-order equations

$$\begin{aligned}
&\dot{x} = y;\\
&\dot{y} = -x - 2\mu d y + \mu\left(\dot{\omega}_1 \sin\varphi_1 + \omega_1^2 \cos\varphi_1\right);\\
&\dot{\varphi}_1 = \omega_1;\\
&\dot{\omega}_1 = -a_1\dot{\varphi}_1 + b_1 + \mu c_1 \dot{y}\sin\varphi_1.
\end{aligned} \tag{2.4}$$

Then we introduce the polar coordinates, $x = \rho\sin\alpha$ and $y = \rho\cos\alpha$. So that the equations get the following form

$$\begin{aligned}
&\dot{\rho} = \mu\left(\dot{\omega}_1 \sin\varphi_1 + \omega_1^2 \cos\varphi_1\right)\cos\alpha - 2\mu d\rho\cos^2\alpha;\\
&\dot{\alpha} = 1 + 2\mu d\sin^2\alpha - \mu\left(\dot{\omega}\sin\varphi_1 + \omega_1^2\cos\varphi_1\right)\sin\alpha/\rho;\\
&\dot{\varphi}_1 = \omega_1;\\
&\dot{\omega}_1 = -a_1\omega_1 + b + \mu c_1\left(\dot{\rho}\cos\alpha - \rho\dot{\alpha}\sin\alpha\right)\sin\varphi_1.
\end{aligned} \tag{2.5}$$

Now the set (2.5) experiences the transform on the angular variable $\varphi_1 = \phi_1 - \omega_1/a_1$. Then the equations obtain the form close to a standard form

$$\begin{aligned}
&\dot{\rho} = \mu\left[\dot{\omega}_1 \sin\left(\phi_1 - \omega_1/a_1\right) + \omega_1^2\cos\left(\phi_1 - \omega_1/a_1\right)\right]\cos\alpha - 2\mu d\rho\cos^2\alpha;\\
&\dot{\alpha} = 1 + 2\mu d\sin^2\alpha - \mu\left[\dot{\omega}_1\sin\left(\phi_1 - \omega_1/a_1\right) + \omega_1^2\cos\left(\phi_1 - \omega_1/a_1\right)\right]\sin\alpha/\rho;\\
&\dot{\phi}_1 = \Omega_1 + \mu c_1\left(\dot{\rho}\cos\alpha - \rho\dot{\alpha}\sin\alpha\right)\sin\left(\phi_1 - \omega_1/a_1\right)/a_1;\\
&\dot{\omega}_1 = -a_1\omega_1 + b_1 + \mu c_1\left(\dot{\rho}\cos\alpha - \rho\dot{\alpha}\sin\alpha\right)\sin\left(\phi_1 - \omega_1/a_1\right).
\end{aligned} \tag{2.6}$$

Here $\Omega_1 = b_1/a_1$ denotes the partial angular velocity of the rotor. The system of Eq. (2.6) is completely equivalent to the original equations. It is not a standard form, resolved for the first derivatives [24], but such form is most suitable for the qualitative study of stationary regimes of motion, due to the explicit presence of generalized velocities in the right-hand side terms.

Resonance

We study the resonance phenomenon in the dynamical system (2.6). Let $\mu = 0$, then Eq. (2.6) are reduced to the following set: $\dot{\rho} = 0$, $\dot{\alpha} = 1$, $\dot{\phi}_1 = \Omega_1$, $\dot{\omega}_1 = -a_1\omega_1 + b_1$, which has a simple solution

$$\begin{aligned}
&\rho = \rho(0);\\
&\alpha = \alpha(0) + \tau;\\
&\phi_1 = \phi_1(0) + \Omega_1\tau;\\
&\omega_1 = \Omega_1\left(1 - \exp(-a_1\tau)\right) + \omega(0)\exp(-a_1\tau),
\end{aligned} \tag{2.7}$$

where $\rho(0)$, $\alpha(0)$, $\phi_1(0)$, $\omega_1(0)$ are the integration constants. Now the solution (2.7) is substituted into the right-hand terms of Eq. (2.6). Then one discards all the terms in order μ2 and higher, as well, to perform the averaging over the period of fast rotating phases. In the problem (2.6), the fast variables are the angles $\alpha(\tau)$ and $\phi_1(\tau)$, accordingly, $\rho(\tau)$ and $\omega_1(\tau)$ are the slow variables. The average of an arbitrary function is calculated as

$$F(\rho,\omega_1)=\langle f(\alpha,\phi_1,\rho,\omega_1)\rangle=\frac{1}{(2\pi)^2}\int_0^{2\pi}d\alpha\int_0^{2\pi}f(\alpha,\phi_1,\rho,\omega_1)d\varphi_1.$$

Now the average $F(\rho,\omega_1)$ is examined for the presence of jumps along a smooth change of system parameters. One of which represents the partial angular velocity Ω_1. It is easy to see that the jump of the average takes place at the value $\Omega_1=1$.

Evolution equations

In the case when the system is far from resonance, i.e., $|\Omega_1-1|>>\mu$, Eq. (2.6) can easily be solved using the Poincaré perturbation method applied to the small nonresonant terms in order μ. However, in the resonant case, as $|\Omega_1-1|\sim 0$, the first-order nonlinear approximation solution should contain the so-called secular terms appearing due to the known problems of small denominators. To overcome such a problem, one usually does the following trick. As soon as the quantities $\alpha(\tau)$ and $\phi_1(\tau)$ are changing rapidly, with approximately the same rate, it is natural to introduce a new generalized slow phase $\Phi(\tau)=\alpha(\tau)-\phi_1(\tau)+(\Omega_1+\varpi_1(\tau))/a_1$, where $\varpi_1(\tau)=\omega_1(\tau)-\Omega_1$ is a small variation of the angular velocity. Then after the averaging over the fast variable α, one obtains the equations for the slow variables only, which are free of secularity. Such equations are called the evolution equations or truncated ones. In the case of the set (2.6), the truncated equations hold true:

$$\begin{aligned}
&\dot\rho=\mu\left((\Omega_1+\varpi_1)^2\cos\Phi-\varpi_1\sin\Phi\right)/2-2\mu d\rho;\\
&\dot\Phi=\Delta-\varpi_1-\mu\left((\Omega_1+\varpi_1)^2\sin\Phi+\varpi_1\cos\Phi\right)/2\rho;\\
&\dot\varpi_1=-a_1\varpi_1-\mu c_1\left(\rho\cos\Phi+\dot\rho\sin\Phi\right)/2,
\end{aligned}\qquad(2.8)$$

where $\Delta=1-\Omega_1$ is the small frequency detuning, $\Phi(\tau)$ is the new generalized phase. Note that for the problem of averaging over the fast variable is enough to write $\dot\alpha\approx 1$.

Stationary oscillations in the absence of energy dissipation

Now the usual condition of a steady motion, i.e., $\dot{\rho} = \dot{\Phi} = \dot{\varpi}_1 = 0$, is applied. We are looking now for the stationary oscillatory regimes *in vacuo*, i.e., $d = 0$. The solution corresponding to these regimes reads

$$\begin{aligned} &\cos\Phi = 0 \quad (\sin\Phi = \pm 1); \\ &\varpi_1 = 0; \\ &\rho = \frac{\mu\Omega_1^2}{2\Delta} = \frac{\mu\Omega_1^2}{2(1-\Omega_1)}. \end{aligned}$$

This solution describes a typical resonant curve near the point $\Omega_1 = 1$. The next stage of the study is to test the stability properties of stationary solutions. To solve this problem, one should obtain the equations in perturbations. The procedure for deriving these equations is that, firstly, one performs the following change of variables

$$\begin{aligned} &\cos\Phi \to \mp\Phi \quad (\sin\Phi \to \pm 1); \\ &\varpi_1 \to \varpi_1; \\ &\rho \to \rho_0 + \rho, \end{aligned}$$

where $\rho_0 = \mu(\Delta - 1)/2\Delta$ is the amplitude of steady-state oscillations, then after replacing the variables, the perturbation equations get the following form

$$\begin{aligned} &\dot{\rho} = -\frac{\mu}{2}\left(\Omega_1^2\Phi + \varpi_1\right); \\ &\dot{\Phi} = -\left(1 + \frac{\mu\Omega}{\rho_0}\right)\varpi_1 + \frac{\mu}{2}\left(\frac{\Omega}{\rho_0}\right)^2\rho; \\ &\dot{\varpi}_1 = -a_1\varpi_1 - \frac{\mu c}{2}\left(\rho_0\Phi + \dot{\rho}\right). \end{aligned}$$

To solve the stability problem evoking the Lyapunov criterion, we formulate the eigenvalue problem defined by the following cubic polynomial, implicitly presented by determinant of the third order

$$\begin{vmatrix} -\lambda & \frac{\mu}{2}\left(\frac{\Omega_1}{\rho_0}\right)^2 & -\left(1 + \frac{\mu\Omega_1}{\rho_0}\right) \\ -\frac{\mu\Omega_1^2}{2} & -\lambda & -\frac{\mu\lambda}{2} \\ \frac{\mu c_1}{2}\rho_0 & -\lambda\frac{\mu c_1}{2} & -\lambda - a_1 \end{vmatrix} = 0.$$

Now we can apply one of the most widely known criteria, for example, the Hurwitz criterion, for the study the stability properties in the space of system parameters. The result is that the descending branch of the resonant curve, when $\Omega_1 > 1$, cannot be practically observed because of the volatility associated with the fact that the driver is of limited power. This cannot maintain the given stationary oscillation of the elastic base near the resonance. This result corresponds to the well-known paradigm associated with the so-called Sommerfeld effect.

Formally, there are stable stationary regimes, as $\Omega_1 \geq 2$. However, this range of angular velocities is far beyond the accuracy of the first-order nonlinear approximation.

Damped stationary oscillations

A small surprise is that the response of the electromechanical system (2.2) has a significant change in the presence of even very small energy dissipation. Depending on the parameters of the set (2.2), the small damping can lead to typical hysteretic oscillatory patterns when scanning the detuning parameter Δ. Though, let the dissipation be sufficiently large, then very simple stable steady-state motions, inherent in almost linear systems, hold true also.

From the stationary condition, one looks for the stationary oscillation regimes ρ_0, ϖ_{10} and Φ_0, as $d \neq 0$. The equations corresponding to these regimes are the following ones

$$\begin{aligned} \rho_0 &= \frac{(1-\Delta+\varpi_{10})^2 \cos\Phi_0}{2d}; \\ \Delta-\varpi_{10} &= \frac{\mu(1-\Delta+\varpi_{10})^2 \sin\Phi_0}{2\rho_0}; \\ \varpi_{01} &= -\frac{\mu c \rho_0 \cos\Phi_0}{2a}. \end{aligned} \qquad (2.9)$$

For a small damping, the solution to these equations describes a typical nonunique dependence between the frequency and amplitude, i.e., $\rho_0(\Delta)$, defined parametrically through the phase Φ_0. Near the resonance, $\Omega_1 = 1$ ($\Delta = 0$), at some given specific parameters of the problem, say $\mu = 0.1$, $d = 0.03$, $a = 1$ and $c = 1$, the sketch of this curve is shown in Fig. 2.1.

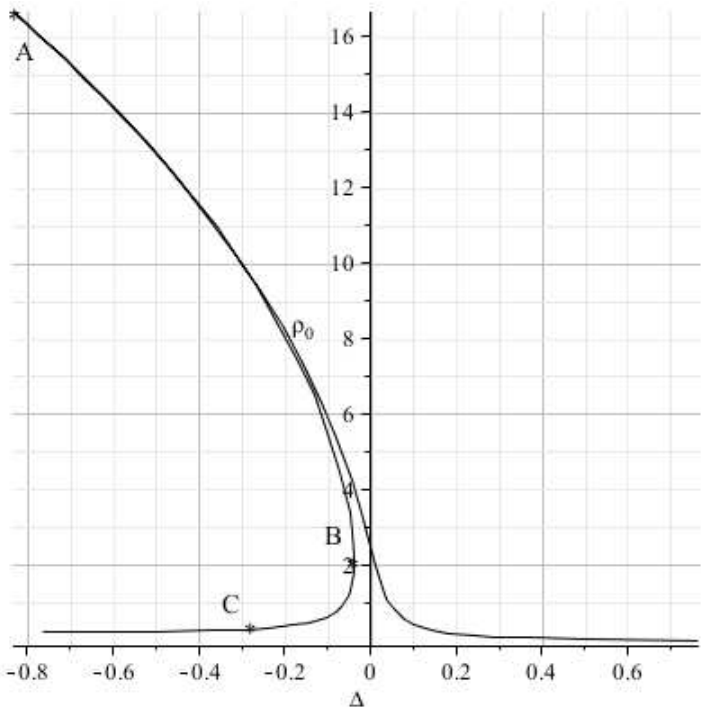

Fig. 2.1 The frequency-amplitude dependence $\rho_0(\Delta)$ near the resonance $\Omega_1 = 1$ (arbitrary units)

To study the stability problem of stationary solutions to the perturbed equations, we should formulate the eigenvalue problem. This leads to the following characteristic cubic polynomial

$$p(\lambda) = g_0\lambda^3 + g_1\lambda^2 + g_2\lambda + g_3$$

with the following coefficients

$$g_0 = 1;$$

$$g_1 = \frac{\mu(1-\Delta+\varpi_{10})(\mu c\rho_0 \sin\Phi_0 + 1-\Delta+\varpi_0)\cos\Phi_0 + 2\rho_0(a_1+\mu d)}{\rho_0\left(1-\mu^2 c_1 \sin^2\Phi_0/4\right)};$$

$$g_2 = \frac{\mu\begin{pmatrix} -\mu\left(\mu c_1\rho_0\sin\Phi_0 + 2c_1\rho_0^2 + 2(1-\Delta+\varpi_{10})^2\right)(\varpi_{10}-\Delta)^2\cos^2\Phi_0/8 \\ +\rho_0\left(\mu^2\rho_0 d c_1\sin\Phi_0 + (1-\Delta+\varpi_{10})^2(a_1+\mu d)\right)\cos\Phi_0/2 \\ -\rho_0 c_1\left(\mu^2(3/2-\varpi_{10}+\Delta)(1-\Delta+\varpi_{10})^2 - 2\rho_0^2\right)\sin\Phi_0/4 + \\ \mu\left(c_1\rho_0^2(\Delta-3-\varpi_0)+\mu(1-\Delta+\varpi_0)^3\right)(1-\Delta+\varpi_0)/4 + 2a_1 d\rho_0^2 \end{pmatrix}}{\rho_0^2\left(1-\mu^2 c_1\sin^2\Phi_0/4\right)};$$

$$g_3 = \frac{\mu^2 \left(\begin{array}{l} \frac{\mu c_1 \rho_0}{2}\left(1-\Delta+\varpi_{10}\right)^3 \cos^3\Phi_0 - \frac{a_1}{2}\left(1-\Delta+\varpi_{10}\right)\left(\left(1-\Delta+\varpi_{10}\right)^3 a_1 + 2\mu c_1 d\rho_0^2\right)\cos^2\Phi_0 \\ + \rho_0\left(1-\Delta+\varpi_{10}\right)^2\left(c_1 \sin\Phi_0/2 + a_1 d\right)\cos\Phi_0 + c_1 d\rho_0^3 \sin\Phi_0 + \\ \left(1-\Delta+\varpi_{10}\right)\left(\left(1-\Delta+\varpi_{10}\right)^3 a + 2\mu c_1 d\rho_0^2\right)/2 \end{array} \right)}{2\rho_0^2\left(1-\mu^2 c_1 \sin^2\Phi_0/4\right)}.$$

It should be noted that the characteristic polynomial coefficients are calculated with a somewhat inflated for the first-order approximation accuracy. In fact, it is easy to prove by series expansion in the small parameter μ. However, the coefficients in the truncated form are such that again lead to a transcendental equation. Therefore, the mathematical significance of such asymptotics is small enough. Now one traces the stability properties by finding the areas of system parameters when applying the Routh-Hurwitz criterion, which states the necessary and sufficient conditions of positivity of the following numbers $T_0 = g_0$, $T_1 = g_1$, $T_2 = g_1 g_3 - g_0 g_2$, $T_3 = T_2 g_3$. These conditions are violated along the amplitude–frequency curve when scanning the parameter between the points **A** and **C**. The characteristic points **A** and **B** originate from the traditional condition that the derivative of function approaches infinity. The point **C** appears due to the multiple and zero valued roots of the characteristic equation $p(\lambda) = 0$, as the determinants in the Routh-Hurwitz criterion approach zero, more precisely, $T_2 = 0$ (Fig. 2.2).

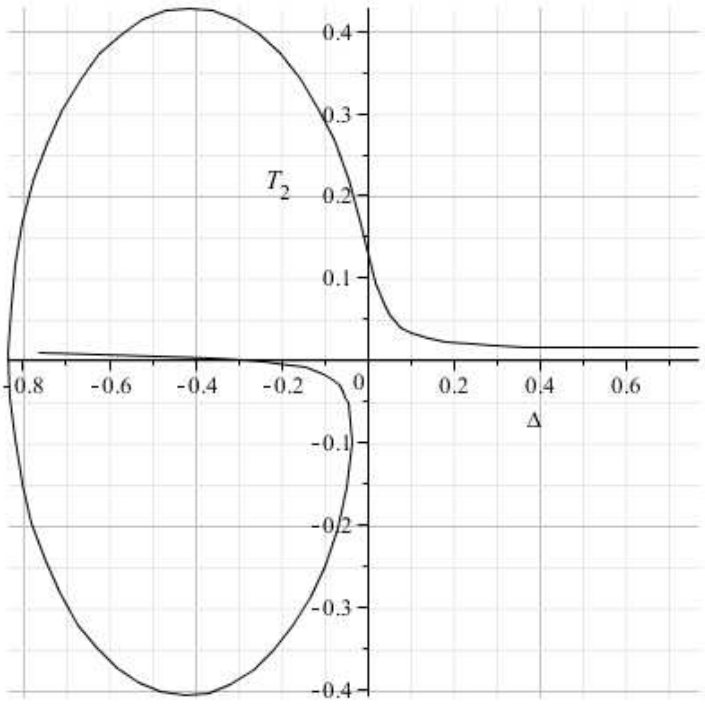

Fig. 2.2 The second determinant of the Routh-Hurwitz criterion versus detuning, $T_2(\Delta)$ ($\mu = 0.1$, $d = 0.03$, $a_1 = 1$, and $c_1 = 1$)

At the direct scanning of the parameter Δ together with increase in the angular velocity of the driver, one can observe a “tightening” of oscillations up to the point **A**. Then, the upper branch of the resonant curve becomes unstable and the stationary oscillations jump at the lower stable branch. At the reverse scan the angular velocity of the driver at the point **C**, in turn, there is a loss of stability of stationary oscillations at the lower branch and the jumping to stable oscillations with the greater amplitude at the upper branch of the resonance curve. The point **B**, apparently, is physically unrealizable mode of oscillations.

However, with the growth of the dissipation, the instability zone shrinks. Then the amplitude–frequency curve becomes unambiguous, and the instability zone is completely degenerated. In this case, the Sommerfeld effect also disappears.

Resume

Near the resonance, the rotor is substantially influenced by the pair of forces acting from the damped vibrating base. The average value of this moment is a positive defined value proportional to the amplitude of vibrations of the base. Therefore, near the resonance, some increase in the angular velocity of the driver is experienced, provided the damping is sufficiently small. This leads to the phenomenon of “pulling” hesitation, despite the fact that the elastic properties of the base are linear. Nonetheless, together with the growth of dissipation, the zone of the Sommerfeld instability narrows down to its complete disappearance. This leads to the idea of efficiency of utilizing vibration absorbers to stabilize the motion of electromechanical systems [26].

SYNCHRONIZATION

The phenomenon of the phase synchronization had being first physically described by Huygens and was intensively studied mathematically only since the mid twentieth century, in parallel with significant advances in electronics [27–29]. Fundamental results on the synchronization in terms of the qualitative theory of differential equations and bifurcation theory prove the resonance nature of this phenomenon [23, 30, 31]. Now, the application of this theory is widely used to solve pressing practical problems in a wide range of activity from microelectronics to power supply [18, 32–35]. Now the research interest in advanced fields of the synchronization theory is concentrated, apparently due to the rapid development of new technologies, on studying complex systems with chaotic dynamics, discrete objects and systems with time delay variables. However, in the traditional areas of human activity such as, for instance, energy and transport, there is also noticeable growth of attention in this phenomenon focused on the searching effective ways to save the energy and integrity of power units. Progressive developments in the scientific researches are constantly improving and expanding in our understanding over the synchronization phenomenon, as a consistent coherent dynamic process. This one occurs usually due to very small, almost imperceptible bonds between the individual elements of the system, which, nevertheless, cause a qualitative change in the dynamical behavior of the object.

The basic equation of the theory of phase synchronization of a pair of oscillators or rotators reads: $d\Psi / dT = \delta + Q\sin\Psi$, where δ is a small frequency (or angular velocity) detuning, Q is the depth of the phase modulation, T is temporal scale. This one being a very simple equation has the general solution in the following form

$$\Psi(T) = 2\arctan\left(\frac{1}{\delta}\left(\tan\left(\frac{T}{2}\sqrt{\delta^2 - Q^2} + \frac{C}{2}\sqrt{\delta^2 - Q^2}\right)\sqrt{\delta^2 - Q^2} - Q\right)\right)$$

where C is an arbitrary constant of integration. From this solution follows a simple stability criterion for the stable phase synchronization: $\delta^2 - Q^2 < 0$. It shows that the phase mismatch δ must be small or, accordingly, the parameter of modulation Q must be sufficiently large, otherwise the synchronization may be destroyed.

A more detailed mathematical study of this problem, referred to a two-rotor system based on an elastic foundation, turns out that the reduced model is incomplete. Namely, one draws somewhat surprising attention to that the model lacks any description of that element of the system which

provides the coupling between the rotors. More detailed studies lead to the following structure of the refined model:

$$\frac{d\rho}{dT} = (S - D)\rho; \quad \frac{d\Psi}{dT} = \delta + Q\sin\Psi + R\rho^2,$$

where $\rho = \rho(T)$ describes a measure of the amplitude of oscillations of the elastic foundation. This additional equation appears as a result of the phase modulation of the angular velocity of rotors due to the elastic vibrations of the base. So that, the perturbed rotors, in turn, cause the resonant excitation of vibrations of the base, described by the first equation. In the study of the refined model, one can explain that the stable synchronization requires the same condition: $\delta^2 - Q^2 < 0$. But, one more necessary condition is required; namely, the coefficient of the resonant excitation of vibrations of the base S should not exceed the rate of energy dissipation D, i.e., $S < D$. The last restriction significantly alters the stability region of the synchronization in the parameter space of the system that will be demonstrated by some specific computational examples.

Equations of motion

We consider the motion of two asynchronous drivers mounted on an elastic base. A mathematical model is presented by the following system of widely cited differential equations [34, 35], which may be considered as a generalization to Eq. (2.1):

$$\begin{aligned} &m\ddot{\eta} + p\eta + 2q\dot{\eta} - m_1 r_1\left(\ddot{\varphi}_1\sin\varphi_1 + \dot{\varphi}_1^{\,2}\cos\varphi_1\right) - m_2 r_2\left(\ddot{\varphi}_2\sin\varphi_2 + \dot{\varphi}_2^{\,2}\cos\varphi_2\right) = 0; \\ &I_1\ddot{\varphi}_1 + H_1(\varphi_1,\dot{\varphi}_1) - L_1(\varphi_1,\dot{\varphi}_1) - m_1 r_1\ddot{\eta}\sin\varphi_1 = 0; \\ &I_2\ddot{\varphi}_2 + H_2(\varphi_2,\dot{\varphi}_2) - L_2(\varphi_2,\dot{\varphi}_2) - m_2 r_2\ddot{\eta}\sin\varphi_2 = 0, \end{aligned} \qquad (3.1)$$

where m is the mass of the base, modeled as a rigid body with one degree of freedom, characterized by a linear horizontal displacement η; p is the coefficient of elasticity of the platform; q is the damping coefficient, mi are the small masses of eccentrics with the eccentricities r_i (radii of inertia); J_i are the moments of inertia of rotors in the absence of imbalance; $H_i(\varphi_1,\dot{\varphi}_1)$ stands for the driving moments; $L_i(\varphi_1,\dot{\varphi}_1)$ denotes the resistance moment of the rotor ($i = 1, 2$). The angles of rotation of the rotors φ_i are measured from the direction of their axis counterclockwise. Assume that the moment characteristics of each driver and torque resistance have, as previously, a simplest form, i.e., $H_i(\varphi_i,\dot{\varphi}_i) = M_i - k_i\dot{\varphi}_i$, $L_i(\varphi_i,\dot{\varphi}_i) = k_{0i}\dot{\varphi}_i$. Here, M_i are the constant parameters, respective for the starting points, k_i and k_{0i} stand for the drag coefficients of the rotors. Respectively, the subscript “1” refers to the first driver while “2” to the second one. If

we allow for such a simple linear model of the moments of static characteristics of the drivers, then the dimensionless form of Eq. (3.1) can be rewritten such as it follows:

$$\begin{aligned}
&\ddot{x}+x+2\mu d\dot{x}-\mu\kappa_1\left(\ddot{\varphi}_1\sin\varphi_1+\dot{\varphi}_1^{\,2}\cos\varphi_1\right)-\mu\kappa_2\left(\ddot{\varphi}_2\sin\varphi_2+\dot{\varphi}_2^{\,2}\cos\varphi_2\right)=0;\\
&\ddot{\varphi}_1+a_1\dot{\varphi}_1-b_1-\mu\kappa_1 c_1\ddot{x}\sin\varphi_1=0;\\
&\ddot{\varphi}_2+a_2\dot{\varphi}_2-b_2-\mu\kappa_2 c_2\ddot{x}\sin\varphi_2=0,
\end{aligned}\qquad (3.2)$$

where μ appears in the role of a small parameter of the problem. The parameters κ_1 and κ_2 are of order of unity such that $\mu_1=\mu\kappa_1$ and $\mu_2=\mu\kappa_2$, where $\mu_i=2m_i r_i/(m_1+m_2)$. We introduce new notations: $a_i=(k_{0i}+k_i)/J_1\omega_0$, $b_i=M_i/J_i\omega_0^2$, $c_i=m(r_1+r_2)/4J_i$ $(i=1,2)$. Here, $\omega_0=\sqrt{p/m}$ is the oscillation frequency of the base in the absence of the devices, $d=(r_1+r_2)\omega_0 q/(m_1+m_2)$ is the dimensionless damping coefficient, x is the new dimensionless linear coordinate measured in fractions of the radius of inertia of the eccentrics. The set (3.2), in contrast to the original equations, depends now on the dimensionless time $\tau=\omega_0 t$.

The problem (3.2) admits an effective study by the method of a small parameter. In order to explore this one, we should transform the system (3.2) to a standard form of the six equations resolved for the first derivatives. The intermediate steps of this procedure are the follows ones. Firstly, we introduce the new variables y, ϖ_1, ϖ_2, associated with the initial dependent variables by differential relations: $\dot{x}=y$, $\dot{\varphi}_1=\varpi_1$, $\dot{\varphi}_2=\varpi_2$. Assume that $\mu=0$ in the set (3.2). Then one defines the transform to the new dependent variables based on the method of varied constants: $\varphi(\tau)=\tau+\alpha(\tau)$, $\varpi_1(\tau)=\nu_1(\tau)\exp(-a_1\tau)$, $\varpi_2(\tau)=\nu_2(\tau)\exp(-a_2\tau)$, $\varphi_1(\tau)=\Omega_1\tau+\beta_1(\tau)$, $\varphi_2(\tau)=\Omega_2\tau+\beta_2(\tau)$, where $x(\tau)=\rho(\tau)\sin\phi(\tau)$ and $y(\tau)=\rho(\tau)\cos\phi(\tau)$, Ω_1 and Ω_2 are the partial angular velocities of devices. Here, $\rho(\tau)$, $\alpha(\tau)$, $\nu_1(\tau)$, $\nu_2(\tau)$, $\beta_1(\tau)$, $\beta_2(\tau)$ are the six new variables of the problem.

The sense of these new variables is following: $\rho(\tau)$, $\alpha(\tau)$ are the amplitude and phase of base oscillations, respectively, $\beta_1(\tau)$, $\beta_2(\tau)$ are the angles and $\nu_1(\tau)$, $\nu_2(\tau)$ are the angular velocities of the rotors. The standard form suitable for further analysis is ready. Because of large records, this standard form is not given, but the interested reader can trace in detail the stages of its derivation [36]. Solution of the system in a standard form is solved as transform series in the small parameter:

$$
\begin{aligned}
&\rho(\tau) \to \rho(T_1, T_2, ...) + \mu\rho^{(1)}(\tau) + \mu^2\rho^{(2)}(\tau) + ...;\\
&\alpha(\tau) \to \alpha(T_1, T_2, ...) + \mu\alpha^{(1)}(\tau) + \mu^2\alpha^{(2)}(\tau) + ...;\\
&\nu_1(\tau) \to \nu_1(T_1, T_2, ...) + \mu\nu_1^{(1)}(\tau) + \mu^2\nu_1^{(2)}(\tau) + ...;\\
&\nu_2(\tau) \to \nu_2(T_1, T_2, ...) + \mu\nu_2^{(1)}(\tau) + \mu^2\nu_2^{(2)}(\tau) + ...;\\
&\beta_1(\tau) \to \beta_1(T_1, T_2, ...) + \mu\beta_1^{(1)}(\tau) + \mu^2\beta_1^{(2)}(\tau) + ...;\\
&\beta_2(\tau) \to \beta_2(T_1, T_2, ...) + \mu\beta_2^{(1)}(\tau) + \mu^2\beta_2^{(2)}(\tau) + ...
\end{aligned}
\qquad (3.3)
$$

Here the kernel expansion depends upon the slow temporal scales $T_n = \mu^n\tau$, which characterize the evolution of resonant processes. The variables with superscripts denote small rapidly oscillating correction to the basic evolutionary solution.

Then it is necessary to identify the resonant conditions in the standard form. The resonance in the system (3.2) occurs within the first-order nonlinear approximation theory, when $\Omega_1 \sim 1$ or when $\Omega_2 \sim 1$ or if the both parameters Ω_2 and Ω_2 are close to unity. All these cases require a separate study. Now we are interested in the phenomenon of the phase synchronization in the system (3.2). This case, in particular, is realized at $\Omega_2 \sim \Omega_1 \neq 1$, though the both partial angular velocities should be sufficiently far and less than unity, in order to overcome the instability predicted by the Sommefeld effect, since the first-order approximation resonance is absent in the system (3.2) in this case. Such a kind of resonance is manifested in the second approximation only.

In addition to the resonance associated with the standard phase synchronization in the system (3.2) there is one more resonance, when $2 - \Omega_1 - \Omega_2 \sim 0$, which apparently has no practical significance, since its angular velocities fall in the zone of instability.

Note that other resonances in the system (3.2) are absent within the first-order nonlinear approximation theory. The next section investigates these cases are in detail.

Matching condition $\Omega_2 - \Omega_1 \sim 0$

After the substitution the expressions (3.3) into the standard form of equations and the separation between fast and slow motions within the first-order nonlinear approximation theory in small parameter μ one obtains the following information on the solution of the system. In the first approximation theory, the slow steady-state motions (when $\tau \to \infty$) are the same as in the linearized set, i.e., $\rho = \text{const}$, $\alpha = \text{const}; \nu_1 = \text{const}$, $\nu_2 = \text{const}; \beta_1 = \text{const}; \beta_2 = \text{const}$. This means that the slowly varying generalized coordinates ρ, α, ν_1 and ν_2, β_1 и β_2 do not depend within the first approximation analysis upon the physical time τ nor the slow time T_1. Solutions

to the small nonresonant corrections appear as it follows: namely, there are small additions to the amplitude and phase of the elastic base:

$$\rho^{(1)}(\tau)=-\frac{\mu}{2A}\left(\begin{array}{l}-\dfrac{\kappa_2\Omega_2^2\cos\left((\Omega_2-1)\tau+\varphi_2-\alpha-\dfrac{\Omega_2}{a_2}\right)}{\Omega_2-1}+\dfrac{\kappa_1\Omega_1^2\cos\left((\Omega_1+1)\tau+\varphi_1+\alpha-\dfrac{\Omega_1}{a_1}\right)}{\Omega_1+1}+\\ +\dfrac{\kappa_2\Omega_2^2\cos\left((\Omega_2+1)\tau+\varphi_2+\alpha-\dfrac{\Omega_2}{a_2}\right)}{\Omega_1+1}+\dfrac{\kappa_1\Omega_1^2\cos\left((\Omega_1-1)\tau+\varphi_1-\alpha-\dfrac{\Omega_1}{a_1}\right)}{\Omega_2-1}\end{array}\right);$$

$$\alpha^{(1)}(\tau)=-\frac{\mu}{2}\left(\begin{array}{l}\dfrac{\kappa_2\Omega_2^2\sin\left((\Omega_2-1)\tau+\varphi_2-\alpha-\dfrac{\Omega_2}{a_2}\right)}{\Omega_2-1}+\dfrac{\kappa_1\Omega_1^2\sin\left((\Omega_1+1)\tau+\varphi_1+\alpha-\dfrac{\Omega_1}{a_1}\right)}{\Omega_1+1}+\\ +\dfrac{\kappa_2\Omega_2^2\sin\left((\Omega_2+1)\tau+\varphi_2+\alpha-\dfrac{\Omega_2}{a_2}\right)}{\Omega_1+1}-\dfrac{\kappa_1\Omega_1^2\sin\left((\Omega_1-1)\tau+\varphi_1-\alpha-\dfrac{\Omega_1}{a_1}\right)}{\Omega_2-1}\end{array}\right),$$

(3.4)

additions to the angles of rotation of rotors:

$$\beta_1^{(1)}(\tau)=\frac{\mu c_1\kappa_1}{2a_1}\left(-\frac{\sin\left((\Omega_1-1)\tau+\varphi_1-\alpha-\dfrac{\Omega_1}{a_1}\right)}{\Omega_1-1}+\frac{\sin\left((\Omega_2+1)\tau+\varphi_2+\alpha-\dfrac{\Omega_2}{a_2}\right)}{\Omega_2+1}\right);$$

$$\beta_2^{(1)}(\tau)=\frac{\mu c_2\kappa_2}{2a_2}\left(-\frac{\sin\left((\Omega_2-1)\tau+\varphi_2-\alpha-\dfrac{\Omega_2}{a_2}\right)}{\Omega_2-1}+\frac{\sin\left((\Omega_1+1)\tau+\varphi_1+\alpha-\dfrac{\Omega_1}{a_1}\right)}{\Omega_1+1}\right),$$

(3.5)

and those to the angular velocities, as well:

$$v_1^{(1)}(\tau)=\frac{\mu c_1\kappa_1 A}{2\left(a_1^2+(1+\Omega_1)^2\right)\left(a_1^2+(1-\Omega_1)^2\right)}\left(\begin{array}{l}(\Omega_1-1)\left(a_1^2+(1+\Omega_1)^2\right)\sin\left((\Omega_1-1)\tau+\varphi_1-\alpha-\frac{\Omega_1}{a_1}\right)+\\+a_1\left(a_1^2+(1+\Omega_1)^2\right)\cos\left((\Omega_1-1)\tau+\varphi_1-\alpha-\frac{\Omega_1}{a_1}\right)-\\-\left((1+\Omega_1)\sin\left((\Omega_1+1)\tau+\varphi_1+\alpha-\frac{\Omega_1}{a_1}\right)\right)+\\+a_1\left(a_1^2+(1-\Omega_1)^2\right)\cos\left((\Omega_1+1)\tau+\varphi_1+\alpha-\frac{\Omega_1}{a_1}\right)\end{array}\right);$$

$$v_2^{(1)}(\tau)=\frac{\mu c_2\kappa_2 A}{2\left(a_2^2+(1+\Omega_2)^2\right)\left(a_2^2+(1-\Omega_2)^2\right)}\left(\begin{array}{l}(\Omega_2-1)\left(a_2^2+(1+\Omega_2)^2\right)\sin\left((\Omega_2-1)\tau+\varphi_2-\alpha-\frac{\Omega_2}{a_2}\right)+\\+a_2\left(a_2^2+(1+\Omega_2)^2\right)\cos\left((\Omega_2-1)\tau+\varphi_2-\alpha-\frac{\Omega_2}{a_2}\right)-\\-\left((1+\Omega_2)\sin\left((\Omega_2+1)\tau+\varphi_2+\alpha-\frac{\Omega_2}{a_2}\right)\right)+\\+a_2\left(a_2^2+(1-\Omega_2)^2\right)\cos\left((\Omega_2+1)\tau+\varphi_2+\alpha-\frac{\Omega_2}{a_2}\right)\end{array}\right).$$

(3.6)

This solution describes a slightly perturbed motion of the base with the same frequencies as the angular velocities of rotors that is manifested in the appearance of combination frequencies in the expression for the corrections to the amplitude and phase (3.4). Corrections to the angles (3.5) and velocities (3.6) also contain the similar small-amplitude combination harmonics at the difference and sum.

Now the solution of the first-order approximation is ready. This one is not suitable for describing the synchronization effect and call to continue further manipulations with the equations along the small-parameter method. Using the solution (3.4–3.6), after the substitution into the standard form, with the help of expressions (3.3), one obtains the desired equation of the second-order nonlinear approximation, describing the synchronization phenomenon of a pair of drivers on the elastic foundation. So that after the second substitution of the modified representation (3.3) in the standard form and the separation of motions into slow and fast ones, we obtain the following evolution equations

$$\begin{aligned}\frac{d\rho}{dT_2} &= (S-D)\rho - P(\Omega_1-\Omega_2)\frac{\sin\Psi}{\rho};\\ \frac{d\Psi}{dT_2} &= \delta + Q\sin\Psi + R\rho^2,\end{aligned} \tag{3.7}$$

where $\Psi(T_2)=\varphi_1(T_2)-\varphi_2(T_2)-\Delta T_2+\Omega_2/a_2-\Omega_1/a_1$ is the new slow variable; $\Delta=\Omega_1-\Omega_2$ denotes the small detuning of the partial angular velocities ($\delta=(\Omega_1-\Omega_2)/\mu^2$); $D=d/\mu^2$ is the rate of energy dissipation. The coefficients of Eq. (3.7) are following:

$$S=\frac{a_1c_1\kappa_1^2\left(3\Omega_1^2+a_1^2+1\right)}{4\left(\Omega_2^2-1\right)\left(a_2^2+(1-\Omega_2)^2\right)\left(a_2^2+(1+\Omega_2)^2\right)}+\frac{a_2c_2\kappa_2^2\left(3\Omega_2^2+a_2^2+1\right)}{4\left(\Omega_1^2-1\right)\left(a_1^2+(1-\Omega_1)^2\right)\left(a_1^2+(1+\Omega_1)^2\right)};$$

$$P=\frac{\kappa_1\kappa_2\Omega_1^2\Omega_2^2\left(1+\Omega_1\Omega_2\right)}{4\left(1-\Omega_1^2\right)\left(1-\Omega_2^2\right)};$$

$$Q=\frac{\kappa_1\kappa_2}{2}\left[\frac{c_1}{a_1}\left(\frac{\Omega_2^2\left(\Omega_2^2-2\right)}{1-\Omega_2^2}\right)+\frac{c_2}{a_2}\left(\frac{\Omega_1^2\left(\Omega_1^2-2\right)}{1-\Omega_1^2}\right)\right];$$

$$R=\frac{c_2^2\kappa_2^2\Omega_2\left(\Omega_2^2+a_2^2+3\right)}{4\left(\Omega_2^2-1\right)\left(a_2^2+(1-\Omega_2)^2\right)\left(a_2^2+(1+\Omega_2)^2\right)}-\frac{c_1^2\kappa_1^2\Omega_1\left(\Omega_1^2+a_1^2+3\right)}{4\left(\Omega_1^2-1\right)\left(a_1^2+(1-\Omega_1)^2\right)\left(a_1^2+(1+\Omega_1)^2\right)}.$$

Let the detuning be zero, then these equations are highly simplified up to the full their separation:

$$\frac{d\rho}{dT_2}=(S-D)\rho;\quad \frac{d\Psi}{dT_2}=Q\sin\Psi+R\rho^2. \tag{3.8}$$

Equations (3.7) represent a generalization of the standard basic equations of the theory of phase synchronization [37], whose structure reads

$$\frac{d\Psi}{dT_2}=\delta+Q\sin\Psi$$

Formally, this equation follows from the generalized model (3.7), if we put ρ = 0, then the general solution has the form

$$\psi(T_2)=2\arctan\left(\frac{1}{\delta}\left(\tan\left(\frac{T_2}{2}\sqrt{\delta^2-Q^2}+\frac{C}{2}\sqrt{\delta^2-Q^2}\right)\sqrt{\delta^2-Q^2}-Q\right)\right),$$

where C is an arbitrary constant of integration. This solution implies the criterion of the stable phase synchronization:

$$\delta^2 - Q^2 < 0 \qquad (3.9)$$

which indicates that in the occurrence of the stable synchronization the phase detuning must be small enough, compared with the phase modulation parameter. If this condition is not satisfied, then the system can leave the zone of synchronization.

On the other hand, the refined model (3.7) says that for the stable synchronization the performance of the above conditions (3.9) is not enough. It is also necessary condition that the coefficient of the resonant excitation S of vibrations in the base should not exceed the rate of energy dissipation D, i.e., $S < D$. The last restriction significantly alters the stability zone of synchronization in the space system parameters that is demonstrated here on the specific computational examples.

Table 3.1 Parameters of stable and unstable regimes of synchronization

	μ	c_1	c_2	κ_1	κ_2	a_1	a_2	Ω_1	Ω_2	$\Delta^2 - Q^2$	S
1	0.1	1	1	0.5	0.5	1	1	0.751	0.75	-0.244	-0.204
2	0.1	1	1	0.5	0.5	1	1	0.251	0.25	-0.072	0.008
3	0.1	1	1	0.6	0.4	1	1	0.25	0.25	-0.075	-0.001
4	0.1	1	1	0.6	0.4	1	1	0.251	0.25	-0.075	0.009
5	0.1	1	1	0.6	0.4	1	1	1.25	1.25	0.239	-0.085
6	0.1	1	1	0.5	0.5	1	1	0.26	0.25	0.998	-0.007

Examples of stable and unstable regimes of synchronization

The table shows the calculation of the different theoretical implementations of stable and unstable regimes of the phase synchronization (Table 3.1). The example 1 (see the first line in the table) demonstrates a robust synchronization with a small mismatch between the angular velocities of drivers, $\delta = 0.1$. The example 2 (see, respectively, the second line in the table, etc.) displays an unstable phase-synchronization regime at the same small difference between the angular velocities, i.e., $\delta = 0.1$. One can reach a stable steady-state synchronization pattern in this example by adding a damping element with the coefficient $D \geq 0.008$. The example number 3 is a robust synchronization for the small differences in eccentrics ($\kappa_1 - \kappa_2 = 0.2$) and equal angular velocities. The example number 4 is an unstable synchronization mode with the same small differences in eccentrics ($\kappa_1 - \kappa_2 = 0.2$) and small mismatch in angular velocities, i.e., $\delta = 0.1$. One can reach a stable regime in this example by adding a dissipative element with the damping coeffi-

cient $D \geq 0.009$. The example number 5 is an unstable synchronization regime. One cannot reach any stable synchronization regime in this example, it is impossible, even when adding any damping element. The example number 6 is an unstable regime of synchronization at different angular speeds. It is also impossible to achieve any sustainable sync mode in this case.

Matching condition $2-\Omega_1-\Omega_2 \sim 0$

After substitution from the expressions (3.3) into the standard form of Eq. (3.2), separation of fast and slow motions within the second-order approximation in the small parameter μ, under the assumption that $2-\Omega_1-\Omega_2 \approx 0$, one obtains the following evolutionary equations

$$\frac{d\rho}{dT_2}=(S-D)\rho-P(2-\Omega_1-\Omega_2)\frac{\sin\Psi}{4\rho};\quad \frac{d\Psi}{dT_2}=Q+\delta-P(2-\Omega_1-\Omega_2)\frac{\cos\Psi}{\rho^2}-R\rho^2. \qquad (3.10)$$

where $\Psi(T_2)=\varphi_1(T_2)+\varphi_2(T_2)-2\alpha(T_2)-\Delta T_2-\Omega_1/a_1-\Omega_2/a_2$ is the new slow variable ($\Delta=2-\Omega_1-\Omega_2$); $\delta=(2-\Omega_1-\Omega_2)/\mu^2$ is the small detuning. The coefficients of Eq. (3.10) are as it follows:

$$S=\frac{a_1c_1\kappa_1^2\left(3\Omega_1^2+a_1^2+1\right)}{4(1-\Omega_1)^2\left(a_1^2+(1-\Omega_1)^2\right)\left(a_1^2+(1+\Omega_1)^2\right)}+\frac{a_2c_2\kappa_2^2\left(3\Omega_2^2+a_2^2+1\right)}{4(1-\Omega_3)^2\left(a_2^2+(1-\Omega_2)^2\right)\left(a_2^2+(1+\Omega_2)^2\right)};$$

$$P=\frac{\kappa_1\kappa_2\Omega_1^2\Omega_2^2}{2(1-\Omega_1)(1-\Omega_2)};$$

$$Q=\frac{\left(\Omega_1^4+\left(2a_1^2-\frac{5}{2}\right)\Omega_1^2+a_1^4+\frac{3}{2}a_1^2+\frac{1}{2}\right)c_1\kappa_1^2}{\left(a_1^2+(1-\Omega_1)^2\right)\left(a_1^2+(1+\Omega_1)^2\right)}+\frac{\left(\Omega_2^4+\left(2a_2^2-\frac{5}{2}\right)\Omega_2^2+a_2^4+\frac{3}{2}a_2^2+\frac{1}{2}\right)c_2\kappa_2^2}{\left(a_2^2+(1-\Omega_2)^2\right)\left(a_2^2+(1+\Omega_2)^2\right)};$$

$$R=\frac{c_1^2\kappa_1^2\Omega_1\left(\Omega_1^2+a_1^2+3\right)}{4(1-\Omega_1)^2\left(a_1^2+(1-\Omega_1)^2\right)\left(a_1^2+(1+\Omega_1)^2\right)}+\frac{c_2^2\kappa_2^2\Omega_2\left(\Omega_2^2+a_2^2+3\right)}{4(1-\Omega_3)^2\left(a_2^2+(1-\Omega_2)^2\right)\left(a_2^2+(1+\Omega_2)^2\right)}.$$

The resonance of this type, as already mentioned, has no practical significance. Let the detuning be zero, then these Eq. (3.10) are highly simplified up to the full their separation:

$$\frac{d\rho}{dT_2}=(S-D)\rho;\quad \frac{d\Psi}{dT_2}=Q-R\rho^2.$$

The formal criterion of stability is extremely simple. Namely, the coefficient of the resonant excitation of vibrations in the base S exceeds no the rate of energy dissipation D, i.e. $S<D$, but the synchronization is awfully destroyed at any positive values of other parameters.

Resume

Synchronous rotations of drivers are almost idle and required no any high-powered energy set in this dynamical mode. Most responsible treatment for the drivers is their start, i.e., a transition from the rest to steady-state rotations [38]. So that, the utilizing vibration absorbers for high-powered electromechanical systems has advantageous for the two main reasons. On the one hand, it provides a control tool for substantially mitigating the effects of transient shocking loads during the time of growth the acceleration of drivers. This contributes to integrities of the electromechanical system and save energy. On the other hand, there is an ability to configure the appropriate damping properties of vibration absorbers to create a stable regime of synchronization when it is profitable, or even get rid of him, to destroy the synchronous movement, creating conditions for a dynamic interchange of drivers.

THERMO-MECHANICAL INSTABILITY IN VIBRATION ABSORBERS

We analyze a problem of the thermo-mechanical instability caused by small changes of a viscous damping in vibration absorbers. The nonlinear coupling between the oscillations and temperature takes place due to a linear thermal dependence of the coefficient of energy dissipation. This provides typical phase– amplitude frequency patterns inherent in unstable regimes. While the damping coefficient decreases with the increase in the temperature, the effect of bifurcated oscillations can be exhibited brightly as some abnormal operating regimes. The vibration absorber appears as a complex dynamical system, behaving strongly upon the ambient temperature. Typical thermo-mechanical instability patterns are traced in detail within a parametric analysis along an approach closed to the Lie method. This study would explain some unwanted dynamical effects accompanying the utilizing of vibration absorbers.

On the one hand, dynamic tests can exhibit abnormal operating regimes accompanied with some overheating of a fluid contained in vibration absorbers. As a result, the amplitude of oscillation can increase dangerously. While on the other hand, the functioning may be quite satisfactory even under almost the same experimental conditions. From a physical viewpoint, it is obvious that the overheating causes a decrease in the fluid viscosity, so that the amplitude of oscillations increases, and then, the efficiency of the set is reduced. These specified abnormal operating regimes require some theoretical explanation. The present study is an attempt along this way. Equations governing the motion of a spring pendulum possessing a sufficiently large coefficient of energy dissipation play the role of the simplified mathematical model of the vibration absorber. It is assumed that the coefficient of energy dissipation depends upon the ambient temperature. Simple temperature dependence between the energy dissipation and temperature characteristics is proposed as a linear function with a small slope, which enter both into the heat balance equation and that describing mechanical vibrations. The equations of the mathematical model are investigated using a small-parameter method under the assumption that the external harmonic excitation is moderate so that it cannot cause significant large-amplitude nonlinear oscillations. The thermal dependence of the dissipative function is assumed to be small, as well. The study of steady-state oscillatory modes reveals dynamic processes treated as dangerous from a viewpoint of the operation of vibration absorbers. These are explicable in terms of the thermo-mechanical instability of a dynamical system near the resonance.

A physical picture of dynamic processes in the vibration absorber is very simple. A drop in the viscosity leads to some increase in the amplitude, which contributes to some additional heat portion. This heat causes some decrease in the viscosity, so that the heat injection should be reduced. It is clear that such a process should be saturated and would approach some stationary state. However, the system under consideration, being nonlinear, has hysteretic steady-state regimes of motion, which can lead to dangerous oscillations even being far from the resonant frequency. Such a situation is modeled by specific examples within a parametric analysis performed to identify the most impact oscillatory patterns. These should help understanding how to use these properties in practice when we investigate a complex technical system, which meets both the electromechanical [1] and thermo-mechanical phenomena, as a rule.

Problems of the thermo-mechanical stability are of interest for researchers both on traditional and new areas. For example, the problems of ultrasonic techniques [39], phase transitions in austenite microstructures [40], the dynamics of materials with memory [41], oscillations in electromechanical systems [42] call some adequate description between the thermal and mechanical effects. Questions of the thermo-mechanical stability in the light of the vibration absorbers have not been methodically studied, being usually restricted by most researchers to some purely mechanical models [43, 44]. The present study represents an attempt to draw readers' attention to this subject, especially supposing high perspectives in magneto-rheological materials [45] combined with active control techniques to provide high effective solutions in a problem of reducing the vibrations in mechanical structures.

A hydraulic vibration absorber contains the working and compensation chambers with a viscous liquid. The elastic properties of the hydraulic absorber are formed by the conical shell-shaped elastomer wall and membrane. A damping of vibrations inside the absorber is due to the dissipation of energy of turbulent fluid flowing to and fro in the chambers through the bypass channels (Fig. 4.1). These turbulent flows can lead to the cavitation phenomenon at sufficiently large external loads. It is believed that the cavitation plays the principal role in seal failures of hydraulic absorbers [46]. Though, this fact can obtain some different explanation.

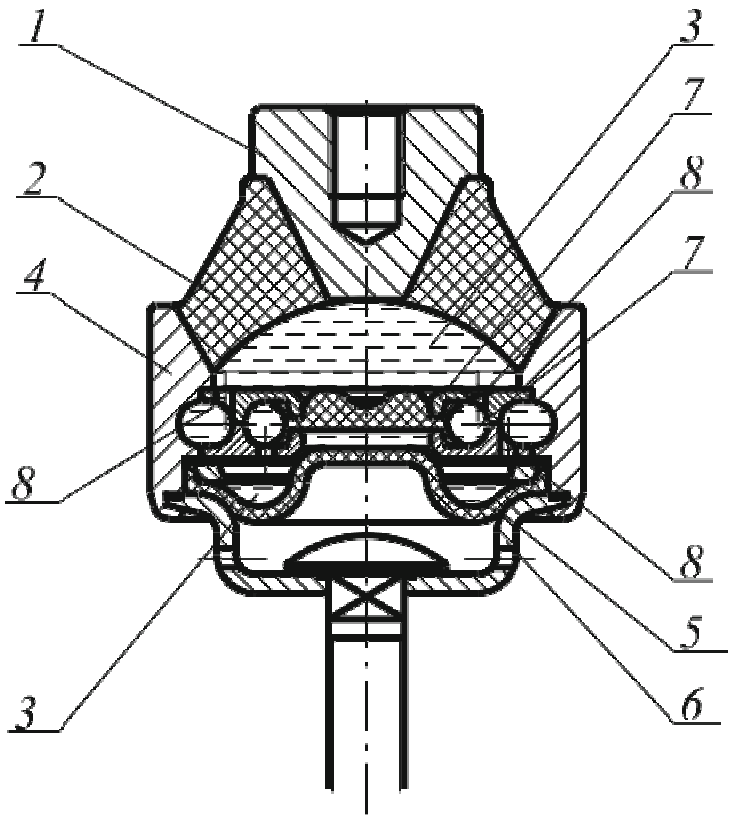

Fig. 4.1 A hydraulic absorber: 1 – support plate, 2 – conical shell-shaped elastomer wall, 3 – liquid chambers, 4 – bearing, 5 – elastic membrane, 6 – pallet, 7 – bulkhead, 8 – throttle channels [46]

During the collapse of cavities in a liquid, shock waves can be generated at the ultrasonic frequencies. The thermodynamics of these waves is non-trivial enough. The collapse of cavities can be accompanied by an adiabatic expansion and cooling of the surrounding liquid in a small neighborhood of the lost cavern, but the temperature can dramatically increase in the center. Although, the total liquid bulk is heated slowly, but steadily, like during an ultrasonic washing. Apparently, this thermal effect is not so significant in terms of the correct functioning of hydraulic absorbers.

However, the shock waves contribute to the erosion of solid surfaces of the structure. The liquid is enriched with a suspension of very small solid particles. The viscosity of this emulsion drops due to the temperature rise, the heat capacity is reduced, but the thermal conductivity increases. The increase in the temperature reduces cavitation risks [47]. But under the resonant excitation of the system at a critical value of viscosity, the temperature rise within the liquid may cause large-amplitude oscillations that can lead to seal failures in the hydraulic absorbers. The present study would show that such processes can really take place.

We trace the influence of temperature effects upon the amplitude–frequency dependence describing the steady-state oscillations in vibration absorbers. The equations governing motion are based on the most basic general physical considerations, which are briefly mentioned in the introduction:

$$\begin{aligned}
&\dot{x} = y;\\
&m\dot{y} + 2\delta(1-\alpha T)y + c(1+\beta x)x = -(P + \mu p\sin\omega t);\\
&CV\dot{T} = 2\delta(1-\alpha T)y^2 - VG(T - T_0),
\end{aligned}$$

where the reduced coefficients of the vibration absorber are following: m is the mass; δ is the damping coefficient c is the coefficient of elasticity; α is the thermal coefficient of viscosity; β is the coefficient of elasticity, which characterizes an asymmetry of deformations; V stands for the volume; P denotes the static load; p is the maximal value of the external harmonic force at the frequency ω; μ is the small dimensionless parameter. These equations, making allowances for the thermal balance, are also characterized by the following parameters: C is the heat capacity; G is the thermal conductivity; $x(t)$ denotes the displacement; $T(t)$ stands for the temperature and T_0 is the ambient temperature. We determinate the static deformation under the static load: $\Delta = -c + \sqrt{c^2 - 4\beta P}/2c\beta$, and the natural frequency of oscillation in the absence of energy dissipation, $\varpi = \sqrt{\sqrt{(c^2 - 4\beta P)}/m}$. Then, the following dimensionless variables are introduced:

$$\tau = \varpi t;\ X(\tau) = \frac{-2x(t)c\beta - c + \sqrt{c^2 - 4\beta P}}{\mu l c\beta};\ Y(\tau) = y(t)/\mu l\varpi;\ \lambda(\tau) = \frac{T(t) - T_0}{\mu T_0}.$$

Here $l = \sqrt[3]{V}$ is the characteristic length scale. The equations of motion in these dimensionless variables can be rewritten as

$$\begin{aligned}
&\dot{X} = Y;\\
&\dot{Y} + X + \frac{2\delta}{m\varpi}(1-\alpha T_0)Y + \frac{p}{ml\varpi^2}\sin\left(\frac{\omega t}{\varpi}\right) = -\mu\frac{\left(c\beta l^2 X^2 - 2\alpha T_0\delta l\varpi Y\lambda\right)}{ml\varpi^2};\\
&\dot{\lambda} + \frac{G}{C\varpi}\lambda = \mu\frac{2\delta l^2\varpi^2(1-\alpha T_0)}{CV\varpi T_0}Y^2.
\end{aligned} \qquad (4.1)$$

Upper dots denote a differentiation with respect to the dimensionless time τ. The general solution to the linear subset (4.1), as $\mu \to 0$, is given by the expressions

$$X(\tau)=A\exp\left(\frac{-\delta(1-\alpha T_0)+im\Omega}{m\varpi}\right)\tau+\overline{A}\exp\left(\frac{-\delta(1-\alpha T_0)-im\Omega}{m\varpi}\right)\tau$$

$$+\frac{p}{l}\frac{\left(2\delta\omega(1-\alpha T_0)\cos\left(\frac{\omega\tau}{\varpi}\right)+(\omega^2-\varpi^2)m\sin\left(\frac{\omega\tau}{\varpi}\right)\right)}{m^2(\omega^4+\varpi^4)+4\omega^2\left(\delta^2(1-\alpha T_0)^2-\frac{m^2\varpi^2}{2}\right)};\qquad(4.2)$$

$$Y(\tau)=\dot{X}(\tau);\quad \lambda(\tau)=B\exp\left(-\frac{G\tau}{C\varpi}\right).$$

Here, A is an arbitrary complex constant ($\overline{A}$ corresponds to the complex conjugate); B is a real arbitrary constant; $\Omega=\sqrt{m^2\varpi^2-\delta^2(1-\alpha T_0)^2}/m$ denotes the resonant frequency at which the linear system reaches the amplitude peak at the same frequency of the external excitation.

Evolution equations

To construct the first-order nonlinear approximation asymptotic solution as series in the small parameter μ, the paradigm of the method of arbitrary constant variations is used:

$$\begin{aligned}
&X(\tau)=A(\tau)\exp\phi(\tau)+\overline{A}(\tau)\exp\overline{\phi}(\tau)+u_0(\tau)+\mu u_1(\tau);\\
&Y(\tau)=\dot{\phi}(\tau)A(\tau)\exp\phi(\tau)+\dot{\overline{\phi}}(\tau)\overline{A}(\tau)\exp\overline{\phi}(\tau)+v_0(\tau)+\mu v_1(\tau);\\
&\lambda(\tau)=B(\tau)\exp(-G\tau/C\varpi)+w_0(\tau)+\mu w_1(\tau).
\end{aligned}\qquad(4.3)$$

Here $\phi(\tau)=-(\delta(1-\alpha T_0)/m\varpi+i\Omega/\varpi)\tau$ is the phase ($\overline{\phi}(\tau)$ denotes the complex conjugate). All old constants are now varying at the time: $A=A(\tau)$, $\overline{A}=\overline{A}(\tau)$, $B=B(\tau)$; the functions $u_j(\tau)$, $v_j(\tau)$, $w_j(\tau)$ ($j=0,1$) represent the so-called nonresonant corrections. The order is determined by the index j which should be fully compatible with a standard expansion of the sought function as series in μ. The nonresonant corrections are introduced to construct an asymptotic solution by an appropriate recursive method, due to the smallness of the parameter μ.

The polar coordinates, $a(\tau)$ and $\varphi(\tau)$, are introduced:

$$\begin{aligned}
&A(\tau)=a(\tau)\exp i\varphi(\tau)\exp\left(\frac{-\delta(1-\alpha T_0)\tau}{m\varpi}\right);\\
&\overline{A}(\tau)=a(\tau)\exp(-i\varphi(\tau))\exp\left(\frac{-\delta(1-\alpha T_0)\tau}{m\varpi}\right);\\
&B(\tau)=\Theta(\tau)\exp(G\tau/C\varpi)
\end{aligned}\qquad(4.4)$$

This transform allows tracing the so-called ”fast” and ”slow” motions near the resonance provided that the external excitation of the system (4.1) is small. The ”fast” variable is characterized by the frequency of the external harmonic force ω, while the new phase coordinate $\psi(\tau)=\varphi(\tau)-(\omega-\Omega)\tau/\varpi$ plays as the “slow” one, where the difference $\omega-\Omega$ is associated with the phase-matching condition, i.e., $\psi(\tau)$ should be a small value of order μ. After substituting (4.3) and (4.4) into Eq. (4.1), the averaging procedure provides the following zero-order approximation evolution equations

$$\begin{aligned}
&\dot{a}+\frac{\delta(1-\alpha T_0)}{m\varpi}a-\frac{p}{4\Omega m\varpi l}\cos\psi=0;\\
&\dot{\psi}+\frac{\omega-\Omega}{\varpi}+\frac{p}{4\Omega m\varpi l}\frac{\sin\psi(\tau)}{a}=0;\\
&\dot{\Theta}+G\Theta/C\varpi=0.
\end{aligned} \tag{4.5}$$

The stationary solution to the set (4.5) is obtained by equating all the derivatives to zero:

$$\begin{aligned}
&a_0^2=\frac{p^2}{16l^2m^2\Omega^2\left(\varpi^2+\omega^2-2\omega\Omega\right)};\\
&\psi_0=-\arctan\left(\frac{m(\omega-\Omega)}{\delta(1-\alpha T_0)}\right);\\
&\Theta_0=0.
\end{aligned} \tag{4.6}$$

where a_0 , ψ_0 and Θ_0 denote the steady states to the variables a, ϕ and γ, correspondingly.

The equations describing the zero-order nonresonant corrections read:

$$\begin{aligned}
&\dot{u}_0(\tau)=v_0(\tau)+\frac{p\cos\left(\frac{\omega\tau}{\varpi}\right)}{l\varpi\sqrt{m^2\varpi^2/2-\delta^2(1-\alpha T_0)^2}};\\
&\dot{v}_0(\tau)=-\frac{2\delta(1-\alpha T_0)}{m\varpi}v_0(\tau)-u_0(\tau)+\frac{p\delta(1-\alpha T_0)\cos\left(\frac{\omega\tau}{\varpi}\right)}{2\varpi^2ml\sqrt{m^2\varpi^2/2-\delta^2(1-\alpha T_0)^2}}-\frac{p\sin\left(\frac{\omega\tau}{\varpi}\right)}{2\varpi^2ml}.
\end{aligned} \tag{4.7}$$

After finding a particular solution to Eq. (4.7), the zero-order approximation is completely built. It is obvious that the zero-order approximation stationary solution, in terms of the substitution (4.3), coincides exactly with the corresponding solution to the original linear subset (4.1).

To construct the nonlinear first-order approximation evolution equations, we can again use the same substitution (4.3), pointing out that the zero-order nonresonant correction is already known as the particular solution to the inhomogeneous linear differential set (4.7).

The evolution equations within the first-order nonlinear approximation hold true:

$$\begin{aligned}
&\dot{a}+\frac{(1-\alpha T_0)\delta}{m\varpi}a-\frac{p\cos\psi}{4m\varpi\Omega l}+\mu\widehat{\Theta}\left(\gamma_{11}\sin\psi+\gamma_{12}\cos\psi+\gamma_{13}a\right)=0;\\
&\dot{\psi}+\frac{\omega-\Omega}{\varpi}+\frac{p}{4m\varpi\Omega l}\frac{\sin\psi}{a}+\mu\widehat{\Theta}\left(\gamma_{21}\frac{\sin\psi}{a}+\gamma_{22}\frac{\cos\psi}{a}+\gamma_{23}\right)=0;\\
&\dot{\Theta}+\frac{G}{C\varpi}\Theta+\mu\left(\gamma_{30}+a\left(\gamma_{31}\sin\psi+\gamma_{32}\cos\psi\right)+\gamma_{33}a^2\right)=0.
\end{aligned} \tag{4.8}$$

The coefficients entering these equations are following:

$$\gamma_{11}=\frac{\alpha\delta pT_0\left(2\omega^2(1-\alpha T_0)^2\delta^2+m^2\left(\varpi^2-\omega^2\right)\left(\varpi^2-\omega\Omega\right)\right)}{16m^2\Omega^2\varpi l\left(\omega^2(1-\alpha T_0)^2\delta^2+m^2\left(\varpi^2-\omega^2\right)/4\right)};$$

$$\gamma_{12}=\frac{\alpha\delta^2 pT_0 m\omega(1-\alpha T_0)\left(\varpi^2+\omega^2-2\omega\Omega\right)}{16m^2\Omega^2\varpi l\left(\omega^2(1-\alpha T_0)^2\delta^2+m^2\left(\varpi^2-\omega^2\right)/4\right)};$$

$$\gamma_{13}=-\frac{\delta\alpha T_0}{m\varpi};$$

$$\gamma_{21}=\frac{\alpha\delta^2 pT_0(1-\alpha T_0)\left(\varpi^2+\omega^2-2\omega\Omega\right)\omega}{16m\Omega^2\varpi l\left(\omega^2(1-\alpha T_0)^2\delta^2+m^2\left(\omega^2-\varpi^2\right)^2/4\right)};$$

$$\gamma_{22}=\frac{\alpha\delta pT_0\left(2\omega^2(1-\alpha T_0)^2\delta^2+m^2\varpi^2\left(\varpi^2-\omega^2\right)\left(\varpi^2-\omega\Omega\right)\right)}{16\varpi l\left(\omega^2(1-\alpha T_0)^2\delta^2+m^2\left(\omega^2-\varpi^2\right)^2/4\right)m^2\Omega^2};$$

$$\gamma_{23}=-\frac{\alpha\delta^2 T_0(1-\alpha T_0)}{m^2\Omega\varpi};$$

$$\gamma_{30}=-\frac{p^2\delta T_0(1-\alpha T_0)\varpi\left(2\omega\Omega-\left(\omega^2+\varpi^2\right)\right)}{16CVT_0\Omega^2\left(\omega^2(1-\alpha T_0)^2\delta^2+m^2\left(\omega^2-\varpi^2\right)^2/4\right)};$$

$$\gamma_{31}=-\frac{p\delta T_0(1-\alpha T_0)l\left(\omega\left(\omega^2(1-\alpha T_0)^2\delta^2+m^2\varpi^2\left(\omega^2-\varpi^2\right)/2\right)\right)}{CVT_0\varpi m\Omega\left(\omega^2(1-\alpha T_0)^2\delta^2+m^2\left(\omega^2-\varpi^2\right)^2/4\right)}$$

$$+\frac{2\Omega p\delta T_0(1-\alpha T_0)l\left(\omega^2(1-\alpha T_0)^2\delta^2+m^2\varpi^2\left(\omega^2-\varpi^2\right)/4\right)}{CVT_0\varpi m\Omega\left(\omega^2(1-\alpha T_0)^2\delta^2+m^2\left(\omega^2-\varpi^2\right)^2/4\right)};$$

$$\gamma_{32} = -\frac{p\delta^2 T_0 (1-\alpha T_0)^2 l\left(-2\omega^2\left(\left(\varpi^2 - 3\omega^2\right)/4 + \delta^2\omega^2(1-\alpha T_0)^2\right) - \omega^3\Omega\right)}{CVT_0\varpi\Omega^2\left(\omega^2(1-\alpha T_0)^2\delta^2 + m^2\left(\omega^2-\varpi^2\right)^2/4\right)};$$

$$\gamma_{33} = \frac{\delta(1-\alpha T_0)\varpi\left(\left(\left(\omega^2-\varpi^2\right)^2 - 4\varpi^2\omega^2\right)(1-\alpha T_0)^2\delta^2 m^2 - \varpi^2 l^2\left(\omega^2-\varpi^2\right)^2 m^4\right)}{CVT_0\varpi m^2\Omega\left(\omega^2(1-\alpha T_0)^2\delta^2 + m^2\left(\omega^2-\varpi^2\right)^2/4\right)}$$

$$+\frac{4\delta^5\omega^2\varpi l^2(1-\alpha T_0)^5}{CVT_0\varpi m^2\Omega\left(\omega^2(1-\alpha T_0)^2\delta^2 + m^2\left(\omega^2-\varpi^2\right)^2/4\right)}.$$

The structure of the evolution Eq. (4.8) is transparent enough. It is obvious that the intensity of the thermo-mechanical effect is determined by the small parameter μ. If this parameter is zero, then there is no temperature effect on the mechanical motion. If we assume the thermal viscosity parameter to be zero, then the coefficients γ_{11}, γ_{12}, γ_{13} and γ_{21}, γ_{22}, γ_{23} should be also zero in the equations for the amplitude and phase. There is no temperature effect on the mechanical motion again. Let us remove these limiting cases from consideration, and then the nontrivial nonlinear thermo-mechanical coupling becomes apparent.

Phase–amplitude frequency response with thermal effects

The equations determining the steady-state oscillatory modes follow directly from the evolution Eq. (4.8) if we put all the velocities equal to zero. As a result one obtains the set of three transcendental equations for the same number of unknowns $\hat{a}$, $\hat{\psi}$ and $\hat{\Theta}$:

$$\begin{aligned}
&\frac{\delta(1-\alpha T_0)}{m\varpi}\hat{a} + \frac{p}{4m\varpi\Omega l}\cos\hat{\psi} + \mu\hat{B}\left(\gamma_{11}\sin\hat{\psi} + \gamma_{12}\cos\hat{\psi} + \gamma_{13}\hat{a}\right) = 0;\\
&\frac{\omega-\Omega}{\varpi} + \frac{p}{4m\varpi\Omega l}\frac{\sin\hat{\psi}}{\hat{a}} + \mu\hat{B}\left(\gamma_{21}\frac{\sin\hat{\psi}}{\hat{a}} + \gamma_{22}\frac{\cos\hat{\psi}}{\hat{a}} + \gamma_{23}\right) = 0;\\
&G\hat{\Theta}/C\varpi + \mu\left(\gamma_{30} + \hat{a}\left(\gamma_{31}\sin\hat{\psi} + \gamma_{32}\cos\hat{\psi}\right) + \gamma_{33}\hat{a}^2\right) = 0.
\end{aligned} \qquad (4.9)$$

The unknown quantities $\hat{a}$, $\hat{\psi}$ and $\hat{\Theta}$ characterizing the amplitude, phase and the temperature, respectively, can be parameterized in different ways. Let these be the functions of the external frequency ω. Then, one can build the so-called amplitude–phase frequency curves, taking into account temperature effects. For clarity, we may consider the specific values of individual parameters to the system (4.1). Let the values of these parameters are: $V = 39.5\times10^{-6} m^3$; $m = 0.5 kg$; $c = 5\times10^4 Nm^{-1}$; $\delta = 100 kg/s$; $P = 10^3 N$; $p = 500N$; $\alpha = 10^{-3} K^{-1}$; $\beta = 3.14 m^{-1}$; $C = 10^3 kg/ms^2K$; $G = 10^2 WK^{-1}m^{-3}$; $T_0 = 300K$; $l = 0.034m$. Then, there is the possibility to trace the behavior of the amplitude and phase characteristics of the stationary processes depend-

ing upon the small parameter. The steady-state characteristics when the parameter is small enough, e.g., $\mu = 10^{-2}$, are shown in Fig.4.2. The frequency in all the pictures is normalized by the value $\varpi = 294.2\ Hz$, so that the maximal amplitude should be near unity. The amplitude, $\hat{a}(\nu)$, and temperature, $\hat{\Theta}(\nu)$, are presented as functions of the dimensionless frequency $\nu = \omega/\varpi$.

It is obvious that the set of stationary states is composed of two distinct subsets, namely **H** and **L**, which we call the high- and low-temperature branches, respectively. The amplitude– and phase–frequency branches, characterizing the low-temperature subset **L**, are almost indistinguishable from the related curves (4.6), characterizing the linear subsystem. At the same time, the high-temperature subset H appears entirely due to the nonlinearity. This subset consists of both stable and unstable fixed points separated by limits where the derivatives become infinite. Obviously, the stable stationary regimes H cannot be reachable from any initial conditions. For example, to excite any stable high-temperature stationary regime, the liquid inside the absorber should be pre-heated up to some predetermined temperature. Moreover, the frequency of the external harmonic signal should be placed within the specified band. At the same time, the stationary regimes, correspondent to the low-temperature subset **L,** are achieved almost at any initial conditions. Let the small parameter μ increases. How significant are the changes over the amplitude and temperature characteristics? The low-temperature branch L changes slowly. The amplitude varies slowly than the temperature, but the resonance peak is shifted slightly into the high-frequency band. In turn, the high-temperature branch **H** changes very rapidly with the growth of the small parameter μ. Starting with a certain critical value of this parameter, the high-temperature characteristic **H** is united with the low-temperature branch **L**. This causes the thermo-mechanical instability of the system, which is expressed in a high jump in the oscillation amplitude and a significant increase in the temperature in the vicinity of the resonance frequency and even some higher, as well. Figure 4.3 illustrates the stationary states near the critical point. The path (a, b, c, d, e, a) in this figure represents the hysteresis loop when the external frequency is scanned to and fro. The system under consideration (4.8) is complex enough to evaluate analytically their stability proper- ties. Nonetheless, numerical tests can confirm oscillatory patterns naturally observed in systems with a hysteresis. Point out that the thermo-mechanical instability in vibration absorbers is obviously unacceptable in practice.

Moreover, we should not forget that Fig. 4.3 demonstrates the results provided by the first-order approximation nonlinear model (4.8). Though, direct numerical calculations of the original equations of motion (4.1) in some characteristic points confirm that the thermo-mechanical instability

actually takes place. It turns out that the solution to the first-order nonlinear approximation Eq. (4.8) practically coincides with those of the initial problem (4.1) at small amplitudes in the vicinity of the resonant frequency. Some discrepancies between the exact and approximate solutions naturally become solid with increasing in the external periodic load. It means that the second-order nonlinear approximation equations play an actual role from the viewpoint of a more detailed description of the frequency–amplitude dependences. But this question, being a nontrivial one, is beyond the scope of present study.

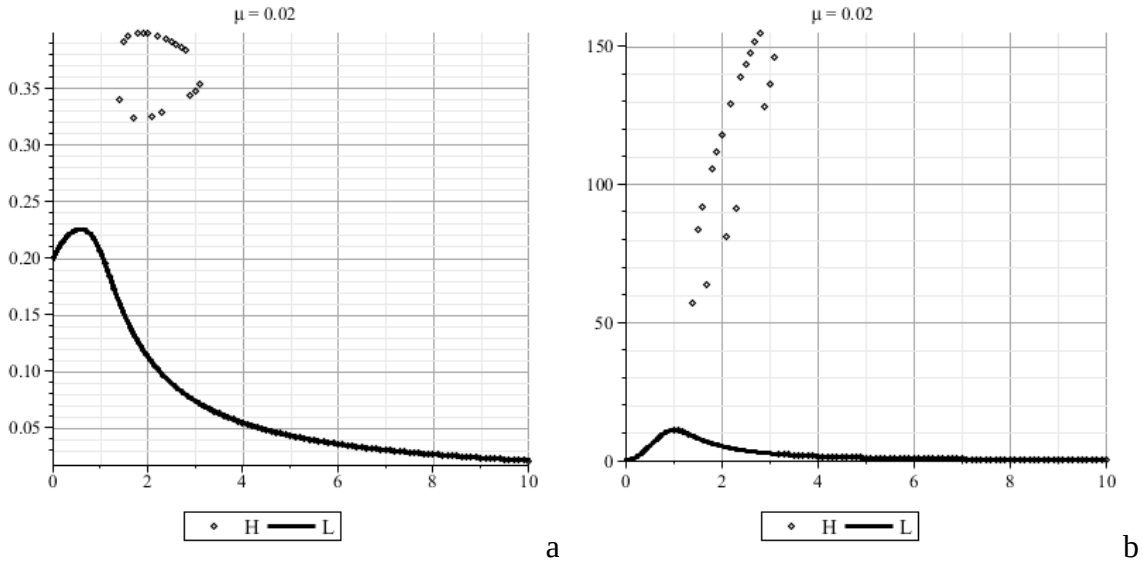

Fig. 4.2 Amplitude (a) and temperature (b) as functions of the dimensionless frequency ν

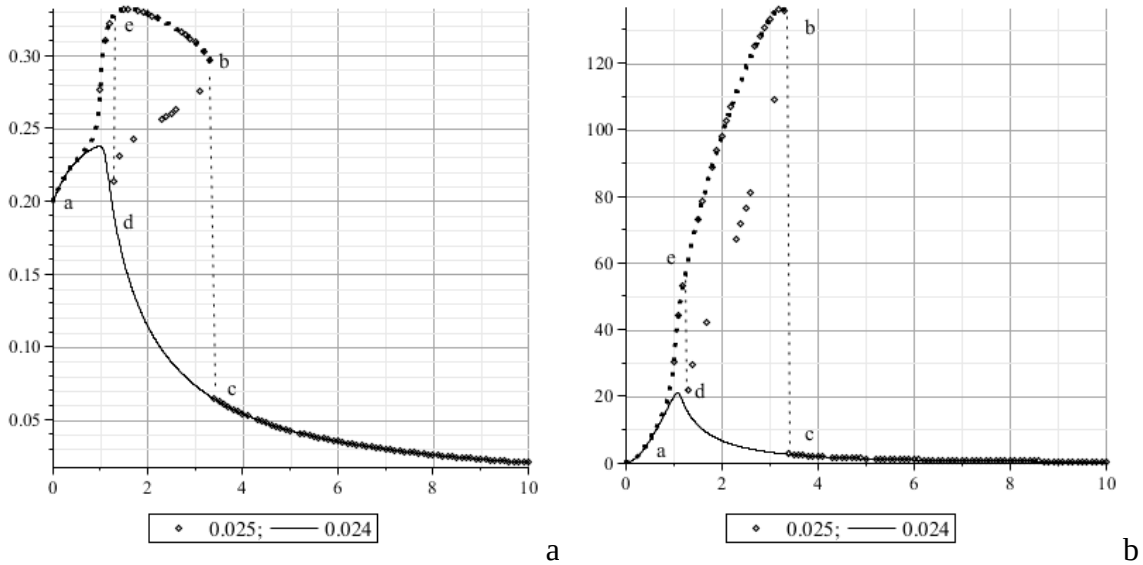

Fig. 4.3 Thermo-mechanical instability. Amplitude response (a) and temperature (b) versus the dimensionless frequency ν. *Numbers* mark different values of the small parameter μ

Parametric analysis of the stationary solutions

To carry out a parametric analysis of stationary solutions to the nonlinear evolution equations of the first-order approximation, the left-hand side of Eq. (4.9) are indicated as it follows:

$$
\begin{aligned}
P &= \frac{\delta(1-\alpha T_0)}{m\varpi}\bar{a} + \frac{p}{4m\varpi\Omega l}\cos\bar{\psi} + \mu\bar{\Theta}(\gamma_{11}\sin\bar{\psi} + \gamma_{12}\cos\bar{\psi} + \gamma_{13}\bar{a});\\
Q &= \frac{\omega-\Omega}{\varpi} + \frac{p}{4m\varpi\Omega l}\frac{\sin\bar{\psi}}{\bar{a}} + \mu\bar{\Theta}\left(\gamma_{21}\frac{\sin\bar{\psi}}{\bar{a}} + \gamma_{22}\frac{\cos\bar{\psi}}{\bar{a}} + \gamma_{23}\right);\\
R &= \frac{G}{C\varpi}\bar{\Theta} + \mu\left(\gamma_{30} + \bar{a}(\gamma_{31}\sin\bar{\psi} + \gamma_{32}\cos\bar{\psi}) + \gamma_{33}\bar{a}^2\right).
\end{aligned}
\tag{4.10}
$$

The unknown quantities $\bar{a}$, $\bar{\psi}$ and $\bar{\Theta}$ describing, as before, the amplitude, the phase and temperature, respectively, are now considered to be smooth functions of the small parameter μ. The functions $P(\bar{a},\bar{\psi},\bar{\Theta})$, $Q(\bar{a},\bar{\psi},\bar{\Theta})$ and $R(\bar{a},\bar{\psi},\bar{\Theta})$ are differentiable almost everywhere in the space of the system parameters. Then, the parametric analysis of stationary solutions is available with the help of the Lie series [23,48]. These functions P, Q and R should be once differentiated by the variable μ in Eq. (4.9), then these equations are resolved to the implicit set for the first derivatives. The result appears as the following three ordinary differential equations

$$
\frac{d\bar{a}}{d\mu} = \zeta_{\bar{a}}(\bar{a},\bar{\psi},\bar{\Theta}); \quad \frac{d\bar{\psi}}{d\mu} = \zeta_{\bar{\psi}}(\bar{a},\bar{\psi},\bar{\Theta}); \quad \frac{d\bar{\Theta}}{d\mu} = \zeta_{\bar{B}}(\bar{a},\bar{\psi},\bar{\Theta}).
\tag{4.11}
$$

It is obvious that expression (4.10) represent explicit solutions to the set (4.11) with the initial conditions defined by the known parameters $\bar{a}(0)$, $\bar{\psi}(0)$ and $\bar{\Theta}(0)$. These parameters are completely determined by the right-hand sides of Eq. (4.6), i.e., $\bar{a}(0) = a_0$, $\bar{\psi}(0) = \psi_0$ and $\bar{\Theta}(0) = \Theta_0$. The structure of these equations is not so easy, but it can be effectively studied in detail using available parsing algorithms [49]. Point out that explicit solutions to Eq. (4.11) may be represented with the help of the Lie series:

$$
\begin{aligned}
\bar{a}(\mu) &= a_0 + \mu\,\mathrm{G}\,a_0 + \frac{\mu^2}{2}\mathrm{G}^2 a_0 + \ldots;\\
\bar{\psi}(\mu) &= \psi_0 + \mu\,\mathrm{G}\,\psi_0 + \frac{\mu^2}{2}\mathrm{G}^2\psi_0 + \ldots;\\
\bar{\Theta}(\mu) &= \Theta_0 + \mu\,\mathrm{G}\,\Theta_0 + \frac{\mu^2}{2}\mathrm{G}^2\Theta_0 + \ldots
\end{aligned}
\tag{4.12}
$$

Here $\mathrm{G} = \zeta_{a_0}(a_0,\psi_0,\Theta_0)\frac{\partial}{\partial a_0} + \zeta_{\psi_0}(a_0,\psi_0,\Theta_0)\frac{\partial}{\partial\psi_0} + \zeta_{B_0}(a_0,\psi_0,\Theta_0)\frac{\partial}{\partial\Theta_0}$ is the differential operator.

Dependence of steady-state solutions upon the small parameter μ

The numerical result to Eq. (4.11) is shown in Fig.4.4, as an illustrative example. The values of the system parameters are the same as previously. The peaks of the displacement and temperature are formed even away from the resonant frequency Ω, as we can see in Fig.4.4. A typical resonant pattern should take place when the frequency of the external signal ω tends to the resonant frequency of the system Ω. At the same time, the amplitude peak, accordingly to the linear theory, is near the resonant frequency $\Omega = 125.6\,Hz$, while the natural frequency should be about $\varpi = 294.2\,Hz$ in the absence of damping. It means that there is a frequency shift caused by the nonlinearity. This one is described mainly by the term $\mu\gamma_{23}\widehat{\Theta}$, entering into the equation for the "slow" phase of the set (4.7). This one is resumed as if the system (4.1) tends to approach *in vacuo* pattern due to such a kind of compensation.

Steady states versus the nonlinear elastic parameter β

The steady states obtained by scanning the parameter β characterizing the asymmetry of the elastic characteristics are shown in Fig.4.5. There is no significant impact on the dynamics of the vibration absorber even with a significant change in this parameter. This result is generally confirmed by experimental tests with the vibration absorbers. In fact, the static deformation appears in the presence of the static load P only. This means that the natural frequency of oscillation in the absence of energy dissipation, $\varpi = \sqrt{\sqrt{\left(c^2 - 4\beta P\right)/m}}$, changes slowly with the growth of the static load P, namely, as a square root, if the first-order nonlinear approximation analysis is considered. Though, the so-called self-action effect, inherent in, say, the well-known Düffing-type equations, should be assuredly manifested when deriving the second-order nonlinear approximation evolution equations.

Steady states versus the static load P

The steady states along the variable parameter P, characterizing the static load, are illustrated in Fig.4.6. It is clearly that the static load does not influence significantly on the dynamics of the vibration absorber. This is generally confirmed in practice.

Steady states versus the damping coefficient δ

The steady states at various values of the damping coefficient δ are shown in Fig.4.7. As we can observe, the thermo-mechanical instability can be suppressed by large values of the damping parameter, for instance at $\delta = 190\,\text{kg/s}$. Though, if this parameter exceeds the damping limit

$\delta^* = 210.12$ kg/s, then the system (4.7) cannot be treated as the oscillatory one, because of exponential dynamical patterns, if the eigenvalue problem is considered. Point out that such patterns with awfully transient dynamics are usually unacceptable in practice of vibration absorbers. At small values of damping, as $\delta = 100$ kg/s, the path (a, b, c) indicates stable steady- state regimes in direct scanning over the small parameter μ, while those are denoted as (c, d, a) in the case of the reverse tracing that is shown in Fig.4.7.

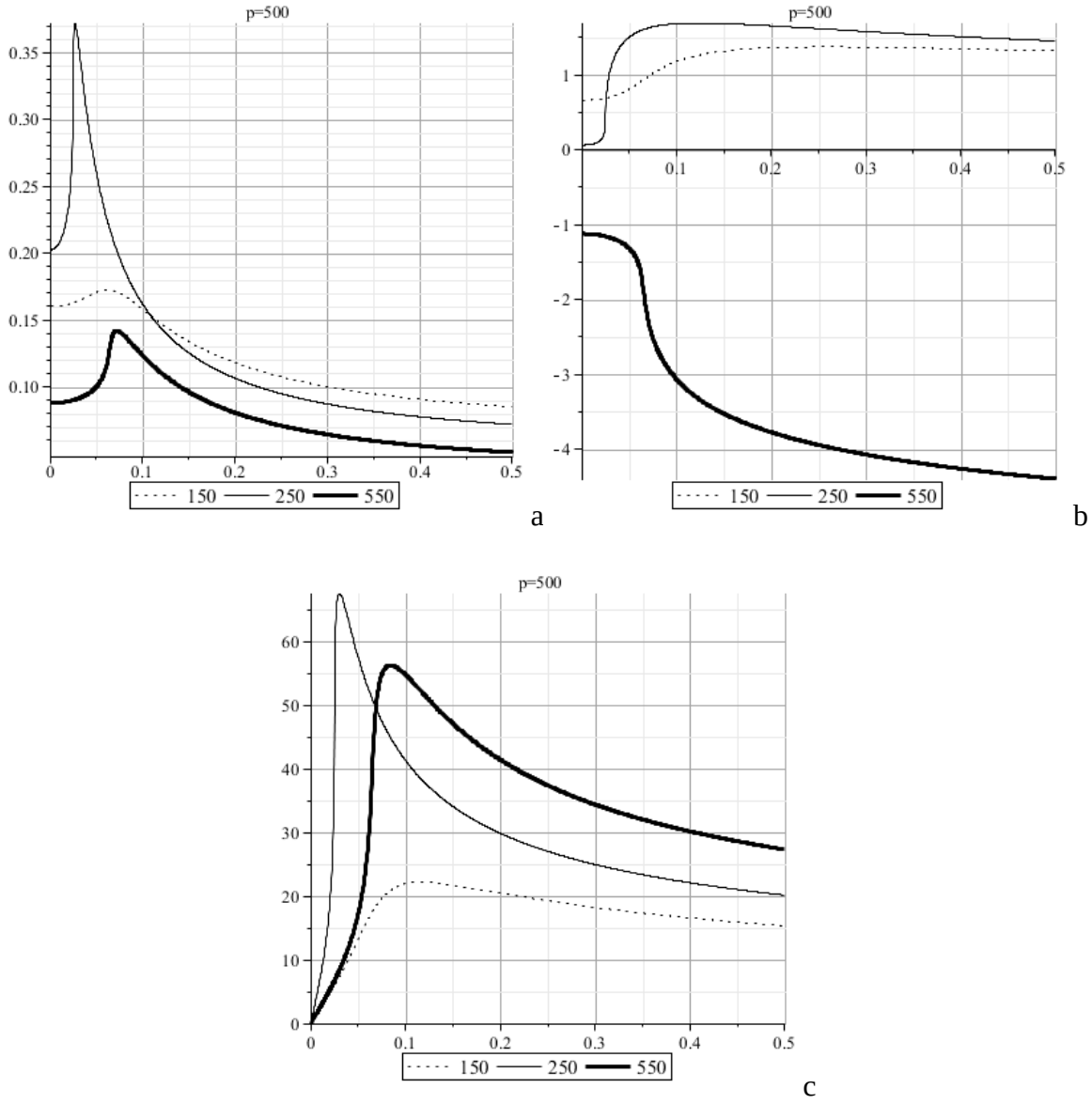

Fig. 4.4 Stationary solutions. Amplitude (a), phase (b) and temperature (c) versus the small parameter μ. Numbers mark the calculated values of the external signal frequency ω in Hertz

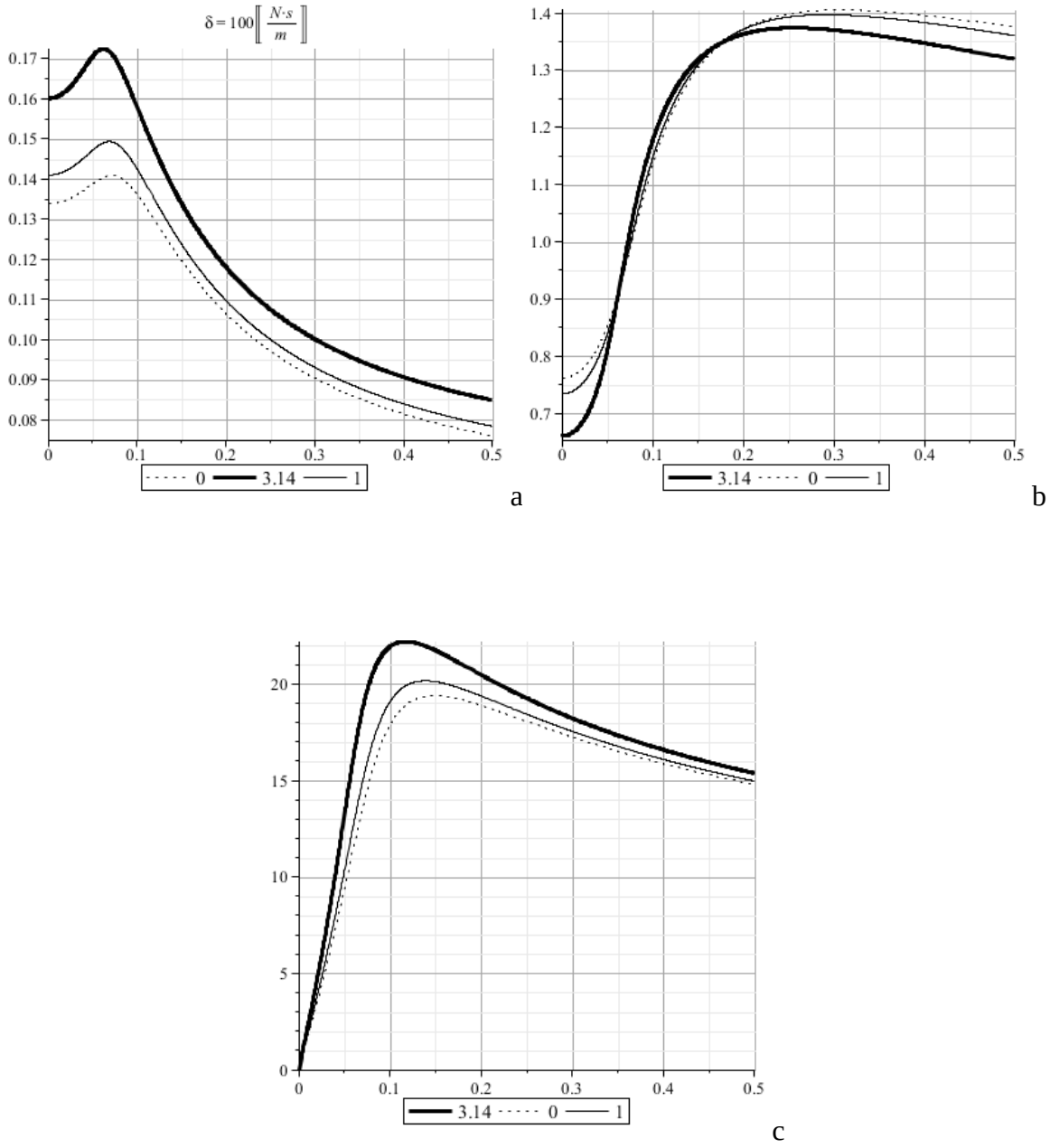

Fig. 4.5 Stationary states. Amplitude (a), phase (b) and temperature (c) versus the small parameter μ. Numbers mark the calculated values for the nonlinear elasticity β (units m^{-1})

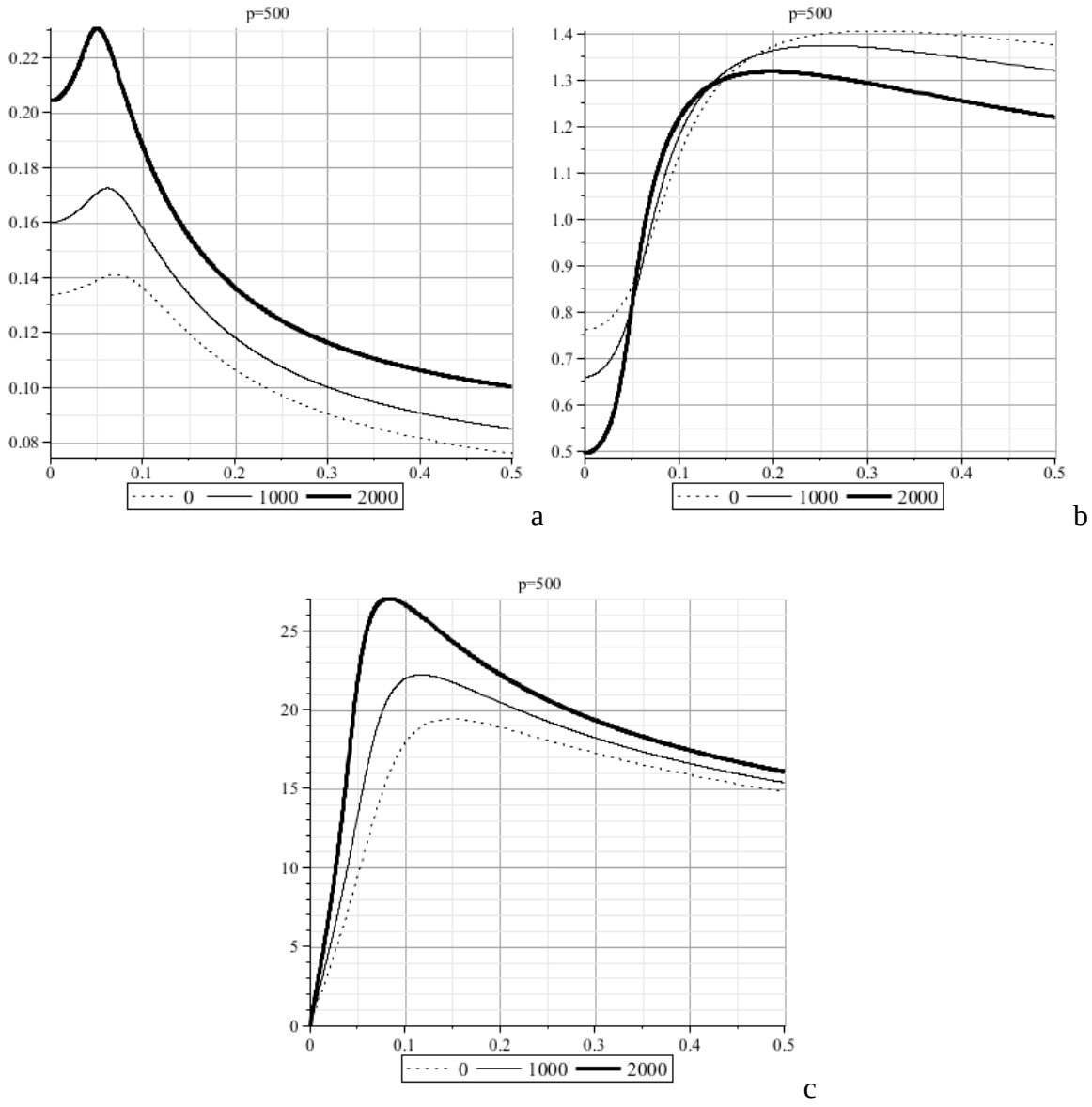

Fig. 4.6 Stationary states. Amplitude (a), phase (b) and temperature (c) versus the small parameter μ. Numbers mark the calculated values of the static load P (units Newton)

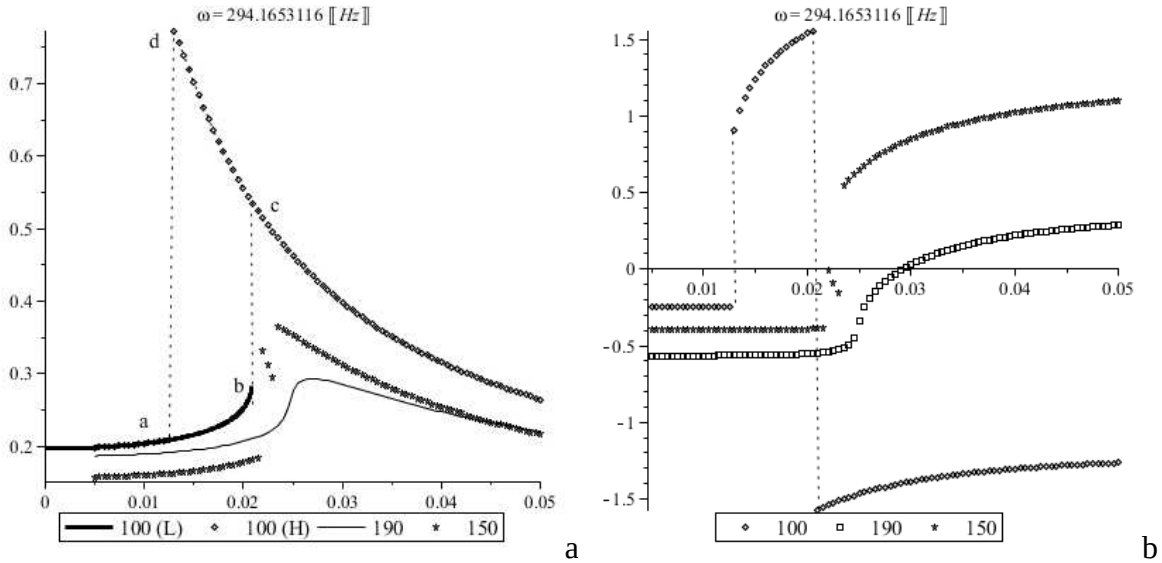

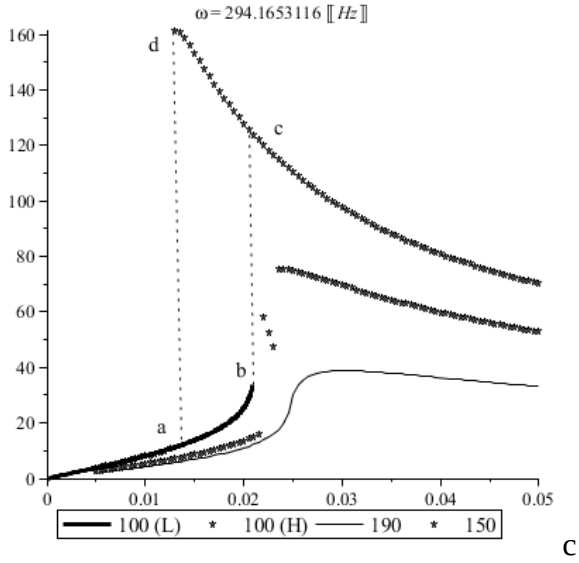

Fig. 4.7 Stationary states. Amplitude (a), phase (b) and temperature (c) versus the small parameter μ. Numbers mark the calculated values of the damping coefficient δ

Resume

A mathematical model describing the thermo-mechanical instability in the vibration absorbers have been traced in this chapter. This instability is caused by the nonlinear resonant phenomena. The temperature of the fluid inside the vibration absorber increases under the external harmonic excitation, so that the viscosity decreases, while the amplitude of mechanical vibrations increases, as well. However, the decrease in the viscosity restricts the heat injection. This leads to the nonlinear steady states. In the vicinity of the resonant frequency, the system exhibits brightly expressed amplitude–frequency dependences, which provide some hysteretic patterns of oscillations. Parametric analysis of the system reveals that the thermal viscosity parameter appears as the most sensitive parameter from the viewpoint of the thermo-mechanical instability. This parameter approaches a critical value at sufficiently small variations in the system. This means that the using of liquid materials with a very small thermal viscosity coefficient is absolutely ineffective for the vibration absorber, since any inner matter, such as particles of metal or polymer, can easily increase the value of the thermal viscosity up to the critical value. This can lead to unwanted and uncontrolled dynamical patterns.

The model of the thermo-mechanical instability proposed in the present study is extremely simple, though being not so trivial in terms of the used algorithms [49]. It is clear that some aspects of the problem should be improved using numerical methods [50] with allowances for more appropriate physical relationships between the viscosity and temperature [51], some various effects of nonlinearity are of high interest [52, 53], as well.

GEOMETRICAL NON-LINEARITY STABILIZES A WAVE SOLID-STATE GYRO

It was recognized long ago that quasi-harmonic standing waves in a thin-walled axisymmetric resonator, mounted on a rotating platform, are subject to a precession. This significant phenomenon is naturally associated with a concept of a solid-state wave gyro, or an inertial instrument used to measure angular rotation rate, as if any wave may be interpreted as a material particle moving in a rotating frame of reference. Because there are no typical mechanical parts, these wave sensors can be utilized with a lot of advantages. To run such a gyro in vita, one should excite and keep on by certain means a standing wave in the thin-walled axisymmetric resonator. Up to now, there are known two ways how to do it, and namely, using either external or parametric resonant mechanisms of excitation. Although both cases necessarily require an additional feedback control device in order to stabilize instable or other parasite oscillations of the resonator. This chapter, following the study of nonlinear waves in a thin circular ring, demonstrates that the solid-state wave gyro may be naturally stabilized just at the expense of the geometrical nonlinearity by combining advantages of both the positional resonant excitation and the parametric resonance.

Modern solid-state wave gyros based on hemispherical high-purity quartz resonators are associated with satellite guidance systems intended for long-term missions extending up to 15 years [54]. It was found long ago that any flexural standing mode in a rotating thin-walled axisymmetric resonator is subject to a precession, because of the so-called wave inertia effect [55]. This means that the precessing wave responds effectively on the rotation, like a material point tends to conserve the spatial position in an inertial frame of references. The wave mode turns about the symmetry axis of the resonator with the angular velocity, $\kappa(n)\theta$, against the platform rotating with the angular velocity θ. Here, $\kappa(n)$ denotes a negative-definite function describing, in particular, specificities of the resonator geometry. This coefficient depends sensitively upon the profile of the precessing standing mode with the wave number n. For instance, experiments with the primary flexural waveform ($n = 2$) in a small hemispherical shell, rotated after the wave excitation about the sensitive axis at the angle $\pi/2$, showed that the summary angle of rotation of this mode is about 63° [55]. This example serves as a prototype of an angle sensor. The principle of operation of this sensor is based, accordingly to the wave-participle dualistic paradigm, on the inertia of waves in solids. Such a gyro possesses a lot of advantages compared to a conventional one [56–58], because of absence of typical mechanical parts.

For operating the wave solid-state gyro, the system should be forced to vibrate in a flexible mode of the axisymmetric resonator. The amplitude of these oscillations has to be maintained on some acceptable level in the presence of energy dissipation. The presence of damping requires pumping permanently the energy into these oscillations by external forces. There are known two main schemes for the wave excitation, using the presence of energy dissipation. The presence of damping requires pumping permanently the energy into these oscillations by external forces. There are known two main schemes for the wave excitation, using the resonant properties of dynamical systems [56]. The first type is called a positional excitation. This means that the external force is modulated harmonically, both in the time and in the space, with the spectral parameters which should be close to the corresponding parameters of a driven mode in the resonator. The second kind is associated with a parametric excitation of vibrations, when the periodic variation in some suitable parameter of the system, e.g. the midline tension of the axisymmetric resonator, is homogeneous one with respect to the circumferential coordinate. The spectral parameters should also be comparable with those of the driven oscillatory mode of the resonator. In the first case, resonantly forced oscillations occur at any value of the external excitation. However, the excited standing wave is spatially glued to the base of the resonator. Consequently, the wave gyro cannot measure the applied rotation rate permanently, but just before the decaying, because of energy dissipation, flexural mode may be reliably recognized. In the second case, there is a threshold of excitation, such that if the level of excitation is small enough, then the parametrically excited vibrations do not occur, but if this threshold is slightly exceeded, the motion becomes unstable. Therefore, an additional device is necessary to stabilize the gyro. This study shows that the wave gyro can stabilized naturally due to the geometrical nonlinearity of the thin-walled resonator. To reach this conclusion, one should build a structural model of the wave gyro, which has to establish a relationship between the parameters responsible for the nonlinear phenomena, the external driving, and energy dissipation. There is no doubt that the wave gyro may be represented by a thin circular ring in the simple case.

Equations governing the motion in a thin circular ring

Let us consider plane vibrations of a thin ring of the thickness h and the radius R, which can rotate with an angular velocity $\theta(t)$ about the sensitive axis. The dynamical processes are studied in the long-wave approximation. To derive the equations of motion, one can use the theory of thin-walled shells based on the Kirchhoff–Love hypotheses. The distribution of displacements inside the ring can be written as it follows [59, 60]:

$$u_{(s)} = v - \varsigma\left(w_s - v/R\right); \quad u_{(\varsigma)} = w,$$

where $v = v(s,t)$ and $w = w(s,t)$ are the circumferential and radial displacements, correspondingly, dependent upon the circumferential coordinate s and the physical time t. These are measured from points located along the midline of the ring at the distance ς in the frame of reference associated with the rotating platform. Expression for the densities of the kinetic energy K and the potential energy are given by the following forms

$$\mathrm{K} = \frac{\rho h}{2}\left[\left(v_t + \theta w + R\theta\right)^2 + \left(w_t - \theta v\right)^2\right]; \quad \Pi = \frac{EF\kappa^2}{2R^2}v^2 + \frac{E}{2}\int_{-h/2}^{h/2} e_{ss}^2 d\varsigma$$

where E stands for the Young's modulus; F denotes the cross-section square; ρ is the mass density; κ is a tunable coefficient characterizing the stiffness between the rotating platform and the ring; $e_{ss} = v_s + w/R + \xi\left(w_{ss} - v_s/R\right) + w_s^2/2$ denotes the circumferential deformation. Equations governing motion possess the following variational form

$$\begin{aligned} &\left(L_{\dot{v}}\right)_t + \left(L_{v_s}\right)_s - L_v = Q_{(v)} - \mathrm{R}_{\dot{v}}; \\ &\left(L_{\dot{w}}\right)_t + \left(L_{w_s}\right)_s - L_w - \left(L_{w_{ss}}\right)_{ss} = Q_{(w)} - \mathrm{R}_{\dot{w}}, \end{aligned} \tag{5.1}$$

where $L = \mathrm{K} - \Pi$ is the Lagrangian density; $Q_{(v)}$ and $Q_{(w)}$ denotes the external forces; $\mathrm{R} = \eta K$ is the energy dissipation function of the rate η. The explicit form of these equations, provided that the damping is neglected, reads as follows:

$$\begin{aligned} &\ddot{v} + 2\theta\dot{w} + \dot{\theta}\left(R + w\right) - \theta^2 v - c^2 V_s + \frac{c^2 a^2}{R}W_{ss} + \frac{\kappa^2 c^2}{R^2}v = \frac{c^2}{2}\left(w_s^2\right)_s + Q_{(v)}; \\ &\ddot{w} - 2\theta\dot{v} + \dot{\theta}v - \theta^2\left(R + w\right) + \frac{c^2}{R}V + c^2 a^2 W_{sss} = c^2\left(Vw_s\right)_s - \frac{c^2}{2R}w_s^2 + \frac{c^2}{2}\left(w_s^3\right)_s + Q_{(v)} \end{aligned} \tag{5.2}$$

where $V = v_s + w/R$ and $W = w_s - v/R$ are introduced for brevity. After the introducing the dimensionless variables: $v = u_0 v'$; $w = u_0 w'$; $\varphi = s/R$; $t = R\tau/c$; $\theta' = R\theta/c$, where $u_0 = \max\left(\sqrt{v^2 + w^2}\right)$; $c = \sqrt{E/\rho}$ stands for the typical wave propagation velocity; $a = h/\sqrt{12}$ is the radius of inertia of a cross-section, Eq. (5.2)can be rewritten in the form:

$$\begin{aligned} &\ddot{v} + 2\theta\dot{w} + \dot{\theta}\left(\mu^{-1} + w\right) - \theta^2 v - V_\varphi + \varepsilon^2 W_{\varphi\varphi} + \kappa^2 v = \frac{\mu}{2}\left(w_\varphi^2\right)_\varphi + Q_v; \\ &\ddot{w} - 2\theta\dot{v} + \dot{\theta}v - \theta^2\left(\mu^{-1} + w\right) + V + \varepsilon^2 W_{\varphi\varphi\varphi} = \mu\left[\left(Vw_\varphi\right)_\varphi - w_\varphi^2/2\right] + \mu^2\left(w_\varphi^3\right)_\varphi/2 + Q_{(v)}. \end{aligned} \tag{5.3}$$

where $\varepsilon = h/\sqrt{12}R << 1$ characterizes a small thickness of the ring; $\mu = u_0 / R << 1$ is a small parameter introduced as a bookkeeping device for procedures of the perturbation analysis[13]; $V = v_\varphi + w$ and $W = W_\varphi - v$. Primes indicating the dimensional variables have been omitted. The set (5.3) should be complemented by the natural periodicity conditions

$$v(\varphi,\tau) = v(\varphi + 2\pi,\tau); \quad w(\varphi,\tau) = w(\varphi + 2\pi,\tau).$$

Note that the role of the coefficient κ, characterizing the stiffness, is twofold. On the one hand, this one plays as a necessary structural element of the gyro. On the other hand, let us suppose this parameter to be zero, and then, the motion governed by Eq. (5.3) becomes infinite one due to the rotation, at least within the linear approximation, though the dynamical system possesses the first integral in this case.

Dispersion relations

To study the kinematics of waves under the rotation rate, it is useful to compare the spectrum of linear oscillations in a uniformly rotating ring with that in the rest. Let us suppose that the rotation is absent, and then the normal modes of vibrations can be represented by standing waves as a superposition of wave pairs traveling toward with the same by absolute values, wave numbers, equal frequencies, and identical amplitudes, as well. However, the frequency spectrum of the corresponding oscillatory modes is deformed in a rotating ring. This means that one cannot observe standing modes. Instead, the precessing waves, traveling in accordance with the angular rate, appear as a reaction on the rotation. Moreover, some asymmetry appears in the wave polarization vectors[14]. The precession rate of these waves is proportional to the difference between the frequencies in the wave couple resulted as a standing wave, if the ring is in the rest. At the constant angular rate, the wave precession appears as a kinematic effect due to the rotation of the platform. Although the expression for the precession will be done below in the case of the uniformly rotating ring, nonetheless, it is expected that the result would be generalized for small arbitrary values of the angular velocity and angular acceleration of the rotating platform [56]. Let

---

[13] Formally, the small parameters ε and μ are the same, though the parameter μ scales simultaneously both the amplitudes and the angular rate. The parameter ε characterizes just geometry of the problem.

[14] The exception takes place in the case if the midline of the ring resonator is supposed to be unstretchable one [56, 61–64].

the angular rate of the rotating platform be constant, then a formal oscillatory solution to the linear subset resulted from Eq. (5.3):

$$\ddot{v} + 2\mu\Omega\dot{w} - \mu^2\Omega^2 v - V_{\varphi} + \varepsilon^2 W_{\varphi\varphi} + \kappa^2 v = 0;$$
$$\ddot{w} - 2\mu\Omega\dot{v} - \mu^2\Omega^2 w - \mu^2\Omega^2 / \varepsilon + V + \varepsilon^2 W_{\varphi\varphi\varphi} = 0.$$

has the following form

$$v(\tau,\varphi) = -\frac{\mu\Omega^2}{\varepsilon\left(\mu^2\Omega^2 - 1\right)} + B\exp i\left(n\varphi + \omega\tau\right); \quad w(\tau,\varphi) = A\exp i\left(n\varphi + \omega\tau\right),$$

where the constant radial displacement is caused by the centrifuge forces; the amplitudes, A and B, are linearly interrelated, i.e., $B = pA$. The interrelation coefficients, p, are defined by the high-and low-frequency branches:

$$p_{k,n} = -\frac{i\left(2\mu\Omega p_{k,n} + n\left(1+\varepsilon^2 n^2\right)\right)}{\left(1+\varepsilon^2\right)n^2 + \kappa^2 - \left(\omega_{k,n}^2 + \mu^2\Omega^2\right)} \tag{5.5}$$

The high-frequency branch is indexed by $k = 1$, while the low-frequency one by the number $k = 2$. These coefficients satisfy the orthogonality condition, $p_{1,n}p_{2,n} = -1$, for any wave number n (the oscillations are decoupled at $n = 0$, if the platform is in the rest). Each natural frequency, marked by $\omega_{k,n}$, refers to a normal wave. Absolute values of the interrelation coefficient corresponding to the low-frequency branch, which is of interest within the present study, versus the modal number are plotted in Fig. 5.1.

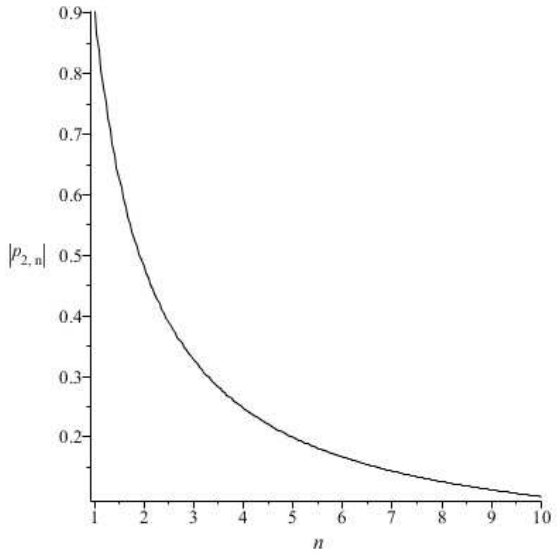

Fig. 5.1 The modulus of the interrelation coefficient to the low-frequency branch (ε=0.01, κ=0.45, Ω=0)

The natural frequencies, $\omega_{k,n}$, are defined by the following dispersion relation

$$\left(\left(1+\varepsilon^2\right)n^2+\kappa^2-\left(\omega_{k,n}^2+\mu^2\Omega^2\right)\right)\left(1+\varepsilon^2 n^4+\kappa^2-\left(\omega_{k,n}^2+\mu^2\Omega^2\right)\right)-\left(2\mu\Omega p_{k,n}+n\left(1+\varepsilon^2 n^2\right)\right)^2=0. \tag{5.6}$$

If the angular velocity is zero: $\Omega\equiv 0$, then this relation turns into the simple biquadratic equation:

$$-\varepsilon^2 n^6-\varepsilon^2\left(-\omega^2-2+\kappa^2\right)n^4+\left(\left(\omega^2-1\right)\varepsilon^2+\omega^2\right)n^2-\omega^4+\left(1+\kappa^2\right)\omega^2-\kappa^2=0. \tag{5.7}$$

The roots of this dispersion relation (5.7) for the free linear vibrations of the ring are shown in Fig. 5.2. The dispersion relation (5.6) possesses four real roots for each n, as well. One pair of roots refers in general to the low-frequency flexural modes, while the second one belongs to the circumferential ones. In the case of a small angular rate ($\Omega << \omega_{k,n}$), the roots of the dispersion relation (5.6) may be constructed asymptotically using the Lie series method [65], if one supposes that the frequencies are differentiable functions dependent upon the angular rate. For example, the first-order approximation analysis reveals the asymmetry in the natural frequencies at the uniform rotation:

$$\omega_{k,n}(\Omega)=\omega_{k,n}(0)+\frac{2\mu\Omega n\left(1+\varepsilon^2 n^2\right)}{1+\varepsilon^2 n^4+\left(1+\varepsilon^2\right)n^2+\kappa^2-2\omega_{k,n}^2(0)}+O\left(\Omega^2\right). \tag{5.8}$$

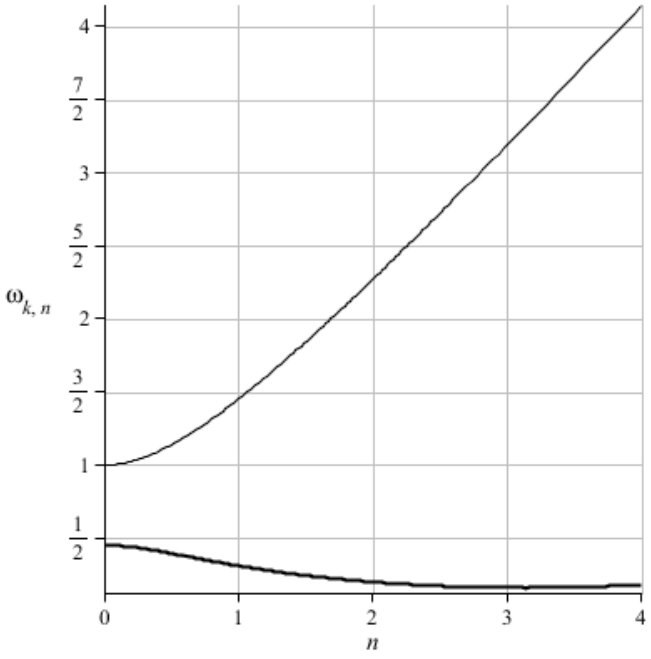

Fig. 5.2 The high-and low-frequency dispersion branches for waves on the fixed platform (ε=0.01, κ=0.45, Ω=0)

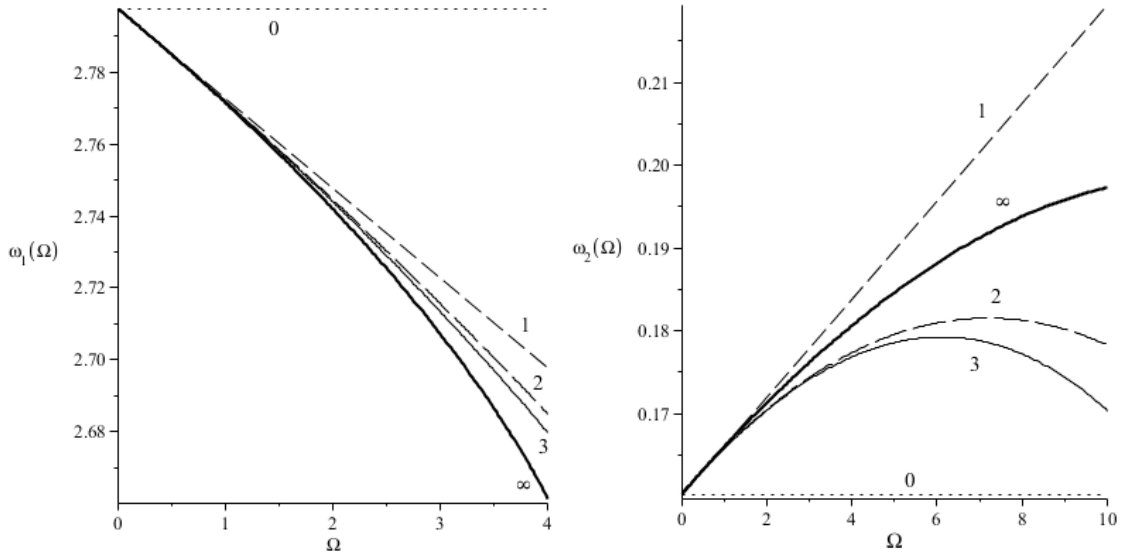

Fig. 5.3 The dispersion branches, modal number $n = 3$. Partial sums to the Lie series at ε=0.01, κ=0.45. The numbers refer to the order of approximation

An illustrative example shown in Fig. 5.3 demonstrates that the first-order approximation curve is completely enough for definite conclusions in the frame of the present study. Obviously, if $\Omega \neq 0$, then the second term in (5.8) splits the double-degenerated roots to Eq. (5.7). Figure 5.4 illustrates this in somewhat caricature manner, since the angular rate should be huge enough to visualize the change in patterns.

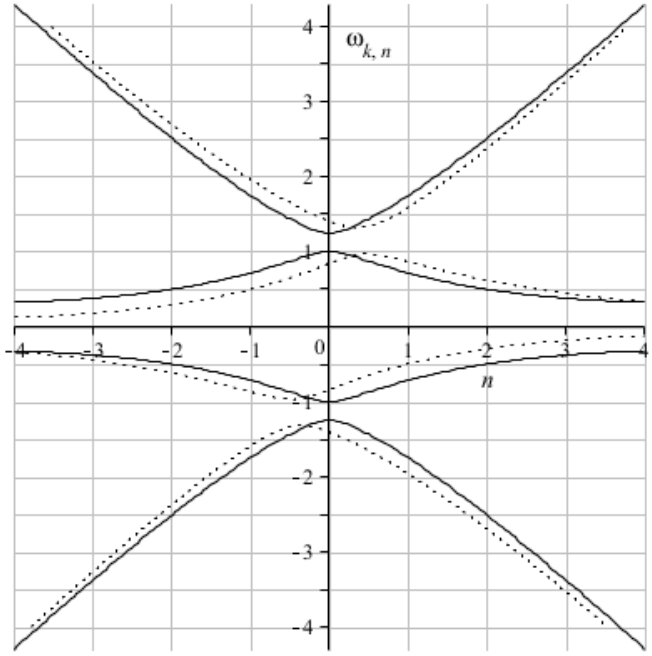

Fig. 5.4 Dispersion diagram for the precessing waves at the uniform rotation (ε=0.01, κ=0.45, Ω=10). The solid curves are the same as plotted in Fig. 5.2

The roots to the dispersion equation (5.6) are antisymmetric ones with respect to the angular rate: $\omega_{k,n}(\Omega) = -\omega_{k,n}(-\Omega)$. Each frequency, $\omega_{k,n}$, consists of the antisymmetric, $\omega_{k,n}^{(a)} = -\omega_{k,-n}^{(a)}$, and the symmetric, $\omega_{k,n}^{(s)} = \omega_{k,-n}^{(s)}$, parts, i.e., $\omega_{k,n}(\Omega) = \omega_{k,n}^{(a)} + \omega_{k,n}^{(s)}$. Simple estimations show that $\omega_{k,n}^{(a)} = O(\Omega)$ and $\omega_{k,n}^{(s)} = \omega_{k,n}(0) + O(\Omega^2)$. The antisymmetric part is satisfactorily approximated by the formula (5.8), which determines the wave precession versus the wave number n. It is obvious that in the rest, i.e. $\Omega = 0$, the coupling coefficients (5.5) are antisymmetric functions; $p_{k,n} = -p_{k,-n}$. This causes a formation of a standing mode coupled by a pair of waves traveling in opposite directions with the same frequencies and identical amplitudes, although, this symmetry is broken in a rotating ring. Therefore, standing waveforms cannot exist even at the uniform rotation. However, if the angular rate is small in comparison with the natural frequencies, then one can interpret the wave motion as a slowly precessing standing waveform, because the asymmetry in the coupling coefficients has the same measure as the angular velocity.

Note that the point $n = 0$ corresponds to the axisymmetric radial oscillation. This osculation is typical one for any axially symmetric resonator. This one is not subject to the Coriolis forces at least within the first-order approximation nonlinear analysis[15].

Nonlinear oscillations in a ring

It is subtle to consider a thin circular ring as a simple model of a solid-state wave gyro, when tracing the precession of flexural oscillations in the absence of damping. However, the energy dissipation always presents in practice. Therefore, this requires some external feedback control to supply the wave motion. All the known types of excitation related to the solid-state wave gyro, briefly mentioned in the introduction, are not quite satisfactory from the viewpoint of actuation, driving, or stability properties. Since the linear theory is not able to achieve the desired goal, it is necessary to look for other theoretical tools within the nonlinear wave dynamics. The idea is to use the exclusive property of the axisymmetric mode of the ring to control the amplitude of flexural waves in the gyro in the presence of energy dissipation, just to use this one as a "mediator" in the dynamical process.

[15] The trajectories of points occupying the midline of the ring, involved into the huge uniform rotation, move along the elliptic orbits elongated by the Coriolis forces. The corresponding motions are strictly oriented in the radial direction if the platform is in the rest.

Triple-mode resonant interactions

Let us suppose that the angular rate is small, i.e. $\theta(\tau) \sim \mu$ and $d\theta / d\tau \sim \mu^2$, then the first-order nonlinear approximation solution to Eq. (5.3) can be sought as a resonant triad consisting of the axisymmetric radial oscillation and a pair of quasi-harmonic waves [66–68]:

$$\begin{aligned} v(\tau,\varphi) &= \sum_{k=1}^{3} p_k A_k(T) \exp i\phi_k + \mu v^{(1)}(\tau,\varphi) + O(\mu^2\tau) + (*); \\ w(\tau,\varphi) &= \sum_{k=1}^{3} A_k(T) \exp i\phi_k + \mu w^{(1)}(\tau,\varphi) + O(\mu^2\tau) + (*), \end{aligned} \tag{5.9}$$

where $A_k(T)$ $\left(k = \overline{1,3}\right)$ are the slowly varying complex wave amplitude ($T = \mu\tau$ is the slow time scale); $v^{(1)}$ and $w^{(1)}$ denote nonresonant corrections supposed to be free of secular terms in order $O(T)$; $\phi_1 = n\varphi + \omega_1\tau; \phi_2 = -n\varphi + \omega_1\tau;$ $\phi_1 = \omega_3\tau$ are the fast rotating phases; $(*)$ refers to the complex conjugate of the preceding terms. The frequencies ω_1, ω_2, ω_3 and the wave numbers $\pm n$ satisfy both the dispersion relation (5.7) and the following phase matching conditions

$$\omega_3 = \omega_1 + \omega_2 + \mu\Delta\omega \tag{5.10}$$

where $\Delta\omega$ denotes a small phase matching detuning. The average Lagrangian of the system under consideration is given by the standard formula

$$\langle L \rangle = \left(\frac{1}{2\pi}\right)^3 \int_0^{2\pi}\int_0^{2\pi}\int_0^{2\pi} L d\phi_1 d\phi_2 d\phi_3 . \tag{5.11}$$

Let us suppose that this one can be represented as a formal series in .:

$$\langle L \rangle = \langle L_0 \rangle + \mu\langle L_1 \rangle + \mu^2 \langle L_2 \rangle + ...$$

then the zero-order approximation produces the dispersion relation in the form $\langle L_0 \rangle = 0$ [69]. This means that the term $\langle L_1 \rangle$ describes a nontrivial nonlinear case within the first-order nonlinear approximation analysis. The corresponding average Hamiltonian of the system is following [70]:

$$\langle H \rangle = \sum_{k=1}^{3} A_{k,T} \frac{\partial \langle L_1 \rangle}{\partial A_{k,T}} + \overline{A}_{k,T} \frac{\partial \langle L_1 \rangle}{\partial \overline{A}_{k,T}} - \langle L_1 \rangle .$$

Let the high-frequency mode of the triad be the axisymmetric oscillation at the frequency $\omega_3 = 1$. This high-frequency radial motion is supposed to be in phase with a pair of secondary

flexural modes with the wave numbers $\pm n$, traveling at the same frequencies, $\omega = \omega_1 = \omega_2$, close to $\omega_3 / 2$, accordingly to the phase matching conditions (5.10). In this case, the average Hamiltonian can be rewritten in more detail:

$$\langle H \rangle = 2i \sum_{j=1}^{2} \omega_j \left(\overline{p}_j - p_j \right) \left| A_j \right|^2 + \varepsilon n^2 \left[\overline{A}_1 \overline{A}_2 A_3 \exp\left(i \Delta \omega T \right) + A_1 A_2 \overline{A}_3 \exp\left(- i \Delta \omega T \right) \right]. \tag{5.12}$$

The truncated evolution equations within the first-order nonlinear approximation, generated by the average Hamiltonian (5.12), are the following

$$\begin{aligned}
\frac{dA_1}{dT} &= \frac{2\Omega\left(\overline{p}_1 - p_1 \right)}{1 + p^2} A_1 - \frac{i \varepsilon n^2}{\omega\left(1 + p^2 \right)} \overline{A}_2 A_3 \exp\left(i \Delta \omega T \right); \\
\frac{dA_2}{dT} &= \frac{2\Omega\left(\overline{p}_2 - p_2 \right)}{1 + p^2} A_2 - \frac{i \varepsilon n^2}{\omega\left(1 + p^2 \right)} \overline{A}_1 A_3 \exp\left(i \Delta \omega T \right); \\
\frac{dA_3}{dT} &= -i \varepsilon n^2 A_1 A_2 \exp\left(- i \Delta \omega T \right),
\end{aligned} \tag{5.13}$$

where $p_k = (-1)^k in\left(1 + \varepsilon^2 n^2 \right) / \left(\left(1 + \varepsilon^2 \right) n^2 - \omega^2 \right)$. These coefficients are equal by absolute values, i.e., $p = \left| p_1 \right| = \left| p_2 \right|$, due to the symmetry of the problem. Note that the case under consideration is associated with the principal parametric resonance. After the exchange of variables:

$$\begin{aligned}
A_1 &= a_1 \exp\left(\frac{2\left(\overline{p}_1 - p_1 \right)}{1 + p^2} \int_0^T \Omega(\varsigma) d\varsigma \right); \\
A_2 &= a_2 \exp\left(\frac{2\left(\overline{p}_2 - p_2 \right)}{1 + p^2} \int_0^T \Omega(\varsigma) d\varsigma \right); \\
A_3 &= a_3,
\end{aligned} \tag{5.14}$$

Equations (5.13) can be rewritten as

$$\begin{aligned}
\frac{da_1}{dT} &=_1 - \frac{i \varepsilon n^2}{\omega\left(1 + p^2 \right)} \overline{a}_2 a_3 \exp\left(i \Delta \omega T \right); \\
\frac{da_2}{dT} &= - \frac{i \varepsilon n^2}{\omega\left(1 + p^2 \right)} \overline{a}_1 a_3 \exp\left(i \Delta \omega T \right); \\
\frac{da_3}{dT} &= -i \varepsilon n^2 a_1 a_2 \exp\left(- i \Delta \omega T \right),
\end{aligned} \tag{5.15}$$

One can see that the equations (5.15) are independent upon the angular velocity, Ω, of the base. These equations are similar to the well-known Euler kinematic equations describing the rotations

of a body about a single fixed point, which can be integrated exactly in terms of the Jacobi elliptic functions [8]. These equations describe the so-called break-up instability over the high-frequency mode of the triad with respect to small perturbations from the two low-frequency satellites [66].

Now, let us exploit the axisymmetric mode in the ring as a "mediator" to pump the energy into the driven flexural modes in the presence of energy dissipation.

Forced motion of the resonant triad

Let the energy of dissipation be comparable with the work of the external force exciting the axisymmetric mode in the system (5.3):

$$Q_v = -2\mu\eta\dot{v}; \quad Q_w = -2\mu\left(\eta\dot{w} - Q\cos\varpi\tau\right), \tag{5.16}$$

where η is the damping rate[16]; Q stands for the magnitude of the external harmonic force oscillated at the given frequency ϖ, which is close to that of the axisymmetric mode, i.e., $\varpi - 1 = \mu\delta << 1$, where δ denotes a small detuning. In the absence of damping, the average Hamiltonian (5.12) is modified as it follows

$$\begin{aligned}\left\langle H\right\rangle = 2i\sum_{j=1}^{2}\omega_j\left(\overline{p}_j - p_j\right)\left|A_j\right|^2 + \varepsilon n^2\left[\overline{A}_1\overline{A}_2A_3\exp\left(i\Delta\omega T\right) + A_1A_2\overline{A}_3\exp\left(-i\Delta\omega T\right)\right] - \\ - Q\left[A_3\exp\left(-i\delta T\right) + \overline{A}_3\exp\left(i\delta T\right)\right]/2\end{aligned} \tag{5.17}$$

This produces the evolution equations

$$\begin{aligned}\frac{dA_1}{dT} &= -\eta A_1 + \frac{2\Omega\left(\overline{p}_1 - p_1\right)}{1+p^2}A_1 - \frac{i\varepsilon n^2}{\omega\left(1+p^2\right)}\overline{A}_2A_3\exp\left(i\Delta\omega T\right);\\ \frac{dA_2}{dT} &= -\eta A_2 + \frac{2\Omega\left(\overline{p}_2 - p_2\right)}{1+p^2}A_2 - \frac{i\varepsilon n^2}{\omega\left(1+p^2\right)}\overline{A}_1A_3\exp\left(i\Delta\omega T\right);\\ \frac{dA_3}{dT} &= -\eta A_3 + iQ\exp\left(i\delta T\right)/2 - i\varepsilon n^2A_1A_2\exp\left(-i\Delta\omega T\right),\end{aligned} \tag{5.18}$$

[16] The damping coefficient can be different for each mode of oscillation. The corresponding modification of the model equations does not lead to a new qualitative result.

with allowances for an ad hoc extension related to the dissipative function R , entering the set (5.1). Analogously, after the exchange of variables (5.14), these evolution equations obtain the following form

$$\begin{aligned}
\frac{da_1}{dT} &= -\eta a_1 - \frac{i\varepsilon n^2}{\omega\left(1+p^2\right)}\bar{a}_2 a_3 \exp\left(i\Delta\omega T\right);\\
\frac{da_2}{dT} &= -\eta a_2 - \frac{i\varepsilon n^2}{\omega\left(1+p^2\right)}\bar{a}_1 a_3 \exp\left(i\Delta\omega T\right);\\
\frac{da_3}{dT} &= -\eta a_3 + iQ\exp\left(i\delta T\right)/2 - i\varepsilon n^2 a_1 a_2 \exp\left(-i\Delta\omega T\right),
\end{aligned} \tag{5.19}$$

After the exchange of variables, $a_j(T) = b_j(T)\exp\left(i\varphi_j(T)\right)$, this set (5.19) produces the following equations resolved in the real-valued amplitudes and phases:

$$\begin{aligned}
\frac{db_1}{dT} &= -\eta b_1 + \frac{\varepsilon n^2 b_2 b_3}{\omega\left(1+p^2\right)}\sin\psi;\\
\frac{db_2}{dT} &= -\eta b_2 + \frac{\varepsilon n^2 b_1 b_3}{\omega\left(1+p^2\right)}\sin\psi;\\
\frac{db_3}{dT} &= -\eta b_3 - \varepsilon n^2 b_1 b_2 \sin\psi + Q\sin\left(\delta T - \varphi_3\right)/2;\\
\frac{d\psi}{dT} &= -\Delta\omega + \frac{-2\varepsilon n^2\left(b_1^2\left(\omega\left(1+p^2\right)b_2^2 - b_3^2\right) - b_2^2 b_3^2\right)\cos\psi + \omega b_1 b_2 Q\left(1+p^2\right)\cos\left(\delta T - \varphi_3\right)}{2\omega\left(1+p^2\right)b_1 b_2 b_3};\\
\frac{d\varphi_3}{dT} &= -\varepsilon n^2 b_1 b_2 \sin\psi / b_3 + Q\cos\left(\delta T - \varphi_3\right)/2,
\end{aligned} \tag{5.20}$$

where $\psi(\tau) = \varphi_3(\tau) - \varphi_2(\tau) - \varphi_1(\tau) - \Delta\omega T$ is the generalized phase. It should be noted that these equations can be interpreted as a phenomenological generalization of the evolution equations (5.15) or a structural scheme of the object under the study.

The stationary solutions to Eq. (5.19) consist of two subsets:

$$b_1 = b_2 = 0; \quad b_3 = \frac{K\left(1+p^2\right)\eta\omega}{\varepsilon n^2}, \tag{5.21}$$

and

$$b_1 = b_2 = \frac{\sqrt{2}\sqrt{1+p^2}\sqrt{K-1}}{\varepsilon n^2}; \quad b_3 = \frac{\eta\omega\left(1+p^2\right)}{\varepsilon n^2}, \tag{5.22}$$

where $K = \varepsilon n^2 Q / \left(4\left(1+p^2\right)\eta^2\omega^2\right)$ is the control parameter analogous to the Reynolds number in the hydrodynamics [71, 72]. The first stationary set (5.21) is stable in the range $0 \le K \le K^*$, where $K^* = 1$ denotes the critical value of the bifurcation number. This stationary solution is totally defined by linear properties of the dynamical system (5.3). In turn, at the point K^*, this trivial stationary solution bifurcates, because of loss of stability, and is changed by the new stationary state (5.22), which is stable one as $K > 1$[17]. As the control parameter K is increasing further, the external source pumps the energy into the low-frequency flexural modes across the high-frequency axisymmetric mode (Fig. 5.5). This makes an effective nonlinear mechanism of energy transfer. The intensity of the low-frequency flexural modes increases with the number K, while the amplitude of the high-frequency axisymmetric mode b_3 is saturated at the constant level $b_3 = \eta\omega\left(1+p^2\right)/\varepsilon n^2$. It is not difficult to verify that the system (5.19) has no any bifurcation, if any low-frequency mode is subject to the direct resonant excitation.

When passing to the old variables of the problem, the corresponding solution obtains the following form

$$\begin{aligned} v(\tau,\varphi) &= -4pb_1\cos\left(\psi(\tau)-n\varphi\right)\cos\left(\omega+\mu\left(\frac{\delta+\Delta\omega}{2}\right)\right)\tau + O\left(\mu^2\tau\right); \\ v(\tau,\varphi) &= -4b_1\sin\left(\psi(\tau)-n\varphi\right)\cos\left(\omega+\mu\left(\frac{\delta+\Delta\omega}{2}\right)\right)\tau - 2b_3\sin\varpi\tau + O\left(\mu^2\tau\right), \end{aligned} \tag{5.23}$$

where $\psi(\tau) = \dfrac{4p}{1+p^2}\int_0^\tau \Omega(\varsigma)d\varsigma$ is the precession rate.

[17] The system under consideration though being stable nonetheless is not Gurwitzian one, since the phase of the precessing flexural mode is an arbitrary value. For instance, the following set of phases: $\varphi_1 = -\pi/2 + \delta T/2 + \Delta\omega T/2$, $\varphi_1 = -\pi/2 + \delta T/2 + \Delta\omega T/2$, $\varphi_1 = -\pi/2 + \delta T$ is appropriate as a solution. Though, the equality $\psi = \pi/2$ should be always fixed.

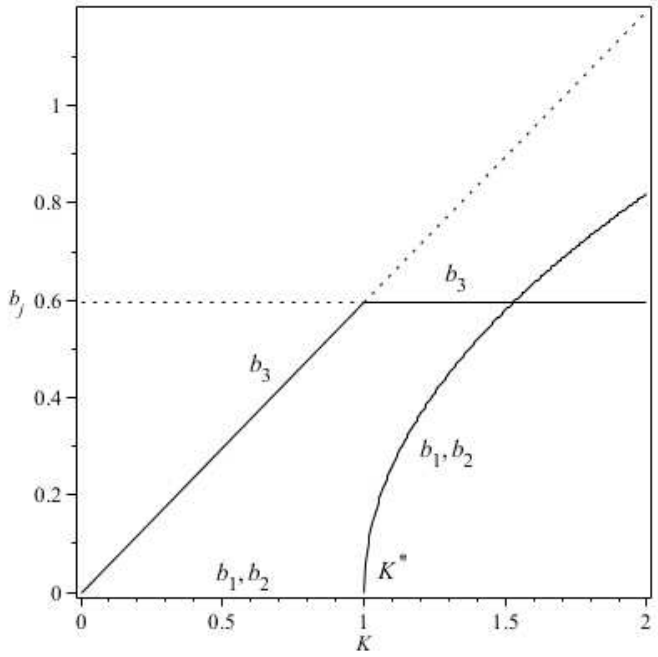

Fig. 5.5 Mode $n = 7$. The bifurcation diagram (η=0.1, ε=0.01, κ=0.45)

Typical frames of the wave precession, accordingly to these expressions, are shown in Fig. 5.6. Here, the stiffness κ is tuned into the triple-wave resonance over the seventh flexural mode.

Two resonant triads are in phase

Let us suppose that the stiffness .increases. This means that at least one more triad can be involved into the nonlinear resonant coupling. In this case, the substitution to Eq. (5.3) has the following form

$$\begin{aligned} v(\tau,\varphi) &= \sum_{k=1}^{5} p_k A_k(T)\exp i\phi_k + \mu v^{(1)}(\tau,\varphi) + O\left(\mu^2\tau\right) + (*); \\ w(\tau,\varphi) &= \sum_{k=1}^{5} A_k(T)\exp i\phi_k + \mu w^{(1)}(\tau,\varphi) + O\left(\mu^2\tau\right) + (*), \end{aligned} \tag{5.24}$$

where $A_k(T)$ $\left(k = \overline{1,5}\right)$ are the slowly varying complex amplitudes (the amplitude subset $\{A_1, A_2, A_3\}$ composes the first triad, while $\{A_3, A_4, A_5\}$ enters the second one); the wave numbers n_1 and n_2 refer to the first and the second triad, correspondingly; $\phi_1 = n_1\varphi + \omega_1\tau$, $\phi_2 = -n_1\varphi + \omega_1\tau$, $\phi_3 = \omega_3\tau$, $\phi_4 = n_2\varphi + \omega_2\tau$, $\phi_5 = -n_2\varphi + \omega_2\tau$ are the fast rotating phases.

Let the set of frequencies $\{\omega_1, \omega_2, \omega_3\}$ and the wave numbers $\pm n_1$ satisfy both the dispersion relation (5.7) and the following phase matching conditions

$$\omega_3 = \omega_1 + \omega_2 + \mu\Delta\omega_1, \tag{5.25}$$

where $\Delta\omega_1$ denotes a small phase matching detuning. Almost the same conditions are valid for the second set of frequencies $\{\omega_3, \omega_4, \omega_5\}$:

$$\omega_3 = \omega_4 + \omega_5 + \mu\Delta\omega_2 . \tag{5.26}$$

Figure 5.7 displays graphically the phase matching conditions when the system parameters are specially tuned into the double triple-wave resonance over the modes number two and seven.

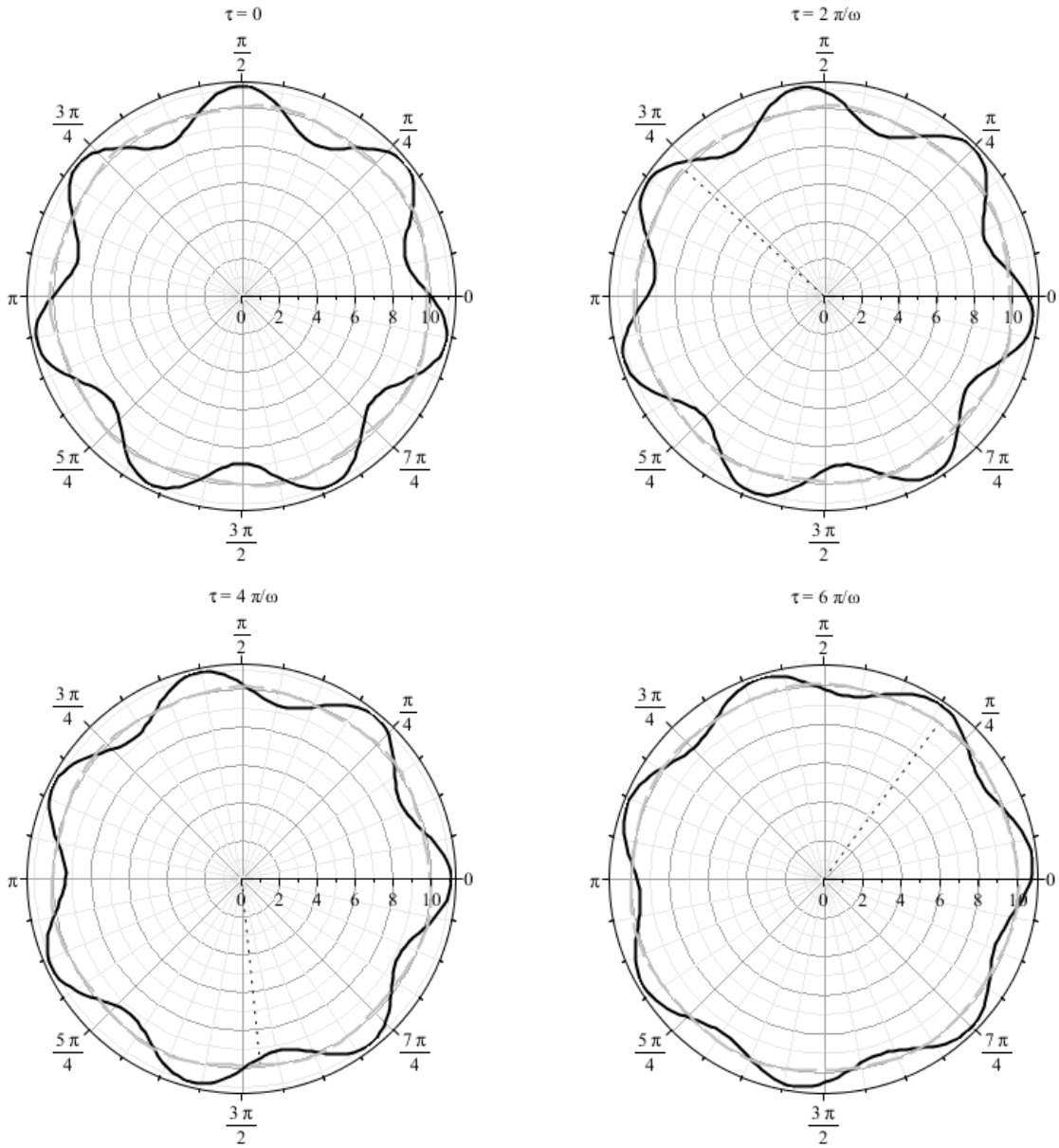

Fig. 5.6 The wave precession. Modal number $n = 7$. Solid lines refer to flexural mode, while the dashes to the circumferential one (η=0.1, $\mu = \varepsilon$=0.01043764232, κ=0.45, Ω=0.085, Q=0.1). The dotted radius indicates the rotation angle $\Omega\tau$.

In this case, the corresponding average Hamiltonian (5.17) may be modified as it follows

$$\langle H\rangle = 2i\sum_{j=1}^{2}\omega_j\left(\overline{p}_j - p_j\right)\left|A_j\right|^2 + \varepsilon n_1^2\left[\overline{A}_1\overline{A}_2A_3\exp\left(i\Delta\omega_1 T\right) + A_1A_2\overline{A}_3\exp\left(-i\Delta\omega_1 T\right)\right] +$$
$$+ 2i\sum_{j=1}^{2}\omega_j\left(\overline{p}_j - p_j\right)\left|A_j\right|^2 + \varepsilon n_1^2\left[\overline{A}_4\overline{A}_5A_3\exp\left(i\Delta\omega_2 T\right) + A_4A_5\overline{A}_3\exp\left(-i\Delta\omega_2 T\right)\right] -$$
$$- Q\left[A_3\exp\left(-i\delta T\right) + \overline{A}_3\exp\left(i\delta T\right)\right]/2.$$

This one produces the evolution equations, analogous to the set (5.18):

$$\frac{dA_1}{dT} = -\eta A_1 + \frac{2\Omega\left(\overline{p}_1 - p_1\right)}{1+\left|p_1\right|^2}A_1 - \frac{i\varepsilon n_1^2}{\omega_1\left(1+\left|p_1\right|^2\right)}\overline{A}_2A_3\exp\left(i\Delta\omega_1 T\right);$$
$$\frac{dA_2}{dT} = -\eta A_2 + \frac{2\Omega\left(\overline{p}_2 - p_2\right)}{1+\left|p_2\right|^2}A_2 - \frac{i\varepsilon n_1^2}{\omega_1\left(1+\left|p_2\right|^2\right)}\overline{A}_1A_3\exp\left(i\Delta\omega_2 T\right);$$
$$\frac{dA_3}{dT} = -\eta A_3 + iQ\exp\left(i\delta T\right)/2 - i\varepsilon n_1^2A_1A_2\exp\left(-i\Delta\omega_1 T\right) - i\varepsilon n_2^2A_4A_5\exp\left(-i\Delta\omega_2 T\right); \qquad (5.27)$$
$$\frac{dA_4}{dT} = -\eta A_4 + \frac{2\Omega\left(\overline{p}_4 - p_4\right)}{1+\left|p_4\right|^2}A_4 - \frac{i\varepsilon n_2^2}{\omega_2\left(1+\left|p_4\right|^2\right)}\overline{A}_5A_3\exp\left(i\Delta\omega_2 T\right);$$
$$\frac{dA_5}{dT} = -\eta A_5 + \frac{2\Omega\left(\overline{p}_5 - p_5\right)}{1+\left|p_5\right|^2}A_5 - \frac{i\varepsilon n_2^2}{\omega_2\left(1+\left|p_5\right|^2\right)}\overline{A}_4A_3\exp\left(i\Delta\omega_2 T\right);$$

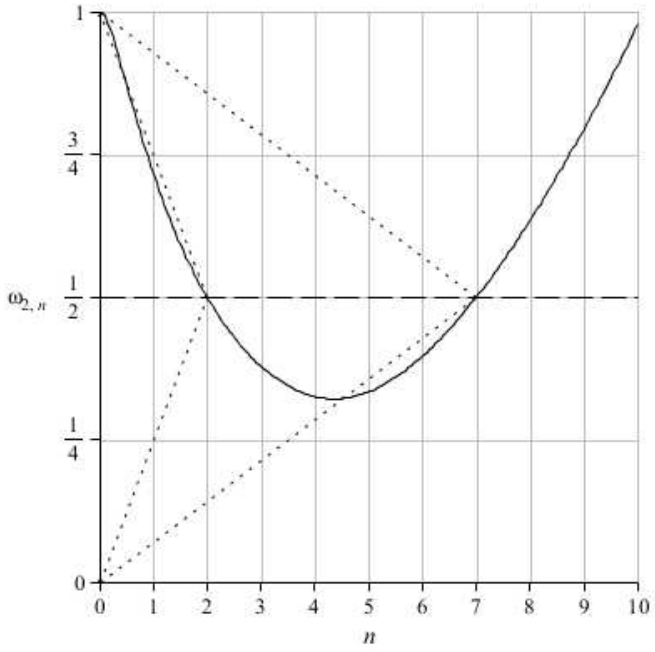

Fig. 5.7 Low-frequency dispersion branch. Triple-wave phase matching. The modes numbers $n_1 = 7$ and $n_2 = 2$ are in phase with the axisymmetric radial oscillation (η=0.1, ε=0.0098, κ=1.25)

The stationary solutions to Eq. (5.19) consist of three subsets:

$$b_1 = b_2 = 0; \quad b_3 = \frac{K_1\left(1+p_1^2\right)\eta\omega_1}{\varepsilon n_1^2}, \tag{5.28}$$

$$b_1 = b_2 = \frac{\eta\sqrt{\omega_1}\sqrt{1+p_1^2}\sqrt{K_1-1}}{\varepsilon n_1^2}; \quad b_3 = \frac{\eta\omega_1\left(1+p_1^2\right)}{\varepsilon n_1^2}, \tag{5.29}$$

$$b_4 = b_5 = \frac{\eta\sqrt{\omega_4}\sqrt{1+p_2^2}\sqrt{K_2-1}}{\varepsilon n_2^2}; \quad b_3 = \frac{\eta\omega_2\left(1+p_2^2\right)}{\varepsilon n_2^2}, \tag{5.30}$$

where $K_1 = \varepsilon n_1^2 Q/\left(2\left(1+p_1^2\right)\eta^2\omega_1\omega_3\right)$ and $K_2 = \varepsilon n_2^2 Q/\left(2\left(1+p_2^2\right)\eta^2\omega_3\omega_4\right)$ are the control parameters corresponding to the first and second triads, respectively. The first stationary set (5.28) is stable in the range $0 \le K_1 \le K_1^*$, where $K_1^* = 1$ denotes the critical value of the bifurcation number. This stationary solution is also defined by linear properties of the dynamical system (5.3), as in the case discussed above. Near the point K_1^* the set (5.28), as it is expected, loses stability and is changed by the new stationary state (5.29), which would be stable one at $K_1 > 1$. At the same time, together with the parameter K_1, the control parameter K_2 increases up to its critical value K_2^*, though the system has no any reaction. This means that the stationary set (5.30) is unstable one, because the critical value K_2^* is reached at much more large magnitude of the external force Q in comparison with that of the value K_1^* (Fig. 5.8). The first triad (the precessing wave number $n_1 = 7$) would always dominate under the second triad (the wave number $n_2 = 2$). Therefore, the typical frames of the wave precession would be similar to those illustrated in Fig. 5.6. So that one may conclude that the stiffness κ can be effectively used to tune the gyro in the triple-wave resonance.

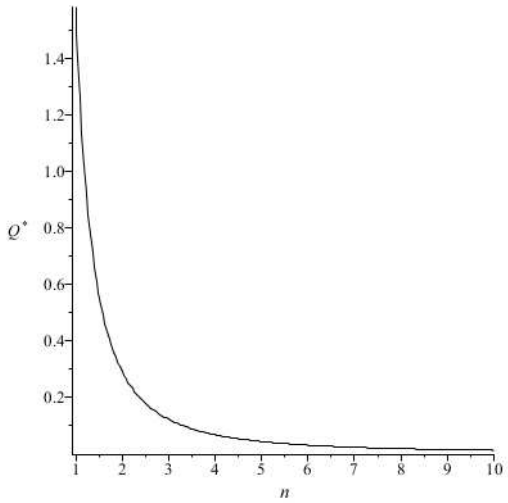

Fig. 5.8 The critical force magnitudes Q^* versus the wave number n (η=0.1, ε=0.0098, κ=1.25)

Resume

Long ago, in 1851, Foucault demonstrated that a pendulum could be used as a vibratory gyro. The wave precession phenomenon caused by rotation of thin-walled cylinders and bells was first discovered and analytically described by Bryan [55]. This physical effect has inspired, in the 1960s, development of a thin-walled hemispherical solid-state gyro. The fused-quartz hemispherical resonator of the wave gyro is naturally actuated and sensed using modern MEMS-technologies, following a concept of the rate integrating sensor [54]. Gyro units based on resonators with high Q-factors have achieved a significant performance in the competition with their laser analogs. Today, the related technologies are evoked within a lot of commercial projects through the development of micromachined gyros.

One more type of wave excitation in a wave solid-state gyro has been proposed in this study, when tracing the breakup instability of the high-frequency mode entering the triple-wave resonant ensemble. This case combines simultaneously both the advantages of the positional and the parametric types of wave excitation. It was shown that the equations governing the evolution of the amplitude envelopes in the resonant triad, written in a special nonstationary frame of reference, do not depend implicitly upon the angular velocity of the ring. The breakup instability of the high-frequency axisymmetric mode in the resonant triplet gives arise to slowly precessing flexural waves in the presence of energy dissipation. A characteristic number as a dimensionless combination of system parameters, including the magnitude of the periodic external force, damping coefficient, and the nonlinearity, are revealed. This number controls the bifurcation of oscillatory patterns, when the system passes through a certain critical value, analogously to the Reynolds number in the hydrodynamics. Tracing the patterns of the precessing flexural modes, one can be judges on the angular position of the rotating ring in the absolute space. Note that the nonlinear model of the gyro described in this study requires no any extremely high Q-factor of the resonator, or some feedback control, as well. This model assumes that the gyro can be tuned in the given precessing regime by controlling the stiffness between the ring resonator and the rotating platform.

SELF-EXITED RESONANT BOLOMETER

Recent cosmology experiments have revealed an accelerated expansion of the Universe and anisotropies in the Cosmic Microwave Background radiation. There are known several cosmology instruments such as balloon telescope BOOMERanG, OLIMPO, B-POL etc., for detecting relict Big Bang waves. The experimental observations inspire novel challenges in theoretical scenarios based on accurate measurements using modern ultra-sensitive detectors. The resonant bolometer, proposed as a mathematical model in the present paper, seems to be one of such promising tools. Moreover, analogous superconducting devices exhibit some promising routes to quantum computations in the recent years.

We study a model of the resonant bolometer converting the electromagnetic radiation energy into thermal one with the help of a heat sensor integrated into a high-quality resonant circuit. Self-excited oscillations in the resonant circuit are supported by a low-noise periodic generator based on physical properties of a Josephson junction. A heat sensor, implemented into the resonant circuit, passes from the superconducting state to the resistive phase under the incoming pulse. The operating temperature of all the sensitive parts of the bolometer is set slightly below the superconducting edge. The measurement procedure is to trace the amplitude and phase modulation at the absorption of the incoming infrared radiation. The sensitivity of this sensor at conventional material parameters would be evaluated as $10^{-12}\,[W]$ by the power input.

The main objective of this chapter is to provide one more idea for the accurate identification of a weak infrared radiation. From a viewpoint of the theory oscillations, the self-exited resonant bolometer can be treated as a self-exited oscillatory system possessing more than two degrees of freedom. In spite of some complexity in a theoretical description, the numerical modeling leads to a conclusion that this system is extremely simple, since any chaotic motion, inherent in complex nonlinear dynamical systems, has not been observed yet. Point out that this is a fairly rare case in the theory of oscillations. It means that, on the one hand, we have got a simple self-exited system characterized by regular dynamics, while, on the other hand, the model of the self-excited resonant bolometer possesses a negative feedback which creates most optimal preconditions for a quickest cooling of the sensor. This would lead to a technical result which improves the sensitivity, accuracy and stability by reducing the measurement errors up to the level limited by thermal fluctuations. The latter circumstance creates perspectives for more efficient identification of unknown parameters in the incoming electromagnetic radiation.

Voltage-temperature circuits

We should note that any conventional bolometer almost always operates using a DC biasing. This represents almost linear systems investigated by tools of spectral methods. Therefore, there is no place to apply the modern theory of nonlinear oscillations. Probably this is caused, on the one hand, by an attractive simplicity of sensors, while, on the other hand, – by advances in nanotechnology, trying to modify the existing models up to ideal limits predicted by the noise theory. The recent actual studies [73–77] deal with the periodically forced models of sensors, based on approaches inherent in nonlinear resonant systems. Point out that the periodical pumping is modeled therein just as trigonometric functions. Although, we should remember that this is power source of additional noise in practice, inherent in any conventional generator of periodical electric signals. Here, we try to overcome this deficiency by combining the DC biasing with the periodical pumping due to the self excitation mechanism. Finally, recent developments in the nanotechnology allow supposing that the dynamical sensors would really take place of traditional sensors.

First, we consider the dynamics of a conventional bolometer represented by an electrically biased Thévenin's circuit. This circuit, connected in series, consists of a bias voltage U_b, an ordinary resistor r, an inductance L and a transition-edge-sensor (TES). Changes in temperature result in changes of the current flowing through the TES-sensor, playing the role of the thermometer whose resistance depends upon the temperature T. At low temperatures, the electrical resistance $\rho(T)$ is zero. Near the critical temperature T_0, the resistance increases together with the temperature. At ambient temperatures, the TES-sensor has a normal resistance ρ_0. The inductance L includes, together with a parasitic one, the inductance of a SQUID interferometer. The electrical capacitance c is neglected in this model.

Let the circuit be biased by nearly constant voltage, at least, at the frequencies lower than the characteristic reciprocal time $(r+\rho)/L$. This also assumes that the resistance r is small enough compared to the resistance ρ_0, otherwise the current biasing would be suitable instead the voltage bias U_b. Therefore, this circuit is described by the following equation:

$$L\frac{dj}{dt} = U_b - j(r+\rho(T)), \tag{6.1}$$

where $j = j(t)$ is the current; t denotes the time. It is supposed that the TES-sensor is integrated with the absorber. The absorber cools into a thermostat having the temperature $T_0 - \Delta T$, where

ΔT is a small temperature detuning, slightly under the sensor phase-transition edge characterized by the value T_0. The Joule heat elevates the temperature of both the TES-sensor and absorber, some above the bath temperature, and dissipates the energy of the conductivity electrons. There is always a finite voltage drop in the direction of the current flow because of the electrical resistance. The useful heating is inspired by the incoming power, described here as a narrow external pulse $P(t)$, and approximated as the Dirac-type function having a small dispersion in the time scale. Thus, the governing equation of the thermal circuit is the following

$$C\dot{T} = R(T)j^2 - Q(T - T_0 + \Delta T) + P(t), \tag{6.2}$$

where $C = \gamma V$ is the heat capacity (γ stands for the volumetric heat capacity; V is the volume of the absorber); Q denotes the thermal conductivity characterizing a cooling rate into the thermostat.

Conductivity electrons are scattered in a random fashion by imperfections in material, and take part in the energy exchange between thermal phonons. Thus, the energy is converted into heat, accordingly the second law of thermodynamics. At ambient temperatures, the resistance is caused by inelastic collisions between electrons and thermal phonons, while the thermal phonons are almost absent at lower temperatures. As the temperature is decreased, the resistance also decreases, and the resistance takes place due to the scattering on impurities, in general. Consequently, the clearance of materials is worth for the bolometer sensitivity. The bolometer efficiency depends also upon the volume, not only upon the quality of a material of the absorber. Naturally, the geometry of the absorber should provide best energy resolution. On the one hand, the absorber design should tend to decrease the heat capacity, while on the other hand, the increasing heat conductivity facilitate a cooling of the absorber together with decreasing the relaxation time.

The electrical resistance at ambient temperatures is caused by the electron-phonon coupling. The electrons are subject to many random collisions with thermal phonons. As a result, the random exchange of energy between the electric current and the thermal reservoir is experienced. In the absence of the net current, the electron gas has the same temperature as the gas of thermal phonons. Consequently, the fluctuations are zero in average, because the system is in the equilibrium. These fluctuations appear as electric noise in conductors. There is a fundamental relationship between the mean-square noise voltage and the electrical resistance at the given temperature:

$$\left\langle |U|^2 \right\rangle = 4k_B TR\Delta f \ ,$$

where $k_B = 1.38059\times10^{-23}\left[m^2 kg/s^2 K\right]$ is the Boltzmann constant; T is the temperature of the resistor R; Δf denotes the frequency bandwidth. The mean noise voltage U is zero. This noise, called as the Johnson noise [78, 79], represents an ordinary "white noise". Its intensity directly depends upon the temperature. Naturally, the real noise would be somewhat larger than the fundamental Johnson noise because of variety of physical effects, such as a tunneling of electrons or random magnet flux in a superconductor, etc.

Example

Let us consider the set of equations just discussed above:

$$L\frac{dj}{dt} = U_b - \left(\rho(T) + r\right)j; \quad V\gamma\frac{dT}{dt} = \rho(T)j^2 - Q\left(T - T_0 + \Delta T\right) + P(t). \tag{6.3}$$

Here $\rho(T) = \rho_0\left(1 + \mathrm{e}^{-4(T-T_0)/\Delta}\right)^{-1}$ is the TES-sensor resistance, characterized by is the resistance at the normal state ρ_0; Δ characterizes the rate of the phase transition between the normal and superconductive states; $P(t) = P_0\,\mathrm{sech}\left((t-t_0)/D\right)$ is the incoming power. Let us suppose that $\Delta = 0.5[K]$; $D = 0.5[s]$; $t_0 = 25[s]$ (Fig. 6.1). The other system parameters are the following: $T_0 = 3.5[\mathrm{K}]; \Delta T = 0.3[\mathrm{K}]$; $Q = 10^{-7}[W/K]$; $L = 0.5[\mathrm{H}]$; $\gamma = 5\times10^{-2}[sW/Km^3]$; $r = 10^{-1}[\Omega]$; $\rho_0 = 1.0[\Omega]$; $V = 10^{-5}[m^3]$.

The initial conditions to the correspondent Cauchy problem (6.3) are defined from the equilibrium:

$$U_b - \left(\rho_0\left(1 + \mathrm{e}^{-4(T-T_0)/\Delta}\right)^{-1} + r\right)j = 0; \quad \rho_0\left(1 + \mathrm{e}^{-4(T-T_0)/\Delta}\right)^{-1} j^2 - Q\left(T - T_0 + \Delta T\right) = 0.$$

Let the voltage be a given constant $U_b = 1.0\times10^{-8}[V]$ at the initial temperature $T(0) \approx 3.2[K]$, then the stationary current should be equal to $j(0) = 6.0\times10^{-8}[A]$.

After the transform: $t = (L/\rho)\tau$; $j(t) = (U_b/\rho)J(\tau)$; $T(t) = (T_0 - \Delta T)\Theta(\tau)$, the set (6.3) can be expressed in terms of new dimensionless coordinates:

$$\frac{dJ}{d\tau} = 1 - \left(\tilde{\rho}(\Theta) + r\right)J/\rho; \quad \frac{d\Theta}{d\tau} = \frac{L}{V\gamma\rho}\left(\frac{\tilde{\rho}(\Theta)U_b^2 J^2}{\rho^2\left(T_0 - \Delta T\right)} + \frac{\tilde{P}(\tau)}{\left(T_0 - \Delta T\right)} - Q(\Theta - 1)\right), \tag{6.4}$$

where $\widehat{P}(\tau) = P_0 \operatorname{sech}\left(\frac{L}{\rho D}(\tau - \rho t_0 / L)\right)$ and $\widehat{\rho}(\Theta) = \rho\left(1 + \mathrm{e}^{-4((T_0 - \Delta T)\Theta(\tau) + T_0)/\Delta}\right)^{-1}$.

Let us consider a perturbed version of Eq. (6.1) in the resistive state:

$$L\frac{dj}{dt} = U_b - j(r+\rho) + \int_{-\infty}^{\infty} U_\omega \exp(i\omega t + \varphi_\omega) d\omega,$$

where U_ω is a contribution of the voltage noise at the given frequency ω; φ_ω are arbitrary phases.

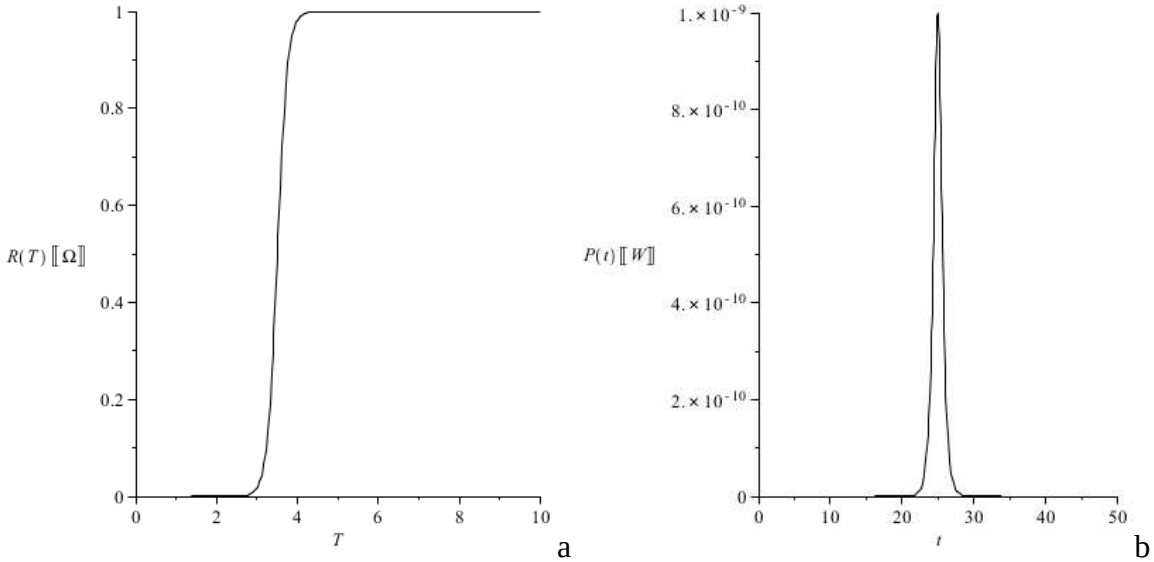

a b

Fig. 6.1 The resistance the TES sensor vs. the temperature (a) and the incoming power vs. the time (b)

Therefore, a spectral component of the current noise is expressed as $j_\omega = U_\omega / (r + \rho + i\omega L)$. To define the output noise, one must integrate this function over the total frequency range. The mean square of the total random current reads

$$\frac{1}{2\pi}\int_{-\infty}^{\infty} |j_\omega|^2 d\omega = \frac{1}{2\pi}\int_{-\infty}^{\infty} \frac{|U_\omega|^2 d\omega}{(r+\rho)^2 + (\omega L)^2} = \frac{4k_B T \Delta f}{r+\rho},$$

or, that is the same

$$\frac{2k_B T}{L} = \frac{4k_B T \Delta f}{r+\rho}.$$

Here $\Delta f = (r+\rho)/2L$ is the noise bandwidth, expressed in Hertz. This means that the total voltage mean square $\left\langle |U|^2 \right\rangle = 4k_B T(R+r)\Delta f$ is evaluated as $\sqrt{\left\langle |U|^2 \right\rangle} \approx 1.9\times 10^{-11}[V]$, in our above numerical example. Thus, the corresponding noise bandwidth would be about $5\,[Hz]$.

Moreover, the temperature fluctuations $\left\langle |\theta|^2 \right\rangle = k_B T^2 / V\gamma$ take place in any small body possessing the thermal capacity $C = V\gamma$ at the temperature T. This fundamental contribution always limits a best obtainable resolution by noise caused by intrinsic thermal fluctuations. This one is estimated as almost negligible value $\sqrt{\left\langle |\theta|^2 \right\rangle} = 1.8\times 10^{-8}[K]$, in our numerical example. Thus, the set of the modified equations (6.3) reads as it follows

$$L\frac{di}{dt} = U_b - \left(\rho(\hat{T}) + r\right)i + \xi_1(t); \quad \frac{d\hat{T}}{dt} = \left(\rho(\hat{T})i^2 - Q(\hat{T} - T_0) + P(t)\right)/V\gamma,$$

where $\xi_1(t) = \eta_1(t)\sqrt{4k_B\hat{T}(t)\left(\rho(\hat{T}) + r\right)\Delta f}$ and $\xi_2(t) = \eta_2(t)\sqrt{k_B\hat{T}^2(t)/V\gamma}$ are independent random functions. The perturbed temperature $\hat{T}$ is resulted after the transform $T(t) \to \hat{T}(t) + \xi_2(t)$. The mean values of the functions $\xi_1(t)$ and $\xi_2(t)$ are zeroes and possess the Dirac function correlations. The result of the numerical experiment, shown in Fig. 6.2, explains roughly the basic noise effect on the sensitivity of the bolometer (the magnitude of the incoming power P_0 is scanned from $10^{-11}\,[W]$ to $10^{-9}\,[W]$).

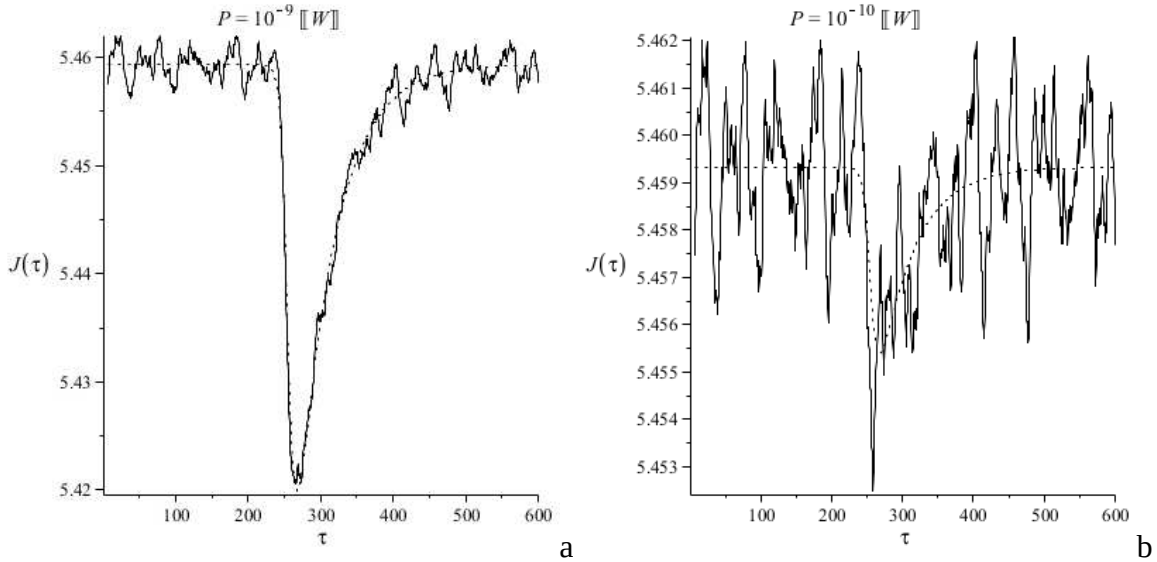

a b

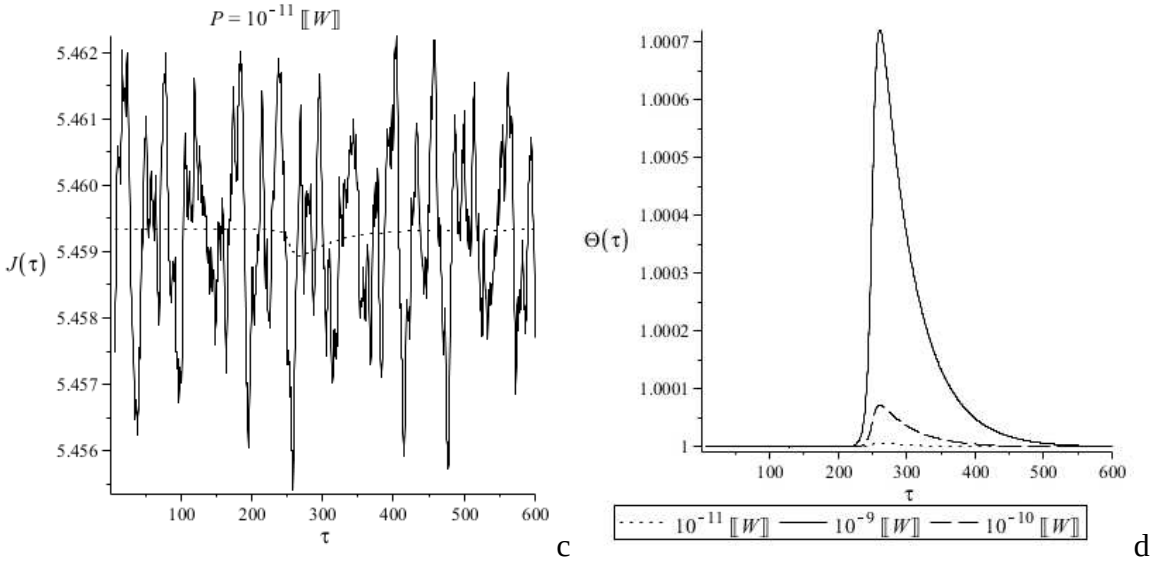

c d

Fig. 6.2 The current and temperature across the TES-sensor vs. the dimensionless time. The regular component of the response, depicted by point lines, becomes almost undistinguished at the current noise background together with decreasing the incoming power signal – (a, b, c). The temperature change by scanning the incoming power – (d)

Van der Pol generator with a TES-sensor

Van der Pol generator represents a classic model in the theory of nonlinear oscillations, in physics, electronics, biology, neurology, sociology, etc. The governing equation has been studied over wide parameter regimes, beginning from quasi-harmonic patterns to relaxation oscillations. Van der Pol generator is a simplest self-exited system that may be modified to investigate much more complicated nonlinear systems.

Let the electrical circuit of a bolometer is consistent with the van der Pol generator, though the TES sensor is used there instead of the normal resistor. Then the governing equations can be written as it follows

$$\begin{aligned} &L\frac{dj}{dt} + q/c + \rho j = -\varepsilon\left(q^2 - \delta\right); \quad \frac{dq}{dt} = j; \\ &V\gamma\frac{dT}{dt} = \rho j^2(t) - Q\left(T - T_0 + \Delta T\right) + P(t), \end{aligned} \tag{6.5}$$

Thus, the electric circuit consists of a resistor $\rho(T) = \rho_0\left(1 + \mathrm{e}^{-4(T-T_0)/\Delta}\right)^{-1}$ possessing superconductive properties at low temperatures beneath the value T_0; an inductance L; a capacitor c; all connected in series. The parameters ε and δ, inherent in any van-der-Pol generator, are respective for a self-excited biasing. The equation describing the heat circuit is the same as described in the previous sections.

The dynamical variables of the system are the temperature of the TES-sensor $T(t)$; the current flowing through this one $j(t)$, evolved in the time t. The TES-sensor plays as the thermometer. Changes in the temperature result in the evolution of the amplitude envelope of the current, under the incoming power $P(t) = P_0 \operatorname{sech}((t - t_0)/D)$. The inductance L is supposed to include that of a SQUID coil, for measurements.

After the transfer from the actual variables to the polar coordinates: $q(t) = A(t)\sin(\omega t + \varphi(t))$; $j(t) = \omega A(t)\cos(\omega t + \varphi(t))$, and the averaging over the fast rotating phases, Eq. (6.5) are rearranged into the following form

$$\dot{A} = -A\left[4(\rho - \varepsilon\delta) + \varepsilon A^2\right]/8L; \quad \dot{\varphi} = 0;$$

$$\dot{T} = \left[\rho\omega^2 A^2 - Q(T - T_0 + \Delta T) + P(t)\right]/\gamma V,$$

where $\omega = 1/\sqrt{cL}$ is the frequency of the electric circuit in the absence of resistance and excitation.

Let us suppose that that the normal resistance is large enough, i.e., $\rho_0 > \varepsilon\delta$. If the initial value of the amplitude is equal to 0 or $2\sqrt{\delta}$, then the amplitude $A(\tau)$ remains the same for all the time in the absolute absence of perturbations. However, it is well known that the stationary solution $A(\tau) = 0$ exhibits unstable properties at $\rho \sim 0$ (the superconductive state), while the same trivial state becomes stable one at the normal resistance $\rho \sim \rho_0$.

At the superconducting state, the stationary amplitude of oscillations is saturated, i.e., $A(t) = 2\sqrt{\delta}$. At the time $t = t_0$, the resistor ρ, under the incoming power $P(t)$, passes from the superconducting state, $\rho \sim 0$, to the resistive phase, $\rho \sim \rho_0$. Let us suppose that the phase transition between the superconducting and the resistive states of the system is performed beginning from the point $t = t_0$. Then the amplitude would relax beginning from the value $2\sqrt{\delta}$, and almost to zero, following the time history

$$a(\tau) = \frac{2\sqrt{\rho_0 - \varepsilon\delta}\exp(-(\rho_0 - \varepsilon\delta)(\tau - t_0)/2)\sqrt{\delta}}{\sqrt{\rho_0 - \exp(-(\rho_0 - \varepsilon\delta)(\tau - t_0))\varepsilon\delta}}.$$

Some definite time Δt is necessary to heat and then to cool the absorber up to the superconductive temperature. After the absorption of the incoming power, the resistor ρ returns from the resistive state to the initial stable stationary superconducting state, and the amplitude evolves accordingly to the following law

$$b(t)=\frac{2\exp(\varepsilon\delta(\tau+\Delta t-t_0)/2)\sqrt{\delta}a(t_0)}{\sqrt{(\exp(\varepsilon\delta(\tau+\Delta t-t_0))-1)a^2(t_0)+4\delta}}.$$

The locus between the curves $a(\tau)$ and $b(\tau)$, defined by the equation $a(\tau)=b(\tau)$, at some point $t=t_1$, defines an approximate solution to the problem in the form of the following piecewise function, $A(\tau)=\{a(\tau),\quad \tau<t_1; b(\tau),\quad \tau\geq t_1\}$, shown in Fig. 6.3. Here, the system parameters are selected in arbitrary units: $T_0=3.5$, $\Delta T=0.1$, $P_0=10^{-2}$, $\Delta=0.05$, $D=0.5$, $\gamma=0.05$, $V=1$, $Q=0.035$, $L=1$, $\rho=0.8$, $\omega=1$, $\delta=0.01$, $\varepsilon=0.035$.

One can conclude that the stable stationary solution is zero at the resistive state, i.e., $A=0$, while the stationary amplitude would be equal to $A=2\sqrt{\delta}$ at the superconducting state. The time interval, defining the transition between these two states in the system, is governed by the following heat balance equation

$$\dot{T}=\begin{cases}-Q(T-T_0)/\gamma V, & \tau<t_0;\\ \left[\rho\omega^2 b^2(\tau)-Q(T-T_0)\right]/\gamma V+P(\tau)/\gamma V, & t_1>\tau\geq t_0;\\ -Q(T-T_0)/\gamma V; & \tau\geq t_1.\end{cases}$$

This is a linear nonautonomous equation which can be easily integrated (Fig. 6.4).

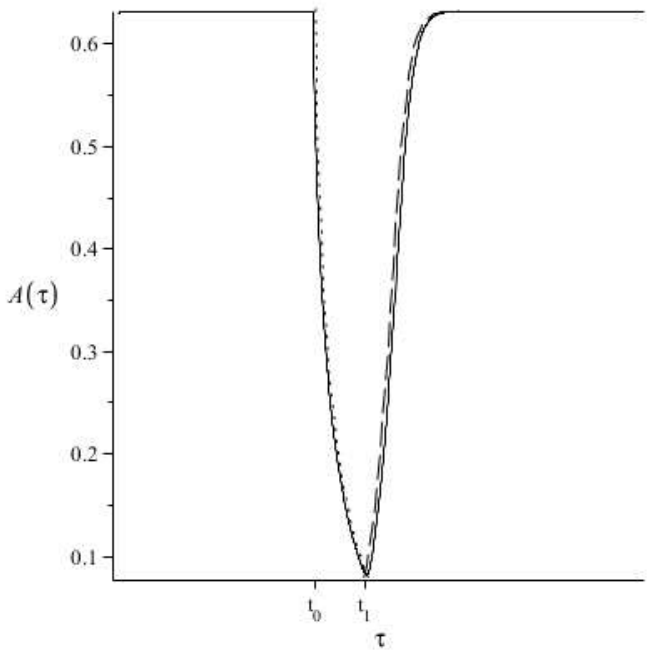

Fig. 6.3 Amplitude envelope vs. time in a comparison between the exact (solid line) and approximate solutions (dotted and dash lines)

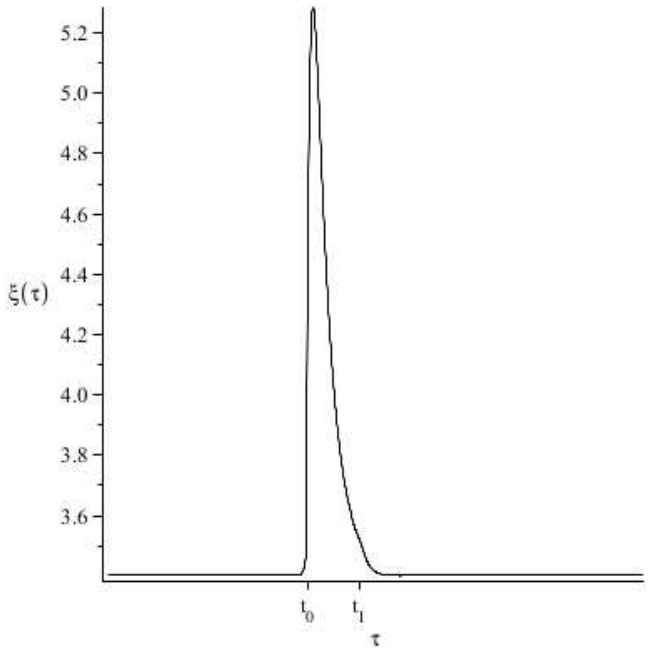

Fig. 6.4 Temperature vs. time

Figures 6.3 and 6.4 explain that the single undefined parameter of the problem is the time interval of absorption $\Delta t = t_1 - t_0$. This one can be defined experimentally using above formulae by solving the inverse problem.

Example

Let the realistic system parameters be the following: $T_0 = 3[K]$, $\Delta T = 0.1[K]$, $P_0 = 10^{-10}[W]$, $\Delta = 0.05\|K\|$, $D = 0.35[s]$, $\gamma = 0.5[sW/Km^3]$, $V = 10^{-11}[m^3]$, $Q = 10^{-11}[W/K]$, $L = 2{,}5\times 10^{-10}[H]$, $\rho = 10^{-11}[\Omega]$, $c = 0.95\times 10^{10}[F]$, $\delta = 0.9[C^2]$, $\varepsilon = 0.35\times 10^{-10}[\Omega/C^2]$.

After the transform $t = \sqrt{cL}\tau$; $T(t) = (T_0 - \Delta T)\Theta(\tau)$; $q(t) = \sqrt{\delta}x(\tau)$; $i(t) = \sqrt{\delta}y(\tau)/\sqrt{cL}$, Eq. (6.5) can be rewritten as

$$\begin{aligned}
&\frac{dx}{d\tau} = y;\\
&\frac{dy}{d\tau} = -x - \hat{\rho}(\Theta)\frac{\sqrt{c}}{\sqrt{L}}y + \varepsilon\delta\frac{\sqrt{c}}{\sqrt{L}}\left(y - x^2\right);\\
&\frac{d\Theta}{d\tau} = \frac{\hat{\rho}(\Theta)\delta y^2}{V\gamma\sqrt{cL}(T_0 - \Delta T)} - \frac{Q(\Theta - 1)}{V\gamma} + \frac{\hat{P}(\tau)}{V\gamma(T_0 - \Delta T)},
\end{aligned}$$

where $\hat{P}(\tau) = P_0\,\mathrm{sech}\left(\left(\sqrt{cL}\tau - t_1\right)/D\right) + 2P_0\,\mathrm{sech}\left(\left(\sqrt{cL}\tau - t_2\right)/D\right)$ ($t_1 = 18[s]$ and $t_1 = 57[s]$); $\hat{\rho}(\Theta) = \rho\left(1 + \mathrm{e}^{-4((T_0 - \Delta T)\Theta(\tau) + T_0)/\Delta}\right)^{-1}$ (Fig. 6.5).

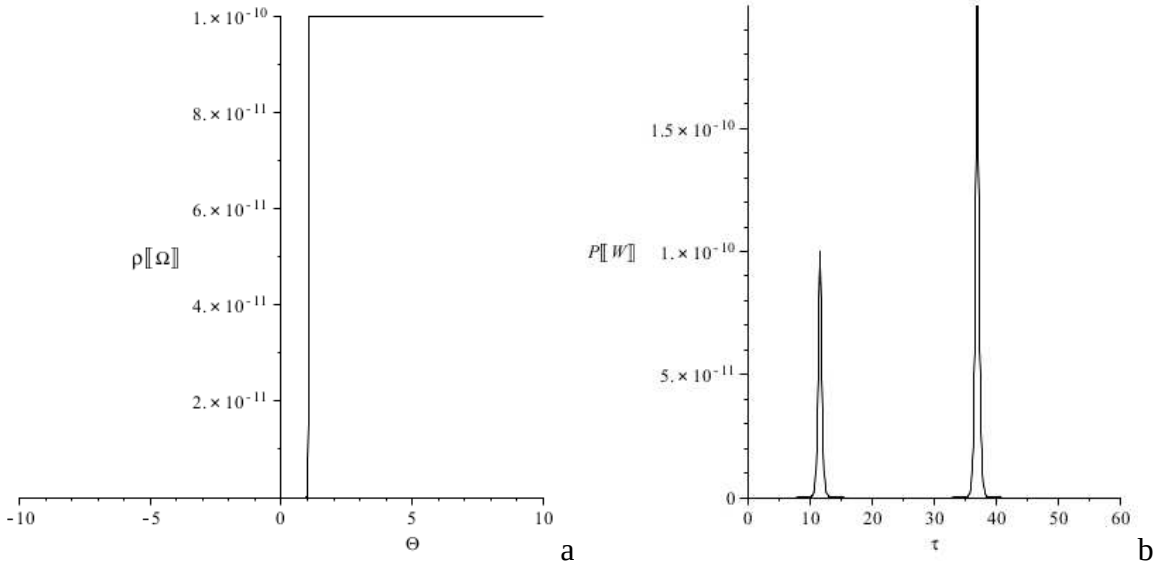

Fig. 6.5 The resistance of the sensor vs. the temperature (a); the incoming power vs. the time (b)

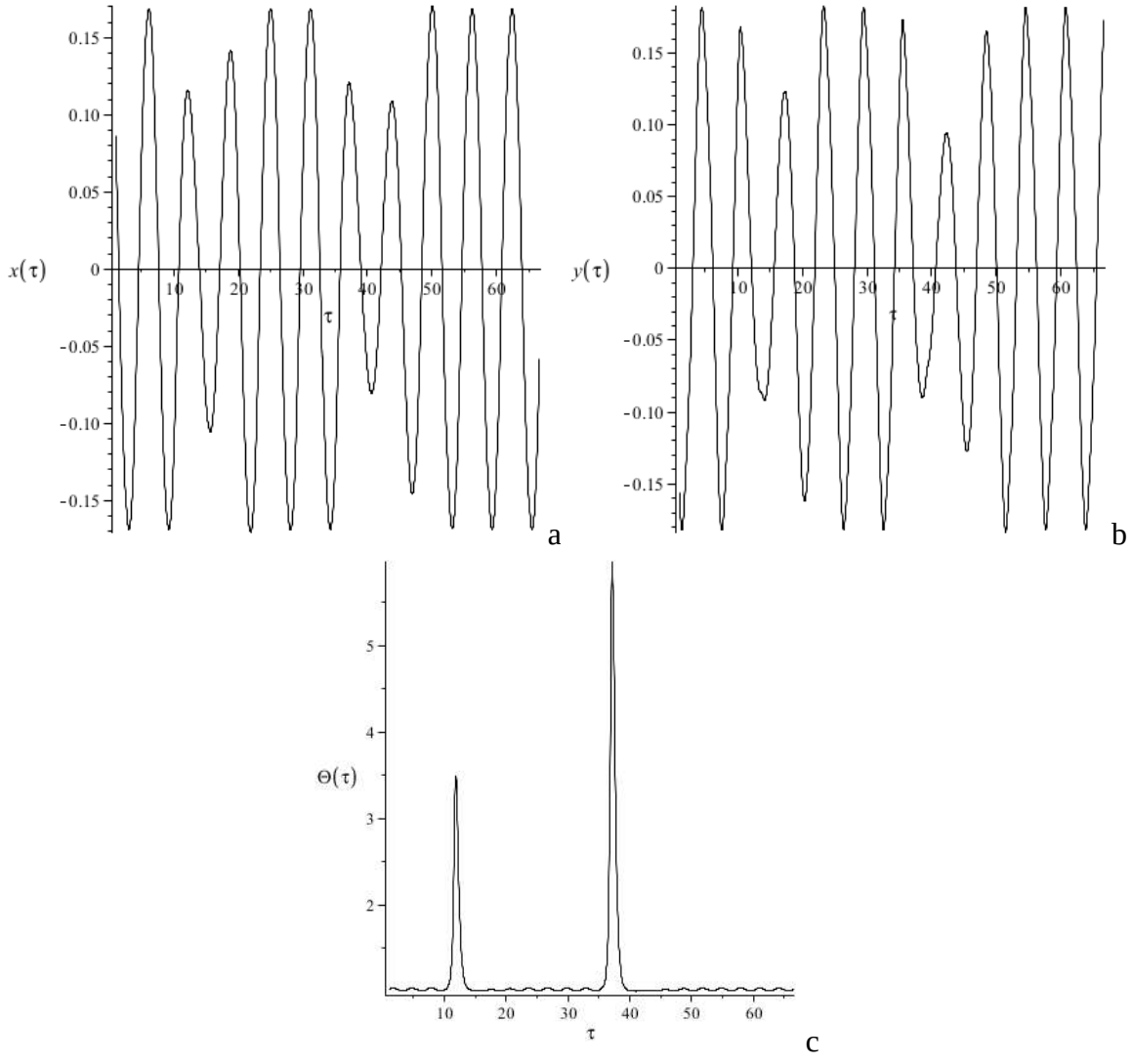

Fig. 6.6 The time history: (a) – charge; (b) – current; (c) – temperature

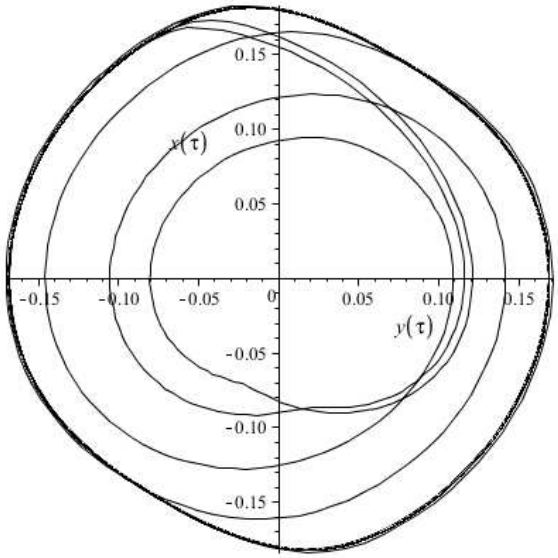

Fig. 6.7 Perturbed limit cycle

In our numerical example, results of the numerical experiment are shown in Fig. 6.6 and Fig. 6.7. The root of voltage mean square is evaluated as $\sqrt{\left\langle |U|^2 \right\rangle} \approx 1.6\times10^{-16}[V]$, while that of the temperature fluctuations is about $\sqrt{\left\langle |\theta|^2 \right\rangle} \approx 2.8\times10^{-5}[K]$.

The heart of any Van der Pol generator is a semiconductor. Any traditional semiconductor produces large noise at ambient temperatures, and plays as an isolator near the absolute zero. Therefore, we should look for other self-excitation mechanisms to achieve a required accuracy in the weak incoming power detection.

Josephson-type generator loaded in parallel to the resonant RLC-circuit

Consider a Josephson junction biased by a constant DC current i. Let us neglect the heat effects, then the equations of the Josephson generation holds true [80–82]:

$$C\frac{dv}{dt}+\frac{v}{\rho}+J\sin\varphi=i;\quad \frac{d\varphi}{dt}=\frac{2ev}{\hbar}. \tag{6.6}$$

Here $v(t)$ is the voltage across the contact; $\varphi(t)$ is the Josephson phase; J denotes the critical current; e stands for the absolute value of the electron charge; $\hbar$ is the Planck's constant; C and ρ are the capacitance and junction resistance, respectively. There is no generation of oscillations provided that the current flow through the Josephson junction is less than its critical value, i.e., $i<J$ [83, 84]. In this case, the stationary value of the Josephson transition phase φ_0 is determined from the following simple equation $J\sin\varphi_0=i$. The generation occurs when the current exceeds the critical value, i.e., $i\geq J$.

Let a high-quality RLC-circuit be connected in parallel to the Josephson junction. The system also operates by applying a DC bias (Fig. 6.8). The symbol JJ denotes the Josephson junction in this figure. The equations of Josephson oscillations are modified as it follows:

$$\begin{aligned}
&C\frac{dv}{dt}+\frac{v}{\rho}+J\sin\varphi=i-j;\quad \frac{d\varphi}{dt}=\frac{2ev}{\hbar};\\
&V_{TES}\Gamma_{TES}\frac{dT}{dt}=rj^2(t)-V_{TES}\Sigma_{TES}\left[T^n-(T_0-\Delta T)^n\right];\\
&V_{JJ}\Gamma_{JJ}\frac{d\Theta}{dt}=(i-j)v-V_{JJ}\Sigma_{JJ}\left[\Theta^n-(T_0-\Delta T)^n\right];\\
&l\frac{dj}{dt}+\frac{q}{c}+rj=v;\quad \frac{dq}{dt}=j.
\end{aligned} \tag{6.7}$$

Here V_{TES} is the volume of the absorber integrated with the heat-sensitive element; $\Gamma_{TES}=\Gamma_{TES}(T)$ is the specific heat capacity of the absorber; Σ_{TES} stands for the coefficient of thermal conductivity; $n=5$[18]; $T(t)$ is the temperature of the heat-sensitive element; $T_0-\Delta T$ denotes the constant temperature of the coolant tank; ΔT is the temperature set some below the phase transition edge. The parameters of the superconducting junction are the following: V_{JJ} is the volume of the junction; $\Gamma_{JJ}=\Gamma_{JJ}(\Theta)$ stands for the specific heat capacity of the junction; Σ_{JJ} is the coefficient of thermal conductivity; $\Theta(t)$ is the junction temperature, while $q(t)$ and $j(t)$, respectively, are the charge and current flow through the resonant circuit with typical parameters of an inductance l, a capacitance c, and a resistance r. All the remaining symbols are the same as above.

The critical current of the junction in the vicinity of the critical temperature is defined by the formulae [85, 86]:

$$J=\frac{\pi}{2e\rho}\Delta\tanh\left(\frac{\Delta}{k_B\Theta}\right);\ \Delta=3.52k_BT_{c,JJ}\sqrt{1-\frac{\Theta}{T_{s,JJ}}}\,.$$

[18] Point out that the electron-phonon coupling has been measured experimentally in many materials. The coupling power is approximated by the following phenomenological dependence $P_{e-h}=\Sigma V\left(T^n-T_0^n\right)$. Here n is integer number, about four or five; $\Sigma\sim10^9\left[WK^{-5}m^3\right]$ is the constant; T is the temperature of the electron gas; T_0 is the temperature of the phonon gas in the thermostat, and V stands for the volume in which the electron-phonon coupling occurs. Thus, the electron-phonon coupling determines the coupling between the bolometer and the cold bath.

Here Δ is the energy gap of the superconductor as the function of the temperature $\Theta(t)$; $T_{s,JJ}$ is the value of the critical temperature; k_B denotes the Boltzmann constant. To obtain the dependence of the critical current J upon the temperature $\Theta(t)$, one should solve a somewhat difficult integral equation [84]. However, the behavior of this solution is very simple (Fig. 6.9); we know; if $\Theta = 0$, then $2\Delta / k_B T_{s,JJ} \approx 3.52$, else if $\Theta \geq T_{s,JJ}$, then $\Delta = 0$ (i.e., the junction resistance is converted into a standard constant value ρ at the ambient temperatures).

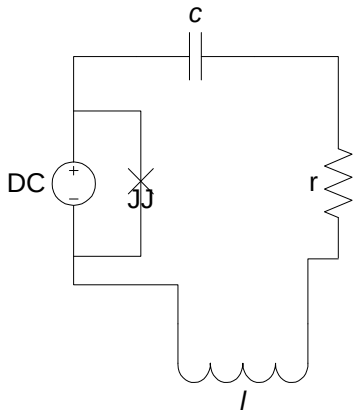

Fig. 6.8 Josephson generator connected in parallel to the RLC-circuit

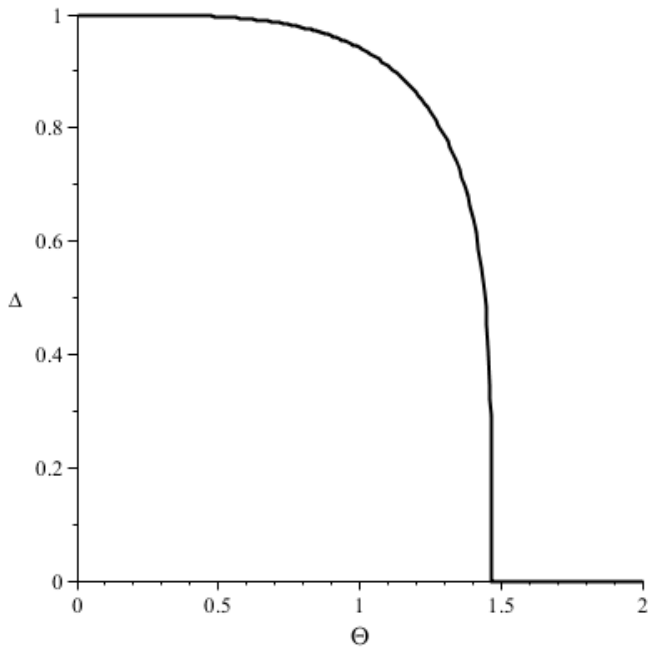

Fig. 6.9 The energy gap versus temperature (arbitrary units)

Typical temperature patterns of the resistance $r = R(T)$ and the heat capacity $\Gamma_{TES}(T)$ of the absorber are schematically plotted in Fig. 6.10, in arbitrary units.

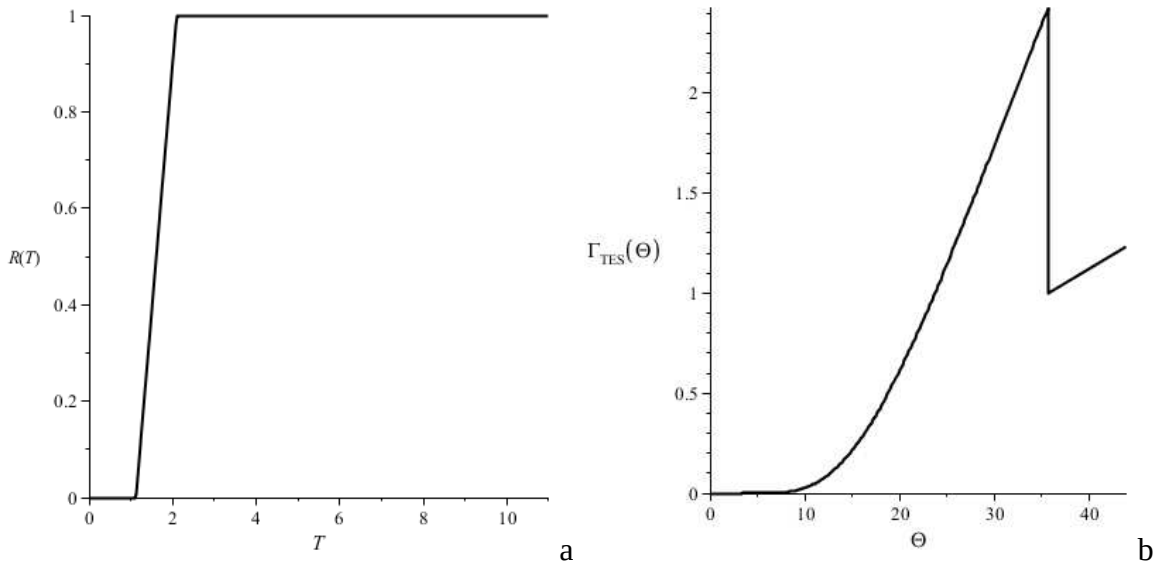

Fig. 6.10 Typical temperature dependences (a – resistive element; b – heat capacity)

The temperature dependence of the specific heat may be approximated by the formula [80]:

$$\Gamma_{JJ}(\Theta)=\begin{cases} y\gamma_{JJ}T_{c,JJ}\exp\left(-1.76T_{c,JJ}/\Theta\right), & \Theta\le T_{c,JJ};\\ \gamma_{JJ}\Theta, & \Theta>T_{c,JJ}. \end{cases} \tag{6.8}$$

The value y is determined from the following condition

$$\frac{c_{es}-\gamma_{JJ}T_{c,JJ}}{\gamma_{JJ}T_{c,JJ}}=1.43. \tag{6.9}$$

Here c_{es} is the heat coefficient in the vicinity of the superconducting edge, while γ_{JJ} denotes the heat coefficient at ambient temperatures; $T_{c,JJ}$ denotes the critical temperature. The formula describing the function $\Gamma_{TES}(T)$ is completely analogous to the above expressions (though $T_{c,TES}$ is used instead the temperature $T_{c,JJ}$, and so on, all the related indexes are changed, as well).

Let us suppose that the bolometer runs in the idle regime. We neglect the temperature effects. An approximate analytical solution to Eq. (6.7) may be represented in the form

$$\begin{aligned} &j(t)=\Omega a_1\cos(\Omega t+\alpha);\quad q(t)=ci\rho+a_1\sin(\Omega t+\alpha);\\ &v(t)=i\rho+\Omega a_2\cos(\Omega t+\beta);\quad \varphi(t)=\Omega t+\frac{2ea_2\sin(\Omega t+\beta)}{\hbar}. \end{aligned} \tag{6.10}$$

Here $\Omega=2ei\rho/\hbar$ denotes the frequency of the Josephson generator in the absence of the resonant circuit. The phases and amplitudes are defined from the following set of equations (solutions these equations tends to be more accurate at $J<<i$):

$$
\begin{aligned}
&\Omega^2 a_2 \sin(\beta) + \frac{\Omega a_1 \cos(\alpha)}{C} + \frac{\Omega a_2 \cos(\beta)}{C\rho} = 0;\\
&-\Omega^2 a_2 \cos(\beta) - \frac{\Omega a_1 \sin(\alpha)}{C} - \frac{\Omega a_2 \sin(\beta)}{C\rho} + \frac{J}{C} = 0;\\
&-\Omega^2 a_1 \cos(\alpha) - \frac{r\Omega a_1 \sin(\alpha)}{l} + \frac{a_1 \cos(\alpha)}{lc} + \frac{\Omega a_2 \sin(\beta)}{l} = 0;\\
&\frac{r\Omega a_1 \cos(\alpha)}{l} - \Omega^2 a_1 \sin(\alpha) - \frac{\Omega a_2 \cos(\beta)}{l} + \frac{a_1 \sin(\alpha)}{lc} = 0.
\end{aligned}
\qquad (6.11)
$$

Let us assume that the generation frequency Ω is close to the natural frequency of the resonant circuit $\omega = 1/\sqrt{lc}$. The solutions to the set (6.11) demonstrate a typical behavior of dynamical systems near the resonance. Figure 6.11 displays a numerical example at the frequency $\Omega = 0.254\times10^{11}[Hz]$, provided that the resistance, $r = 1.16\times10^{-3}\,[\Omega]$, is small enough. The points in this figure correspond to the parameters a_1 and α. The dimensionless frequency detuning is normalized to unity with respect to the resonant frequency Ω. The dimensionless amplitude a_1 is normalized by the value $ci\rho = 1.295\times10^{-15}[C]$, while the amplitude a_2 – by $i\rho/\Omega = 3.291\times10^{-16}[Wb]$. The parameters of the numerical estimation are the following: $J = 8.363\times10^{-5}$ [A]; $c = 1.549\times10^{-11}[F]$; $i = 8.363\times10^{-5}$ [A]; $r = 1.16\times10^{-3}\,[\Omega]$; $l = 10^{-12}$ [m]; $\rho = 7.872\times10^{-10}[\Omega]$; $C = 1.4\times10^{-11}[F]$.

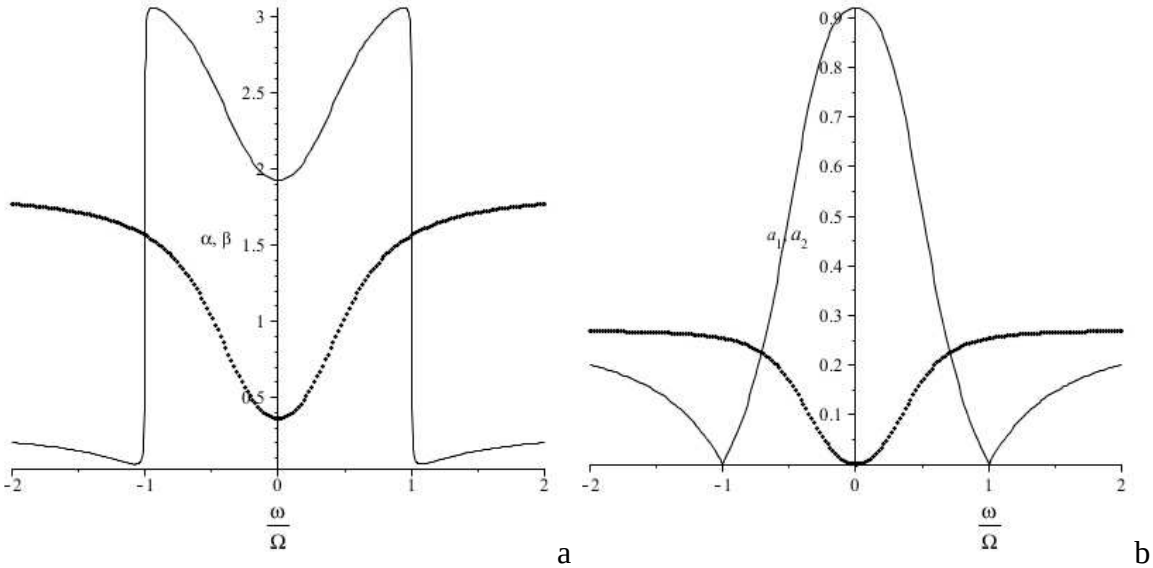

a b

Fig. 6.11 Phase and amplitude response (a – the parameters α and β; b – the parameters a_1 and a_2)

As one can see, the resonant excitation alters significantly the phase and amplitude dependences at small variations near the resonant point $\omega/\Omega = 1$, so that this model leads us to an idea of a highly sensitive sensor.

First, consider the time history of the process governed by Eq. (6.7) at the initial conditions

$$\varphi(0)=0;\ v(0)=0;\ j(0)=0;\ T(0)=T_0-\Delta T;\ \Theta(0)=T_0-\Delta T.$$

The calculation uses the dimensionless variables:

$$\tau=\omega t;\ G(\tau)=j(t)/i;\ \Phi(\tau)=\varphi(t);\ Q(\tau)=q(t)/i\rho c;\ G(\tau)=2ev(t)/\hbar\omega.$$

Specific numerical parameters are shown in the Table 6.1. These are taken as typically encountered ones from the listed bibliography in an attempt to rely already achieved level in technologies.

Table 6.1 The idle sensor parameters with the constant small resistance r

$J=8.363\times10^{-5}$ [A];	$V_{TES}=10^{-19}[m^3]$;
$T_0=T_{s,TES}=0.27$[K]; $T_{s,JJ}=0.351$[K]	$r=1.16\times10^{-3}$ [Ω];
$\Delta T=0.03$[K];	$\Sigma_{TES}=2.5\times10^{9}[W/K^5m^3]$;
$c=1.549\times10^{-11}[F]$;	$\gamma_{TES}=6.9\times10^{-5}[Ws/K^2m^3]$;
$i=8.363\times10^{-5}$ [A];	$V_{JJ}=10^{-15}[m^3]$;
$l=10^{-12}$ [H];	$\Sigma_{JJ}=2.5\times10^{9}[W/K^5m^3]$;
$\rho=7.872\times10^{-10}$[Ω];	$\gamma_{JJ}=6.9\times10^{-3}[Ws/K^2m^3]$.
$C=1.4\times10^{-11}[F]$;	

The oscillatory patterns are shown in Fig. 6.12.

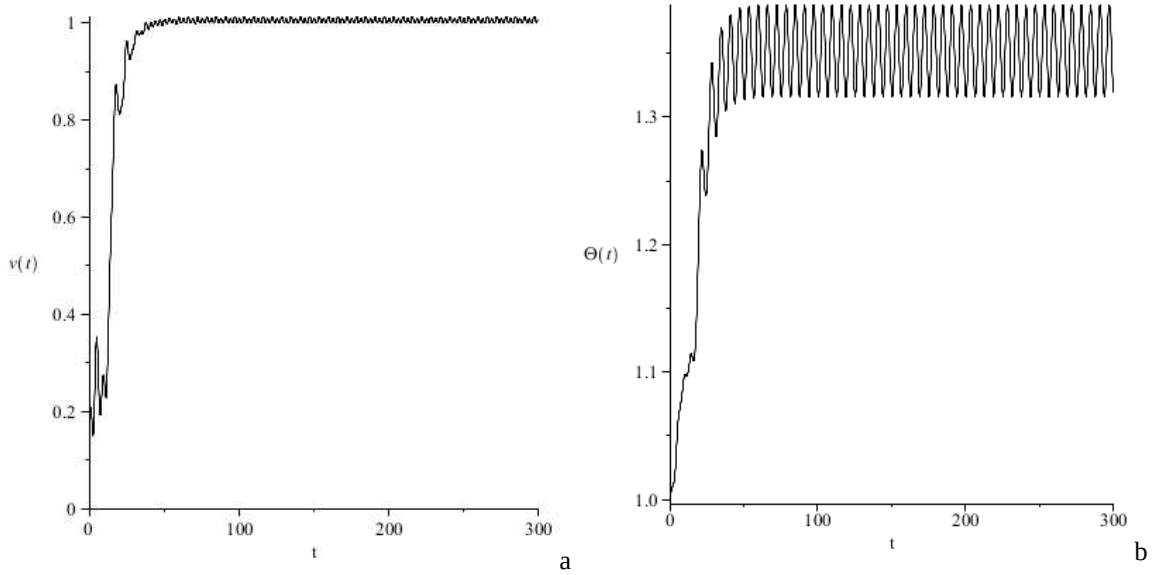

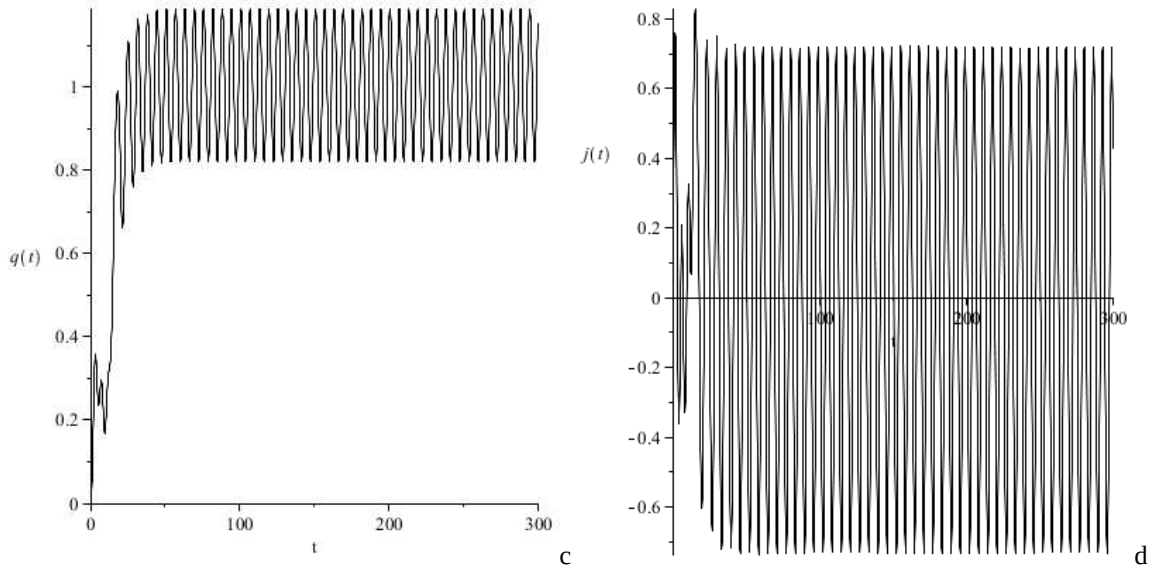

Fig. 6.12 Dynamical response (a – voltage in the junction; b – temperature of the Josephson junction; c – charge in the RLC–circuit; d – current in the RLC–circuit).

Sensor Model

As we can trace, the dynamical system representing the terahertz generator integrated with the resonant RLC–circuit is extremely sensitive to changes in the resistance, since the circuit is tuned into the resonance with the generator. This property is used to identify small thermal changes. Figure 6.13 shows a scheme of the sensor with the TES–type resistor included in the oscillatory circuit parallel to the generator. The magnetic flux near the inductive element may be measured with the help of a quantum interferometer.

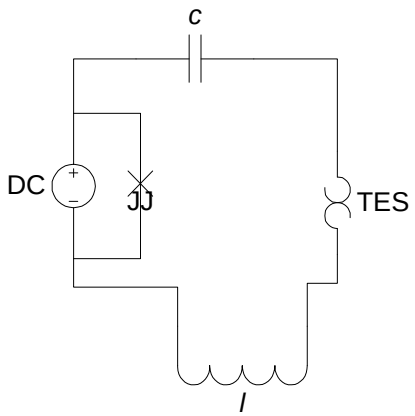

Fig. 6.13 Self-excited resonant bolometer

The following set is derived by modifying Eq. (6.7), making allowances for the resistance of TES–type:

$$
\begin{aligned}
&C\frac{dv}{dt}+\frac{v}{\rho}+J\sin\varphi=i-j;\quad \frac{d\varphi}{dt}=\frac{2ev}{\hbar};\\
&l\frac{dj}{dt}+\frac{q}{c}+R(T)j=v;\quad \frac{dq}{dt}=j;\\
&V_{TES}\Gamma_{TES}(T)\frac{dT}{dt}=R(T)j^2-V_{TES}\Sigma_{TES}\left[T^n-(T_0-\Delta T)^n\right]+P(t);\\
&V_{JJ}\Gamma_{JJ}(\Theta)\frac{d\Theta}{dt}=(i-j)v-V_{JJ}\Sigma_{JJ}\left[\Theta^n-(T_0-\Delta T)^n\right]
\end{aligned}
\qquad (6.12)
$$

Here $P(t)$ is the external power; Δt is the characteristic pulse duration over the time. The remaining notations are the same. In contrast to model (6.7), the set (6.12) cannot be subject to effective analytical study. In this case one may rely to numerical calculation only. In order to test the dynamics governed by the model (6.12), we use the system parameters from Table 6.2. The additional parameters are the following: $r=11.6[\Omega]$; $\max(P)=10^{-12}[W]$; $\frac{dR}{dT}\frac{T}{R}=50$; $\Delta t=10^{-12}[s]$.

The results are presented in Fig. 6.14 (the same dimensionless variables). Obviously, the effects of absorption of the external pulse can be clearly observed due to dynamical changes in the amplitude and phase. In particular, as we can observe, the time point correspondent to the pulse absorption is characterized by almost zeros in the current and voltage. This means that the model of the self-excited resonant bolometer possesses by the effective feedback which creates most optimal preconditions for a quickest sensor cooling.

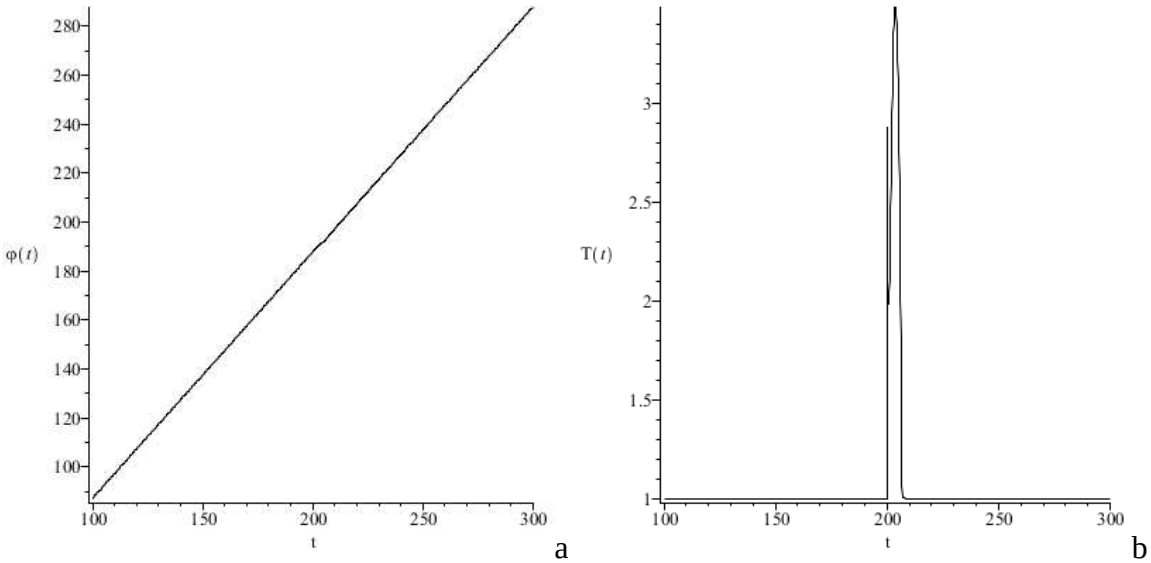

a b

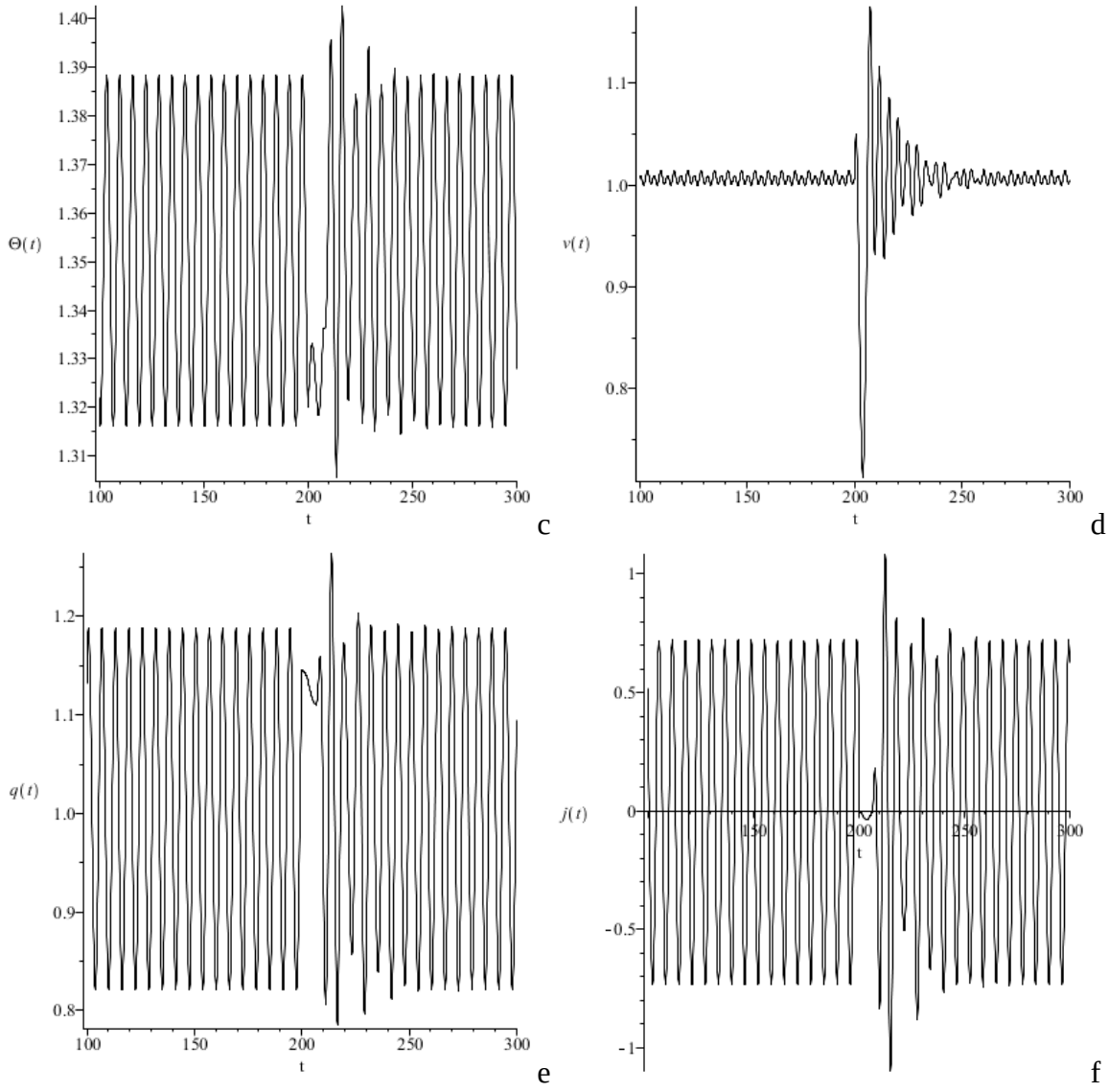

Fig. 6.14 Bolometer dynamics (a – Josephson phase; b – temperature of the resistive element over the time; c – temperature of the junction; d – voltage; e – charge; f – current). The pulse comes at the time of 200 dimensionless units

This would lead to a technical result which should improve the sensitivity, accuracy and stability of the sensor by reducing the measurement errors up to the level restricted by thermal fluctuations.

Finally, the physical processes in the self-excited resonant bolometer may be consumed by the following elementary acts. The low-noise high-frequency generator of oscillations is represented by a terahertz Josephson junction, which is loaded by the resonant RLC-circuit in parallel. The inductive element of the circuit allows for an accurate readout from the sensor with the help of a quantum interferometer. The frequency of electric oscillations is generated in the circuit at the same frequency as that of emitted electromagnetic waves in the case of the critical biasing. Let

the resonant circuit be tuned into the resonance with the Josephson generator, and then the maximal loading is provided. This resonance is accompanied by decreasing in the amplitude of oscillations in the generator, while the amplitude increases in the circuit at the same time. The resonance creates stationary self-excited oscillatory regimes, which exhibit stable patterns at terahertz frequencies. If the sensor is out of balance, because of the absorption of the external pulse, then the negative feedback reacts extremely quickly to return the sensor to its original unperturbed state (Fig. 6.14).

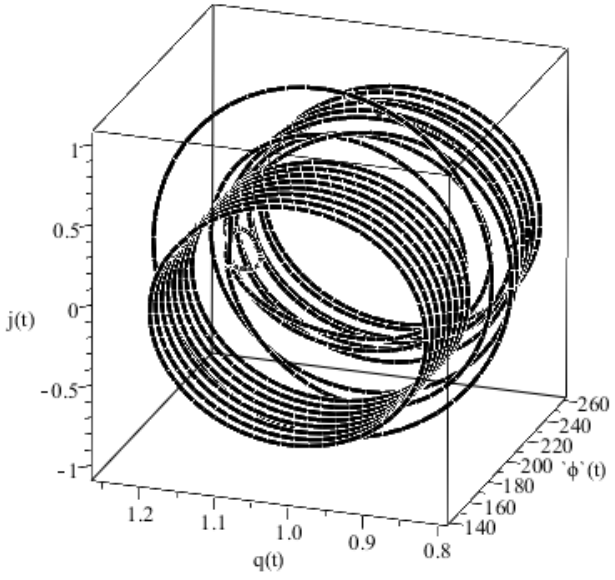

Fig. 6.15 Bolometer dynamics in the phase-space cross section

Noise-equivalent power

If the temperature of the physical body is above the absolute zero, then thermal fluctuations appear always [87, 88]. The main objective is that these fluctuations have to be small compared to the useful signal. The noise-equivalent power due to the electron scattering on phonons is estimated by the following formulae:

$$NEP_{TES} = 20k_B V_{TES}\Sigma_{TES}T^6(t);\ NEP_{JJ} = 20k_B V_{JJ}\Sigma_{JJ}\Theta^6(t). \quad (6.13)$$

The estimations of noise generated by the electron scattering reads:

$$NEV_r = 4rk_B T(t);\ NEV_\rho = 4\rho k_B \Theta(t). \quad (6.14)$$

The evaluation of noise due to the dynamical recharge of capacitors is the following:

$$NV_c = k_B T(t)/c\,;\ NV_C = k_B \Theta(t)/C\,. \tag{6.15}$$

Thus, the noise evaluation for the example present above would be roughly:
$NEP_{TES} = 2.425\times10^{-32}[W^2/Hz]$; $NEP_{JJ} = 9.933\times10^{-31}[W^2/Hz]$; $NEV_r = 5.381\times10^{-22}[V^2/Hz]$;
$NEV_\rho = 1.855\times10^{-23}[V^2/Hz]$; $NV_c = 7.486\times10^{-13}[V^2]$; $NV_C = 3.313\times10^{-13}[V^2]$.

Let us consider the dimensionless transient process in the bolometer, related to the time history shown in the previous figures. This the time range is about 100 units, i.e., the physical time interval is about $2.473\times10^{-9}[s]$ (Fig 6.6). Thus, the frequency bandwidth, $\Delta\omega$, can be estimated as $4.044\times10^{8}[Hz]$. Alternatively, the noise generated due to the recharge of capacitors is not a new kind of noise, since $NEV_r\Delta\omega \sim NV_c$ and $NEV_\rho\Delta\omega \sim NV_C$, accordingly to the spectral theory. Therefore, the total noise should be about $10^{-12}[W]$ in the power. Since the critical noise has the same order as the power of the external pulse, P, related to the numerical example, we have evaluated a threshold of sensitivity of the bolometer to infrared signals. Finally, the interested reader can trace in detail all the numerical examples used in this study [89].

Resume

The reliability of the mathematical model describing dynamical regimes in the self-exited resonant bolometer may be confirmed by many resent successes in nanotechnologies, referred in the text and references in a part. In particular, the patent US8063369 uses several interconnected in a cascade TES-type sensors providing a very sharp response of the bolometer. The main difference of this prototype from the self-excited resonant bolometer is that a constant bias voltage is used to power the cell of detectors. Note that the constant bias, either the current or voltage, would naturally limit the effectiveness of the feedback which should promote a rapid cooling of the detector up to the operating point. Unlike this, the self-exited resonant bolometer has a variable biasing, both in the current and voltage. This supports some fruitful conditions for the feedback properties to reduce the time constant of the bolometer.

Consider the effectiveness of resonant circuits in the excising design of bolometers. A sensitive element in the resonant circuit may play the role as a capacitor or inductor. An example can be found in the patent US6534767. It is well known that the capacitance or inductance both depend on the ambient temperature, which affects changes in the impedance. This causes variations of the resonant frequency which may be registered through the phase-locked loops. The main deficiency of such a prototype is that it is designed using ferroelastic materials, which able to exhibit

the desirable qualities at relatively high temperatures only and cannot provide accurate measurements, because of thermal noise.

A low-noise high-frequency generator of oscillations in the resonant bolometer can be represented by a terahertz Josephson junction, as the best candidate, which is loaded by the resonant RLC-circuit in parallel [90]. The junction, at the critical biasing, generates a localized electromagnetic radiation. The frequency of electric oscillations in the circuit occurs at the same frequency as the frequency of the emitted electromagnetic waves. Then the resonant circuit is tuned into the resonance with the Josephson generator to provide its maximal loading. The resonance creates the stationary self-excited oscillatory regimes, which are stable at terahertz frequencies. When the sensor is out of balance, because of the absorption of the external pulse, the negative feedback reacts extremely quickly to return the sensor to its original unperturbed state. The inductive element of the circuit allows for an accurate readout from the sensor with the help of a quantum interferometer. In particular, the patent US8026487 describes a superconducting tunable coherent terahertz generator based on the resonant coupling between the Josephson oscillations and the fundamental mode of the cavity resonator, which leads to a powerful terahertz radiation.

Note that the self-excited resonant bolometer represents a mesoscopic device. Then its efficiency is restricted by the geometrical dimensions of the system. The mathematical description represented in the chapter is based on the semi-classical physical methods. Let the dimensions decrease with the increasing the purity of a sensor material, then the bolometer turns into a typical quantum system. It is possible that perspective sensor elements can be composed of monatomic metallic layers covered by graphene sheets. This would ensure a minimization of the heat capacity, as well as graphene sheets, accordingly to the state-of-the-art, exhibit extremely high thermal properties which would support a maximization of the thermal conductivity. To implement such elements in the bolometer we may pay attention on new intercalation technologies [91]. NEMS terahertz resonators are also of higher interest [92]. The permanent evolution of nanotechnologies would provide the appearance of very rapid and efficient devices such as quanta counters. Such devices would manifest themselves as awfully quantum objects. However, their manufacturing, but not only the mathematical description, seems to be not so easy [93].

RESONANT ENSEMBLES OF STATIONARY QUASI-HARMONIC WAVES IN A ONE-DIMENSIONAL ANHARMONIC CHAIN

We study nonlinear resonant interactions between quasi-harmonic waves in a one-dimensional anharmonic chain, based on a simple mathematical model originated from the geometry of central and noncentral interactions between particles, within the so-called harmonic approximation. The investigation is carried out by standard asymptotic methods of the nonlinear dynamics. Triple-wave resonant ensembles are revealed within the first-order approximation analysis. These triads are formed both due to the quadratic nonlinearity of the system, and due to satisfying the phase-matching conditions. The resonant triads can be of three different types only, though the each resonant triad consists necessarily of one longitudinal and two transversal wave modes. In turn, these resonant triads can be nonlinearly coupled. This leads to a creation of resonant chains assembled from resonant triads of three different types, having spectral scales in the general case. Cascade processes of energy exchange between the oscillatory modes are characterized not only by complex chaotic dynamics inherent in nonintegrable Hamiltonian dynamical systems, but also by the presence of multi-mode stationary motions, which are stable by the Lyapunov criterion. In an ideal crystal structure such stationary coherent wave ensembles can significantly influence upon heat properties of the system, especially at low temperatures. This is one more relevance of their theoretical and experimental study in micromechanics.

The growing researcher interest in various low-dimensional objects of micromechanics, possessing a spatially periodic structure, inspires theoretical and experimental investigations in the field of nonlinear acoustics, based even on well-known models of chains and lattices of material particles.

Naturally, at the problem formulation, any theory should take into account that the basic techniques of experiments could be focused on the study of the dynamical response of the system to most simple test signals. The spectrum in the response to sufficiently intense input high-frequency signals, due to nonlinear processes, can be quite complex to identify the structure of the object under investigation. Therefore, one of the most important problems is to describe theoretically those frequency bands in which the dynamics of the system would be most predictable, as well it is possible. An appropriate strategy can be based on the simplest classical models, which can be naturally extended, if necessary, straightforwardly to quantum models which describe adequately the properties of a real microsystem.

In this study, we present a complete classification of triple-wave resonances in a simple model of anharmonic chain, taking into account both central and noncentral interactions between the particles within the harmonic approximation. It is shown that a low-frequency quasi-harmonic longitudinal wave, caused by central interactions, is almost always unstable. This, comparatively long longitudinal wave breaks up into a couple of secondary mid-frequency transverse waves, provided that the group velocity of this primary mode does not exceed that of extremely long longitudinal waves.

In the short-wave range, the triple-wave interactions are much more complicated. In the case, when the group velocity of the primary unstable transverse waves exceeds that of extremely long longitudinal waves, a multi-wave cascade process can be created, since a lot of resonant triads can be simultaneously involved in the nonlinear interaction due to the phase matching between waves. This means that the high-frequency transverse waves, the group velocity of which exceeds the group velocity of extremely long longitudinal waves, are always unstable with respect to small perturbations. However, together with increasing number of waves involved in this cascade process, the spectral parameters of the oscillatory modes do not increase. This means that the energy flux is redistributed mainly from the high-frequency band to the low-frequency part of the spectrum of vibrations, and the number of modes, involved in the cascade process, is always a finite or countable number, at least within the first-order nonlinear approximation.

Cascade processes of energy exchange between the oscillatory modes are characterized not only by a complex chaotic dynamics inherent in nonintegrable Hamiltonian dynamical systems, but also by the presence of multi-wave stationary motions, stable by the Lyapunov criterion.

In microsystems, such stationary wave ensembles may be associated with coherent processes which can significantly influence on the macroscale physical properties such as a specific heat and other phenomenological parameters of the system, especially at low temperatures. Note that a significant progress in theoretical and experimental study on the area of nonlinear cascade processes had been achieved in fluid mechanics [94]94–96]. From a viewpoint of the solid acoustics, this theory still requires further development, and therefore, this would be focused in this study. Nowadays, a hot point of interest concerns with a problem of heat transfer in low-dimensional solids possessing a crystal structure. The heat transport in crystalline insulators is carried due to elemental excitations, also named as phonons or elastic quasi-harmonic oscillations of the lattice. The two most important nonlinear effects in crystalline solids are the thermal expansion and the phonon thermal conductivity. The thermal current can arise as a population of

phonons deviates from its equilibrium state, because of both the diffusion and decay. Multi-wave resonant interactions in insulators, such as the triple-phonon break-up processes, change the quasiparticle population accordingly to the Bose gas model. Apart the scattering on impurities, the triple-phonon interactions cause a finite thermal transport at expense of mechanisms of the so-called the Umklapp processes [97]. Thus, the thermal resistivity should necessary present at least at higher temperatures. At low temperatures the Umklapp processes are weakly expressed, as a rule. This means that the heat transfer in low-dimensional system can possess features inherent in ballistic phonon propagation, similar to the stationary multi-wave resonant processes which are of main interest in this chapter.

Equations of motion and dispersion relations

We consider mechanical vibrations of a simple one-dimensional chain consisting of particles of equal masses m, placed along a straight line at equal distances a, being at the rest. Each particle has two degrees of freedom on the plane of oscillation. The forces between the particles are both central and noncentral. Accounting for noncentral interatomic interactions leads to appearance of so-called *transverse* or *bending* oscillatory modes. An absolute elongation of a segment in the chain, λ_n, and the curvature of the median line, κ_n, in the vicinity of the atom number *n* can be expressed as it follows:

$$\lambda_n = \sqrt{\left(a + \left(u_n - u_{n-1}\right)\right)^2 + \left(w_n - w_{n-1}\right)^2} - a\,;$$

and

$$\kappa_n = \arctan\left(\frac{w_n - w_{n-1}}{a + u_n - u_{n-1}}\right) - \arctan\left(\frac{w_{n+1} - w_n}{a + u_{n+1} - u_n}\right),$$

where $u_n = u_n(t)$ and $w_n = w_n(t)$ are the longitudinal and transverse components of the displacement of centers of masses, respectively, which are naturally oriented relatively the Cartesian axes. Then the Lagrangian of the system in the harmonic approximation takes the form

$$L = \frac{m}{2}\sum_{n=-Z}^{Z}\left(\dot{u}_n^2 + \dot{w}_n^2\right) - \frac{1}{2}\sum_{n=-Z}^{Z}\left(\alpha\lambda_n^2 + \beta\kappa_n^2\right), \tag{7.1}$$

where the phenomenological constants α and β characterize the stretching and transverse motions of the chain, respectively; the dot denotes derivative with respect to the time t. The number of elemental cells Z in the chain is supposed to be large enough, i.e., $Z \to \infty$.

Equations governing the dynamics of the chain of particles are derived with the help of the Euler-Lagrange variational principle. For the convenience of asymptotic procedures we introduce a small parameter $\mu << 1$, using the following similarity transform: $u_n(t) \to \mu u_n(t)$, $w_n(t) \to \mu w_n(t)$. The small parameter is arbitrary, for example, one can assume that $\mu a = \max(u_n(t), w_n(t))$.

In the linear limit, as $\mu \to 0$, equations of motion read as it follows:

$$\begin{aligned} m\ddot{u}_n &= \alpha(u_{n-1} - 2u_n + u_{n+1}); \\ m\ddot{w}_n &= \beta(-w_{n-2} + 4w_{n-1} - 6w_n + 4w_{n+1} - w_{n+2}). \end{aligned} \tag{7.2}$$

Let the number of particles in the chain tends to infinity, then a solution to Es. (7.2) can be expressed in the integral form:

$$\begin{aligned} U_n(t) &= \int_{-\infty}^{\infty} \left(A_l(k) \exp i\phi_l(k,t) + A_l^*(k) \exp(-i\phi_l(k,t))\right) dk; \\ W_n(t) &= \int_{-\infty}^{\infty} \left(A_b(k) \exp i\phi_b(k,t) + A_b^*(k) \exp(-i\phi_b(k,t))\right) dk, \end{aligned} \tag{7.3}$$

where $A_l(k)$ and $A_b(k)$ are the complex amplitudes ($A_l^*(k)$ and $A_b^*(k)$ are the corresponding complex conjugates of the preceding terms); $\phi_l(k,t) = \omega_l(k)t + kan$ and $\phi_b(k,t) = \omega_b(k)t + kan$ denote fast-rotating phases of the transverse and longitudinal waves, respectively; $\omega_l(k)$ and $\omega_b(k)$ stand for the natural frequencies of the normal harmonic waves, depending upon the wave number k. Spectral parameters of the set (7.2) are completely characterized by the following dispersion relations

$$\omega_l(k) = \sqrt{\frac{2}{m}\alpha(1 - \cos ka)}; \quad \omega_b(k) = 2\sqrt{\frac{\beta}{m}}\frac{(1 - \cos ka)}{a}, \tag{7.4}$$

which are presented in Fig. 7.1.

These dispersion curves have three characteristic points:

- The *group-matching* point in the long-wave range (indicated by G_1 in Fig. 7.1), where the group velocity of the extremely long longitudinal wave coincides with the group velocity of the transverse wave: $\left|ak_{g_1}\right| = \arcsin\left(\sqrt{\alpha/\beta}a/2\right)$.

- There is also a point of *group synchronism* in the short-wave range (marked by G_2 in Fig. 7.1), where the group velocity of the extremely long longitudinal wave coincides with the group velocity of the transverse wave: $\left|ak_{g_2}\right| = \pi - \arcsin\left(\sqrt{\alpha/\beta}a/2\right)$.
- The *phase-matching* point (marked as P in Fig. 7.1) in which the phase velocities of longitudinal waves coincide with that of and transverse waves: $\left|ak_{ph}\right| = \pi - \arccos\left(\left(\alpha a^2 - 2\beta\right)/2\beta\right)$.

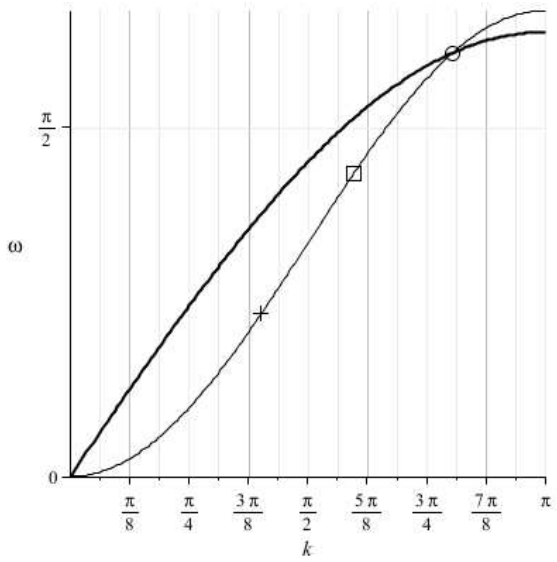

Fig. 7.1 The dispersion relation of longitudinal and transverse waves in the chain

For most known natural materials possessing a periodic structure, a reaction of a sample on a transverse deformation is usually small, so the inequality $\alpha << \beta a^2$ holds true. This means that the transverse waves typically have comparatively low frequencies compared to those of longitudinal waves. Therefore, in the nonlinear formulation of the problem, it is expected that the high-frequency longitudinal waves should be unstable with respect to small low-frequency transverse perturbations. Though, one should pay attention that many artificial materials, appearing in recent times, commonly called *metamaterials*, which can have extremely unexpected and paradoxical properties. For example, for some "telescopic" metamaterials the relation $\alpha \approx \beta a^2$ can be true. This indicates, in turn, that the transverse waves may possess enough energy for efficient interaction between longitudinal waves due to nonlinearity. Therefore, in this study we formulate the general problem, namely, a question is not only in the study of the nonlinear wave dynamics in natural materials, but also in metamaterials in which a resistance on bending deformations can be compared with that of tension and compression caused be longitudinal waves.

Average Lagrangian. Hamiltonian

Let the small parameter of the problem μ be nonzero and finite. Then the solution (7.3) to the linearized set (7.2) can be successfully utilized to have useful information about basic properties of the weakly nonlinear system characterized by the Lagrangian (7.1). This is achieved by varying the arbitrary constants of integration in the time, the role of which in the present study is played by the complex amplitudes of quasi-harmonic waves: A_l, B_l, A_b and B_b.

If $\mu \neq 0$, then the solution of any quasilinear system is developed in the same form as the expression (7.3), using a formal modification of variables: $A_l(k) \to A_l(k,t)$, $B_l(k) \to B_l(k,t)$, $A_b(k) \to A_b(k,t)$ and $B_b(k) \to B_b(k,t)$. Obviously, the time variations of amplitudes would be the brighter with growth of the parameter μ, so that the introduction of new scales of slow times, i.e. $\tau_n \to \mu^n t$, is actual.

In addition, following the general procedure constructing the asymptotic solution, the expression (7.3) should be modified by adding small corrections to the kernel solution in the form of an expansion in the small parameter μ:

$$\begin{aligned} U_n(t) &= \int_{-\infty}^{\infty} \left(A_l(k,\tau_1,\tau_2,...) \exp i\phi_l(k,t) + A_l^*(k,\tau_1,\tau_2,...) \exp\left(-i\phi_l(k,t)\right) \right) dk + \sum_{m=1}^{\infty} \mu^m u_n^{(m)}(t); \\ W_n(t) &= \int_{-\infty}^{\infty} \left(A_b(k,\tau_1,\tau_2,...) \exp i\phi_b(k,t) + A_b^*(k,\tau_1,\tau_2,...) \exp\left(-i\phi_b(k,t)\right) \right) dk + \sum_{m=1}^{\infty} \mu^m w_n^{(m)}(t). \end{aligned} \tag{7.5}$$

The small corrections, if it is necessary, would be determined step by step during the constructing the asymptotic solutions with a given accuracy.

The Lagrange function, after the substituting therein the anzats (7.5), and subsequent averaging over the fast rotating phases $\phi_l(k,t)$ and $\phi_b(k,t)$, appears in the form of so-called average Lagrangian $\langle L \rangle$ whose arguments are the complex amplitudes of the quasi-harmonic waves with their time derivatives, as well. These arguments, *inter alia*, are proportional to the canonically conjugate variables. If one enters by a standard way the generalized moments

$$p_{A_l} = \frac{\partial \langle L \rangle}{\partial \dot{A}_l}; \; p_{A_l^*} = \frac{\partial \langle L \rangle}{\partial \dot{A}_l^*}; \; p_{A_b} = \frac{\partial \langle L \rangle}{\partial \dot{A}_b}; \; p_{A_b^*} = \frac{\partial \langle L \rangle}{\partial \dot{A}_b^*},$$

then the average Lagrangian $\langle L \rangle$ can be transformed into the averaged Hamiltonian $\langle H \rangle = \dot{A}_l p_{A_l} + \dot{A}_l^* p_{A_l^*} + \dot{A}_b p_{A_b} + \dot{A}_b^* p_{A_b^*} - \langle L \rangle$. The advantages of the Hamiltonian description,

compared with the Lagrangian one, are that, at least, one integral of motion is already known *a priori*, namely $\langle H \rangle = H_0$, where H_0 is an arbitrary constant of integration.

Resonance

The average Hamiltonian, as a power series in μ, has a transparent structure:

$$\langle H \rangle = \mu^2 \langle H_2 \rangle + \mu^3 \langle H_3 \rangle + ... \tag{7.6}$$

The first term $\langle H_2 \rangle$ is identical zero by virtue of the dispersion relations (7.4). The term $\langle H_3 \rangle$ is a cubic polynomial dependent upon the new generalized coordinates and momenta, namely, complex conjugate amplitudes of longitudinal and transverse waves and their derivatives. This term holds all the information on the dynamic properties of the system within the first-order nonlinear approximation. If $\langle H_3 \rangle$ not identical zero, then the system explores the *first-order* resonance. An alternate method, looking for the presence of resonance in the system, can be as it follows. The initial system of differential equations is reduced to the so-called *standard form*. The general solution to the linearized subset of the standard form is substituted into the right-hand terms of the standard form, containing the nonlinear terms. Next, the right-hand terms are averaged over fast rotating phases, and if the average is not zero or contains jumps at scanning the spectral parameters of the system, this means that the resonance presents in the system [24].

In particular, the dynamical system represented by the average Lagrangian $\langle L \rangle$ or the average Hamiltonian $\langle H \rangle$, experiences the resonance due to nonlinear interactions between modes being in the triple-wave phase matching. As a result resonant ensembles known as the triads are formed. There are no other resonances, except for the triple-wave resonances in the first-order nonlinear approximation in the system under investigation. Consequently, in the absence of resonance, the nonlinearity of system can be neglected, since a linear description of the system would be adequate in this particular case.

Components of resonant ensembles

The set of nonlinearly interacting triads is called within this study as a *multi-wave resonant ensemble*. For the occurrence of nonlinear triple-mode resonant interaction between waves, any dynamical system requires an appropriate type of quadratic nonlinearity in the equations of motion, together with fulfilling the following phase-matching conditions [98]

$$\omega_1 = \omega_2 + \omega_3 + \Delta\omega; \quad k_1 = k_2 + k_3 + \Delta k. \tag{7.7}$$

Here ω_n are the natural frequencies and k_n are the corresponding wave numbers of waves; $\Delta\omega \sim \mu \min(\omega_n)$ denotes a possible frequency detuning, assumed to be small compared to all the natural frequencies. The eigenfrequencies are numbered following the natural order: $\omega_1 \geq \omega_2 \geq \omega_3$. It should be emphasized that the phase-matching conditions are only the necessary conditions for the creation of the *resonant triad* or *triplet*. The sufficient conditions arise at suitable structure of nonlinear terms in the equations governing the motion. Based on the analysis of the dispersion properties and the structure of nonlinearity, one can establish that the triple-mode resonance in a simple anharmonic chain of particles can be of three different types, though each triple can consist of one longitudinal and two transverse waves. Similar dynamical processes can be observed in a straight elastic bar in the long-wave limit [100].

T_{lbb} -type triad

The high-frequency mode in a resonant triad of the first type, which will be referred as T_{lbb}, is the primary longitudinal wave (symbol l in the abbreviation is given for the longitudinal mode while the symbol b corresponds to the transverse mode). The ordering in the indexes agrees with that of frequencies in the phase matching conditions (7.7). Solutions to the dispersion equation (7.4), satisfying the phase-matching conditions (7.7), in the absence of detuning, $\Delta\omega = 0$, can be determined graphically [66, 99–101]. These solutions do exist in the wide permissible range of wave numbers, but only when the wave number of the longitudinal mode k_1 does not belong to the following "forbidden" interval:

$$k_1 \notin \left[\arctan\left(\frac{8\sqrt{\alpha\beta}\left(\alpha a^2 - 4\beta\right)a}{\alpha^2 a^4 - 24\beta\alpha a^2 + 16\beta^2} \right) / a, \quad 2\pi - \arctan\left(\frac{8\sqrt{\alpha\beta}\left(\alpha a^2 - 4\beta\right)a}{\alpha^2 a^4 - 24\beta\alpha a^2 + 16\beta^2} \right) / a \right]. \qquad (7.8)$$

In the case of long-wave processes, $|ak_1| \leq \pi - \arccos\left(\left(\alpha a^2 - 2\beta\right)/2\beta\right)$, the secondary transverse waves propagate in opposite directions, since $k_2 k_3 < 0$. The kinematic scheme of "longwave" T_{lbb}-type triplet on the dispersion diagram is shown in Fig. 7.2.

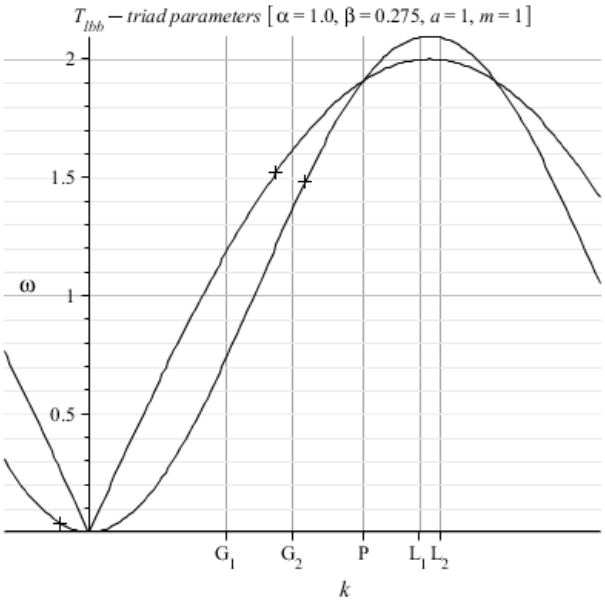

Fig. 7.2 The "longwave" phase matching due to the T_{lbb}-type triple-wave resonance. The lower point of the group matching is indicated as G_1; the higher point of the group matching – by symbol G_2; the phase matching point is indicated as P; the points L_1 and L_2 refer to the lower and upper boundaries of the "forbidden" zone for longitudinal waves

The "shortwave" resonant processes, at $|ak_1| > \pi - \arccos\left(\left(\alpha a^2 - 2\beta\right)/2\beta\right)$, are characterized by the same direction of travelling, both for the primary longitudinal and secondary transverse waves. A scheme of "shortwave" T_{lbb}-triplet is shown in Fig. 7.3.

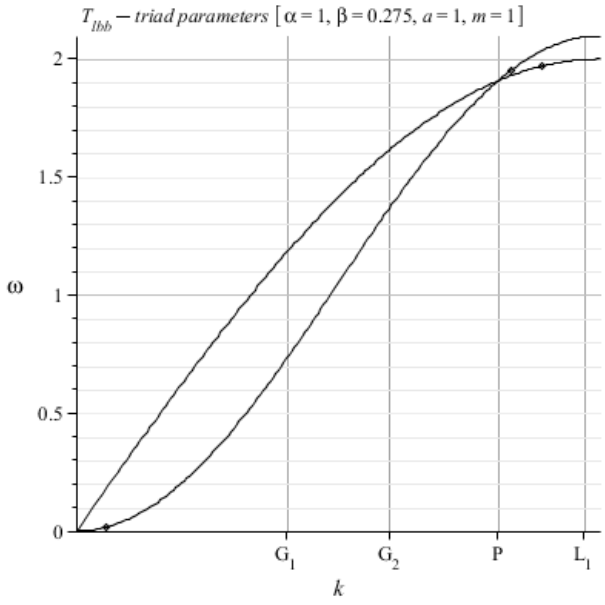

Fig. 7.3 The phase matching of the "shortwave" resonant triplet wave of T_{lbb}-type

T_{blb} -type triad

Let the high-frequency mode of the triplet of the second type, namely T_{blb} -triad, is the primary transverse wave number 1, while the numbers 2 and 3 correspond to the secondary longitudinal and transverse waves, respectively. Then the phase-matching conditions for these three waves exist only in the interval $|k_1 a| \geq \arcsin\left(a\sqrt{\alpha/\beta}/2\right)$. Figure 4 shows a "longwave" triplet of the second type, wherein the all the three waves, obviously, travel in the same direction.

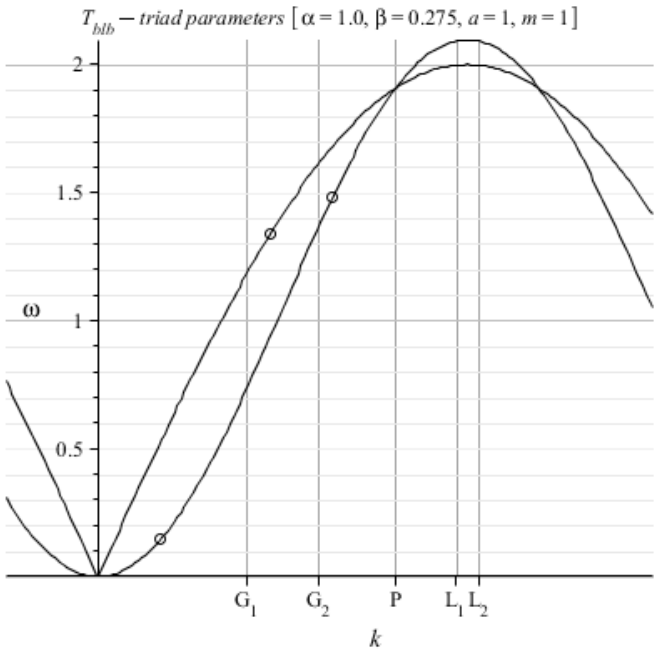

Fig. 7.4. Scheme of the "longwave" T_{blb} - type triad

T_{bbl} -type triad

Finally, a scheme of the third-type triad, named as T_{bbl} -triad, is given in Fig. 7.5. The properties of this triad are similar to that of the T_{blb} -type triad. However, as it is obvious that the two secondary waves, namely the longitudinal and transverse modes, can be both unstable: the longitudinal mode splits into a pair of transverse waves (to create a new smaller-scale T_{lbb} -triad), while the secondary transverse mode breaks up into the longitudinal and the transverse waves (to form a smaller-scale T_{blb} -type triad, in turn).

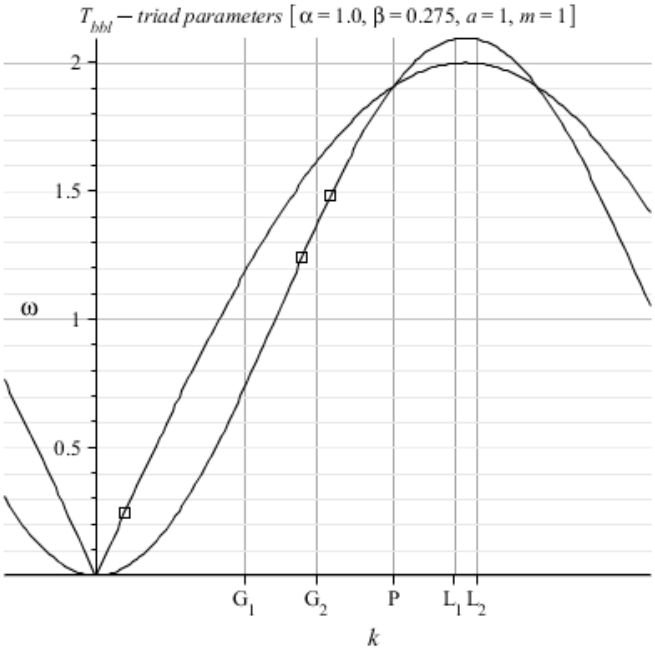

Fig. 7.5 The scheme of the "shortwave" T_{bbl} - type triad

Summarizing the above information, related the various types of resonant triads in the chain, one should pay attention to that if the high-frequency decay mode is the longitudinal wave, then the triple-frequency resonant interactions are always allowed by the phase-matching conditions (T_{lbb} -triads), except for the "forbidden" zone (7.8). If the primary mode is the high-frequency transverse wave, then the triple-wave resonant processes are possible only in the case when the group velocity of this wave is not less than that of longitudinal waves (T_{blb} -triad), i.e., the spectral parameters of the unstable transverse modes must always be above the "longwave" group-matching point. The third type of triple-wave interaction (T_{bbl} -triad) is clearly manifested in the shortwave processes, when the spectral parameters of the unstable transverse wave exceed those determined by the "shortwave" group-matching point. Figure 6 shows a cumulative result illustrating some fragments of the triple-wave resonant interactions, have been exemplified above in Fig. 7.2 – 7.5. Actually, the study of elementary properties of such cascade processes becomes of interest in this chapter.

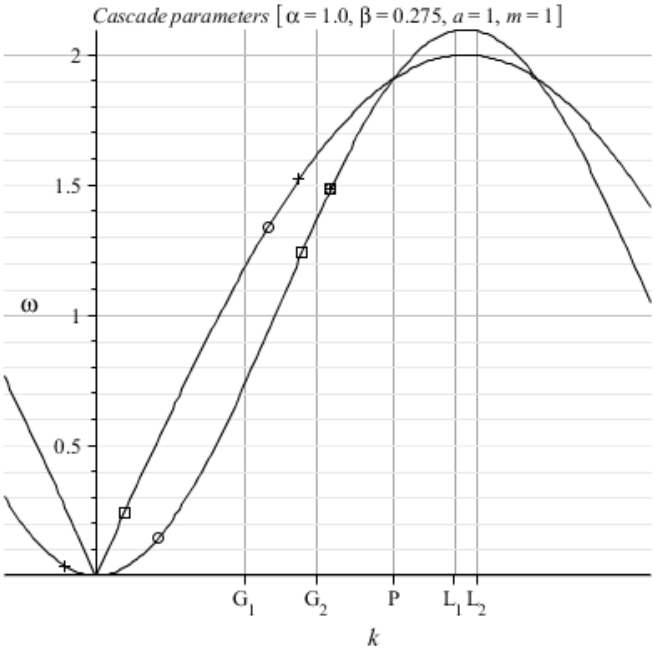

Fig. 7.6 A fragments of cascade interactions between modes belonging to triplets of T_{lbb}-, T_{blb}- and T_{bbl}-types

Evolution equations

T_{lbb}-type triad

Let the high-frequency mode of the resonant triad be a longitudinal wave. Then, after substituting the following representation of the solution:

$$u_n(t) = A_1(\tau)\exp i(\omega_1 t + k_1 an) + c.c.;$$
$$w_n(t) = A_2(\tau)\exp i(\omega_2 t + k_2 an) + A_3(\tau)\exp i(\omega_3 t + k_3 an) + c.c., \tag{7.9}$$

into the Lagrangian (7.1), where ω_m and k_m are the spectral parameters of waves entering the resonant triple; $A_m(\tau)$ are the complex amplitudes of quasi-harmonic waves that slowly varying in the time $\tau = \mu t$; *c.c.* denotes the complex conjugate of the preceding terms, the evolution equations describing the evolution of the first-type triad take the following form:

$$2m\omega_j \frac{dA_j}{d\tau} = \frac{\partial H_{lbb}}{\partial A_j^*}; \quad 2m\omega_j \frac{dA_j^*}{d\tau} = -\frac{\partial H_{lbb}}{\partial A_j}. \tag{7.10}$$

Here $H_{lbb} = c_{lbb}\left(A_1^* A_2 A_3 \exp(-i\Delta_{lbb}) - A_1 A_2^* A_3^* \exp i\Delta_{lbb}\right)$ is the average potential of the T_{lbb}-type triplet; $\Delta_{lbb} = (\omega_1 - \omega_2 - \omega_3)t + (k_1 - k_2 - k_3)an$ stands for a small phase-matching deruning; c_{lbb}

is the coefficient of the nonlinear interaction, characterized by vanishing at the phase matching point (Fig. 7.7).

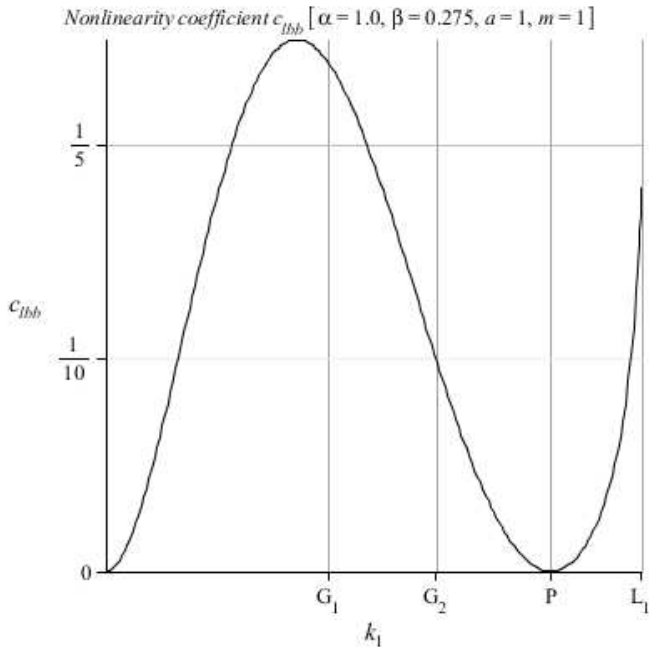

Fig. 7.7 The nonlinearity coefficient of the T_{lbb} -type triad vs. wave number

The analytical value of this nonlinearity coefficient reads as it follows:

$$c_{lbb} = \frac{2\alpha}{a}\left(\sin(ak_2) + \sin(ak_3) - \sin\left(a\left(k_2 + k_3\right)\right)\right) + \\ + \frac{2\beta}{a^3}\left(\begin{array}{l} 5\sin(ak_2) + 5\sin(ak_3) - 6\sin\left(a\left(k_2 + k_3\right)\right) - \sin(2ak_3) + \\ + \sin\left(a\left(2k_2 + k_3\right)\right) + \sin\left(a\left(k_2 + 2k_3\right)\right) - \sin(2ak_2) \end{array}\right). \tag{7.11}$$

T_{blb} - and T_{bbl} - type triads

The evolution equations of the triad of the second type are completely analogous to the written set (7.10):

$$2m\omega_j \frac{dA_j}{d\tau} = \frac{\partial H_{blb}}{\partial A_j^*}; \quad 2m\omega_j \frac{dA_j^*}{d\tau} = -\frac{\partial H_{blb}}{\partial A_j}, \tag{7.12}$$

where $H_{blb} = c_{blb}\left(A_1^* A_2 A_3 \exp\left(-i\Delta_{blb}\right) - c.c.\right)$; $\Delta_{blb} = \left(\omega_1 - \omega_2 - \omega_3\right)t + \left(k_1 - k_2 - k_3\right)an$. The coefficient of nonlinear interaction is expressed by the following formula:

$$c_{blb} = \frac{2\alpha}{a}\left(\sin\left(a\left(k_2+k_3\right)\right)-\sin\left(ak_2\right)-\sin\left(ak_3\right)\right)- \\ -\frac{2\beta}{a^3}\left(\begin{array}{l}5\sin\left(a\left(k_2+k_3\right)\right)-5\sin\left(ak_3\right)-6\sin\left(ak_2\right)+\sin\left(2ak_3\right)+\\ -\sin\left(2a\left(k_2+k_3\right)\right)+\sin\left(a\left(k_2-k_3\right)\right)+\sin\left(a\left(2k_2+k_3\right)\right)\end{array}\right). \tag{7.13}$$

Obviously, this coefficient equals zero below the “longwave” group matching point and vanishes at the phase velocity matching point. One can observe a change in the sign near the “shortwave” group-matching point. In addition, near this “shortwave” group-matching point, the nonlinearity coefficient c_{blb} can produce one more branch (Fig. 7.8). Ambiguity of the nonlinearity coefficient means that for a given value of the wave number of the unstable mode k_1, two cascade processes can be developed simultaneously. An example of such two triads, initiating the two cascades, is shown in Fig. 7.9.

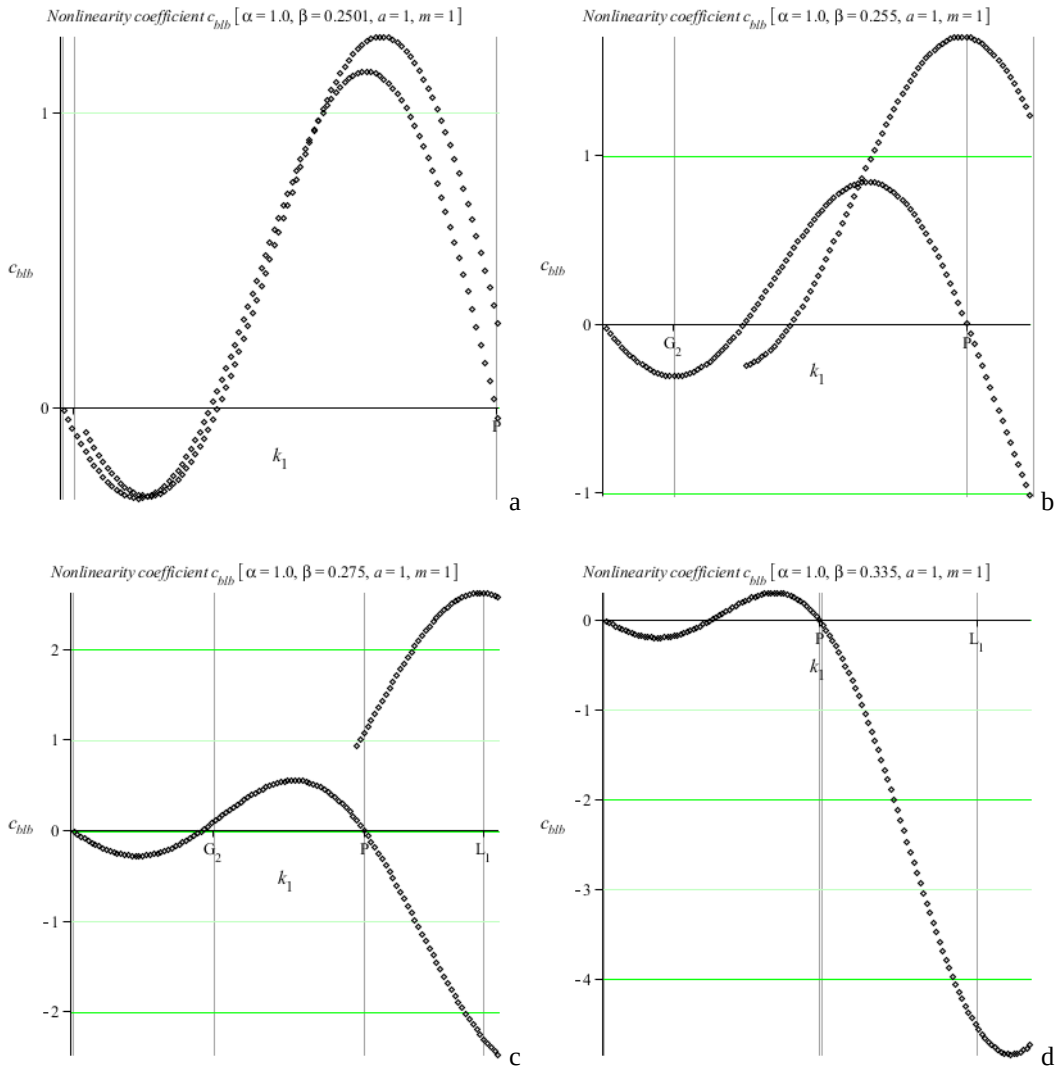

Fig. 7.8 Branches of the nonlinearity coefficient of the T_{blb}-type triad vs. increasing values of the parameter β

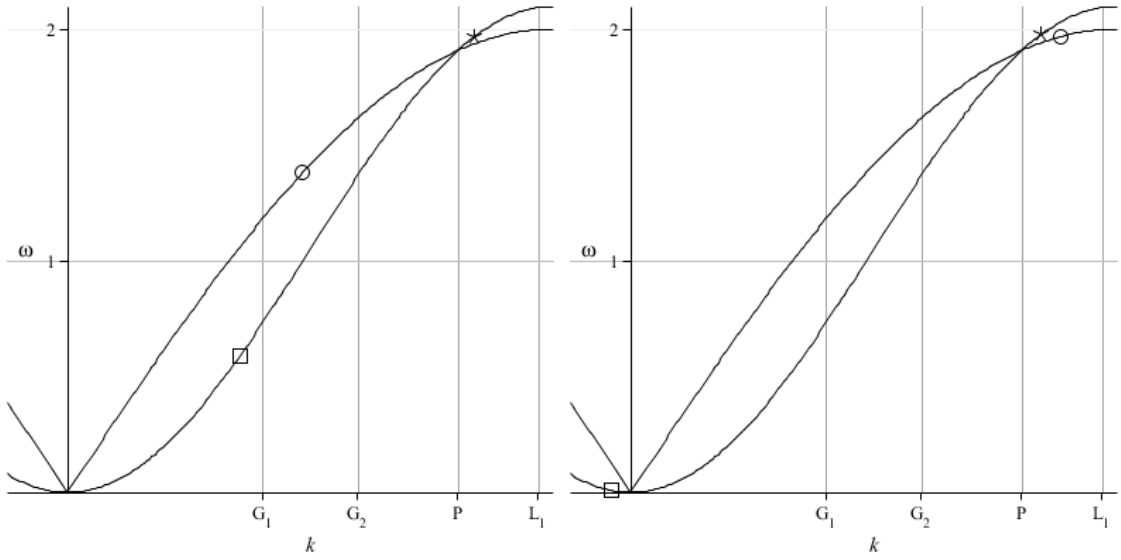

Fig. 7.9 Two different T_{blb}-type triads with the same unstable high-frequency mode marked by a star

The evolution equations and the formula for the coefficient of nonlinearity T_{bbl}-type triad are formally described by the already existing expressions (7.12) and (7.13).

Conservation laws for isolated triads

The evolution equations presented, e.g. in the form of Eq. (7.10), possess the first integrals. One of them, obviously, is the average Hamiltonian, $H_{lbb} = \text{constant}$, while the others are known as the Manley-Rowe relations:

$$\omega_1 |A_1(\tau)|^2 + \omega_2 |A_2(\tau)|^2 = c_{1,2}; \quad \omega_2 |A_2(\tau)|^2 - \omega_3 |A_3(\tau)|^2 = c_{2,3}, \tag{7.14}$$

where $c_{1,2}$, $c_{2,3}$ are arbitrary integration constants determined from the initial conditions to the Cauchy problem. These integrals of motion are sufficient for complete integrability of Eq. (7.10) or Eq. (7.12). The general solution is determined by Jacobi elliptic functions. A particular form of these solutions and some typical wave patterns, illustrating, in particular, processes of the so-called *decay instability* over the high-frequency mode of a triad had been described in the paper [102].

Cascade interaction between triads

The waves entering the resonant triads in the chain of material particles can effectively interact, being the components of triads of three different types and different spectral states. To formulate the problem of multi-wave resonant interaction in terms of the nonlinearly coupled triads pos-

sessing different types and spectral scales, one can follow the main ideas traced in papers [103–105].

There is one, not the only, main sequence governing the development of the nonlinear coupling between the resonant triads, provided that each triad can be treated now as an elemental structural element in cascade wave processes. To trace this sequence, one can suppose that the longitudinal high-frequency mode, say, inside a given triad $T_{lbb}^{(1)}$, is unstable with respect to small transverse perturbation. Thus, the secondary transverse mode of this triad at the mid-frequency $\omega_2^{(1)}$, again, due to the phase-matching conditions, plays the role of the unstable high-frequency transverse mode, though, inside the new $T_{blb}^{(2)}$-triad of a smaller scale at the frequency $\omega_1^{(2)}$, which, naturally, coincides with the mid-frequency $\omega_2^{(1)}$. In turn, the longitudinal mode at the mid-frequency $\omega_2^{(2)}$, being a member of the $T_{blb}^{(2)}$-triad, becomes unstable within the $T_{lbb}^{(3)}$-triad of the smallest scale, etc.

It should be noted that in this model, describing a successive "engagement" of triads, one specific $T_{lbb}^{(N)}$-type resonant triad always presents. This is located in the lower part of the spectrum, which is appropriately to call as "terminator". This triad prevents the further development of the cascade down the spectrum, representing the isolated triple-wave resonant ensemble. The group velocities of the transverse modes, entering this terminator, are always less than that of the extremely long longitudinal wave.

In addition to this "main sequence of the engagement" of resonant triads inherent in low-frequency processes in the chain of particles, there is one more, somewhat sophisticated type of the cascade processes. On the one hand, this scenario is inspired by the existence of different patterns inside T_{blb}-type triads having the same high-frequency transverse mode (Fig. 7.9), while on the other hand, with the occurrence of the third-type triples, namely T_{bbl}-triads (Fig. 7.5).

Recall that the T_{bbl}-type triad is characterized that the both secondary modes, namely the transverse and longitudinal ones, are unstable with respect to small perturbations. The break-up of the primary high-frequency transverse mode of the T_{bbl}-triad is accompanied by the simultaneous excitation of a new pair of triads of T_{lbb}- and T_{blb}-types, the high-frequency components of which, in turn, are the secondary low-frequency modes of the T_{bbl}-triad (Fig. 7.6). In this case, the triad chain branches, and this structure would be appropriate to call *a resonant lattice*, since this dynamical system would consist of several elemental resonant cascades. Namely, the secondary transverse mode of oscillations, being a child of the parent T_{bbl}-triad, is the unstable mode

entering into the subsidiary T_{lbb}-type triad. This T_{blb}-triad, in turn, contains the unstable transverse mode generating a new cascade of interactions accordingly to the "main sequence" scenario. The second longitudinal mode of the subsidiary T_{lbb}-triad, being unstable one, creates a new cascade of interactions between the oscillatory modes also in agree with this "main sequence" of junctions between the resonant triads. It should be noted that the total number of resonant triads, accordingly the above described model of break-up instability, is small, since the secondary mode of this T_{bbl}-type triads is always the unstable mode inside other triads possessing another pattern than the T_{bbl}-type.

Generally, the patterns of resonant interactions in the modal cascade can be represented as a tree-like graph. Subtrees of this tree are formed at the nodes related to the T_{bbl}-type triads and some T_{blb}-type triads, which are discussed above, and the crown of this tree is formed by the terminating triads of T_{lbb}-type. Similar graphs and the related dynamic processes are studied in detail in papers [106, 107].

Evolution equations of the triad chain

If one accepts the above proposed scheme of "main sequence of junctions" between the resonant triads, then the average Hamiltonian of the triad chain, consisting of N triplets, can be written as it follows

$$H = \sum_{j=1}^{N} \beta_j \left(A^*_{2j-1} A_{2j} A_{2j+1} \exp\left(-i\Delta_j\right) - A_{2j-1} A^*_{2j} A^*_{2j+1} \exp i\Delta_j \right) \tag{7.15}$$

where β_j are the nonlinearity coefficients related to the jth resonant triplet (these coefficients, in turn, alternate by pairs, c_{lbb} and c_{blb}, with account for the scale of spectral state of triples); Δ_j are possible small phase detunings $\left(j = \overline{1,N}\right)$; A_n $\left(n = \overline{1,2N+1}\right)$ are the complex amplitudes of waves, slowly varying in the time τ. The natural ordering of these amplitudes is adopted in indices: A_{2j-1} relate to the high-frequency unstable modes, A_{2j} are to the so-called "idle" modes, while A_{2j+1} denote the "signal" ones [98]. The evolution equations of the triad chain are derived from the Hamiltonian formalism of mechanics:

$$2m\omega_n \frac{dA_n}{d\tau} = \frac{\partial H}{\partial A^*_n}; \quad 2m\omega_n \frac{dA^*_n}{d\tau} = -\frac{\partial H}{\partial A_n} \quad \left(n = \overline{1,2N+1}\right). \tag{7.16}$$

If one passes from the complex amplitudes to the polar coordinates

$$A_n(\tau)=a_n(\tau)\exp i\varphi_n(\tau)\quad\left(n=\overline{1,2N+1}\right),$$

then Eq. (7.16) take the form

$$\begin{aligned}
&\dot a_1=-\frac{\beta_1}{2m\omega_1}a_2a_3\cos\psi_1;\\
&\dot a_{2j}=\frac{\beta_j}{2m\omega_{2j}}a_{2j-1}a_{2j+1}\cos\psi_j\quad\left(j=\overline{1,N}\right);\\
&\dot a_{2j+1}=\frac{\beta_j}{2m\omega_{2j+1}}a_{2j-1}a_{2j}\cos\psi_j-\frac{\beta_{j+1}}{2m\omega_{2j+1}}a_{2j+2}a_{2j+3}\cos\psi_{j+1}\quad\left(j=\overline{1,N-1}\right);\\
&\dot a_{2N+1}=\frac{\beta_N}{2m\omega_{2N+1}}a_{2N-1}a_{2N}\cos\psi_N
\end{aligned}\tag{7.17}$$

and

$$\begin{aligned}
&\dot\varphi_1=-\frac{\beta_1}{2m\omega_1}\frac{a_2a_3}{a_1}\sin\psi_1;\\
&\dot\varphi_{2j}=\frac{\beta_j}{2m\omega_{2j}}\frac{a_{2j-1}a_{2j+1}}{a_{2j}}\sin\psi_j\quad\left(j=\overline{1,N}\right);\\
&\dot\varphi_{2j+1}=\frac{\beta_j}{2m\omega_{2j+1}}\frac{a_{2j-1}a_{2j}}{a_{2j+1}}\sin\psi_j-\frac{\beta_{j+1}}{2m\omega_{2j+1}}\frac{a_{2j+2}a_{2j+3}}{a_{2j+1}}\sin\psi_{j+1}\quad\left(j=\overline{1,N-1}\right);\\
&\dot\varphi_{2N+1}=\frac{\beta_N}{2m\omega_{2N+1}}\frac{a_{2N-1}a_{2N}}{a_{2N+1}}\sin\psi_N,
\end{aligned}\tag{7.18}$$

where the angular variables $\psi_j(\tau)=\varphi_{2j-1}(\tau)-\varphi_{2j}(\tau)-\varphi_{2j+1}(\tau)\quad\left(j=\overline{1,N}\right)$ are called as *generalized phases*, and $a_n(\tau)=|A_n(\tau)|\quad\left(n=\overline{1,2N+1}\right)$ are the modulii of the complex amplitudes. The last group of $2N+1$ equations for the individual phases can be rewritten in the form of N equations for the generalized phases:

$$\begin{aligned}
&\dot\psi_1=\frac{\beta_1}{2m}\left(\frac{a_2a_3}{\omega_1a_1}-\frac{a_1a_3}{\omega_2a_2}-\frac{a_1a_2}{\omega_3a_3}\right)\sin\psi_1-\frac{\beta_2}{2m}\frac{a_4a_5}{\omega_3a_3}\sin\psi_2;\\
&\dot\psi_j=\frac{\beta_{j-1}}{2m}\frac{a_{2j-2}a_{2j-3}}{\omega_{2j-1}a_{2j-1}}\sin\psi_{j-1}+\frac{\beta_j}{2m}\left(\frac{a_{2j}a_{2j+1}}{\omega_{2j-1}a_{2j-1}}-\frac{a_{2j-1}a_{2j+1}}{\omega_{2j}a_{2j}}-\frac{a_{2j-1}a_{2j}}{\omega_{2j+1}a_{2j+1}}\right)\sin\psi_j-\\
&\qquad\frac{\beta_{j+1}}{2m}\frac{a_{2j+2}a_{2j+3}}{\omega_{2j+1}a_{2j+1}}\sin\psi_{j+1}\quad\left(j=\overline{2,N-1}\right);\\
&\dot\psi_N=\frac{\beta_{N-1}}{2m}\frac{a_{2N-2}a_{2N-3}}{\omega_{2N-1}a_{2N-1}}\sin\psi_{N-1}+\frac{\beta_N}{2m}\left(\frac{a_{2N}a_{2N+1}}{\omega_{2N-1}a_{2N-1}}-\frac{a_{2N-1}a_{2N+1}}{\omega_{2N}a_{2N}}-\frac{a_{2N-1}a_{2N}}{\omega_{2N+1}a_{2N+1}}\right)\sin\psi_N.
\end{aligned}\tag{7.19}$$

It would be noted, if the chain consists of N triplets, then the theory of differential equations specifies that the first-order resonance has the order of N [24].

Conservation laws of the cascade process

Together with the obvious integral of motion (7.15), which is naturally interpreted as the law of *energy conservation*, that is valid for any number of resonantly interacting waves, the set (7.17) and (7.18), in the case $N=1$, as it was shown above, has a pair of independent conditions known as the Manly-Rowe relations (7.14). The existence of these integrals of motion is sufficient for complete integrability. However, the system (7.17), (7.18) becomes nonintegrabile beginning from the number $N=2$.

Let us introduce the following notation $E_n=\omega_n^2\left|A_n\right|^2$. If $N=2$, then the conservation laws in the form of the Manley-Rowe relations:

$$\frac{E_1}{\omega_1}+\frac{E_2}{\omega_2}=\text{constant};\quad \frac{E_2}{\omega_2}-\frac{E_3}{\omega_3}-\frac{E_4}{\omega_4}=\text{constant};\quad \frac{E_4}{\omega_4}-\frac{E_5}{\omega_5}=\text{constant}, \tag{7.20}$$

prescribe the following energy partition between the odd modes of oscillation:

$$\frac{E_1}{\omega_1}+\frac{E_3}{\omega_3}+\frac{E_5}{\omega_5}=\text{constant},$$

and the law of the total mechanical energy conservation

$$\frac{E_1}{\omega_1}+\frac{E_2}{\omega_2}+\frac{E_3}{\omega_3}+\frac{E_4}{\omega_5}+\frac{E_5}{\omega_5}=\text{constant}.$$

If $N=2$, then the set (7.17), (7.18), together with the of the Manley-Rowe relations (7.20), has four obvious independent integrals of motion. The order of the set (7.17), (7.18) is seven, i.e., one should determine the five amplitudes and two generalized phases [108]. However, the number of available integrals of motion is insufficient for the complete integrability in quadratures. Suppose that the following inequality $N>2$ holds true, then the amount of “missing” integrals of motion just increases. For example, if $N=3$, the system (7.17), (7.18), together with the Hamiltonian (7.15) has only five independent integrals of motion:

$$\frac{E_1}{\omega_1}+\frac{E_2}{\omega_2}=\text{constant};$$
$$\frac{E_2}{\omega_2}-\frac{E_3}{\omega_3}-\frac{E_4}{\omega_4}=\text{constant};\quad \frac{E_4}{\omega_4}-\frac{E_5}{\omega_5}-\frac{E_6}{\omega_6}=\text{constant};$$
$$\frac{E_6}{\omega_6}-\frac{E_7}{\omega_7}=\text{constant},$$

which produce the energy partition between the odd modes of oscillation, analogously to the previous case:

$$\sum_{j=1}^{4}\frac{E_{2j-1}}{\omega_{2j-1}}=\text{constant}\,,$$

and the law of conservation of the total mechanical energy:

$$\sum_{n=1}^{7}E_n=\text{constant}\,.$$

Now the order of the set (7.17), (7.18) is already ten: one has got seven unknown real amplitudes and three generalized phases.

In the general case of N interacting triads, the set (7.17), (7.18) has $N+2$ obvious independent integrals of motion:

$$\begin{aligned}
&\frac{E_1}{\omega_1}+\frac{E_2}{\omega_2}=\text{constant};\\
&\frac{E_{2j}}{\omega_{2j}}-\frac{E_{2j+1}}{\omega_{2j+1}}-\frac{E_{2j+2}}{\omega_{2j+2}}=\text{constant};\ \left(j=\overline{1,N-1}\right)\\
&\frac{E_{2N}}{\omega_{2N}}-\frac{E_{2N+1}}{\omega_{2N+1}}=\text{constant}\,.
\end{aligned}\qquad (7.21)$$

The energy partition between odd modes of oscillations takes place in the form

$$\sum_{j=1}^{N+1}\frac{E_{2j-1}}{\omega_{2j-1}}=\text{constant}$$

and the total mechanical energy is naturally conserved:

$$\sum_{n=1}^{2N+1}E_n=\text{constant}\,.$$

The order of the set (7.17), (7.18) is equal to $3N+1$ (i.e., there are $2N+1$ unknown amplitudes and N unknown generalized phases). The available set of conservation laws is obviously insufficient for the complete integrability in terms of quadratures. Therefore, one should recognize numerical methods to be the only effective way to study the problem in detail. It should be noted that the numerical simulation confirms that the problem becomes very difficult even at $N=2$. This indicates inefficiency of looking for additional conservation laws, different from the Manley-Rowe relations (7.21), in order to significantly reduce the order of the differential equations (7.17) and (7.18) until the complete integrability. An algorithm dealing with such quadratic conservation laws is described in detail in the work [109].

Stationary waves in resonant chains

In general, the evolution of waves described by the nonlinear Hamiltonian system (7.17) and (7.18) is very complex, including variety of chaotic motions, limited by the energy conservation law $H=\text{constant}$ and the Manley-Rowe relations (7.21). Among the entire set of motions, the natural interest is attracted to the stable stationary multi-mode quasi-periodic oscillations which can appear in the microsystem under small nonconservative perturbations, such as temperature effects. Indeed, at certain relations between the amplitudes and phases of quasi-normal waves, the chain of resonant triads can be involved into a so-called *reactive* nonlinear interaction [110], which conserves the shape of the resonant ensemble. Simplest stationary solutions to the set (7.17) and (7.18) are the harmonic waves, periodic in the space and time.

Spatially homogeneous solutions

We study the properties of stationary waves. A particular interest is in the amplitude dispersion, i.e., the dependence between the additive corrections, Ω_j, to the natural frequencies of quasi-normal waves ω_j and the amplitudes a_j. To determine the parameters of spatially homogeneous stationary solutions of system (7.17), (7.18):

$$A_n(\tau)=a_n\exp i(\Omega_n\tau+\xi_n)\quad\left(n=\overline{1,2N+1}\right), \tag{7.22}$$

we explore $2N+1$ equations (7.19), which imply the following relations

$$\Omega_1 = \frac{\beta_1 a_2 a_3}{\omega_1 a_1};$$
$$\Omega_{2j} = \frac{\beta_j a_{2j+1} a_{2j-1}}{\omega_{2j} a_{2j}}; \quad \left(j = \overline{1, N}\right)$$
$$\Omega_{2j+1} = \frac{\beta_j a_{2j-1} a_{2j} + \beta_{j+1} a_{2j+2} a_{2j+3}}{\omega_{2j+1} a_{2j+1}}; \quad \left(j = \overline{1, N-1}\right) \tag{7.23}$$
$$\Omega_{2N+1} = \frac{\beta_N a_{2N-1} a_{2N}}{\omega_{2N+1} a_{2N+1}}$$

and the phase-matching conditions for nonlinear corrections:

$$\Omega_{2n-1} - \Omega_{2n} - \Omega_{2n+1} = 0; \quad \xi_{2n-1} - \xi_{2n} - \xi_{2n+1} = \psi_n^0, \tag{7.24}$$

where ψ_n^0 are arbitrary constants of the generalized phases. The phase-matching conditions (7.24) are determined by necessity for the existence of nontrivial steady states; therefore, the generalized phases should satisfy the following restrictions:

$$\psi_j = \pi / 2 + \pi m_j, \tag{7.25}$$

where m_j are arbitrary integers. The latter manifests the phenomenon of phase synchronization in the system, which can lead to a neutrally stable periodic or quasi-periodic motion, similar to the stable planetary orbits in the Hamiltonian mechanics [111].

To obtain the solution of the set (7.23) and (7.24), one can use the method of mathematical induction. For a single triad, as $N = 1$, the system (7.23), (7.24) gets the following form

$$a_1^2 = \frac{\Omega_2 \Omega_3 \omega_2 \omega_3}{\beta_1^2};$$
$$a_2^2 = \frac{\Omega_1 \Omega_3 \omega_1 \omega_3}{\beta_1^2};$$
$$a_3^2 = \frac{\Omega_1 \Omega_2 \omega_1 \omega_2}{\beta_1^2}.$$

If $N = 3$, then the solution to Eq. (7.23), (7.24) has the form

$$a_1^2=\frac{\Omega_2\omega_2}{\Omega_1\omega_1}a_2^2=\frac{\Omega_2\Omega_3\omega_2\omega_3}{\beta_1^2}-\left(\frac{\beta_2}{\beta_1\beta_3}\right)^2\frac{\Omega_2\Omega_6\Omega_7\omega_2\omega_6\omega_7}{\Omega_4\omega_4};$$

$$a_3^2=\frac{\Omega_1\Omega_2\omega_1\omega_2}{\beta_1^2};$$

$$a_4^2=\left(\frac{\beta_2}{\beta_1\beta_3}\right)^2\frac{\Omega_1\Omega_2\Omega_6\Omega_7\omega_1\omega_2\omega_6\omega_7}{\Omega_4\omega_4};$$

$$a_5^2=\frac{\Omega_6\Omega_7\omega_6\omega_7}{\beta_3^2};$$

$$a_6^2=\frac{\Omega_7\omega_7}{\Omega_6\omega_6}a_7^2=\frac{\Omega_5\Omega_7\omega_5\omega_7}{\beta_3^2}-\left(\frac{\beta_2}{\beta_1\beta_3}\right)^2\frac{\Omega_1\Omega_2\Omega_7\omega_1\omega_2\omega_7}{\Omega_4\omega_4}.$$

Finally, for $N=5$ the solution is as it follows

$$a_1^2=\frac{\Omega_2\Omega_3\omega_2\omega_3}{\beta_1^2}-\left(\frac{\beta_2}{\beta_1\beta_3}\right)^2\frac{\Omega_2\Omega_6\Omega_7\omega_2\omega_6\omega_7}{\Omega_4\omega_4}+\left(\frac{\beta_2\beta_4}{\beta_1\beta_3\beta_5}\right)^2\frac{\Omega_2\Omega_6\Omega_{10}\Omega_{11}\omega_2\omega_6\omega_{10}\omega_{11}}{\Omega_4\omega_4\Omega_8\omega_8};$$

$$a_2^2=\frac{\Omega_1\Omega_3\omega_1\omega_3}{\beta_1^2}-\left(\frac{\beta_2}{\beta_1\beta_3}\right)^2\frac{\Omega_1\Omega_6\Omega_7\omega_1\omega_6\omega_7}{\Omega_4\omega_4}+\left(\frac{\beta_2\beta_4}{\beta_1\beta_3\beta_5}\right)^2\frac{\Omega_1\Omega_6\Omega_{10}\Omega_{11}\omega_1\omega_6\omega_{10}\omega_{11}}{\Omega_4\omega_4\Omega_8\omega_8};$$

$$a_3^2=\frac{\Omega_1\Omega_2\omega_1\omega_2}{\beta_1^2};$$

$$a_4^2=\left(\frac{\beta_2}{\beta_1\beta_3}\right)^2\frac{\Omega_1\Omega_2\Omega_6\Omega_7\omega_1\omega_2\omega_6\omega_7}{(\Omega_4\omega_4)^2}-\left(\frac{\beta_2\beta_4}{\beta_1\beta_3\beta_5}\right)^2\frac{\Omega_1\Omega_2\Omega_6\Omega_{10}\Omega_{11}\omega_1\omega_2\omega_6\omega_{10}\omega_{11}}{(\Omega_4\omega_4)^2\Omega_8\omega_8};$$

$$a_5^2=\frac{\Omega_6\Omega_7\omega_6\omega_7}{\beta_3^2}-\left(\frac{\beta_4}{\beta_3\beta_5}\right)^2\frac{\Omega_6\Omega_{10}\Omega_{11}\omega_6\omega_{10}\omega_{11}}{\Omega_8\omega_8};$$

$$a_6^2=\frac{\Omega_5\Omega_7\omega_5\omega_7}{\beta_3^2}-\left(\frac{\beta_2}{\beta_1\beta_3}\right)^2\frac{\Omega_1\Omega_2\Omega_7\omega_1\omega_2\omega_7}{\Omega_4\omega_4}-\left(\frac{\beta_4}{\beta_3\beta_5}\right)^2\frac{\Omega_5\Omega_{10}\Omega_{11}\omega_5\omega_{10}\omega_{11}}{\Omega_8\omega_8}+$$

$$+\left(\frac{\beta_2\beta_4}{\beta_1\beta_3\beta_5}\right)^2\frac{\Omega_1\Omega_2\Omega_{10}\Omega_{11}\omega_1\omega_2\omega_{10}\omega_{11}}{\Omega_4\omega_4\Omega_8\omega_8};$$

$$a_7^2=\frac{\Omega_5\Omega_6\omega_5\omega_6}{\beta_3^2}-\left(\frac{\beta_2}{\beta_1\beta_3}\right)^2\frac{\Omega_1\Omega_2\Omega_6\omega_1\omega_2\omega_6}{\Omega_4\omega_4};$$

$$a_8^2=\left(\frac{\beta_4}{\beta_3\beta_5}\right)^2\frac{\Omega_5\Omega_6\Omega_{10}\Omega_{11}\omega_5\omega_6\omega_{10}\omega_{11}}{(\Omega_8\omega_8)^2}-\left(\frac{\beta_2\beta_4}{\beta_1\beta_3\beta_5}\right)^2\frac{\Omega_1\Omega_2\Omega_6\Omega_{10}\Omega_{11}\omega_1\omega_2\omega_6\omega_{10}\omega_{11}}{\Omega_4\omega_4(\Omega_8\omega_8)^2};$$

$$a_9^2=\frac{\Omega_{10}\Omega_{11}\omega_{10}\omega_{11}}{\beta_5^2};$$

$$a_{10}^2=\frac{\Omega_{11}\omega_{11}}{\Omega_{10}\omega_{10}}a_{11}^2=\frac{\Omega_{10}\Omega_{11}\omega_{10}\omega_{11}}{\beta_5^2}-\left(\frac{\beta_4}{\beta_3\beta_5}\right)^2\frac{\Omega_5\Omega_6\Omega_{11}\omega_5\omega_6\omega_{11}}{\Omega_8\omega_8}-$$

$$-\left(\frac{\beta_2\beta_4}{\beta_1\beta_3\beta_5}\right)^2\frac{\Omega_1\Omega_2\Omega_6\Omega_{11}\omega_1\omega_2\omega_6\omega_{11}}{\Omega_4\omega_4\Omega_8\omega_8}.$$

Solutions to the set (7.23), (7.24) for an arbitrary value N are given in the Appendix.

Obviously, the set (7.23) and (7.24) is underdetermined one. Therefore, to study the properties of stationary processes, it is necessary to allow for a number of assumptions, but without losing the generality. For example, suppose that the initial phases of individual waves, $\xi_j = \xi_j^0$, are known, and the nonlinear corrections to the frequencies, Ω_j, are directly proportional to those of normal waves, ω_j, with the proportionality coefficient $\kappa = \Omega_j / \omega_j$. Then the algebraic system of equations (7.23), (7.24) has a unique solution a_j, if this set is consistent. In this case, the spatially homogeneous solution of the problem can be interpreted as rotations of the imaging point around a $2(2N+1)$-dimensional torus in the phase space. The radius vectors on this torus are the constant amplitudes of waves, a_j, and the corresponding angular coordinates vary linearly, i.e., $\Omega_j \tau + \xi_j^0$. In the given particular case the motion will be strictly periodic, because both the frequencies ω_j and the nonlinear corrections to them Ω_j satisfy the phase-matching conditions (7.25). This means that all phase curves are closed, and not everywhere covers the torus, having a finite number of rotations. The amplitudes of the stationary waves are directly proportional to the ratio $\kappa = \Omega_j / \omega_j$, which plays a role analogous to the temperature of the thermostat. For instance, let κ be zero, then all amplitudes are also zeroes. Examples of stationary solutions for a cascade consisting of five triads, in the case of the amplitude proportional dispersion, at $\kappa = 1$, are shown in Fig. 7.10.

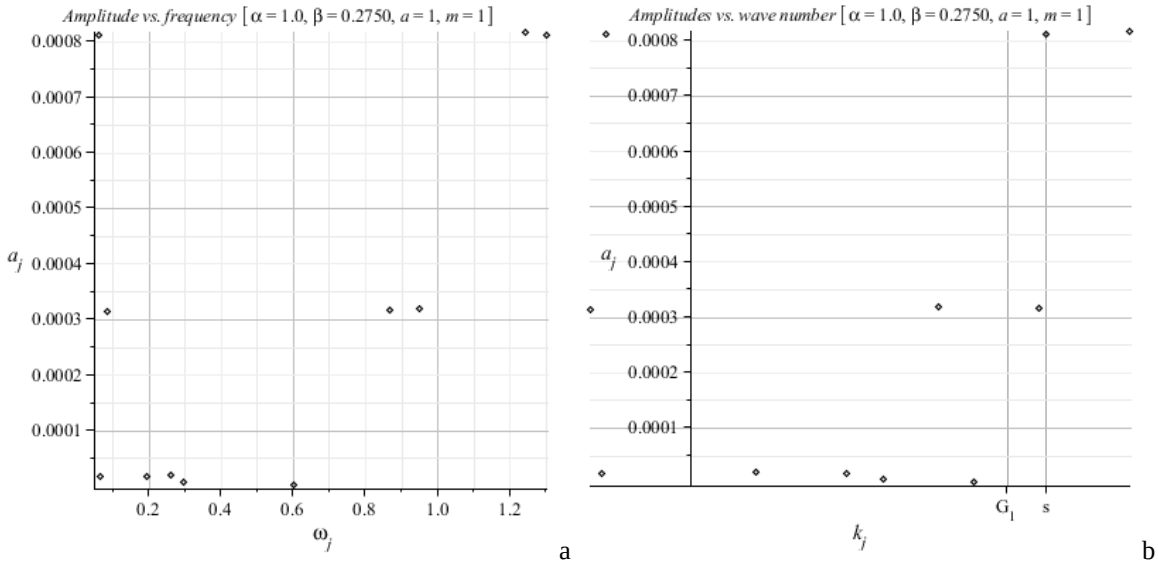

Fig. 7.10 The amplitudes of stationary wave at the amplitude-proportional dispersion (a – dependence vs. the frequency; b – the same, vs. the wave number)

Let us suppose that the nonlinear corrections, Ω_j, are not proportional to the natural frequencies, ω_j, but to the wave numbers: $\Omega_j = k_j$. Then one obtains somewhat different stationary distribu-

tion (Fig. 7.11), although the modal cascade consists of the same five triads, as in the previous example shown in Fig. 7.10.

Besides the parameters specified in the above examples for the five interacting triads, one can find such sets of the frequency corrections Ω_j, also formally satisfying the phase-matching relations (7.25), but such that the stationary solutions are absent. This means that although there are infinitely many of various stationary solutions, nonetheless, some selection rule that limits this set should exist there. The study of this question is nontrivial task, since the method for constructing the stationary solutions does not operate with elementary functions (cf. the Appendix).

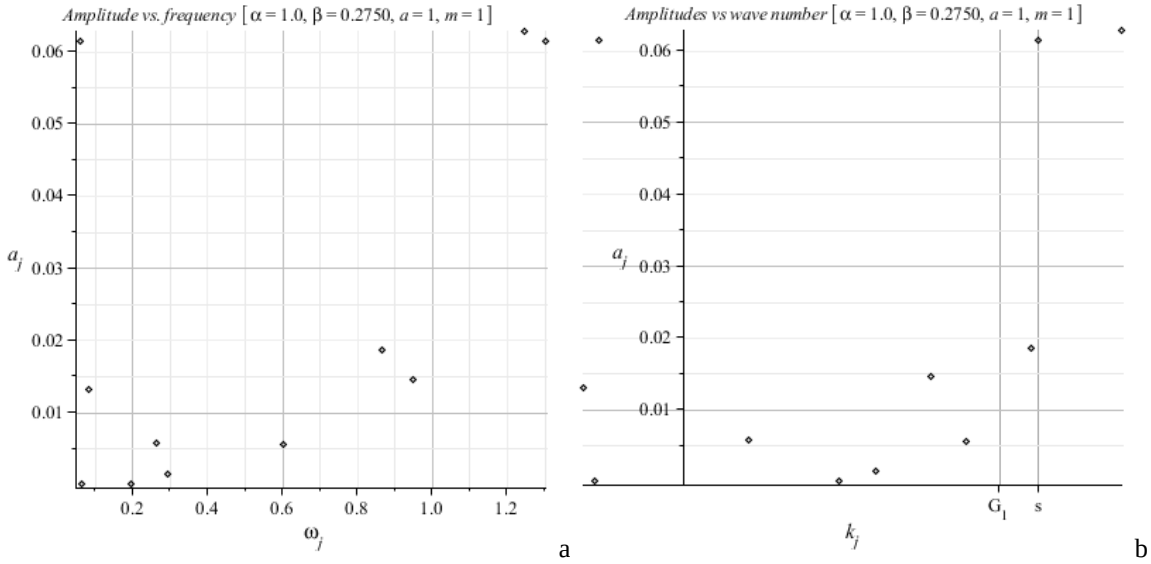

Fig. 7.11 The stationary values of amplitudes at frequency corrections proportional to the wave numbers (a – dependence upon the frequency; b – the same, vs. the wave number)

Energy distribution of stationary waves in the cascade

From the solutions to the algebraic equations (7.23) and (7.24) one can deduct an important conclusion on the patterns of the energy distribution between the quasi-harmonic modes of oscillations for the spatially homogeneous process. Namely, the energy of the modes with even indices is in the one-third ratio to those with odd indices. Moreover, the energy parts between the transverse modes with odd indices and longitudinal modes, also with odd ones, are equal. In other words, if the “total energy” of the stationary process is defined by the expression

$$\sum_{j=1}^{2N+1} \Omega_j \omega_j a_j^2 = E \,,$$

then the following outstanding relation:

$$\sum_{j=1}^{N}\Omega_{2j}\omega_{2j}a_{2j}^2=\sum_{j=1}^{(N+1)/2}\Omega_{4j-1}\omega_{4j-1}a_{4j-1}^2=\sum_{j=1}^{(N+1)/2}\Omega_{4j-3}\omega_{4j-3}a_{4j-3}^2=\frac{E}{3}$$

holds true. In particular, this fundamental law can be traced in Fig. 7.10 and Fig. 7.11, though this is not so obvious at the first sight. This situation confirms that the analytical conclusions are always more capacious than any graphic illustration. It may be noted that in the case of a single triad, the stationary solution is exactly associated with the equipartition by the Rayleigh-Jeans law.

Equation for small perturbations and stability of steady states

Perturbed motions in the chain, composed of N resonant triads near the stationary solutions, are prepared as it follows

$$A_j(\tau)=\left[a_j+b_j(\tau)\right]\exp i\left(\Omega_j\tau+\xi_j+\eta_j(\tau)\right), \tag{7.26}$$

where a_j are the constants characterizing the stationary values of the amplitudes of waves; $b_j=b_j(\tau)$ are small perturbations of these variables in the time τ; $\eta_j=\eta_j(\tau)$ stand for small perturbations to the individual phases of waves $\varphi_j(\tau)$ near the stationary values of the generalized phases of resonant triads ψ_n (7.25). The indexes vary within the following limits: $j=\overline{1,2N+1}$ and $n=\overline{1,N}$. If the perturbations b_j and η_j are absent, then the solution (7.26) is stationary and spatially homogeneous, i.e., the parameters a_j, Ω_j and ξ_j satisfying Eq. (7.23), (7.24).

The dynamics of the perturbed system near the stationary orbits is characterized by the following Lagrangian

$$\begin{aligned}l=&i\sum_{n=1}^{N}\beta_n a_{2n-1}a_{2n}a_{2n+1}\left(\eta_{2n-1}-\eta_{2n}-\eta_{2n+1}\right)^2+4i\sum_{n=1}^{2N+1}\omega_n b_n a_n\left(\frac{d\eta_n}{d\tau}\right)+2i\sum_{n=1}^{2N+1}\omega_n b_n^2\Omega_n-\\&-2i\sum_{n=1}^{N}\beta_n\left(a_{2n-1}b_{2n}b_{2n+1}-b_{2n-1}a_{2n}b_{2n+1}-b_{2n-1}b_{2n}a_{2n+1}\right)^2.\end{aligned} \tag{7.27}$$

This expression can be obtained from the original Lagrangian system (7.1), if one, after the substitution of the expression (7.26) therein, would neglect the higher-order terms, beginning from the cubic nonlinearity.

The set of linear differential equations of motion for small perturbations, generated by the Lagrangian l, if one takes into account the phase-matching conditions (7.24), reads as it follows:

$$
\begin{aligned}
&\dot{b}_1 = \frac{\beta_1 a_2 a_3 (\eta_1 - \eta_2 - \eta_3)}{2\omega_1};\\
&\dot{b}_{2n} = -\frac{\beta_n a_{2n-1} a_{2n+1} (\eta_{2n-1} - \eta_{2n} - \eta_{2n+1})}{2\omega_{2n}};\\
&\dot{b}_{2n+1} = -\frac{\beta_n a_{2n-1} a_{2n} (\eta_{2n-1} - \eta_{2n} - \eta_{2n+1})}{2\omega_{2n+1}} - \frac{\beta_{n+1} a_{2(n+1)-1} a_{2(n+1)} (\eta_{2(n+1)-1} - \eta_{2(n+1)} - \eta_{2(n+1)+1})}{2\omega_{2n+1}};\\
&\dot{b}_{2N+1} = -\frac{\beta_N a_{2N-1} a_{2N} (\eta_{2N-1} - \eta_{2N} - \eta_{2N+1})}{2\omega_{2N+1}},
\end{aligned}
\tag{7.28}
$$

and

$$
\begin{aligned}
&\dot{\eta}_1 = -\frac{\beta_1 (a_2 a_3 b_1 - a_1 a_3 b_2 - a_1 a_2 b_3)}{2\omega_1 a_1^2};\\
&\dot{\eta}_{2n} = \frac{\beta_n (a_{2n} a_{2n+1} b_{2n-1} - a_{2n-1} a_{2n+1} b_{2n} + a_{2n-1} a_{2n} b_{2n+1})}{2\omega_{2n} a_{2n}^2};\\
&\dot{\eta}_{2n+1} = \frac{\beta_n (a_{2n} a_{2n+1} b_{2n-1} + a_{2n-1} a_{2n+1} b_{2n} - a_{2n-1} a_{2n} b_{2n+1})}{2\omega_{2n+1} a_{2n+1}^2} -\\
&\quad - \frac{\beta_{n+1} (a_{2(n+1)} a_{2(n+1)+1} b_{2(n+1)-1} - a_{2(n+1)-1} a_{2(n+1)+1} b_{2(n+1)} - a_{2(n+1)-1} a_{2(n+1)} b_{2(n+1)+1})}{2\omega_{2n+1} a_{2n+1}^2};\\
&\dot{\eta}_{2N+1} = \frac{\beta_N (a_{2N} a_{2N+1} b_{2N-1} + a_{2N-1} a_{2N+1} b_{2N} - a_{2N-1} a_{2N} b_{2N+1})}{2\omega_{2N+1} a_{2N+1}^2}.
\end{aligned}
\tag{7.29}
$$

The characteristic equation to this set of ordinary differential equations has $2(2N+1)$ roots. Among these roots $2N+2$ are zeroes, while the remaining $2N$ roots are nontrivial complex conjugate roots. Moreover, these are the different purely imaginary ones. Obviously, the presence of zero roots is because of that not all the sought variables in the set (7.28) and (7.29) are independent. One can always reduce the order of the original set by introducing N generalized phases $\eta_{2n-1} - \eta_{2n} - \eta_{2n+1}$ $\left(n = \overline{1, N}\right)$, instead of using the individual phases η_j $\left(j = \overline{1, 2N+1}\right)$. In addition, the amplitude of the stationary waves, b_j $\left(j = \overline{1, 2N+1}\right)$, are coupled by $N+1$ independent constraints, in the form of the Manley-Rowe relations (7.21).

As a result, the total number of constraints, imposed on the system, is equal to $2N+2$. This one coincides with the number of zero roots. The rest of $2N$ purely imaginary roots are inherent in linear pendulum-like oscillatory systems possessing N degrees of freedom.

A concluding remark is that the measure of the perturbed motion of the triad chain near the stationary orbits should coincide with that of the small perturbations. In this interpretation, the stationary spatially homogeneous solutions are stable by the Lyapunov criterion. To prove the stability properties, one can also use the method of Lyapunov functions. Naturally, an appropriate

role of the Lyapunov function can play the Hamiltonian obtained by a suitable canonical transformation of the Lagrangian (7.27).

Heat Transport in low-dimensional systems

The quality of the heat transport depends upon the phonon scattering induced by crystalline defects. It is well known that the mean free path, $l = v_g \tau$, is associated with the motion of a phonon, travelling by inertia during some characteristic relaxation time τ, where v_g denotes the group velocity of the quasi-harmonic wave packet. Since the dispersion of longitudinal waves prescribes much greater group velocities than those of transverse waves, one can reasonably suppose that the thermal conductivity should be mainly caused by longitudinal phonons. It is evident from many experiments on glass and other bulk substances that the wave refraction appears due to the presence of small uncorrelated impurities. This is exhibited be the Rayleigh scattering, which traditionally answers on the question "why sky is blue" by predicting a transparency for the longwave packets along the beam of radiation. Point out that the Rayleigh scattering appears mainly because of random fluctuations, in contrast with the Brillouin scattering, when the parameters of a wave guide are regularly correlated because of dynamical processes. In any case of scattering, one can suppose that the lifetime should decrease with increasing number of atoms in the unit cell, and therefore the thermal energy conversion through materials should be much more efficient in lower dimensional materials at the nanoscale [112].

The heat flowing per second through unit cross section area in isotropic media can be evaluated following the phenomenological Fourier law: $\mathbf{q} = -k\nabla T$, where k is the coefficient of thermal conductivity, while sign minus directs the heat to travel always from the hot region to the cold one, accordingly to the second law of thermodynamics. In the case of a one-dimensional wire, when the temperature difference between the hot and cold ends is small, the heat flowing per second is approximated by the formula $q = k\Delta T / L$, where L denotes the length between the two thermal baths.

To study a heat current in a perturbed Hamiltonian multi-particle system, one should connect it to heat baths. For instance, the Langevin model is resulted by modifying the equation of motion of those particles which are immediately in a contact with two thermostats [113]:

$$\dot{p}_1 = -\partial H / \partial q_1 + \eta_1(t); \quad \dot{q}_1 = \partial H / \partial p_1$$

$$\dot{p}_n = -\partial H / \partial q_n; \quad \dot{q}_n = \partial H / \partial p_n \quad \left(n = \overline{2, N-1}\right) \tag{7.30}$$

$$\dot{p}_N = -\partial H / \partial q_N + \eta_N(t); \quad \dot{q}_N = \partial H / \partial p_N.$$

where $\eta_1(t)$ and $\eta_N(t)$ are the Gaussian stochastic white-noise forces with zero mean, which maintain the constant temperatures T_1 and T_N of two reservoirs. The forces $\eta_1(t)$ and $\eta_N(t)$ are supposed to be such that mean values of the kinetic energy on the ends of the system model the temperature effect: $\left\langle p_1^2 / 2m_1 \right\rangle = KT_1$; $\left\langle p_N^2 / 2m_N \right\rangle = KT_N$. The energy balance equation can be written as it follows

$$dH / dT = q,$$

where $q = \eta_1(t) p_1 / m_1 + \eta_N(t) p_N / m_N$ is the power of stochastic forces. The thermal conductivity can be evaluated as $k = qL / \Delta T$. Thus, the thermal conductivity can be calculated using either spectral analytical approach, applicable for some linear systems, or numerical Monte Carlo methods in the general case.

A question "does the Fourier law hold true in low-dimensional systems" has attracted increasing attention in recent years [112, 113]. The thermal conductivity can be evaluated in terms of the spatial size of the system, i.e., $k \sim \beta L^{\alpha}$. A normal diffusion implies a normal heat conduction obeying the Fourier law ($\alpha = 0$), an anomalous heat conduction is characterized by a divergent thermal conductivity ($\alpha > 0$), while an anomalous heat conduction has an insulator thermal conductivity ($\alpha < 0$). For instance, a ballistic thermal transport inherent in the quasiharmonic wave motion, leads to a divergent thermal conductivity, i.e. $\alpha \sim 1$. One can refer to a numerical evidence for the universal law ($\alpha \sim 1/3$) in one-dimensional systems, although nowadays many puzzles remain so far, including the accuracy of model (7.30).

Resume

The present theory of stationary cascade processes is valid only when the energy of nonlinearly interacting oscillators does not exceed the critical value determined by the equality $\hbar\omega_j = k_B T$, where $\hbar$ is the Planck constant; ω_j are the classic natural frequencies of normal modes; k_B denotes the Boltzmann constant; T is the temperature of a thermostat. The motion of the system in this limit is represented by long-wavelength acoustic waves, the propagation of which is inevitably accompanied by the energy dissipation. Therefore, the formation of stationary resonant proc-

esses, excepting trivial ones, is impossible. However, this is not so, if the energy of oscillators is comparable to that of thermal phonons, i.e., $\hbar\omega_j$. But in the latter case, it is absolutely necessary to have a quantum description, which inevitably leads a number of specific features. Quantum effects imply the vacuum states of the system, due to the non-commutatively properties of the creation ($\hat{a}^+$) and annihilation ($\hat{a}$) operators of phonons, as well as the appearance of discrete energy levels. Following a standard procedure of second quantization [114, 115], the Hamiltonian operator of the system, corresponding to the classical Hamiltonian

$$H = \sum_{n=-Z}^{Z} \frac{\partial L}{\partial \dot{U}_n} \dot{U}_n + \sum_{n=-Z}^{Z} \frac{\partial L}{\partial \dot{W}_n} \dot{W}_n - L\,,$$

where L is the Lagrangian of the original system (7.1), after the normalizing transformation, taking into account the processes allowed only the law of conservation of energy, is resulted in the following form

$$\hat{H} = \sum_{j=1}^{2N+1} \hbar\omega_j \left(\hat{a}_j^+ \hat{a}_j + \frac{1}{2} \right) + \left(\frac{\hbar}{2m} \right)^{3/2} \sum_{j=1}^{N} \frac{\beta_j}{\sqrt{\omega_{2j-1}\omega_{2j}\omega_{2j+1}}} \left(\hat{a}_{2j-1} \hat{a}_{2j}^+ \hat{a}_{2j+1}^+ - \hat{a}_{2j-1}^+ \hat{a}_{2j} \hat{a}_{2j+1} \right). \tag{7.30}$$

The first term in this operator (7.30) describes the excitation of oscillatory modes, at the frequency ω_j, by quanta of energy $\hbar\omega_j$. The individual modal energy equals to $\left(n_j + 1/2\right)\hbar\omega_j$, where the integer n_j determines the degree of excitation in the given oscillator or the number of phonons. The quantity $\hbar\omega_j/2$ corresponds to the vacuum states of the system in the absence of photons. The second term relates to the wave resonant coupling between phonons or the binding energy.

Following the Heisenberg picture, the time evolution equations of the creation and annihilation operators:

$$\frac{d\hat{a}^+}{dt} = \frac{i}{\hbar}\left(\hat{H}\hat{a}^+ - \hat{a}^+ \hat{H} \right); \quad \frac{d\hat{a}}{dt} = \frac{i}{\hbar}\left(\hat{H}\hat{a} - \hat{a}\hat{H} \right) \tag{7.31}$$

are analogous to equations governing the resonant triads (7.16). The evolution equations (7.31) have the same number of conservation laws and the total energy of quanta is also the same, as it follows from Manly-Rowe conditions (7.21). Therefore, it is natural to expect that the properties of stationary solutions to Eq. (7.31) will be similar to those obtained in the classical approximation within a context of this study. However, one should pay attention to the fact that Eq. (7.31), in a contrast to the set (7.16), may have solutions which are not reducible to the classical solu-

tions [116, 117], since the occupation numbers and the phase of oscillators, being the canonical variables are not commuting quantities. This fact should be studied in detail.

Moreover, one more question arises immediately. In the general case, the average degree of excitation of each oscillator at the given temperature T is determined by the Bose-Einstein statistics: $n_j = \left(\exp\left(\hbar\omega_j / k_B T\right) - 1\right)^{-1}$. However, for the stationary processes, for example, in a metamaterial, the phenomenological parameters of which satisfy the relation $\alpha \approx \beta a^2$, the Bose-Einstein distribution could be unfair. It argues that the Bose-Einstein statistics assumes zero binding energy of oscillators, in average. In the case of stationary cascade processes, the phase coherence, similar to the phase matching conditions (7.25), is necessary. Thus, the binding energy cannot be zero. Moreover, this is a sign-definite quantity. If the binding energy would be negative, it indicates the spontaneous formation of a coherent dynamic structure composed of nonlinear interacting oscillators, since the energy of this structure is less than that of the corresponding system of decoupled oscillators. Otherwise, in order to maintain the structure, the energy is required from outside, which would be equal or even some higher than the binding energy, and, therefore, this system becomes unstable. Thus, if the stable stationary cascade processes are physically realistic, then it can open an opportunity to create new MEMS devices with highly efficient heat and thermal conductivity parameters. But this is a topic requiring much more careful study.

CONCLUSION

When I was younger, I had a chance to practice as an engineer. I went to the task of calculating the stress-strain state of a thick cylindrical tube. This problem was complicated by a high temperature and high pressure picks inside the tube. After collecting a lot of information on thermophysical properties of the tube material, plastic flow models, etc., the time come to dive in a FEM simulation. Barely nine months, as the first results appeared. It was necessary to analyze the obtained results on the adequacy. There were reasons to think: what it was a difficult work, this absorbed all my small student skills. But all should not be hastily for me, and, after a week or two, one experienced engineer «hurried» with a little help, seeing the futility of my troubles in ensuring that everything is calculated OK. He pulled off a book from the shelf, opened this one to the right page and said “Read it”. There was a very simple formula from the well-known Lamé problem describing a deformed state in pipes under internal pressure; of course, I was well acquainted with this theory. Seeing that I have instantly read, my helper took a calculator in a couple of minutes, and then, slightly glancing at the listing of my calculations, said, “Look at”. And there was a small miracle: the result on the calculator with a precision of three decimal points was exactly the same as in my sophistical calculations. Not showing him my admiration, I said that I had no doubt of the validity in the result, but still – why have we so difficult and for a long time worked over the evidence truth, in the walls of this esteemed company. He smiled and said “when you grow up, maybe, you will know why”. Perhaps, it was my first lesson in a practical engineering. After the while, I have understood why sometimes developers propose to the user that product which is wanted to. But still, it is better to write computer games to the public, than to play them; at least, this will not be bored.

It seems that a practical engineering activity requires a certain mental alertness. It is better not to rush in the pursuit of the result, in order to get a «decent remuneration». For example, consider the deformation of a straight elastic thread:

$$\varepsilon = \sqrt{(1+u_x)^2 + w_x^2} - 1,$$

where u and w are longitudinal and transverse components of the displacements of points of the thread along the Cartesian axes x. Subscript denotes differentiation with respect to the spatial coordinate. This expression is easy to obtain, based on the Pythagorean Theorem. Let us interest in small deformations, and then the formula can be simplified by getting rid of radical, using a formal Taylor series expansion:

$$\varepsilon = u_x + u_x^2/2 + w_x^2/2 .$$

Now check the result. Let there are no transverse displacements, then the exact formula gives the correct result $\varepsilon = u_x$. But, the approximated formula contains the following error: $u_x^2/2$. What to do? Formally, the series expansion is valid. This is a convergent series, but the expansion looks to be much more complicated than the original function.

Let us consider another example. Someone needs to move the drawer in the kitchen, perhaps, without worrying of the safety for the floor surface. How, will it be easier to cope with the case: to pull or push it? Obviously, it is easier to pull this one. Let us try to formalize the problem: all is known: the mass of the box, the coefficient of dry friction, etc. Let us believe in the "school" formula for the dry friction. And, it turns out that the direction, along which this cargo is replaced, should not affect on the mechanical work performed at the same distance. This is, of course, for the first formal look. But, really, it is not so. How to be?

Let us consider one more example as a destructive obsession of paradigms. Consider the differential equation modeling the oscillator with a specific restoring force:

$$\ddot{x} + \left| x^{\alpha-1} \right| x = 0 .$$

It is obvious that solutions to this equation have essentially different left- and right-side limits near the origin, as power series. Nevertheless, many researchers, mainly from the East Europe, believe in the smooth exact solution to this equation in the form of the so-called Ateb-function. The interested reader can easily find them in relevant works traced in the World Wide, accompanied by «proofs» with expanding these mythical functions in Taylor or Fourier series, and their various applications in «practice», as well. Obviously, that is wrong, since we deal with nonsmooth functions. At the same time, one can find informative and scholarly works over the related questions in the qualitative theory of ordinary differential equations with nonanalytic right-hand terms. *Erratum humanum est. De omnibus dubitandum est.*

REFERENCES

[1] Kovriguine, D.A.: Synchronization and sommerfeld effect as typical resonant patterns. *Arch. Appl. Mech*. 82(5), 591–604 (2012)

[2] Kovriguine, D.A.: Thermo-mechanical instability in vibration absorbers. *Arch. Appl. Mech*. 83(9), 1295–1308 (2013)

[3] Kovriguine, D.A.: Vibration Absorbers Govern the Synchronized Motion, In book: *Railways: Types, Design and Safety Issues*, Editors: Cacilie Reinhardt and Klaus Shroederpp, Nova Publisher, ISBN: 978-1-62417-139-0, 51–96 (2013)

[4] Kovriguine, D.A.: Geometrical nonlinearity stabilizes a wave solid-state gyro. *Arch. Appl. Mech*. 84(2), 159–172 (2014)

[5] Kovriguine, D.A. Non-linear Self-Exited Resonant Bolometer, *Uni. J. Non-linear Mech.,* **1**, 45–55 (2013)

[6] Mathieu, Emile: *Cours de physique mathématique*. Paris, Gauthier-Villars (1873)

[7] Abramowitz, M.: *Handbook of Mathematical Functions with Formulas, Graphs, and Mathematical Tables*, Stegun, Irene A., eds. New York, Dover Publications, ISBN 978-0-486-61272-0 (1972)

[8] Janke, E., Emde, F., Lösch, F.: *Tafeln* Höherer *Funktionen. Sechste auflage*. Neubearbeitet von F.Losch, B.G.Teubuer. Verlagsgesellschaft. Stuttgard (1960)

[9] Yakubovich, V. A., Starzhinskii, V. M.: *Linear Differential Equations with Periodic Coefficients*. John-Wiley & Sons, New York-Toronto (1975)

[10] B. van der Pol: A theory of the amplitude of free and forced triode vibrations. *Radio Rev.* **1**, 754-762 (1920)

[11] Kauderer, H.: *Nichtlineare Mechanik*, Springer, Berlin (1958)

[12] Landau, L.D. and Lifshitz, E. M.: *Mechanics.* 3rd ed., Pergamon, Oxford (1976)

[13] Kovriguine, D.A., Maugin, G.A. and Potapov, A.I.: Multiwave non-linear couplings in elastic structures. I. One-dimensional examples. *Int. J. of Solids and Struct.* 39(21-22), 5571–5583 (2002)

[14] Sommerfeld, A.: Beitrage zum dynamischen ausbau der festigkeislehre. *Z. Ver. Deut. Ing*. 46, 391–394 (1902)

[15] Frolov, K.V.: Vibrations of machines with limited capacity power source and the variable parameters. In: Frolov, K.V. (ed.) *Nonlinear Oscillations and Transient Processes in Machines.* Nauka, Moscow. 5–16 (1972) [in Russian]

[16] Kononenko, V.O.: *Nonlinear Vibrations of Mechanical Systems*. Nauk. Dumka, Kiev, (1980) [in Russian]

[17] Blekhman, I.I.: *Synchronization in Nature and Technology*. Nauka, Moscow (1977) [in Russian]

[18] Blekhman, I.I., Landa, P.S., Rosenblum, M.G.: Synchronization and chaotization in interacting dynamical systems. *Appl. Mech. Rev*. 11(1), 733–752 (1995)

[19] Nagaev, R.F.: *Quasiconservative Systems*. Nauka, St. Petersburg (1996) [in Russian]

[20] Krasnopolskaya, T.S., Shvets, A.Y.: Chaos in dynamics of machines with a limited power-supply. In: Okrolnick, L. (ed.) *8-th World Congress on the Theory of Machines and Mechanisms.* **1**, 181–184. Czech. Acad. Sci., Prague (1991)

[21] Krasnopolskaya, T.S., Shvets, A.Y.: Chaos in vibrating systems with limited power-supply. *Chaos* **3**, 387–395 (1993)

[22] Krasnopolskaya, T.S.: Acoustic chaos caused by Sommerfeld effect. *J. Fluids Struct*. **8**, 803–815 (1994)

[23] Arnold, V.I.: *Geometrical methods in the theory of ordinary differential equations*. Springer, Berlin (1988)

[24] Zhuravlev, V.F., Klimov, D.M.: *Applied Methods in Oscillation Theory*. Nauka, Moscow (1988) [in Russian]

[25] Leonov, G.A., Ponomarenko, D.V., Smirnova, V.B.: *Frequency-domain Methods for Nonlinear Analysis. Theory and applications*. World Science, Singapore (1996)

[26] Dantas, M.J.H., Balthazar, J.M.: On the existence and stability of periodic orbits on non ideal problem: general results. *Z. Angew Math. Phys*. **58**, 940–956 (2007)

[27] Appleton, E.V.: The automatic synchronization of triode oscillator. *Proc. Cambridge Phil. Soc.* **21**, 231–248 (1922)

[28] Van der Pol, B.: Forced oscillations in a circuit with non-linear resistance. *Phil. Mag*. **3**, 64–80 (1927)

[29] Andronov, A.A., Witt, A.A.: By the mathematical theory of capture. *Zhurn. Math. Phys*. 7(4), 3–20 (1930)

[30] Tricomi, F.: Integrazione di unequazione differenziale presentasi in electrotechnica. *Annali Della Roma Schuola Normale Superiore de Pisa.* 2(2), 1–20 (1933)

[31] Leonov, G.A.: Discontinuous load rating problem for inductor motors. *Tech. Mech*. 24(3–4), 271–276 (2004)

[32] Blekhman, I.I., Fradkov, A.L., Nijmeijer, H., Pogromsky, A.Y.: On self-synchronization and controlled synchronization. *Syst. Control Lett*. **31**, 299–305 (1997)

[33] Blekhman, I.I., Fradkov, A.L., Tomchina, O.P., Bogdanov, D.E.: Self-synchronization and controlled synchronization: gen- eral definition and example design. *Math. Comput. Simul*. 58(4–6), 367–384 (2002)

[34] Blekhman, I.I., Fradkov, A.L.: On general definitions of synchronization. In: Blekhman, I.I. (ed.) *Selected Topics in Vibrational Mechanics*. World Scientific, Singapore, 179–188 (2004)

[35] Rosenblum, M.G., Pikovsky, A.S., Kurths, J.: Phase synchronization of chaotic oscillators. *Phys. Rev. Lett*. **76**, 1804–1807 (1996)

[36] http://kovriguineda.ucoz.ru/index/motors/0-28/

[37] Haken, H.: *Advanced Synergetics: Instability Hierarchies of Self-Organizing Systems and Devices*. Springer, New-York (1993)

[38] Rumyantsev, S.A., Azarov, E.B.: Study of transient dynamics vibrating and transporting machines using a mathematical model. *Transp. Ural* 4(7), 45–51 (in Russian) (2005)

[39] Astashev, V.K., Babitsky, V.I., Kolovsky, M.Z.: *Dynamics and Control of Machines*. Series: Foundations of Engineering Mechanics. Springer, Berlin (2000)

[40] Wang, L.X., Melnik, R.V.N.: Numerical model for vibration damping resulting from the first-order phase transforma- tions. *Appl. Math. Model*. **31**, 2008–2018 (2007)

[41] Lacarbonara, W., Bernardini, D., Vestroni, F.: Nonlinear thermomechanical oscillations of shape-memory devices. *Int. J. Solids Struct*. **41**, 1209–1234 (2004)

[42] Tiseo, B., Concilio, A., Ameduri, S., Gianvito, A.: A shape memory alloys based tunable dynamic vibration absorber for vibration tonal control. *J. Theor. Appl. Mech*. 48(1), 135–153 (2010)

[43] Landa, P.S., Duboshinskii, Y.B.: Self-oscillatory systems with high-frequency energy sources. *Sov. Phys. Usp*. **32**, 723–731 (1989)

[44] Tondl, A.: To the problem of self-excited vibration suppression. *Eng. Mech*. 5(4), 297–307 (2008)

[45] Kandaurova, G.S.: New phenomena in the low-frequency dynamics of magnetic domain ensembles. *Phys. Usp*. **45**, 1051–1072 (2002)

[46] Gordeev, B.A., Okhulkov, S.N., Osmekhin, A.N., Gorskov, V.P.: Long-term sealing loss of hydraulic bearings. *Russ. Eng. Res*. 31(7), 647–650 (2011)

[47] Webb, I.R., Payne, S.J., Coussios, C.C.: The effect of temperature and viscoelasticity on cavitation dynamics during ultrasonic ablation. *J. Acoust. Soc. Am*. **130**, 3458–3466 (2011)

[48] Bruno, A.D.: *Local Methods in Nonlinear Differential Equations*. Nauka, Moscow (1979)

[49] http://kovriguineda.ucoz.ru/index/absorber/0-32/

[50] Liu, H.P., Wu, T.X.: Modelling and performance analysis of rail vibration absorber by FE and BE Methods. In: *Noise and Vibration Mitigation for Rail Transportation Systems. Notes on Numerical Fluid Mechanics and Multidisciplinary Design*. **118**, 135–142 (2012)

[51] Fogelson, R.L., Likhachev, E.P.: Temperature dependence of viscosity. *Tech. Phys*. 71(8), 128–131 (2001)

[52] Samani, F.S., Pellicano, F.: Vibration reduction of beams under successive traveling loads by means of linear and nonlinear dynamic absorbers. *J. Sound Vib*. 331(10), 2272–2290 (2012)

[53] Agnes, G.S., Inman, D.J.: Nonlinear piezoelectric vibration absorbers. *Smart Mater. Struct*. **5**, 704–714 (1996)

[54] Lynch, D.D.: HRG development at Delco, Litton, and Northrop Grumman. In: *Proceedings of of Anniversary Workshop on Solid-State Gyroscopy*, 19–21 May 2008. Yalta, Ukraine. Kyiv-Kharkiv. ATS of Ukraine, ISBN:978-976-0-25248-5 (2009)

[55] Bryan, G.H.: On the beats in the vibrations of a revolving cylinder or bell. *Proc. Camb. Philos. Soc. Math. Phys. Sci*. VII(III), 101–111 (1890)

[56] Zhuravlev, V.F., Klimov, D.M.: *Wave Solid-State Gyro*. Nauka Publisher, Moscow (1985) [in Russian]

[57] Bose, A., Puri, S., Banerjee, P.: *Modern Inertial Sensors and Systems*. Prentice-Hall of India, New Delhi, II (2008)

[58] Osiander, R., Darrin, M.A.G., Champion, J.L.: *MEMS and Microstructures in Aerospace Applications*. Taylor & Francis Publisher, London. ISBN:0824726375 (2005)

[59] Flügge, W.: *Stresses in Shells*, 2nd edn. Springer, New-York (2005)

[60] Donnell, L.H.: *Beams, Plates and Shells*. McGraw-Hill, New-York (1979)

[61] Lindberg, H.E.: Stress amplification in a ring caused by dynamic instability. *Trans. ASME J. Appl. Mech*. 41(2), 390–400 (1974)

[62] Glynn, C.C.: On the resonant nonlinear travelling waves in a thin rotating ring. *Int. J. Non-Linear Mech*. 17(5/6), 327–341 (1982)

[63] Natsiavas, S.: On the dynamics of rings rotating with variable spin speed. *Nonlinear Dyn*. **7**, 345–363 (1995)

[64] Martynenko, Y.G., Merkuryev, I.V., Podalkov, V.V.: Control of nonlinear vibrations of vibrating ring microgyroscope. *Mech. Solids* 43(3), 379–390 (2008)

[65] Hydon, P.E.: *Symmetry Methods for Differential Equations. A Beginner's Guide*. University of Surrey, Guildford. ISBN:9780521497862 (2000)

[66] Phillips, O.M.: *The Dynamics of the Upper Ocean*. Cambridge University Press, Cambridge, MA (1977)

[67] Kovriguine, D.A., Potapov, A.I.: Nonlinear oscillations in a thin ring—I, II. *Acta Mech*. **126**, 189–212 (1998)

[68] Kovriguine, D.A.: On non-linear resonant excitation of a wave solid-state gyro. In: Jezequel, L. (ed.) *Proceedings of International Congress MV2: New Advances in Modal Synthesis of Large Structures, Non-linear, Damped and Non-deterministic Cases*. École Centrale de Lyon, **2**, 575–586 (1995)

[69] Whitham, G.B.: *Linear and Nonlinear Waves*. Wiley-Interscience, New-York (1995)

[70] Zakharov, V.E., Kuznetsov, E.A.: Hamiltonian formalism for nonlinear waves. *UFN* 167(11), 1137–1167 (1997)

[71] Gledzer, E.B., Dolzhansky, F.W., Obukhov, A.M.: *Systems of Hydrodynamic Type and Their Applications*. Nauka Publisher, Moscow (1981) [in Russian]

[72] Nayfeh, A., Balachandran, B.: *Applied Nonlinear Dynamics: Analytical, Computational and Experimental Methods*. Wiley, New-York (1995)

[73] Mazin, B.A., Bumble, B. et al. Position sensitive x-ray spectrophotometer using microwave kinetic inductance detectors. *Appl.Phys.Lett*. **89** 222507–222510 (2006)

[74] Day P, Le Duc H, et al. (2003) A broadband superconducting detector suitable for use in large arrays. *Nature*. **425**, 817–820

[75] Shitov, S.V.: Bolometer with high-frequency readout for array applications. *Tech.Phys.Lett*. 37(10), 932–934 (2011)

[76] Segev, E., Suchoi, O. et al.: Self-oscillations in a superconducting strip-line resonator integrated with a DC superconducting quantum interference device. *Appl.Phys.Lett*. **95**, 152509-152509 (2009)

[77] Vijay, R., Devoret, M.H. and Siddiqi, I.: Invited review article: The josephson bifurcation amplifier. *Rev. Sci. Instrum*. 80(11), 111101-1:17 (2009)

[78] Nyquist, H.: Thermal Agitation of Electric Charge in Conductors. *Phys.Rev*. **32**, 110934 113 (1928)

[79] Aldert van der Ziel: *Noise in Solid State Devices and Circuits*. Wiley-Interscience (1986)

[80] Josephson, B.D.: Possible new effects in superconductive tunneling. *Phys. Lett*. **1**, 251–253 (1962)

[81] Feynman. R.P., Leighton, R.B. and Sands, M.: *The Feynman Lectures on Physics*. Vol. 3: *Quantum Mechanics*. Massachusetts, Addison-Wesley (1965)

[82] Ginzburg, V.L.: On superconductivity and superfluidity. *Physics-Uspekhi*. **47**(11) 1155-1170 (2004)

[83] Cooper, L.N.: Bound electron pairs in a degenerate Fermi gas. *Phys.Rev*. **104**, 1189–1190 (1956)

[84] Bardeen, J., Cooper L.N., Schrieffer. J.R. Microscopic theory of superconductivity. *Phys.Rev*. **106**, 162–164 (1957)

[85] Bardeen, J., Cooper L.N., Schrieffer, J.R.: Theory of superconductivity. *Phys.Rev*. 108(5), 1175–1204 (1957)

[86] Buckingham, M.J.: Schematic diagram of the apparatus for infrared measurements. *Phys.Rev*. **101**, 1431–1432 (1956)

[87] Johnson, J.B.: Thermal agitation of electricity in conductors. *Phys. Rev*. **32**, 97–109 (1928)

[88] Mather, J.C.: Bolometer noise: nonequilibrium theory. *Appl Opt*. 21(6), 1125–1129 (1982)

[89] http://kovriguineda.ucoz.ru/index/bolometer/0-31/

[90] Tachiki, M., Ivanovic, K,, Kadowaki, K.: Emission of terahertz electromagnetic waves from intrinsic Josephson junction arrays embedded resonance in LCR circuits. *Phys.Rev.B*. **83**, 014508–014515 (2011)

[91] Riedl, C., Coletti, C. et al.: Quasi-free-standing epitaxial graphene on SiC obtained by hydrogen intercalation. *Phys.Rev.Lett*. **103**, 246804–246807 (2009)

[92] Yuehang, Xu, Changyao, Chen et al.: Radio frequency electrical mechanical transduction of graphene resonators. *Appl.Phys.Lett*. **97**, 243111–243113 (2010)

[93] Nakamura. Y. et al.: Control of coherent macroscopic quantum states in a single-Cooper-pair box. *Nature*. **398**, 786–788 (1999)

[94] Henderson, D.M., Hammack, J.L.: Experiments on ripple instabilities. Part 1. Resonant triads. *J. Fluid Mech*. 184(11), 15–41 (1987)

[95] Perlin, M., Henderson, D. and Joe Hammack: Experiments on ripple instabilities. Part 2 Selective amplification of resonant triads. *J. Fluid Mech*. 219(10), 51–80 (1990)

[96] Chow, C.C., Henderson, D. and Harvey Segur: A generalized stability criterion for resonant triad interactions. *J. Fluid Mech*. 319(6), 67–76 (1996)

[97] Nika, D.L., Pokatilov E.P., Askerov, A.S. and A. A. Balandin: Phonon thermal conduction in graphene: Role of Umklapp and edge roughness scattering. *Phys. Rev. B* **79**, 155413– (2009)

[98] Kaup, P.J., A. Reiman & A. Bers: Space-time evolution of nonlinear three-wave interactions. Interactions in a homogeneous medium. *Rev.of Modern Phys.* 51(2), 275–309 (1979)

[99] Kovriguine, D.A., Potapov, A.I.: Nonlinear Waves in Elastic Bar. *Eur. J. Mech. A/Solids*, 15(6), 1049–1075 (1996)

[100] Ziman, J. M.: *Electrons and phonons*. Clarendon Press: Oxford (1960)

[101] Ball, F. K.: Energy transfer between external and internal gravity waves. *J. Fluid Mech*., **19**, 465–478 (1964)

[102] Kartashova, Elena: Nonlinear resonances of water waves. *DCDS-B*, 12(3), 607–621 (2009)

[103] Richardson, L.F.: *Weather Prediction by Numerical Process*. Cambridge University Press (2007)

[104] Landau, L.D.: To the problem of turbulence. *DAN SSSR*. **44**, 339–344 (1944)

[105] Zakharov, V.E.: The Hamiltonian formalism for nonlinear waves in dispersive media. *Proceedings of Higher Education, Radio.* 17(4), 431–453 (1974) [in Russian]

[106] L'vov, Victor S., Pomyalov, A., Procaccia, I. and Oleksii Rudenko: Finite-dimensional turbulence of planetary waves. *Phys. Rev., E* **80**, 066319 – (2009)

[107] Bustamante, M.D., Kartashova, E.: Resonance Clustering in Wave Turbulent Regimes: Integrable Dynamics. *Commun. Comput. Phys*. **10**, 1211–1240 (2011)

[108] Kovriguine, D. A.; Maugin, G. A.; Potapov, A. I.: Multiwave non-linear couplings in elastic structures. Part II: two-dimensional example. *J. Sound and Vibration*. 263(5), 1055–1069 (2003)

[109] Harper, K.L., Bustamante, M.D. and Nazarenko S.V.: Quadratic invariants for discrete clusters of weakly interacting waves. *J. Phys. A: Math. Theor*. **46**. 245501–, (2013)

[110] Sukhorukov, A.P.: *Nonlinear wave interactions in optics and radio physics*. Moscow, Nauka (1988) [in Russian]

[111] Arnold, V.I.: Small denominators and problems of stability of motion in classical and celestial mechanics. *Advances Mathematical Sciences* ie XVIII, Issue 6 (114), 91–192 (1963) [in Russian]

[112] Pichanusakorn, P., Bandaru, P.: Nanostructured thermoelectrics. *Materials Science and Engineering: R: Reports.* 67(2–4). 19–63 (2010)

[113] Abhishek Dhar: Heat Transport in low-dimensional systems. *Adv. in Physics*, 57(5), 457–537 (2008)

[114] Pitaevskii, L.P., Lifshitz, E.M.: *Physical Kinetics*. **10** (1st ed.). Butterworth-Heinemann Ltd. (1981)

[115] Harrison, Walter A.: *Solid state theory*. New York, Dover Publications (1980)

[116] Misochko, O. V.: Nonclassical states of lattice excitations: squeezed and entangled phonons. *Phys. Usp*. **56**, 868– (2013)

[117] Kazakovtsev, D.V., Levinson, I.B.: Propagation of phonon pulses in the regime of spontaneous phonon decay. *JETP Lett*. 27 (3), 181–183 (1978)

APPENDIX

Algorithm to find stationary oscillations of the triad chain

The method of mathematical induction is utilized to construct solutions to Eqs. (7.23) and (7.24).

Step 1.

Let $N=1$. Consider the vector 3×1:

$$M_{1,1}=\begin{bmatrix}1\\1\\1\end{bmatrix}$$

and the scalar $E_{1,1}=\Omega_1\Omega_2\Omega_3\omega_1\omega_2\omega_3/\beta_1^2$, characterizing the modal energy in the chain consisting of a single resonant triad. Vector $\left[\Omega_1\omega_1 a_1^2/4 \quad \Omega_2\omega_2 a_2^2/4 \quad \Omega_3\omega_3 a_3^2/4\right]^T = M_{1,1}E_{1,1}$ gives the solution to the problem at $N=1$.

Step 2.

Let $N=3$. We consider the matrices $M_{1,3}$ and $M_{3,3}$, dimension 7×2:

$$M_{1,3}=\begin{bmatrix}1&0\\1&0\\1&0\\0&0\\0&1\\0&1\\0&1\end{bmatrix};\ M_{3,3}=\begin{bmatrix}0&1\\0&1\\0&0\\0&-1\\0&0\\0&1\\0&1\end{bmatrix}$$

and vectors

$$V_{1,3}=\left[E_{1,1} \quad E_{1,3}\right];\ V_{3,3}=\left[0 \quad E_{3,3}\right],$$

where $E_{1,3}=\dfrac{\Omega_5\Omega_6\Omega_7\omega_5\omega_6\omega_7}{\beta_3^2}$; $E_{3,3}=\left(\dfrac{\beta_2}{\beta_1\beta_3}\right)^2\dfrac{\Omega_1\Omega_2\Omega_6\Omega_7\omega_1\omega_2\omega_6\omega_7}{\Omega_4\omega_4}$.

The vector $\left[\Omega_1\omega_1 a_1^2/4 \quad \Omega_2\omega_2 a_2^2/4 \quad \Omega_3\omega_3 a_3^2/4\right]^T = M_{1,3}V_{1,3}+M_{3,3}V_{3,3}$ gives a solution of the problem for $N=3$.

Step 3.

Let $N=5$. We introduce the matrices $M_{1,5}$, $M_{3,5}$ and the matrix $M_{5,5}$ of the dimension 11×3:

$$M_{1,5}=\begin{bmatrix}1&0&0\\1&0&0\\1&0&0\\0&0&0\\0&1&0\\0&1&0\\0&1&0\\0&0&0\\0&0&1\\0&0&1\\0&0&1\end{bmatrix};\ M_{3,5}=\begin{bmatrix}0&1&0\\0&1&0\\0&0&0\\0&-1&0\\0&0&1\\0&1&1\\0&1&0\\0&0&-1\\0&0&0\\0&0&1\\0&0&1\end{bmatrix};\ M_{5,5}=\begin{bmatrix}0&0&1\\0&0&1\\0&0&0\\0&0&-1\\0&0&0\\0&0&1\\0&0&0\\0&0&-1\\0&0&0\\0&0&1\\0&0&1\end{bmatrix}$$

as well as, the vectors $V_{1,5}$, $V_{3,5}$ and $V_{5,5}$ (dimension 3×1):

$$V_{1,5}=\begin{bmatrix}E_{1,1} & E_{1,3} & E_{1,5}\end{bmatrix};\ V_{3,5}=\begin{bmatrix}0 & E_{3,3} & E_{3,5}\end{bmatrix};\ V_{5,5}=\begin{bmatrix}0 & 0 & E_{5,5}\end{bmatrix},\ \text{where}$$

$$E_{1,5}=\frac{\Omega_9\Omega_{10}\Omega_{11}\omega_9\omega_{10}\omega_{11}}{\beta_5^2};$$

$$E_{3,5}=\left(\frac{\beta_4}{\beta_3\beta_5}\right)^2\frac{\Omega_5\Omega_6\Omega_{10}\Omega_{11}\omega_5\omega_6\omega_{10}\omega_{11}}{\Omega_8\omega_8};$$

$$E_{5,5}=\left(\frac{\beta_2\beta_4}{\beta_1\beta_3\beta_5}\right)^2\frac{\Omega_1\Omega_2\Omega_6\Omega_{10}\Omega_{11}\omega_1\omega_2\omega_6\omega_{10}\omega_{11}}{\Omega_4\omega_4\Omega_8\omega_8}.$$

The vector $\begin{bmatrix}\Omega_1\omega_1a_1^2/4 & \Omega_2\omega_2a_2^2/4 & \dots & \Omega_{11}\omega_{11}a_{11}^2/4\end{bmatrix}^T=\sum_{i=1}^{3}(-1)^{i+1}M_{2i-1,5}V_{2i-1,5}$ provides the solution to the problem at $N=5$.

Step i.

Let the solution to the set (7.23), (7.24) is available at $N=2i-3$, where i is the number of previous iterations. Auxiliary matrices $M_{1,N-2}$, $M_{3,N-2}$, ..., $M_{N-2,N-2}$ have dimensions $(2N-1)\times(i-1)$. Auxiliary matrix, prepared to get a solution on the next iteration i: $M_{1,N}$, $M_{3,N}$, ..., $M_{N-2,N}$, are obtained by increasing the dimensions of the corresponding matrices at the current iteration, $i-1$ until $(2N+1)\times i$, by adding zeros on the positions that appeared due to

the expansion of all the matrices, except the last column. In this case, the principal minor of the new matrices are the same matrix in the current iteration. The last column of the new matrix is obtained from the previous column by the shift its elements four rows down. The top four positions of the last column of the new matrix are occupied by zeros. The matrix $M_{N,N}$ has the same dimension as the extended matrix. It is filled with zeros except his last column. Positions of the first and the last element in the last column in this matrix are filled by units. Internal positions of elements of this column are filled by quartets of alternate numbers: 1, 0, -1, 0. The dimension of the auxiliary vectors $V_{1,N-2}$, $V_{3,N-2}$, ..., $V_{N,N-2}$ on i-th iteration is $(i-1)\times 1$. Let these vectors are known and have the following form:

$$V_{1,N-2} = \lfloor E_{1,1} \quad E_{1,3} \quad E_{1,5} \quad E_{1,7} \quad ... \quad E_{1,N-2} \rfloor;$$

$$V_{3,N-2} = \lfloor 0 \quad E_{3,3} \quad E_{3,5} \quad E_{3,7} \quad ... \quad E_{3,N-2} \rfloor;$$

$$V_{5,N-2} = \lfloor 0 \quad 0 \quad E_{5,5} \quad E_{5,7} \quad ... \quad E_{5,N-2} \rfloor; \ldots;$$

$$V_{N-2,N-2} = \lfloor 0 \quad 0 \quad 0 \quad 0 \quad ... \quad E_{N-2,N-2} \rfloor.$$

Then the auxiliary vectors solving the problem on the i-th iteration appear as:

$$V_{1,N} = \lfloor V_{1,N-2} \quad E_{1,N} \rfloor;$$

$$V_{3,N} = \lfloor V_{3,N-2} \quad E_{3,N} \rfloor;$$

$$V_{5,N} = \lfloor V_{5,N-2} \quad E_{5,N} \rfloor; \ldots;$$

$$V_{N-2,N} = \lfloor V_{N-2,N-2} \quad E_{N-2,N} \rfloor;$$

$$V_{N,N} = \lfloor 0 \quad 0 \quad ... \quad 0 \quad ... \quad E_{N,N} \rfloor,$$

where the last element of the vector $V_{1,N}$ is calculated by the formula

$$E_{1,N} = \frac{\Omega_{2N-1}\Omega_{2N}\Omega_{2N+1}\omega_{2N-1}\omega_{2N}\omega_{2N+1}}{\beta_N^2},$$

and the remaining unknown elements of the vectors $V_{1,N}$ are calculated with increment two by the index j: $j = 1..(N-1)/2$. The last components of the vectors are given by

$$E_{j+2,N} = E_{j,N}\left(\frac{\beta_{N-j}}{\beta_{N-(j+1)}}\right)^2 \frac{\mu_{N-(j+1)}}{\mu_{N-j}},$$

where $\mu_n = \prod_{i=-1}^{1} \Omega_{2n-i}\omega_{2n-i}$.

For example, if $j = 1$, then the last expression reads

$$E_{3,N} = \left(\frac{\beta_{N-1}}{\beta_{N-2}\beta_N}\right)^2 \frac{\Omega_{2N-5}\Omega_{2N-4}\Omega_{2N}\Omega_{2N+1}\omega_{2N-5}\omega_{2N-4}\omega_{2N}\omega_{2N+1}}{\Omega_{2N-2}\omega_{2N-2}}.$$

Let j be two, then

$$E_{5,N} = \left(\frac{\beta_{N-1}}{\beta_{N-2}\beta_N}\right)^2 \frac{\Omega_{2N-9}\Omega_{2N-8}\Omega_{2N-4}\Omega_{2N}\Omega_{2N+1}\omega_{2N-9}\omega_{2N-8}\omega_{2N-5}\omega_{2N-4}\omega_{2N}\omega_{2N+1}}{\Omega_{2N-6}\Omega_{2N-2}\omega_{2N-6}\omega_{2N-2}}.$$

The vector $\left[\Omega_1\omega_1 a_1^2/4 \quad \Omega_2\omega_2 a_2^2/4 \quad ... \quad \Omega_{2N+1}\omega_{2N+1}a_{2N+1}^2/4\right]^T = \sum_{i=1}^{(N-1)/2} (-1)^{i+1} M_{2i+1,N} V_{2i+1,N}$ gives a solution to the problem for arbitrary value N. Obviously, the induction basis is presented by the steps 1 and 2, the step number i is inductive, while the step 3 is shown for the illustration of calculation only.

Point out that this algorithm for finding the stationary solution represents a standard procedure for calculating the nonelementary functions.

It is important to note that for any even number of nonlinearly interacting triads the stationary solutions are absent. This impacts the fact that the phase synchronization, which leads to stationary regimes of oscillation is possible only for the systems consisting an odd number of triads only.